DEVELOPMENT, CALIBRATION AND APPLICATION OF A 3-D INDIVIDUAL-BASED GAP MODEL FOR IMPROVED CHARACTERIZATION OF EURASIAN BOREAL FORESTS IN RESPONSE TO HISTORICAL AND FUTURE CHANGES IN CLIMATE

KSENIA BRAZHNIK

CHARLOTTESVILLE, VIRGINIA

B.A. CHEMISTRY, VIRGINIA POLYTECHNIC INSTITUTE AND STATE UNIVERSITY, 2002

A DISSERTATION PRESENTED TO THE GRADUATE FACULTY

OF THE UNIVERSITY OF VIRGINIA IN CANDIDACY FOR THE DEGREE OF

DOCTOR OF PHILOSOPHY

DEPARTMENT OF ENVIRONMENTAL SCIENCES

UNIVERSITY OF VIRGINIA

DECEMBER, 2015

Abstract

Climate change is altering forests globally, some in ways that may promote further warming at the regional and even continental scales. The dynamics of complex systems that occupy large spatial domains and change on the order of decades to centuries, such as forests, do not lend themselves easily to direct observation. A simulation model is often an appropriate and attainable approach toward understanding the inner workings of forest ecosystems, and how they may change with imposed perturbations. A new spatially-explicit model SIBBORK has been developed to understand how the Siberian boreal forests may respond to near-future climate change. The predictive capabilities of SIBBORK are enhanced with 3-dimensional representation of terrain and associated environmental gradients, and a 3-D light ray-tracing subroutine. SIBBORK's outputs are easily converted to georeferenced maps of forest structure and species composition.

SIBBORK has been calibrated using forestry yield tables and validated against multiple independent multi-dimensional timeseries datasets from southern, middle, and northern taiga ecotones in central Siberia, including the southern and northern boundaries of the boreal forest. Model applications simulating the vegetation response to climate change revealed significant and irreversible changes in forest structure and composition, which are likely to be reached by mid-21st century. These changes in land cover will inevitably result in changes in the biodiversity, carbon storage, and the ecosystem services provided by the Siberian boreal forest.

Acknowledgements

First and foremost, I would like to thank my husband, Luke, for putting up with me while I learned to program. This was a journey that involved a myriad of emotions and a whole lot of chocolate. I am grateful to my advisor Hank Shugart, who had provided guidance, encouragement, funding and a productive environment for this project. I would also like to thank my brother, Konstantin, who has supported me in finding creative ways to communicate about my research and played an integral role in the creation of the SIBBORK introduction video. Furthermore, I'd like to thank Charlie Hanley, who spent a semester working with me on developing a fire subroutine for SIBBORK.

I am thankful to my committee - Stephan F. J. de Wekker, Paolo D'Odorico and Jennie Chiu - for their guidance. I thank K. Holcomb for programming consultation, D. Ershov for facilitating the Usolsky forest dataset, J. Weishampel for providing a reference 3-D light subroutine, D. Urban and J. Holm for ZELIG v1.0 code and documentation, O. Krankina for fruitful conversation and access to some hard-to-find Russian literature, and Dr. C. Huttig for providing the dataset "Hybrid Biomass and Land Cover Map for Central Siberia", portions of which were used in model validation and generation of several figures in this dissertation.

This research was supported and funded by the Environmental Sciences Department at the University of Virginia, the Virginia Space Grant Consortium Graduate Fellowship grant, a NASA grant (NNX11AE39G) to Hank Shugart, and a NASA grant (UM-3002295358) to the University of Michigan subcontracted to Hank Shugart.

Abstract ii

Acknowledgements iii

1 Numerical modeling Approach to Predicting Ecosystem Change **1**

1.1 Introduction 1

1.2 Forest modeling 5

1.3 Advantages of Spatially-Explicit Forest Models 8

1.4 Motivation 11

1.5 Objectives and Hypotheses 12

2 SIBBORK: Model Development **17**

2.1 Environment 20

2.2 Vegetation Processes 43

2.3 Allometry 49

2.4 Environmental Effects on Vegetation Processes 60

3 Model Calibration and Testing **67**

3.1 Introduction 67

3.2 Methodology 68

3.3 Results 85

3.4 Discussion 91

3.5 Conclusions 95

4 Structure and Dynamics in Complex Terrain and in a Changing Climate **97**

4.1 Introduction 98

4.2 Methods 99

4.3 Results . . . 106
4.4 Discussion . . . 109
4.5 Conclusions . . . 115

5 Model Sensitivity **117**

5.1 Does spatial-explicity matter? . . . 118
5.2 Model sensitivity to spatial resolution . . . 125
5.3 Climate Sensitivity Analysis: spatially-explicit forest responses to climate change in central Siberia . 136

6 Current and Future Developments **143**

6.1 Disturbances and Mitigation . . . 143
6.2 Landscape Fragmentation and Edge Effects . . . 153
6.3 Synthetic data generation for Synthetic Aperture Radar calibration and validation . . . 157

7 Conclusions **159**

8 References **161**

CHAPTER

ONE

NUMERICAL MODELING APPROACH TO PREDICTING ECOSYSTEM CHANGE

"Technical skill is mastery of complexity, while creativity is mastery of simplicity." - Sir E. C. Zeeman (1977)

1.1 Introduction

This work serves to introduce the dynamic gap model SIBBORK (SIBerian BOReal forest simulator, pronounced "cyborg" but with a "k" at the end) as a robust tool for predicting ecosystem change. This contribution estimates changes in the boreal ecosystem, which (1) represents the largest terrestrial biome, (2) contains a disproportionate amount of carbon compared to other terrestrial ecosystems, (3) exchanges carbon with the atmosphere, and (4) has been experiencing accelerated climate change over the last three decades. Boreal forests occupy one sixth of the land cover, yet contain one third of the terrestrial carbon stores (*Shugart et al.*, 1986; *Bolin*, 1986, as referenced in *Bonan*, 1988a; *Conard et al.*, 2002; *Bonan*, 2008). Although most of the carbon in boreal forests is stored in soils and permafrost (*Tarnocai et al.*, 2009), carbon dynamics within the ecosystem depend on the structure and composition of the above-ground vegetation community. Additionally, boreal forests are floristically simple, which renders their species diversity, biomass, and carbon dynamics more susceptible to perturbations, such as climate change (*Shugart et al.*, 1992a; *Bonan*, 2008; *Anderegg et al., 2012*). Changes in forest composition and dynamics may propagate regional and global warming of ambient air and soil temperatures through a complex system of vegetation-atmosphere feedbacks (*Bonan et al.*, 1992; *Betts*, 2000; *Denman et al.*, 2007; *Bonan*, 2008; *Shugart and Woodward*, 2011). Due to its rich carbon stores and low biodiversity, the boreal ecosystem may play a substantial role in the planetary carbon cycle, as the warming predicted and already observed in Eurasian boreal forests is likely to shift their function toward acting as a net source of atmospheric carbon. Predicting future changes in the Eurasian boreal

forest is intrinsically a modeling issue, as the spatial expanse of this ecosystem and the temporal scale of patterns and processes do not lend themselves to direct measurement or observation. Furthermore, models allow us to infer long-term dynamics in hypothetical or potential future environmental conditions (*Busing and Mailly*, 2004). This thesis details the development and application of SIBBORK in a spatially-explicit model-based synthesis of forest dynamics to investigate the structure and processes of this vast boreal landscape on multiple scales of time and geography, and includes an exploration of forest response to climate change with the purpose of understanding how changes in this ecosystem may affect global carbon dynamics.

Complex internal interactions within the boreal ecosystem can amplify climate change at regional and continental levels. Field studies have shown that alterations in land cover, such as shifts in tree line position and forest composition, and changes in vegetation processes, including regeneration and seed dispersal, are already occurring within the Siberian boreal forest (*Tretyakova and Noskova*, 2004; *Soja et al.*, 2006; *Noskova and Tretyakova*, 2006; *Tretyakova*, 2006; *Kharuk et al.*, 2009; *Noskova et al.*, 2009; *Barchenkov*, 2010; *Kharuk et al.*, 2013a,b). These physical changes in forest structure coincide with measurements of greater warming than has been observed elsewhere or predicted by global climate models (*Hansen et al.*, 1999; *Serreze et al.*, 2000; *Soja et al.*, 2007; *Shkol'nik et al.*, 2012). Shifts in species composition can transition a forest from acting as a carbon sink to becoming a source of atmospheric carbon, for example, through feedbacks associated with the replacement of deciduous conifers with evergreen conifers. This transition has already been observed in Canadian boreal forests (*Kurz and Apps*, 1999). Forest composition changes can also lead to decreased stand productivity, increased respiration rates, and changes in disturbance regimes (*Valendik et al.*, 2004a,b). Regional changes in species composition and vegetation cover can lead to changes in regional albedo, which, in turn, modifies the regional radiation budget and affects regional climate (*Bonan et al.*, 1992; *Hayden*, 1998; *Baldocchi et al.*, 2000; *Barlage et al.*, 2005; *Liu et al.*, 2005; *Bonan*, 2008; *Groisman et al.*, 2009; *Shuman et al.*, 2011; *Boisier et al.*, 2013).

The replacement of deciduous Larch species (*Larix spp.*) with evergreen conifer species (*Abies spp.*, *Picea spp.*, *Pinus spp.*) accompanying an increase in ambient winter temperatures (*Soja et al.*, 2007; *Kharuk et al.*, 2009; *Shugart and Woodward*, 2011) represents a specific example of how shifts in species composition can alter the regional climate. Larch is a deciduous conifer and, as such, loses foliage in the fall. Consequently, the regional albedo of larch-dominated forests in the winter is closer to that of snow (*Suzuki and Ohta*, 2003) and reflects the majority of the incoming solar radiation. In contrast, evergreen trees maintain the same albedo throughout the year (*Shugart et al.*, 1992a; *Betts and Ball*, 1997; *Shugart and Woodward*, 2011; *Shuman et al.*, 2011). Additionally, in a snow-free environment the annual average albedo of larch is greater than that of any other conifer (*Hollinger et al.*, 2010). There is evidence that the large-scale replacement of larch and a shift to evergreen dominance by dark conifers decreases the average regional albedo (*Kharuk et al.,* 2007). This drives a positive feedback loop between the ambient temperature

and vegetation cover, which may result in further warming and climate changes through alteration of the surface properties and, therefore, the radiation budget on the regional level (*Bonan et al.*, 1992; *Betts et al.*, 2000; *Bonan*, 2008). This feedback has a potential of generating an estimated annual average positive radiative forcing of approximately 5 W/m^2 (*Shuman et al.*, 2011), which is comparable to double the forcing from CO_2 emissions (*IPCC*, 2013). In this manner, climate-related replacement of a cold-loving species with a heat-tolerant one can propagate changes toward a warmer climate that facilitates continued dominance of the heat-tolerant species. Forest dynamic models can be used to further our understanding regarding how species replacement at different scales may affect the local and regional climate.

Carbon dynamics are not equally predictable at all stages of succession, and forest simulation models can facilitate insight into how climatic changes at different stages of succession may affect ecosystem trajectories and carbon storage capacity. Young forests generally serve as a net carbon sink, followed by a self-thinning period of net carbon release to the atmosphere as trees grow and compete for space and resources. New saplings establish in canopy gaps generated by tree mortality, and eventually the regeneration rate balances out the mortality rate. The role of the forest as a sink for atmospheric carbon greatly depends on the balance of uptake of carbon through photosynthesis and release through decomposition and respiration. Older forests tend toward slower growth and greater decomposition rates (*Kolchugina and Vinson*, 1995; *Schulze et al.*, 1995; *Luyssaert et al.*, 2008), and can act as carbon neutral, weak sinks, or weak sources. During the 20th century, Eurasian boreal forests acted as a weak sink, storing atmospheric carbon in vegetation and soil carbon pools (*Shvidenko and Nilsson*, 2003; *Milakovsky et al.*, 2012). However, two decades ago, over half of the 15 million square kilometers of Russian boreal forests were in the mature and overmature category (*Anonymous*, 1990; *Krankina and Dixon*, 1994; *FAO TBFRA of UN-ECE/FAO*, 2000) - a stage when forest productivity decreases (*Kurz et al.*, 1995b; *Bhatti et al.*, 2003; *Goetz et a.*, 2007), and can transition from acting as a net carbon sink to being carbon neutral or a net source of atmospheric carbon (*Ashton*, 2012).

Consequently, due to the age structure and composition of Russian boreal forests, this vast biome is potentially on the verge of becoming a net carbon source in the near future. The climax species in Eurasian boreal forests are dark conifers, which have a lower net primary productivity than the early successional broadleaf deciduous stands. Lindroth *et al*., (1998) found that the carbon balance of old and middle-aged closed-canopy boreal forests in Scandinavia depends on the thermal regime, and acts as a source of atmospheric carbon during years with abnormal temperature distributions. Similar studies have demonstrated that this thermal dependency exists in other biomes, including tropical rain forests (*Grace at al.*, 1995) and temperate forests (*Goulden et al.*, 1996). The vulnerability of the role of forests as sinks for atmospheric carbon may therefore be enhanced by stand age and exacerbated by climatological changes (*Smith and Shugart*, 1993; *Milakovsky et al.*, 2012). A numerical model of forest dynamics can further our

understanding regarding how these complex relationships and processes affect the overall functioning of a forest as a net carbon source or sink.

Furthermore, disturbances alter the short- and long-term carbon balance in a forest. Mature and overmature stands, and especially dark conifers in Siberia, are affected by insect outbreaks and fires - both types of disturbances that are likely to become more significant with increasing conifer dominance in the region (*Ershov and Isaev*, 2006). Coniferous trees are also more susceptible to insect damage and exhibit higher mortality during insect outbreaks than early-successional broadleaf species (*Lyamzev and Isaev*, 2002). Direct observation of forests in North and South America revealed that climate-related and insect outbreak disturbances cause structural changes in forests, including alterations in stand density, spatial distribution, dominant species, and species composition, because trees have different susceptibilities to selective mortality based on size and the life stage of the individual (*Anderegg et al.*, 2012) and the life history of the species (*Shugart*, 1984; *Coffin and Urban*, 1993). Changes in forest structure and species composition in the large boreal ecosystem may have considerable implications for net primary productivity and carbon balance in the region (*Milakovsky et al.*, 2012). To compound the problem, insect outbreaks may be linked to increases in spread and frequency of wildfires (*Bonan and Shugart*, 1989), which would further decrease the carbon storage and productivity of the region in the short term (*Conard et al.*, 2004). It has been reported that increases in the wildfire and insect-related disturbances in the boreal forests in Canada have already converted those forests to a source of atmospheric carbon (*Kurz and Apps*, 1999). Eurasian boreal forests also have the potential to transition to being a carbon source with intensification in the disturbance regimes.

Although remote sensing and satellite-products are capable of monitoring the regional changes in species composition, albedo, and large-scale disturbances, numerical models are vital for predicting future forest structure and dynamics, evaluating the effectiveness of potential mitigation approaches, assessing the associated implications for regional climate and estimating changes in the carbon budget. The new vegetation model SIBBORK has been developed for the purpose of furthering our understanding of how forest dynamics may change with both abrupt and gradual perturbations, as well as for estimating the future carbon storage capacity under different climate change and disturbance scenarios. SIBBORK does not capture all of these feedbacks and complex interactions, but instead focuses on the climate-vegetation relationship and is used to understand how stand structure and composition of a boreal forest may change with alterations to the temperature and precipitation regimes, as well as intensification of the disturbance regime.

1.2 Forest modeling

A model is a simplified representation of our understanding of reality, in this case - forest ecosystems. As a result, some processes may be represented very simplistically or not at all, and some functionality may be over/underestimated. Many current-generation forest dynamics models are based either on the JABOWA (*Botkin et al.*, 1972a,b) or the FORET models (*Shugart and West*, 1977), developed in the 1970's, both of which are were founded on the assumptions of landscape homogeneity over the size of the plot, single leaf layer canopy on each plot, and no interactions between simulated plots. ZELIG, a descendant of FORET, enhanced parameterization of environmental effects on tree processes (*Smith and Urban*, 1988) using the relationships presented by Pastor and Post (1986). ZELIG has been rigorously tested and implemented in past and current applications for investigation of land cover structure and composition in temperate forests (*Urban et al.*, 1991; *Weishampel et al.*, 1996), coastal forest (*Urban et al.*, 1993; *Busing and Solomon*, 2004), dry tropical forest (*Holm et al.*, 2012), tropical rain forest (*Holm et al.*, 2014), as well as upland and bottomland forests in the arid midwest of the U.S. (Acevedo et al., 1997; Holcomb, 2001). Compared to observations from a Northwest Pacific forest, ZELIG underestimates regeneration, producing a smaller number of young saplings, and overestimates mortality, reducing the number and size of mature and old growth trees (*Pabst et al.*, 2008). Nonetheless, the wide application of ZELIG to a diverse array of forest ecosystems demonstrated the model's robustness and adaptability, and provided a strong reference framework for the development of the new model SIBBORK.

SIBBORK is a spatially-explicit individual-based gap model. Individual-based models track the establishment, growth, and mortality of individual trees. Gap models are a type of individual-based models, in which the processes and structure are simulated on plots approximately the size of the crown of a canopy dominant tree (0.05-0.1ha). A sample plot is shown in Figure 1.1, with a canopy dominant tree and other canopy constituents. Within-plot interactions are through extinction of diffuse radiation entering the canopy at a vertical angle by overhead leaf area. Spatial complexity is conveyed through (1) specification of environmental conditions at the plot level, and (2) interactions of trees on one plot with trees on adjacent and nearby plots. Between-plot interactions are a unique feature of SIBBORK and absent from most forest models. SIBBORK can simulate the structure, biodiversity, and geometry of stand composition on each simulated plot (independent 1-D mode), a north-south oriented transect of plots (interactive 2-D mode), or a grid of plots (interactive 3-D mode), and computes the 3-dimensional canopy interactions between plots in the two interactive modes. Additionally, the environmental conditions and light interactions can be computed in complex terrain, which further expands the application of this model to understanding the behavior of vegetation in mountainous regions and transitional ecotones. The most important assumption of gap models, such as SIBBORK, is that patch dynamics can be abstracted to the landscape scale (*Shugart*, 1984, 1998, 2003), and that average dynamics

from 150 or more replicate plots (*Bugmann et al.*, 1996) represent the larger landscape dynamics. SIBBORK goes further by simulating a grid of plots that cover the area of several hectares (up to 81-ha has been tested). An average of 150 replicate simulations of 81-ha landscape serves to more accurately represent the average dynamics on that landscape.

Fig. 1.1: The spatial unit of the simulation is a plot approximately the size of the crown of a dominant tree. Multiple trees sprout, grow, and die on the plot over the course of the simulation. Note, the plots in SIBBORK are square, whereas in many classical gap dynamics models (FORET, FAREAST), the plots are circular. [Reproduced from Shugart (1987).]

Successional dynamics are simulated as a transition from one species to another through species-specific tolerances and competition for resources. A simulation can be initiated from bare ground or an initial condition. Bare ground represents the conditions following a stand-replacing disturbance, such as a wildfire. The model then simulates the establishment, growth, and mortality of each tree using species-specific tolerances and biotic constraints, such as competition for light and soil moisture (*Shugart*, 1984). Establishment denotes seedling germination and sapling generation. Growth refers to an increase in diameter, height, cumulative leaf area, and biomass of individual trees at annual increments over time. The model computes the maximum potential growth and establishment rates for trees of a given species and size, and modifies them based on the environmental conditions and available resources, which are heterogeneously distributed across the landscape. This results in individuals of the same species experiencing different environmental conditions and growth rates based on their location along resource gradients on the terrain.

Tree mortality may be natural or stress-induced. Natural mortality is species- and age-specific. The probability of this intrinsic mortality is the same regardless of tree age, and results in approximately 1% of individuals surviving past the estimated maximum age for the species in regions without disturbance (*Mielke et al.*, 1978). Stress-related mortality varies spatially and temporally, and facilitates the differential distribution of species across the 3-dimensional landscape gradients.

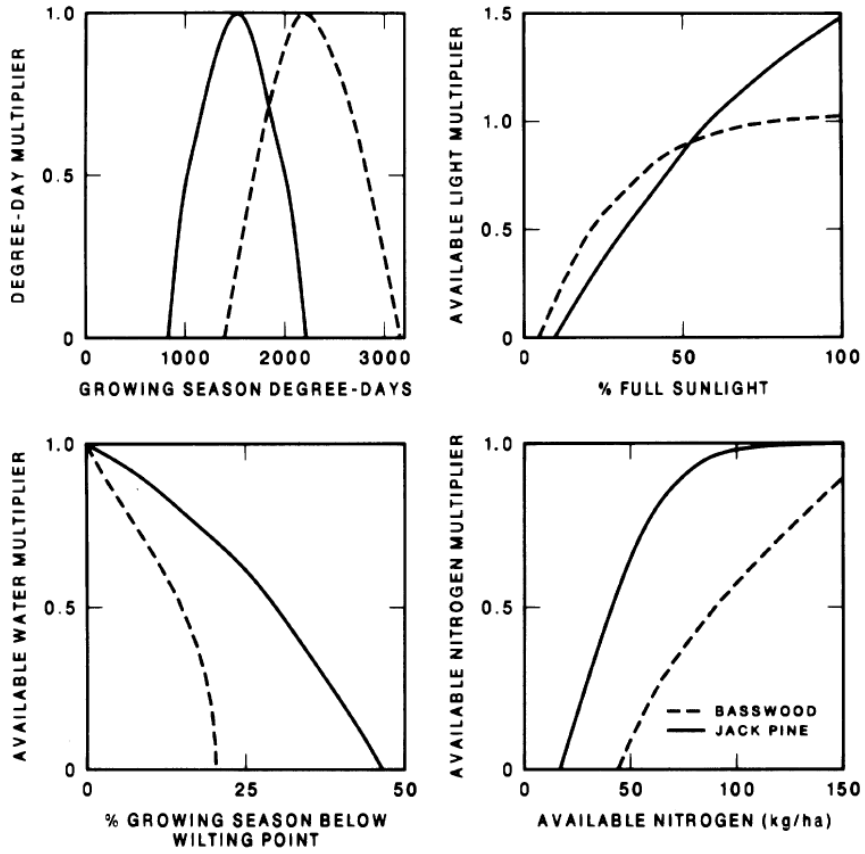

Fig. 1.2: The effects of environmental conditions shown here for Jack Pine. [Reproduced from Pastor and Post (1986).]

Over the course of the simulation, trees interact with surrounding trees and the environment. The growth response to the environmental factors of light availability, soil moisture, ambient temperature, expressed as growing degree days, and soil fertility, expressed as maximum biomass per plot (*Pastor and Post*, 1986), are shown in Figure **??**. Based on a more recent understanding of vegetation response to heat stress (*Bugmann and Solomon*, 2000), the parabolic growing-degree day response has been modified to a nonlinear function of temperature (Figures 2.16b, 2.28c). Recent empirical studies have shown that trees subjected to artificially-warmed environments experienced limited growth only in drought conditions (*McDowell et al.*, 2011; *Bauweraerts et al.*, 2014; *Wertin et al.*, 2012). This modification to the temperature effect on growth transfers the limitation from heat stress to temperature-induced-drought stress,

which appears to more realistically represent tree response to changes in air temperature and soil moisture regimes. The interaction of trees with their environment and other trees in a 3-dimensional spatial domain is the core of the model and makes SIBBORK unique in its representation of important forest processes. SIBBORK development and functionality are described in detail in Chapter 2.

In order to assess the validity of model output, the simulation needs to be tested against field observations. A model can be verified by comparing the output of the model to the data on which it was "trained" - which was used to parameterize the model. Verification assesses how well the numerical model aligns with the conceptual model. Conversely, a model can be validated by comparing the model output to an independent data set, information from which is used to initiate the model, but which was not employed in parameterizing the model. Validation tests the accuracy of the concept map and how well the model can be generalized to new scenarios, environments, and locations (*Cale et al.,*, 1983). The model may need to be revised several times in order to achieve the desired accuracy and realism in representation of forest growth and responses, and to better match the computer simulation to the concept map of forest processes, feedbacks, and interactions. SIBBORK was verified against regional forestry yield tables and validated using an independent forest inventory dataset. Model generalizability was assessed via simulation of new locations outside of the "training" region, and comparison with published datasets and forest descriptions. Model verification and validation are described in detail in Chapter 3.

1.3 Advantages of Spatially-Explicit Forest Models

Forests have been modeled by an array of individual-based models, including homogeneous landscape models (*Shugart*, 1998), Markov and Semi-Markov models (*Acevedo et al.*, 1996), mosaic landscape models, such as a Monte Carlo simulation for point locations (*Yan and Shugart*, 2005), as well as interactive (*Urban*, 1990) and nested landscape models (*Shugart*, 1984; *Urban et al.*, 1993). A spatially-explicit model, however, may more accurately simulate forest vegetation dynamics and predict responses of large heterogeneous landscapes to abrupt disturbances, such as fires and insect outbreaks, as well as more gradual changes in environmental parameters related to climate change, than models lacking spatial complexity. In order to represent the observed climatologic, geologic, topographic, and environmental gradients in the Siberian boreal forest, the model needs to explicitly simulate the large temporal and spatial variability in insolation, soil moisture, as well as air and soil temperatures. Variability in environmental conditions leads to heterogeneous distribution of vegetation across the landscape. A spatially-explicit model can directly simulate some of the fine-scale differences in environmental conditions on the landscape and resolve the environmental biases in the distribution of species in 3-dimensional space based on species-specific tolerances to resource limitations. Shifts in temperature and precipitation regimes can be applied differentially across the landscape, reflecting fine-scale

differences in changing conditions and potential refugia for species that would otherwise be subjected to coarse-scale environmental changes in models that apply homogeneous warming or precipitation changes at the simulation level. For these reasons, a spatially-explicit model may be the more appropriate tool for examining forest responses to local changes in abiotic environmental factors and disturbances, which can then be extrapolated to the landscape scale.

SIBBORK, along with a few other spatially-explicit forest models (SORTIE: *Pacala et al.*, 1993; FORMOSAIC: *Liu and Ashton*, 1998; FORMIND/FORMIX/FOREGG: *Kohler and Huth*, 1998; *Huth et al.*, 1998; *Huth and Ditzer*, 2000; *Kohler at al.*, 2003; *Tietjen and Huth*, 2006; *Kohler and Hurth*, 2007; *Dislich and Huth*, 2012; LANDIS: *Mladenoff and He*, 1999), keeps track of the location of each tree within the geometrical space of the simulation domain. As in LANDIS, the landscape in SIBBORK is simulated as a grid of plots (*Mladenoff*, 2004). However, the advantage of SIBBORK is that it keeps track of individual trees, whereas LANDIS simulates age classes (cohorts). Similar to FORMIX/FORMIND, the x-y location of each tree within a plot is not recorded, and the uncertainty in the location of each tree on the landscape is limited to within a plot. However, the advantage of SIBBORK over the FORMIX/FORMIND models is in (1) the spatial resolution in the vertical dimension, and (2) the species-specific parameterization, compared to plant functional type groups utilized in FORMIX/FORMIND (*Huth et al.*, 1998). Models with spatial complexity explicitly resolve spatial processes and attempt to represent the 3-dimensional space within a patch of forest to varying degrees of detail (*Busing and Mailly*, 2004). Some spatially-explicit models are able to resolve the 3-dimensional structure of canopy and sizes of gaps at different resolution scales: SORTIE - user-specified 1024 m^2 minimum, FORMIND suite - 400 m^2, LANDIS - 100 m^2 to 0.25 km^2, SIBBORK - user-specified 100 m^2 minimum tested. An example of an explicitly-resolved 3-dimensional process is shading of trees by canopies of individuals on the same and adjacent plots. The explicit simulation of shading by trees on surrounding plots allows for the simulation of vegetation responses to disturbances that affect areas larger than a single plot, for example, the regeneration of shade-intolerant trees when gaps the size of multiple plots form as a result of mortality of several canopy dominant trees in a mature forest. Processes larger than the plot size are not resolved in simulations of independent plots. Furthermore, spatially-explicit models may be more suitable for simulation of phenomena that spread in space (*Reiners and Driese*, 2004), such as tree mortality and gap formation on multiple scales, whether due to natural mortality or drought stress, insect outbreaks, or fires (*Sturtevant et al.*, 2009). When individuals on plots interact with each other and the environment in 3-dimensional space, the probability of an event occurring on a plot can be affected by the occurrence of this event, e.g. fire, on adjacent plots. This spatial interaction results in a more realistic representation of process dependencies on the natural landscape.

Characterization of ambient conditions based on the plot's location within the landscape facilitates simulation of fine-scale species distribution. The ability to differentially change climatic conditions based on landscape characteristics enables the simulation of climate change scenarios more similar to those observed and forecast for regions of complex

terrain, such as in southern and eastern Siberia. In the extreme continental locations of the Siberian boreal forest, larger temperature increases have been predicted and observed than anywhere else on our planet (*Denman et al.*, 2007; *IPCC*, 2013). In fact, some of the observed warming trends have been in excess of the model-predicted trends for the region (*Soja et al.*, 2007). Uneven distribution of warming has been observed across Eurasia on multiple scales (*Kharuk et al.*, 2013a,b; *Bulygina et al.*, 2014; *Gruza et al.*, 2015). Several responses of boreal forest constituents to climate change have already been observed, such as the regional northward and upslope shifts in the treeline location (*Esper and Schweingruber*, 2004; *Kharuk et al.*, 2006; *Soja et al.*, 2006), and changes in reproduction capacity and mortality rates of some boreal tree species, including Siberian Larch (*Larix sibirica*), Scots Pine (*Pinus sylvestris*) and silver birch (*Betula pendula*) (*Kharuk et al.*, 2009; *Kharuk et al.*, 2013a,b). Boreal forests exhibit low diversity of tree species, and changes in reproduction, growth or mortality rates of just a few of them can drastically alter the species composition and associated atmosphere-vegetation interactions at local and regional scales. A spatially-explicit model may more realistically capture the northward and upward shifts in species distribution across the simulated terrain, and changes in the differential distribution of species on slopes of different aspects. The application of SIBBORK toward understanding the northward and upward shifts in treeline with changing temperature regimes is described in detail in Chapter 4.

The large-scale effects of climate change on boreal ecosystems have been estimated using an array of non-interactive and non-spatially-explicit approaches. Holdridge life-zone classification has been employed to examine the current climate-vegetation coupling, and then the same coupling was used to generate biome maps for a proposed future distribution of climatological zones (*Emanuel et al*., 1985). A primary limitation of this approach is that the same climate-vegetation coupling may not be valid under new climatological conditions. Nonetheless, if this approach is valid, the southern taiga boreal forest is predicted to become a steppe ecozone (*Emanuel et al.*, 1985; *Monserud et al.*, 1993) with a Global Climate Model prediction of a warmer, drier climate (*Prentice*, 1990; *IPCC*, 2007). Another approach includes a simplified parameterization of species into plant functional types with a limited set of common parameters used in a community land model together with a global climate model (*Lawrence et al*., 2012; *Oleson et al.*, 2013). However, Law (2014) points out the importance of species-specific parameterization, especially for investigation of climate-related changes in ecosystem trajectories, and Ashroft *et al.* (2009) have demonstrated the need for fine-scale spatially-explicit resolution of microclimates in models used to predict vegetation response to climate change. Species-specific parameterizations and spatial complexity are of particular importance in a boreal ecosystem where biodiversity is low and 95% of tree species are represented by six tree genera, and the environmental conditions are characterized by a complex light regime and permafrost. Estimates from models lacking spatial complexity described above predict significant vegetation shifts in regions currently occupied by boreal forests with future climatological changes. These model predictions are in contrast to the results from an investigation of the effect of a 2^o C

increase in annual average temperature using the non-spatially-explicit model FAREAST (UVAFME) with species-specific parameterizations (*Shuman and Shugart*, 2009). Employing the spatially-explicit model SIBBORK toward a similar investigation provides more detail and insight into the smaller-scale processes and changes within the Siberian boreal forest with observed and forecast climatic changes. Details of this investigation are delivered in Chapter 5.

1.4 Motivation

The motivation for this research stems from the need for developing predictive capabilities for the simulation of terrestrial ecosystem dynamics and incorporating projections of regional and global changes. Changes in land cover and biomass affect the carbon stores in vegetation, soils, and permafrost. The less carbon that is sequestered and stored in the terrestrial biome and oceans, the more remains in or is released to the atmosphere. This project is geared toward the understanding of the forest dynamics in the ecosystem that comprises the largest carbon reserve on the Earth's surface via a spatially-explicit modeling approach. The manner in which a landscape may respond to climate change depends on spatial interactions between the different components of the landscape (*Shugart and Woodward*, 2011). Some forest functions and processes, such as evapotranspiration, soil moisture, spread of insect outbreaks and wildfires, depend on spatial parameters, such as topography and whether the neighboring trees are infected or burning. I developed a new spatially-explicit individual-based gap model SIBBORK to incorporate spatial interactions into the simulation of boreal forest dynamics. The new model is based on our current understanding of forest dynamics and internal processes, regional and global datasets, and recent advances in computing technologies. Model development is described in Chapter 2. Model calibration and testing is described in Chapter 3. Model application toward the simulation of northward and upward migration of boreal treeline - a sensitive transition ecotone - is described in Chapter 4. Of particular interest is the assessment of whether spatial complexity in the 3-D interactive mode has better predictive power with regards to species composition, total biomass (carbon storage), and other stand aggregate and species-specific characteristics in a boreal forest, as compared to the independent non-spatially-explicit 1-D point-plot mode. This comparison is presented in Chapter 5, along with climate sensitivity analysis on central Siberian boreal forest. Further applications of SIBBORK toward examination of how mitigation effects, wildfire, and insect outbreaks may affect the contribution of the boreal forest toward the global carbon budget are discussed in Chapter 6.

To narrow down the geographic scope for initial model development, SIBBORK was trained on silvicultural data from the forestry yield tables for southern taiga ecotones of central Siberia, parameterized with meteorological data and soils characteristics from global datasets, and tested against independent datasets from southern and middle taiga ecotones of central Siberia.

1.5 Objectives and Hypotheses

Gap models can be used to predict the distribution and abundance of arboreal species, as well as the succession trajectories and biomass dynamics within a forest. In order to understand the potential uncertainty associated with model predictions for simulation of possible future conditions, we need to evaluate model output under known conditions against observations. The three main questions of this thesis are concerned with the predictive abilities of SIBBORK and whether added spatial complexity results in a gain in prediction accuracy. The first objective addresses model verification, which assesses how well the numerical model aligns with the conceptual model of forest dynamics. Whether initialized from bare ground or from initial conditions, does the simulation appropriately reproduce the observed stand structure and composition of young (less than 100 years old) mixed and mono-species stands? The verification test involves the dataset on which the model has been "trained". The null hypothesis is that there is no statistically significant difference between the field-measured parameters reflected in the regional forestry yield tables (*Shvidenko et al.*, 2006) and the model output for young forest stands. The alternate hypothesis is that there is a statistically significant difference between the yield table data and model output during the first 100 years of simulation. The stand structure parameters evaluated include diameter at breast height (DBH, at 1.37m), height, stem density, and biovolume. Stand dynamics are represented by the changes in these structural parameters over time. We can compare simulated stand dynamics to the timeseries forestry yield table datasets, which reflect average stand structure at decadal time steps. Evaluation of model output against a timeseries dataset, versus a snapshot of conditions at a single point in time, constitutes a more powerful test of the model's predictive abilities (*Bugmann*, 2001).

The second objective addresses model validation, and includes the comparison of model output to an independent dataset not used in training of the model. Validation tests the accuracy of the concept map and how well the model can be generalized to new scenarios, environments, and locations. When initialized from bare ground, does the simulation appropriately reproduce stand structure and composition of mature (older than 200 years old) mixed and mono-species stands? The validation test involves the comparison of model output to an independent forest inventory dataset from the Usolsky forest enterprise in the Krasnoyarsk Region of Russia (*Ershov and Isaev*, 2006). This independent dataset has not been used in the training or verification of the model. When SIBBORK is initiated with climatological and site parameters from the Usolsky forest, but the silvicultural and allometric relationships are not altered, does the model appropriately reproduce stand characteristics from the Usolsky forest? The null hypothesis is that there is no statistically significant difference between the modeled and field-measured stand characteristics from the Usolsky forest for mature stands. The alternate hypothesis is that there are statistically significant differences between the model output and the field data from the Usolsky forest with regards to the stand aggregate and species-specific physiognomy. The characteristics selected for the validation test depend on data availability. The stand structure parameters evaluated

in this test include biovolume and species composition. It is important to create a model that is applicable to the broader Eurasian boreal forests. To assess the model's ability to simulate forests outside of the calibration region (south taiga), published datasets and descriptions of forest composition at different successional stages were utilized for qualitative validation and quantitative assessment of model generalizability to the middle taiga ecotone. The stand structure parameters evaluated in the generalization test included basal area and species composition.

Having created a functional 3-dimensional forest dynamics model, of particular interest is the balance between complexity and realism. The third hypothesis addresses the potential advantages of spatially-explicit forest models by examining the differences between the output from the independent and interactive plot modes in SIBBORK. Is there a statistically significant gain in the accuracy of model prediction for forest biomass and species composition, from inclusion of interactions between trees on model plots through the simulation of a 3-dimensional light regime? A need for this type of comparison in forest gap models had been identified by Busing and Mailly (2004), however, few forest dynamics models can operate in both independent and interactive modes, and none, to date, have been used for the simulation of the Siberian boreal forest. To limit the confounding variables in the comparison, this question is best answered using a single model that operates in both spatially-explicit and independent plot modes, rather than between two different gap models that only function in one mode or the other. For this test, model runs in both modes were initiated from bare ground with the same climatological, site, and silvicultural input parameters, and the evolution of stand structure and composition was compared between the two modes for the first 600 years of the simulation. The stand structure parameters evaluated include stand aggregate and species aggregate DBH, Lorey's height, and biovolume at 10 year intervals. The null hypothesis is that there is no difference between stand structure and dynamics simulated using the 1-D independent mode compared to the 3-D interactive mode. The alternate hypothesis is that there is a statistically significant difference between the outputs from spatially-explicit and non-spatially-explicit simulations, and significant gain in predictive abilities by means of enhanced spatial complexity.

The three hypotheses described above were tested using the new SIBBORK model, forestry yield tables from central Siberia (*Shvidenko et al.*, 2006), Usolsky forest inventory (*Ershov and Isaev*, 2006), and additional datasets and descriptions from the literature (*Basilevich*, 1986; *Alexeyev*, 1998; *Roser et al.*, 2002; *Hytteborn et al.*, 2005; *Shulze et al.*, 2005; *Groisman et al.*, 2013), and are addressed in Chapters 3 and 5. The distribution of stem density and biomass is not normal, which violates the t-test assumption (*Bugmann*, 1996), therefore quantitative model validation was conducted using the nonparametric Smirnov-Kolmogorov test and regression analysis in Statistical Analysis Software (SAS v9.3). The uncertainty of the forestry yield table data is estimated at 4-7%, and the uncertainty of the Usolsky forest inventory is unknown. A model is not meant to reproduce the structure and composition of one specific stand - it is developed for broader applications within a region. Over-tuning the model to the calibration or validation datasets

can decrease the range of model applicability. For this reason, differences between modeled and observed quantities of less than 15% were not considered significant.

Additionally, forest simulation was conducted on artificial south- and north-facing slopes under 1-dimensional and 3-dimensional regimes. This investigation was driven by the question: does the explicit simulation of 3-dimensional topography, and the associated radiation, temperature, and hydrology gradients, result in improved predictive capabilities for species and biomass distribution across complex terrain? Model output was qualitatively compared to altitudinal zonation, as well as the location of the upper and lower timberline in southern Siberian Sayan-Altay mountains described in the literature (*Onuchin*, 1962; *Shumilova*, 1962; *Ogureeva*, 1973; *Gorchakovsky and Shiyatov*, 1978; *Rakovskaya and Davydova*, 1990; *Moiseev*, 2002; *Chytry et al.*, 2008; *Kharuk et al.*, 2010a; *Kharuk et al.*, 2010b; *Kharuk et al.*, 2013a,b). This analysis is described in Chapter 4.

Changes in biomass represent fluctuation of carbon stocks and can give us insight into the storage capacity of the Siberian boreal forest. Previous investigation suggested that the storage capacity in the Siberian boreal forest is limited (*Dixon and Krankina*, 1994; *Shuman*, 2010), which makes the current investigation all the more pertinent. The vast Siberian boreal forest is confined between approximately the 12^o C and 19^o C July isotherms (*Arctic Atlas*, 1985; *Anuchin et al.*, 1986; *MacDonald et al.*, 2000). Tundra is located to the north of the 12^o isotherm, and steppe outcompetes trees in the dry environment south of the 19^o C July isotherm. Together with low biodiversity, the distribution along a narrow climatological gradient renders the Siberian boreal forest susceptible to thermal regime changes as low as $+2^o$ C. Utilizing the ability to simulate interactive and non-interactive plots, SIBBORK was used to examine the changes in biomass dynamics and species composition in the Siberian boreal forest that may be expected as a result of shifts in temperature and precipitation regimes. How do climate change responses in the vegetation differ on an interactive grid of plots compared to independently modeled plots? Monthly temperature and precipitation were gradually varied based on reported (*Blunden et al.*, 2013; *Groisman et al.*, 2013; *Bulygina et al.*, 2014; *Gruza et al.*, 2015) and projected (*Shkol'nik et al.*, 2012; *IPCC*, 2013, RCP8.5 Scenario) climatological changes for central Siberia. Details of the climate sensitivity analysis on the resilience and potential tipping points of the Siberian boreal forest ecosystem are discussed in Chapter 5.

The spatially-explicit nature of the SIBBORK simulation allows us to see how the distribution of vegetation across a simulated landscape changes over time and with changing environmental conditions. This platform facilitates the investigation of how spatial phenomena propagate across and are modified by the conditions on the landscape. SIBBORK opens the possibility of exploring spatial forest processes, such as treeline undulation and seed dispersion, in addition to understanding the forest response to dominant natural disturbances. The disturbance dynamics in the boreal forest biome will likely be affected by shifts in temperature and precipitation regimes (*Dale at al.*, 2001). The extent, duration and frequency of droughts, insect outbreaks, and wildfires are likely to increase (*Conard et al.*, 2002;

Kasischke et al., 2004; *Goetz et al.*, 2007; *Malevsky-Malevich et al.*, 2008; *Mokhov and Chernokulsky*, 2010; *Kharuk et al.*, 2011). Many of these have already been observed (*Soja et al.*, 2007). These disturbances alter the species composition, biomass dynamics, soil temperature and respiration rates, and therefore have a significant effect on the role of the boreal forest as a sink or a source of atmospheric carbon, both through immediate and multi-year effects following the disturbance. Furthermore, the characteristics of the fire regime affect species composition (*Rogers et al.*, 2015), and changes in fire regimes are likely to not only modify the forest age structure, but also the composition and the dominant species in the affected forest stands. Together with an undergraduate student, Charlie Hanley, I explored the effects of simple disturbance (fire) parameterizations on species composition and biomass dynamics. Instead of simulating the actual disturbance phenomena, which are very complex, the *effect* of these disturbances on biomass dynamics and species composition was explored based on published descriptions of species tolerances to different types of wildfires (*Cuevas-Gonzales et al.*, 2009). The effects of current (*Groisman et al.*, 2007; *Loboda and Csiszar*, 2007) and potential future (*Mokhov et al.*, 2006; *Malevsky-Malevich et al.*, 2008; *Mokhov et al.*, 2010) fire regimes on stand structure and composition were explored. Additionally, the potential of SIBBORK coupling with existing wildfire and insect outbreak modules to examine the propagation of these disturbances across the simulated landscape was investigated. The effects of including disturbance on the simulation outcome are described in Chapter 6.

CHAPTER

TWO

SIBBORK: MODEL DEVELOPMENT

"Any model represents an abstraction of reality. The problem is not whether, but what to leave out." - Clark, Jones & Holling (1979)

"Always code as if the guy who ends up using/maintaining your code is a violent psychopath who knows where you live." - John Woods (1991)

The original project direction focused on the re-parameterization of an existing gap dynamics model ZELIG for the simulation of boreal ecosystems. ZELIG was initially developed for temperate forests (*Smith and Urban*, 1988; *Urban*, 1990), and although the 3-D light subroutine has been applied to simulate a high-latitude light environment (*Weishampel and Urban*, 1996), the model had not been previously applied toward the simulation of Eurasian boreal ecosystems, and there were numerous incompatibilities between the existing ZELIG model and boreal forest processes. For example, ZELIG employed the Thornthwaite-Mather equation for the calculation of potential evapotranspiration (PET) based on monthly temperature and precipitation, and latitude corrections for day length. However, the correction factors have not been validated for latitudes above 50^o N (*Botkin*, 1993), which rendered this approach inappropriate for the estimation of the water budget within Siberian boreal ecosystems located between 50^o N and 71^o N. The 3-D light ray tracing subroutine was created for flat terrain and, in its original form (*Weishampel*, 1994), was not compatible with complex terrain features. However, approximately half of the Siberian boreal forest is located in mountainous terrain (*Atlas of the USSR*, 1983), so modifications to the 3-D light ray tracing subroutine were needed in order to more appropriately compute the light environment for these areas. Each process in ZELIG was evaluated for compatibility with application toward the simulation of high-latitude environments and ecosystems and, wherever necessary, new formulations were developed. In order to extend the capabilities of the original ZELIG model to simulate the temperature, radiation, and edaphic gradients encountered in the mountains, model structure and several processes were substantially modified. The resulting gap dynamics model was deemed different enough from ZELIG

to warrant a rebranding and was coined SIBBORK - the SIBerian BOReal forest simulator, which was calibrated to the Krasnoyarsk region in central Siberia.

SIBBORK is a spatially-explicit individual-based gap model for predicting ecosystem change in boreal forests. It was designed as an open source model, utilizing publicly-available software and datasets. The new model is a descendant of ZELIG, an existing individual-based gap dynamics model (*Urban* 1990, 2000; *Urban et al*. 1991, 1993) and retains many of ZELIG's functionalities. First, ZELIG was functionally translated from Fortran to Python for the purpose of interfacing with ArcGIS, since a spatially-explicit model produces spatially explicit output, and GIS (ArcGIS, open source: QGIS, Grass) could be used to display model output in georeferenced space. Thereafter, the model was substantially altered through modifications to the 3-D light subroutine, species-specific parameterizations and governing equations, simulation of canopy architecture and terrain representations, and specification of the simulation area and plot size. Alteration was geared toward improving model functionality based on advances in ecology and technology, and specifically tailored to the boreal forest ecosystem. Additionally, an array of analysis scripts were created for ease of processing output from replicate model runs and for visualization of model outputs. A simplified diagram of process flow in SIBBORK is shown in Figure 2.1.

SIBBORK's predecessor, ZELIG, was originally developed at the University of Virginia based on the FORET model (*Shugart and West*, 1977; *Shugart*, 1984; *Leemans et al.*, 1989), which is not spatially-explicit, for the simulation of North American temperate forests (*Smith and Urban*, 1988; *Urban*, 1990). It has since been adapted to temperate forests in China (*Jiang et al.*, 1999), the Pacific Northwest (*Urban et al.*, 1993; *Busing and Solomon*, 2004), Alaska (*Weishampel et al.*, 1992), the northern hardwood and mixed forests in Canada (*Larocque et al.*, 2006; *Larocque et al.*, 2011), the tropical dry forests in Puerto Rico (*Holm et al.*, 2012; *Bond-Lamberty et al.*, 2015), as well as the tropical forests in the Amazon region (*Holm et al.*, 2014). A detailed process flow diagram for ZELIG is shown in Figure 2.2. The blue rectangles and arrows symbolize the processing, the orange rectangles list the inputs and the green rectangles summarize the outputs for each subroutine.

The current working version of SIBBORK is v3.0, however, each stage in development has it's own importance. SIBBORK v1.0 represents ZELIG (Fortran) functionality, implemented in Python. This version includes 1-D and 2-D light subroutines, in which the light penetration through the canopy is computed solely from directly overhead (1-D), as in classical gap dynamic models, or from overhead and from the south directions (2-D), respectively. The Fortran and Python versions of the model were run concurrently and model output was qualitatively and quantitatively evaluated to validate the functionality of the "translation". There was no difference in model output of tree height, diameter at breast height (DBH), and biomass distributions for monospecies stands simulated via ZELIG v1.0 (Fortran) and SIBBORK v1.0 (Python) starting from bare ground, from identical initial conditions, and with a fixed seed in the random number generators.

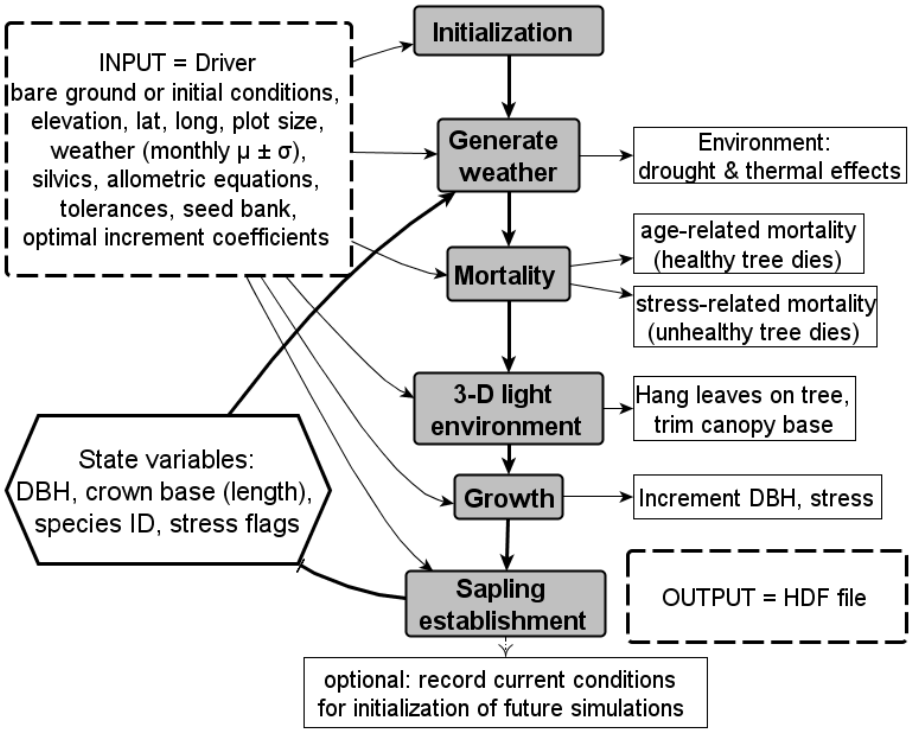

Fig. 2.1: Conceptual diagram of process flow in SIBBORK. Pre-processing includes analysis of climatological, radiation, and edaphic factors for the location of interest and generation of topography using Geographic Information System software. The model is initialized with conditions specified in the driver file. Weather is generated at daily and monthly timesteps. Annually, saplings are established, trees are grown, and some trees die due to natural or stress-related mortality. State variables are updated annually. HDF output file contains a record of state variables at user-specified increments. Height, basal area, biovolume, biomass, and leaf area are computed at the individual level as a function of DBH during post-processing, and optionally aggregared to the stand-level, with the additional option to specify masks based on terrain features.

In SIBBORK v2.0, the weather, sapling establishment, and tree growth subroutines were modified, and the parameterization representing the interaction between trees and the surrounding environment was enhanced. The representation of terrain in the simulation was developed using ArcGIS. The 3-D light subroutine developed by Weishampel (1994) was functionally implemented in Python and significantly modified to enhance the representation of the complex light regime at northern latitudes. Although the 3-D light subroutine worked with complex terrain at this stage, it was very computationally expensive (runtime on a 9-ha 1,000-year simulation was on the order of 12 hours). Model output and state variables were recorded to a hierarchical data format (HDF) file.

Sibbork v3.0 further improved the 3-D light subroutine to facilitate ray-tracing in complex terrain and accelerate it via the Numba library, which compiles the python code. Leaf area calculation was improved using a combination of approaches from the literature and field-based observations. Multiple scripts and a GUI were created to facilitate analysis and visualization of model output, including a timeseries output of simulated forest structure color-coded by species. The functions that have been modified from ZELIG to SIBBORK are outlined in red in Figure 2.2, and added

functionality is shown via red rectangles and arrows. Features that are unique to SIBBORK, compared to ZELIG, are listed in Figure 2.3, and additional model highlights are described in Figure 2.4.

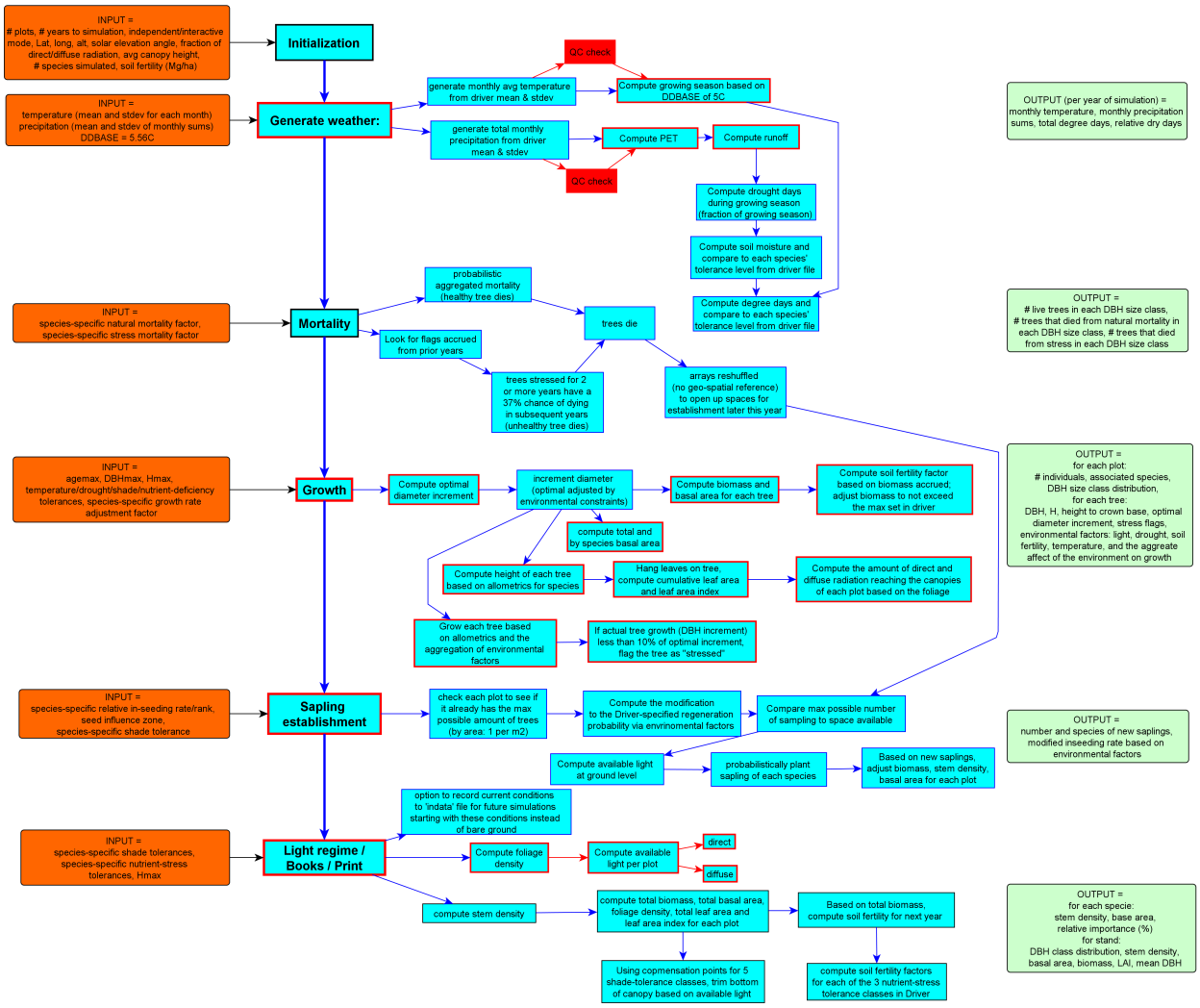

Fig. 2.2: SIBBORK is based on the ZELIG gap model, with significant modifications to the sapling establishment, tree growth, and 3-D light subroutines, as well as environmental interaction parameterizations. New features symbolized via red rectangles/arrows; features modified from ZELIG outlines in red.

2.1 Environment

SIBBORK simulates tree processes in a 3-dimensional environment, which includes topographic, radiation, climatic, and edaphic gradients. Topography and radiation are specified at the plot-level. Topography is specified as elevation above sea level in meters. Within each plot, the elevation is constant and the terrain is uniform. Radiation is computed in ArcGIS and specified as a sum of WHm^{-2} for each month of the year. The radiation calculation takes into account

Function	ZELIG	SIBBORK
Monthly temperature	random from a gaussian around a mean	same, with added QC check
Monthly precipitation	random from a gaussian around a mean	same, but flush negative rain to 0, added QC check
Growing degree base	5.56^o C	broadleaf: 5^o C
Potential Evapotranspiration	Thornthwaite-Mather equation	modified Penman equation
Runoff	uses PET, field capacity and wilting point	same, but uses AET instead of PET
Optimal diameter increment	based on JABOWA	based on Bragg (2001, 2003)
Soil fertility	based on optimal biomass increment	based on actual potential biomass increment
Heat tolerance	parabolic	user-specified: parabolic or non-linear
Stress flags	if does not achieve 10% of optimal diameter increment	species-specific thresholds based on forestry yield tables
Maximum stem density	1 stem / m^2	user-specified
Height	same form polynomial with species-specific coefficients	species-specific equations (incl. piecewise)
Leaf Area	same equation for all species, f(DBH)	species-specific, based on Breda (2003) and forestry yield tables
Plot size	100 m^2	user-specified
Simulation domain	Single plot, transect of plots, or grid of interactive plots	user-specified number of plots in an interactive grid, single plot, transect of plots, or grid of independent plots grid of independent plots
Terrain	Flat	Flat, artificial 3-D, or real 3-D
Light mode	1-D, 2-D, 3-D	1-D, 2-D, or 3-D, with complex terrain
Driver file	fixed-format text	self-documenting python code
Model output file	(pretty-print) text, csv	HDF

Fig. 2.3: Functionality comparison between ZELIG and SIBBORK

latitude, elevation, slope steepness, aspect, direct:diffuse ratio, and atmospheric transmissivity. Soil characteristics include field capacity, wilting point and site index. Field capacity and wilting point are estimated from the total available water. These parameters are specified in the driver and are the same for all plots in the simulation. Conversely, site index is estimated based on forestry yield tables and refers to the limit on gross primary productivity. Site index is a plot-level parameter. Temperature and precipitation represent the simplified weather conditions. Temperature is specified at the plot-level, and is adjusted using the environmental lapse rate based on elevation above or below a reference weather station. Monthly precipitation is the same for all plots, due to lack of field data and uncertainty in downscaling precipitation from climate and meso-scale models. A simplified precipitation gradient can be specified based on slope aspect (windward/leeward), however, all plots with a given slope aspect will receive the same precipitation. Light-ray tracing is computed within a 50-m thick layer of the atmosphere above the ground surface. The 50-m thickness was selected to exceed the maximum observed tree heights in the Siberian boreal forest and to limit the computational space (*Shvidenko et al.*, 2006; *Ershov and Isaev*, 2006; *Neigh et al.*, 2013). Vegetation is simulated within this 3-dimensional environment.

Feature	Description	Origin
Simulation of 3-D space		
Spatially-explicit simulation of 3-D terrain	The model intakes a 2-D matrix that can specify real terrain from a Digital Elevation model or user-generated artificial terrain (flat, sloped, etc.)	A new feature that allows terrain heterogeneity. Plots in a grid (homogeneously flat terrain) were simulated with ZELIG by Weishampel and Urban (1996).
Wrap-around to simulate continuous forest	The southernmost boundary of the simulation area is wrapped around to be continuous with the northernmost boundary, and the eastern boundary is wrapped around to be continuous with the western boundary to ensure continuity with regards to light ray tracing.	This feature remains from the previous versions of ZELIG, however, in SIBBORK this feature can be toggled on/off to simulate forest fragmentation.
3-D light ray tracing that works with the 3-D terrain	Light ray tracing does not allow light to travel through the terrain. To facilitate wrap-around, ray trace is permitted to continue elevated terrain along the edge of the simulation area.	A new algorithm that allows the 3-D light subroutine originally developed by Weishampel (1993) to work with 3-D terrain.
Independent vs. interactive plot modes	Independent mode: trees on a plot receive only from directly overhead and do not shade of trees on other plots. Interactive mode: trees on a plot receive light from 7 paired sun azimuth-elevation angles and shade trees on nearby plots.	An improved version of a feature from ZELIG, which now gives the user the ability to specify the shape and extent of the simulation area, and the plot size.
Differential air (and soil) temperature in complex terrain	Air temperature is computed at the plot level using weather station data, radiation inputs, and seasonal lapse rates.	A new empirically-based algorithm.
Soil moisture and drainage	Soil moisture is computed as a fraction of total available water content based on soil type. Runoff represents gravitational water, and is contributed as runon to the water budget of the plot directly downslope.	A new algorithm based on soil type and terrain characteristics. Soil and water content data are available from global datasets.
Species-specific parameterization		
Total (above- & below-ground) biomass	Most models do not consider or compute below-ground biomass. SIBBORK is parameterized to compute the species-specific total sum of above- and below-ground biomass based on yield tables with this data.	A new empirically-based algorithm that improves simulated biomass estimates at the individual and stand levels.
Foliage biomass	Species-specific piece-wise calculation based on DBH and total biomass.	A new empirically-based algorithm.
Total leaf area	Species-specific computations of leaf area as a function of foliage biomass, leaf area index (LAI), and specific leaf area (SLA).	A new algorithm that synthesizes regional yield table data and published datasets.

Inputs		
JSON (JavaScript Object Notation) file format	Standardized file format with user-friendly formatting and incorporation of documentation strings for every input variable.	A new feature, as previous versions of ZELIG and its derivatives utilize Text file format, in which inputs must be specified at a fixed location within the document with no option of in-line documentation.
Input file pickled and stored with simulation output	The input file is stored with the output HDF file and cannot be altered, therefore preserving the user-specified simulation parameters for future reference.	This is a new feature that permanently associates the input data with the model output generated with those inputs, eliminating the possibility of manually associating the input file with an output file generated from other inputs.
Ease of creating matrix inputs for topography, soil nutrition, and maximum ground-level light gradients.	Although the maximum available light at ground level (also used for top of canopy) is computed using the Solar Radiation Calculator (ref) in ArcGIS, the topography and site index input ASCII files can be generated manually or with a script.	This is a new feature that facilitates generation of artificial terrain (e.g. flat, different slopes and aspects) for model testing, and allows the utilization of actual terrain from a Digital Elevation Model in the simulation.
Outputs		
HDF file format	Multi-dimensional matrix output format that makes it possible to store all of the model output in one file, greatly simplifying the parsing of model output.	A new feature that eliminates the need to parse pretty-print text output documents common to many models, including ZELIG and FAREAST.
2-D and 3-D matrix outputs to visualize the simulated environment and vegetation across the landscape	Information about the simulated environment is stored at the plot level. All tree parameters are stored at the individual level within each plot. This facilitates analysis at the individual, plot, and stand levels.	A new feature that facilitates visualization and animation of model outputs in 4-D space-time in Geographic Information Systems or as matrix-based gifs.
Documentation		
User's Manual, tutorials, and extensive comments within the code and driver file	Documentation of every input parameter, function and subroutine in the model code. Step-by-step tutorials on model implementation, re-parameterization to new species and locations, modification of the HDF output record, and model testing. In-line code commentary.	A new feature that is often overlooked in model development or lost as model development branches.

Fig. 2.4: Description and origins of new and improved SIBBORK v3.0 features.

2.1.1 Spatial domain

Plot Size

The spatial unit of the simulation is a plot approximately the size of the canopy of a dominant tree. Trees of different species will develop crowns of different sizes, however, the average canopy size can be deduced from the ecosystem in focus. Tropical trees, e.g. Bunyan, may develop canopies 20-m across or more, whereas Dahurian larch, which dominates vast regions of north-central Siberia, is characterized by a long, thin, almost-cylindrical canopy of just a few meters in diameter. The goal is to appropriately simulate the leaf area index (LAI), which, in the simulation, is a ratio of total leaf area to plot size. If the plot is significantly smaller than the horizontal canopy cross-section, the simulated LAI will be exaggerated. The plot size is set by the user in the digital elevation input file. In the current analysis and application of SIBBORK, 100 m^2 plots were used. However, analysis assessing the dependence of model output on plot size was conducted and the results are reported in Chapter 5, which confirmed the appropriateness of the 100 m^2 plot size for the central Siberian boreal forest.

Simulation Area

The spatial domain includes all of the plots in the simulation, and is determined by whether the simulation is run in 1-D, 2-D or 3-D mode. In the 1-D mode, the user-specified number of plots are simulated independently, without spatial interactions, and with a simplified light representation (Figure 2.5a). There are two options for simulating independent plots: (1) all plots are collocated at the same point location and experience the same environmental conditions, and (2) plots are distributed in a grid across environmental gradient(s), but trees on a plot do not interact with trees on adjacent and nearby plots. In the latter, each plot can have different environmental conditions from its neighbors, which expands on ZELIG capabilities.

In the 2-D mode, the plots are aligned along a north-south transect (Figure 2.5b). Each plot is adjacent to two neighboring plots - to the north and to the south, respectively, with a wrap-around from the northern-most plot to the southern-most plot. The trees on each plot interact with trees on plots to the north through shading. The shadow is wrapped around from the north edge to enter the simulation domain from the south edge.

In the 3-D mode (Figure 2.5c), the plots are aligned in a grid. Each plot has eight immediate neighbors, and trees on one plot interact with trees on adjacent and nearby plots through shading along seven compass directions: NE, E, SE, S, SW, W, and NW (no shade directly to the south in the extratropical northern hemisphere).

The plot size and the spatial extent of the simulation domain are specified in a 2-D matrix format of plot-level elevations in an ASCII file (DEM), which can be generated in ArcGIS or by the user. Plot-level radiation inputs are computed in

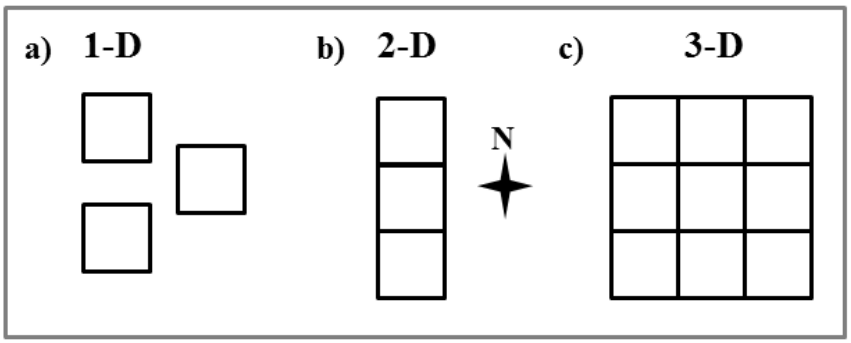

Fig. 2.5: User-specified simulation modes in SIBBORK: (a) Independent plots, no interactions between trees on these plots. (b) Transect of plots oriented south to north. Trees on a plot cast shade onto plots to the north. (c) Grid mode. Trees on a plot cast shade onto plots to the southeast, east, northeast, north, northwest, west and southwest. Each square represents one plot.

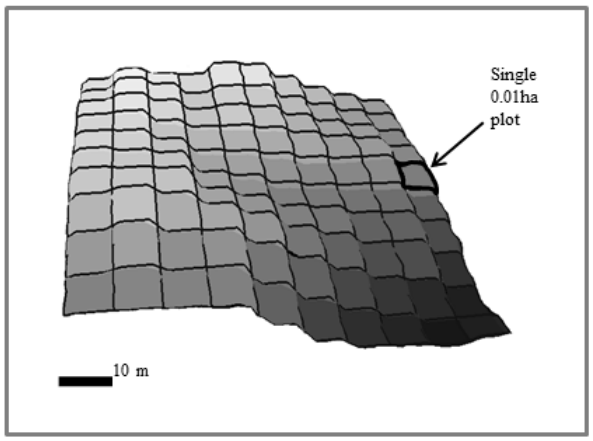

Fig. 2.6: A sample simulation area for 3-D grid mode: 0.01ha plots along a topographic gradient - a gentle, southeast-facing slope. Lower elevations are symbolized by darker grey. Each plot in the 3-D simulation mode has hydrlogic, temperature, and radiation variables based on its location along the simulated terrain.

ArcGIS based on the topography specified in this file. Plot size for calibration and testing of the model remained at 100 m^2 (0.01ha). A sample 1-ha simulation domain is shown in Figure 2.6.

Urban and his colleagues conducted a sensitivity analysis on ZELIG to assess the dependence of model output on the spatial extent simulated (*Urban et al.*, 1991). They found that aggregation at the plot-level compared to larger spatial domains (hectare) results in greater interannual and inter-replicate variability in stand structure. The scale of output aggregation in SIBBORK is user-specified, however, it is important to understand that the simulated changes in stand structure and composition over time will vary depending on whether the analysis is conducted at the fine (plot-level) or coarse (landscape-level) scale.

Initial Conditions

The simulation can be initialized from bare ground or a specific initial condition. Bare ground represents the conditions following a stand-replacing disturbance, such as clear-cutting or an intense wildfire or clear-cutting. Initialization from a set of initial conditions places a specified number of trees of a given species and size on each plot. Initial conditions may be obtained from field measurements, random assignment, or previous model runs, and specify the average tree size and stem density for species of interest. For example, it is possible to initialize the model as a young birch stand with diameters at breast height (DBH) in the range $5 \pm 1cm$, which over the course of the simulation may be replaced by other species.

2.1.2 Weather

Weather conditions affect the duration of the growing season, the annual growing degrees sum, and the soil moisture available for plant growth. Weather is modeled stochastically in the simulation at a daily timestep based the monthly averages of observed temperature and precipitations records from the World Meteorological Organization (WMO) weather station(s) within 100km radius of the location of interest. WMO weather records in Russia extend back 50-120 years, cover all ecotones of interest, and are in the public domain (*NCDC*, 2005a, b).

In order to prevent the occasional simulation of unrealistically high or low temperatures generated from the gaussian distribution centered around the average monthly temperature, a quality control (QC) check has been added. If a temperature is simulated outside of the observed absolute minimum to absolute maximum range, this number is discarded, and another number is generated. The distributions of observed and simulated monthly temperatures are shown in Figure 2.7 for an average growing season at 57^oN 95^oE, elevation 180m above mean sea level (amsl). Using the DEM and the standard environmental lapse rate of 6.5^oCkm^{-1}, temperature is computed for each plot that is at a different elevation than the reference weather station. Air temperature is used to compute the growing degree days above the base temperature of 5^oC. Observed and simulated growing degree day sums for 55 consecutive years (length of record) are shown in Figure 2.8. Monthly precipitation is also simulated from a gaussian distribution using average monthly sums of water-equivalent precipitation. Monthly precipitation totals are increased by 10% to account for potential windloss (*Bonan*, 1988a). The shape of the simulated distribution of monthly precipitation on flat terrain closely resembles the precipitation records acquired at the same elevation (Figure 2.9).

Climate change is simulated in two ways: static and dynamic. Static climate change simply adjusts the simulated monthly temperature and precipitation by a specified coefficient before relaying these values to the vegetation processes. The coefficient of change is constant throughout the simulation. In this manner, vegetation processes can be simulated in an environment that experiences a stable climate of, for example, 2^oC warmer and 10% dryer than the historic record (based on 20^{th} century observations). Dynamic climate change is represented by adjustment coeffi-

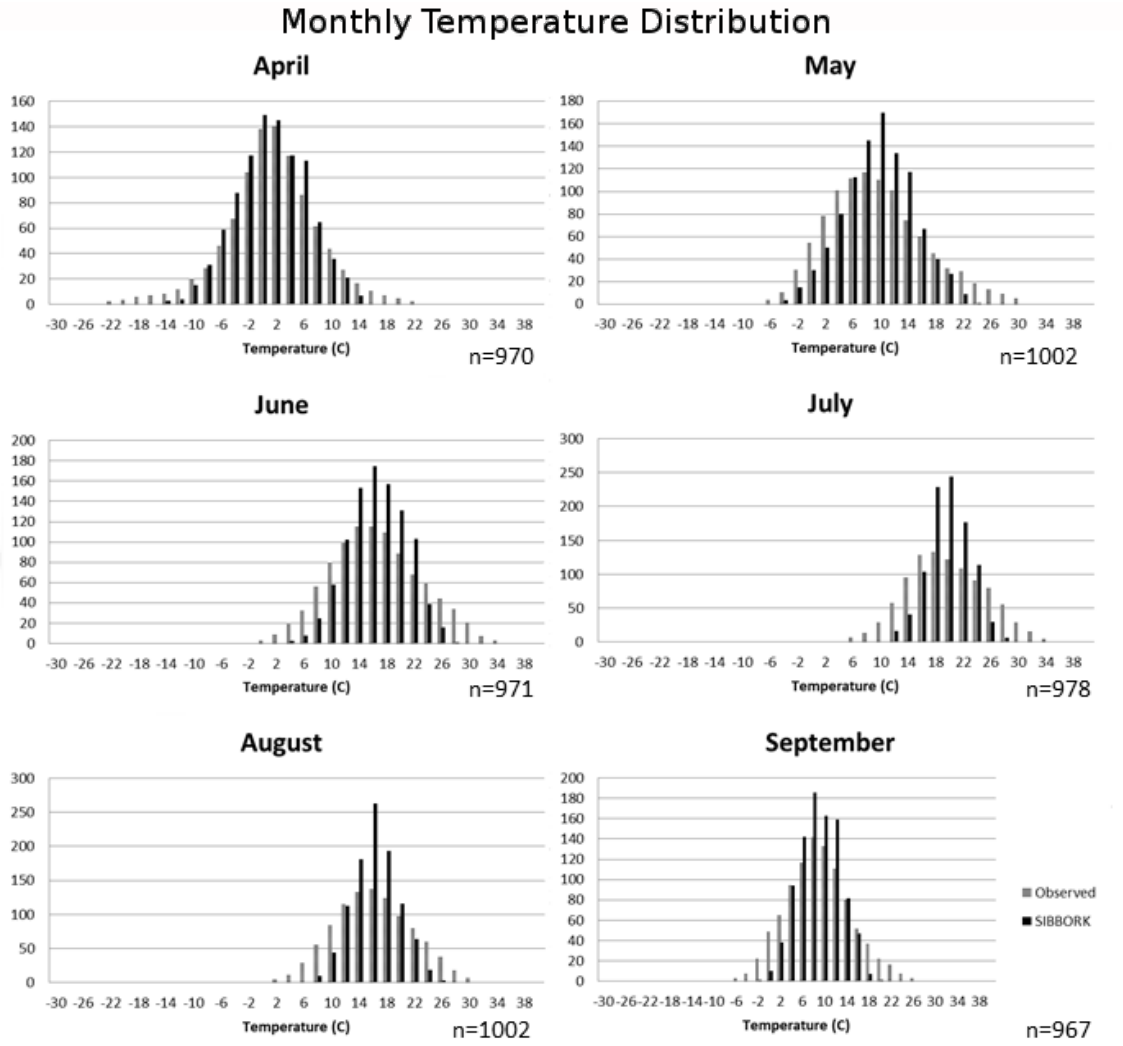

Fig. 2.7: Distributions of observed and simulated daily temperature for the months within the growing season. Although the distribution of observed temperatures is slightly wider, the average simulated annual total heat sum, expressed in growing degree days, is within 2% of the average observed value.

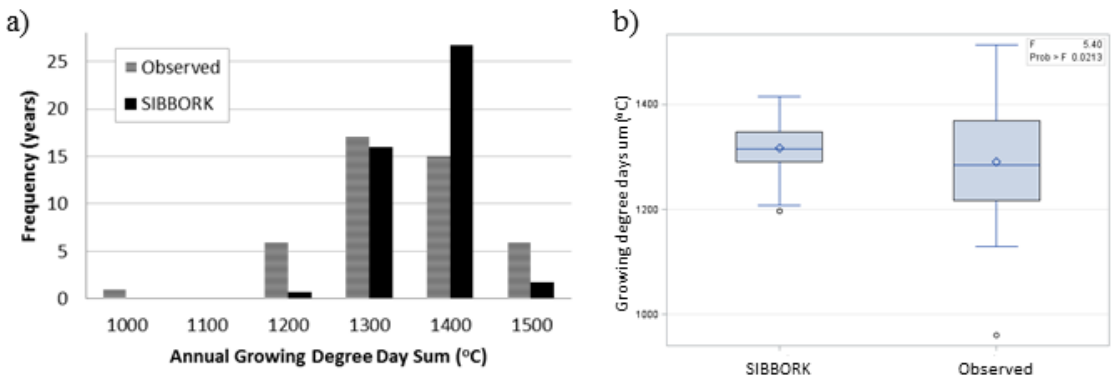

Fig. 2.8: Distributions of observed and simulated growing degree days. (a) Slightly greater variability is exhibited in the data record than in the simulation, however, if a larger sample size is considered, colder and warmer years are also simulated, which expands the variability for the annual growing degree days sum in the simulation. (b) SIBBORK annual growing degree day sums are not statistically significantly different from observed values at the nearest WMO station at the 0.05 level (ANOVA: F=5.4, p<0.0213, n_{obs} =45).

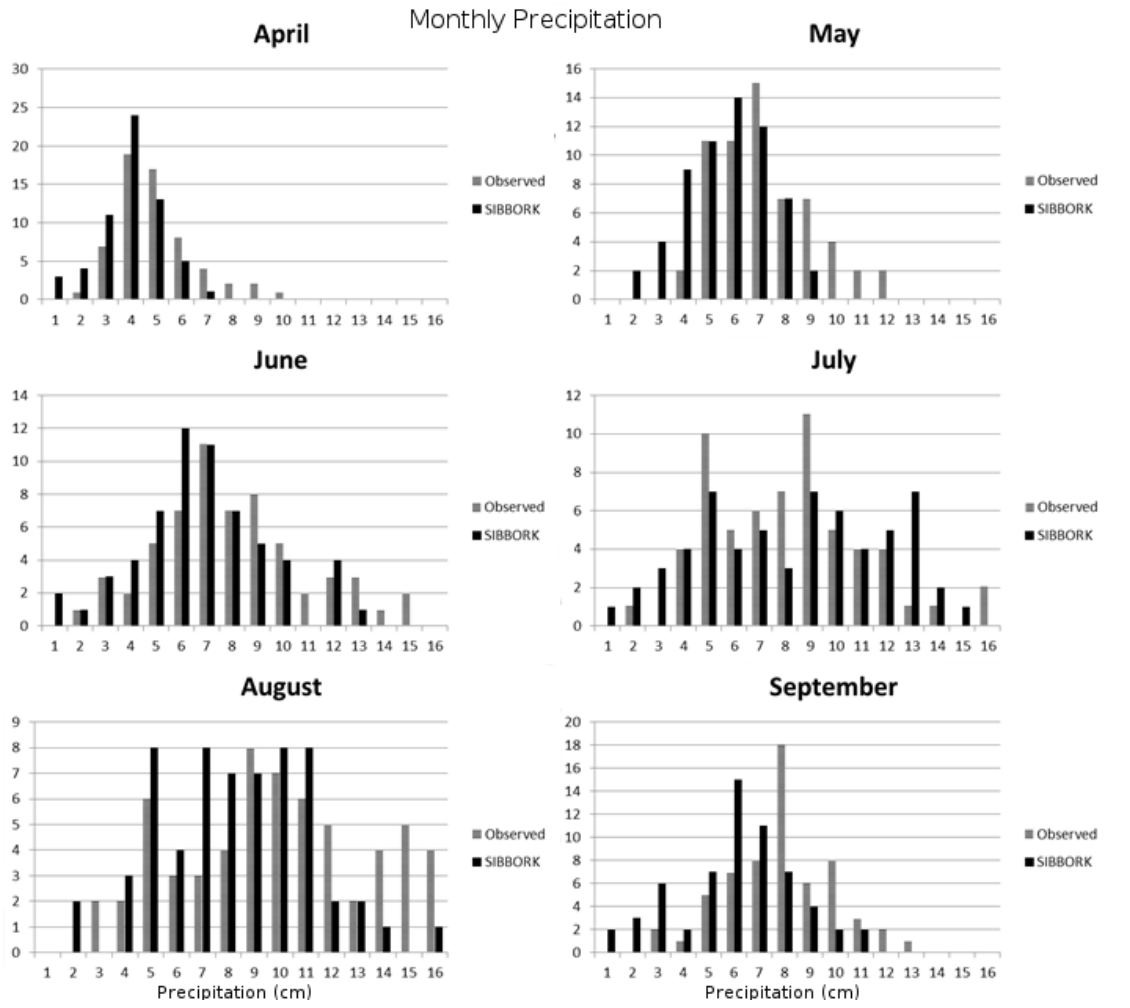

Fig. 2.9: Distributions of observed and simulated daily precipitation exhibit significant overlap throughout the growing season.

cients applied at annual or monthly increments. For example, average monthly temperatures may be linearly increased at a rate of 1^oC per decade and/or precipitation may be decreased at a non-linear rate of 10% per decade (Figure 2.10). Climate change is initialized at a user-specified year in the simulation and continues for a specified duration. This approach is flexible enough to allow forest generation in a stable climate, then apply climate change for a desired period of time, then stabilize the climate at a desired threshold.

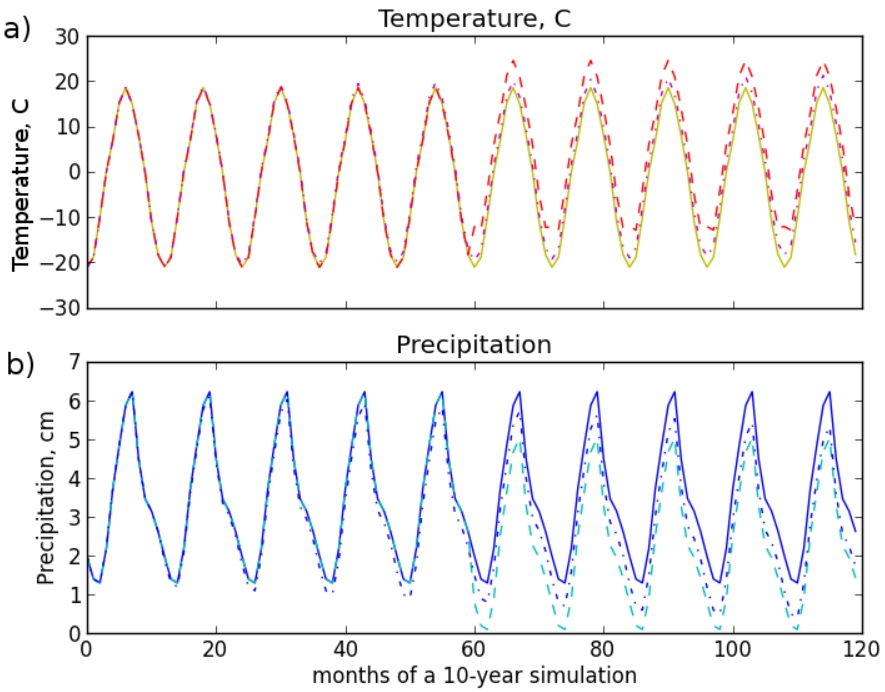

Fig. 2.10: The top graph depicts average monthly temperature (a), whereas the bottom graph depicts average monthly precipitation (b), over the course of a 10 year simulation. The solid lines depict the historical data record. The dashed line in (a) represents a step-wise 7^oC increase in temperature in year 5. The dash-dot line represents a more gradual approach, in which each month's temperature is increased by a small fraction of a degree, so that a total of 1.5^oC warming is observed over the 10 year simulation. In (b), precipitation can also be gradually decreased (dash-dot line) by a few mm per year to a total decrease of 1cm over the course of a 10-year simulation. Alternatively, precipitation can be changed once (decrease in year 5) and then maintained at the new level.

To simulate observed climate change, observed monthly and seasonal trends in temperature and precipitation changes were obtained from the Russian Hydrometeorology Office (*Gruza et al.*, 2015). Near-future climate change may be approximated via extrapolation of the observed trends.

2.1.3 Insolation

Solar radiation is required for photosynthesis, however, vegetation can be shaded by surrounding vegetation and by the terrain. A unique feature of SIBBORK is the incorporation of shading by topographic features, which generates

ecotone	station	location (lat, long)	direct:diffuse ratio
northern taiga	Turukhansk	65.8^o N, 88.0^o E	40 : 60
middle taiga	Vanavara	60.2^o N, 102.2^o E	45 : 55
southern taiga	Irkutsk	52.3^o N, 104.4^o E	50 : 50

Fig. 2.11: World Radiation Data Centre stations used for computing the direct:diffuse ratio for downwelling solar radiation, and for quality control check of computed radiation values in ArcGIS using Solar Area Calculator.

a differential distribution of radiation available for photosynthesis based on the location on the landscape. This is particularly important for the simulation of the southern Siberian boreal forest located in the complex terrain of Altay-Sayan and Zabaikal'e mountain ranges, as well as for the high latitude environment of northern taiga, where the unique annual pattern of radiation exhibits a large component of diffuse radiation for most of the year due to the flat angles of the sun. Available light is partitioned into direct and diffuse components using ratios derived based on radiation datasets from the central Siberian stations (World Radiation Data Centre: wrdc-mgo.nrel.gov).

Incident radiation (direct + diffuse) received at bare ground (or top of the canopy) is computed in WHm^{-2} at a monthly time step using the Area Solar Radiation tool in ArcGIS based on algorithms developed by Fu and Rich (1999a, 1999b, 2002) and the 30m X 30m resolution ASTER Digital Elevation Model (*METI and NASA*, 2011) resampled at a 10m X 10m resolution. In brief, the Area Solar Radiation tool computes incident direct radiation based on a viewshed from a set number of compass directions (user-defined: 8-32). Diffuse radiation is computed using the standard overcast diffuse model, in which incoming radiation depends on the sun's zenith angle. Default atmospheric transmissivity of 0.5 is used for central Siberia, as this fraction represents generally clear skies, and corresponds to the prevailing anticyclonic conditions throughout most of the year in this region. Transmissivity and the direct:diffuse ratio can be decreased to represent the radiation regime of particularly cloudy regions. Using the Area Solar Radiation algorithm, slopes of different grades and aspects receive differential amounts of total radiation throughout the year, which affects the monthly air temperature and the potential evapotranspiration of those locations. The differences in radiation received in complex terrain can be quite significant, as shown for the top of the canopy of a mixed forest in complex terrain (Figure 2.12a) and at the ground level below the canopy assuming a leaf area index of 1.3 (Figure 2.12b). This figure demonstrates the importance of including 3-dimensional terrain in the computation of available light for prediction of species distribution (potential vegetation) across the landscape.

A limitation of the approximation of incident radiation using the Solar Area Radiation calculator in ArcGIS is in the specification of the direct:diffuse light fraction. The same fraction is applied to all locations on the terrain, regardless of slope or aspect. This can be particularly incorrect when considering high latitude light regimes in the northern hemisphere, with larger direct radiation received on the south-facing slopes, and the light regime dominated by diffuse light on north-facing slopes. Based on radiation data from the World Radiation Data Centre (see station list in Figure 2.11), direct:diffuse light fraction computed for locations in southern, middle, and northern taiga are approximately

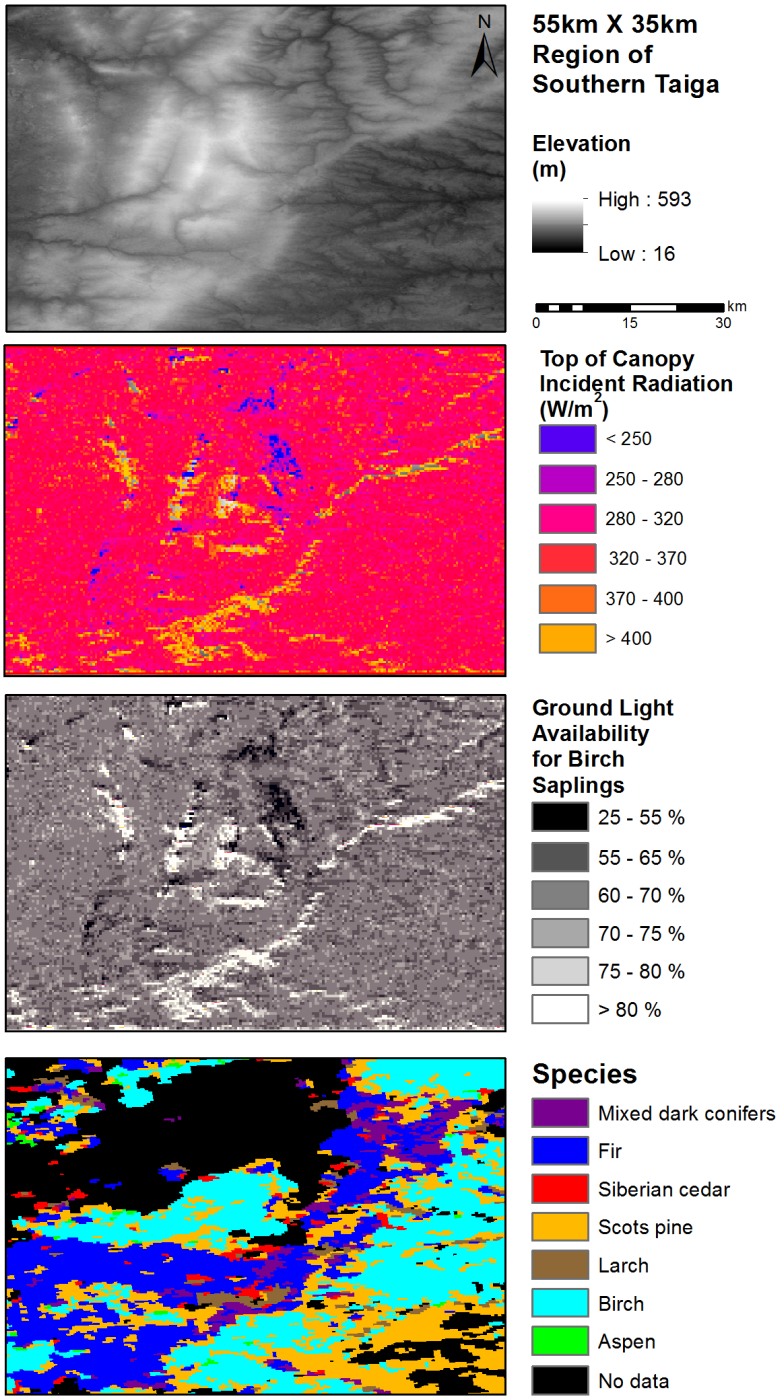

Fig. 2.12: Radiation input differs across the terrain based on elevation, slope, and aspect. (a) An area of complex terrain in southern taiga, east of the Yenisei River (from ASTER DEM, *METI and NASA*, 2011). (b) The average direct radiation experienced on different slopes within complex terrain in central Siberia on June 22nd, computed using ArcGIS Area Solar Calculator tool. (c) Model-predicted available light factor for birch at the ground level based on a closed canopy with a leaf area index of 1.3, computed as a fraction of light incident on top of the canopy, as in (b), or on bare ground. (d) A species composition map (*Bartalev*, 2010; *Bartalev et al.*, 2011; *Huttich et al.*, 2014) shows the observed distribution of birches along upper slopes, including a southeast-facing slope in the lower right quadrant, and an area of higher elevation in the center. Birches are found in this panel predominantly where the available ground-level light in (c) is greater than 50% of what birches require for regeneration.

50:50, 45:55, 40:60, respectively. These ratios are estimated averages for the duration of the growing season at each location, based on data from 1993, which is the most recent year for which data for all three locations is available.

2.1.4 Available Light

Shading by terrain is accounted for in the GIS-generated plot-level radiation values based on the resampled digital elevation model. Shading by vegetation, on the other hand, depends on foliage density and is computed within a 50-m thick layer of the atmosphere above the ground level using the Beer-Lambert Law:

$$AL_h = AL_o \times e^{-k \times DLA} \tag{2.1}$$

where AL_h is the available light at a given height h above the ground, AL_o is the top-of-canopy normalized radiation factor that includes shading due to terrain and aspect, k is a constant that describes light extinction through the canopy, and *DLA* represents the cumulative foliage density above height h. *DLA* is synonymous with leaf area index (LAI). Species-specific values of *k* vary in the range of 0.37 to 0.47 between species (*Breda*, 2003), and even greater variability is observed based on stand density and tree age (*Johansson*, 1989). An average value of 0.4 is employed for the light extinction constant in the simulation. Plotting this equation for LAI values of 1-10 results in Figure 2.13. In broadleaf and light conifer forests, LAI values of 1-5 are common (*Brooks et al.*, 1997a,b; *Kull and Tulva*, 2000; *Shibistova et al.*, 2002a,b; *Shulze et al.*, 2002; *Lindroth et al.*, 2008; *Kobayashi et al.*, 2010), whereas coniferous forests can accumulate LAI of up to 10 (*Chen et al.*, 2005), and LAIs as high at 18 have been reported for some boreal regions (*DeAngelis et al.*, 1981;), but these high values may be an artifact of using 2-sided leaf area to calculate the LAI (*Asner, et al.*, 2003). In general, significantly more shading within and below the canopy is observed within dark conifer forests of Siberia than in broadleaf or mixed stands.

The direct light simulation traces a sun ray from each of the 7 compass directions along a diagonal based on the average sun elevation angle in that direction (no direct light from the north in extratropical northern hemisphere). The direct radiation along each trace is scaled by the contribution of light from each compass direct over the course of the growing season. In contrast, diffuse light is computed along 8 diagonal paths through the canopy and from directly overhead. Light extinction is computed along these ray traces.

The shadow of a typical canopy dominant tree from central Siberia (24m, *Simard et al.*, 2011) can extend up to 100m, depending on foliage density and sun elevation angle. A sensitivity analysis for the maximum distance of a tree's shading effect for direct and diffuse light in the boreal ecosystem revealed that the maximum effect (tree shadow) of a 20m tree on unvegetated flat terrain at 56^oN is approximately 100m for direct radiation, however, this depends on the sun angle. This maximum distance was obtained using the lowest sun elevation angle (5^o) averaged for the

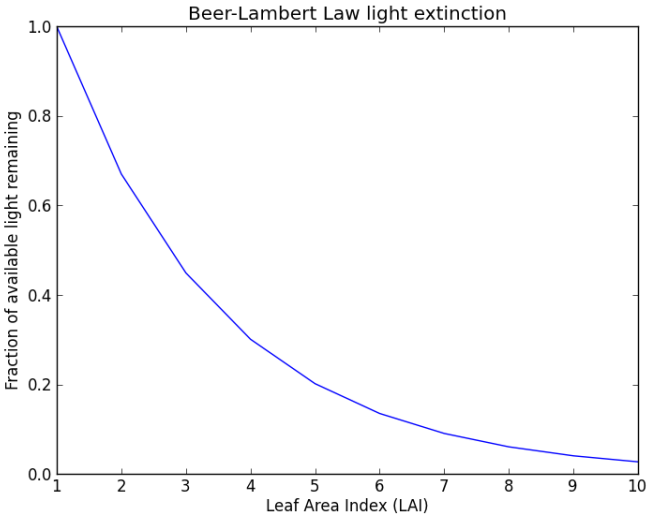

Fig. 2.13: At the top of the canopy, the fraction of available light is 1. Light extinction through the canopy follows an exponential function related to leaf area index (LAI). Broadleaf species generally do not establish in forests with LAI greater than 5, because not enough light filters through the canopy for them to maintain a positive carbon balance.

northeastern section during the growing season. The of effect trees on one plot with regards to diminishing the amount of diffuse light on adjacent and nearby plots extends up to 75m, which corresponds to approximately 7 plots in the simulation. Beyond that distance, the effects are considered negligible. Within a forest, light along a ray trace is likely to diminish due to the leaf area index (LAI) before reaching the distance of maximum shadow length. When the maximum possible tree height was taken into consideration (larch, 41m, *Shvidenko et al.*, 2006), the maximum distance for the shading effect could extend to 450m and 160m for direct and diffuse light, respectively, when computing the shading effect mathematically via the tangent of the sun elevation angle. The values are different, because the angles used to compute shading are different for direct and diffuse light components. The analysis in GIS, however, reveals that the effective shadow from the low sun elevation angle from the NE and NW is insignificant, i.e. less than 1% of direct radiation extinguished along this shadow path, and that the effective shadow length when the sun is in the east or west, at an average sun elevation angle of 19^o, extends 130m for direct and diffuse light. Beyond that distance, 0.5% of the above-canopy radiation is occluded by the tree. This analysis helps to determine the smallest spatial domain that would not cause numerical instability upon wrap-around in the simulation. In the spatially-explicit version of ZELIG, the warp-around was shifted by one grid row, so that a tree does not shade itself (Figure 8.3 in *Shugart et al.*, 1988; Figure 2 in *Weishampel et al.*, 1996). In contrast, in SIBBORK, the shadow is kept in the same grid row upon wrap-around, but the size of the simulation domain is selected to exceed the longest possible shade to avoid having a tree shade itself.

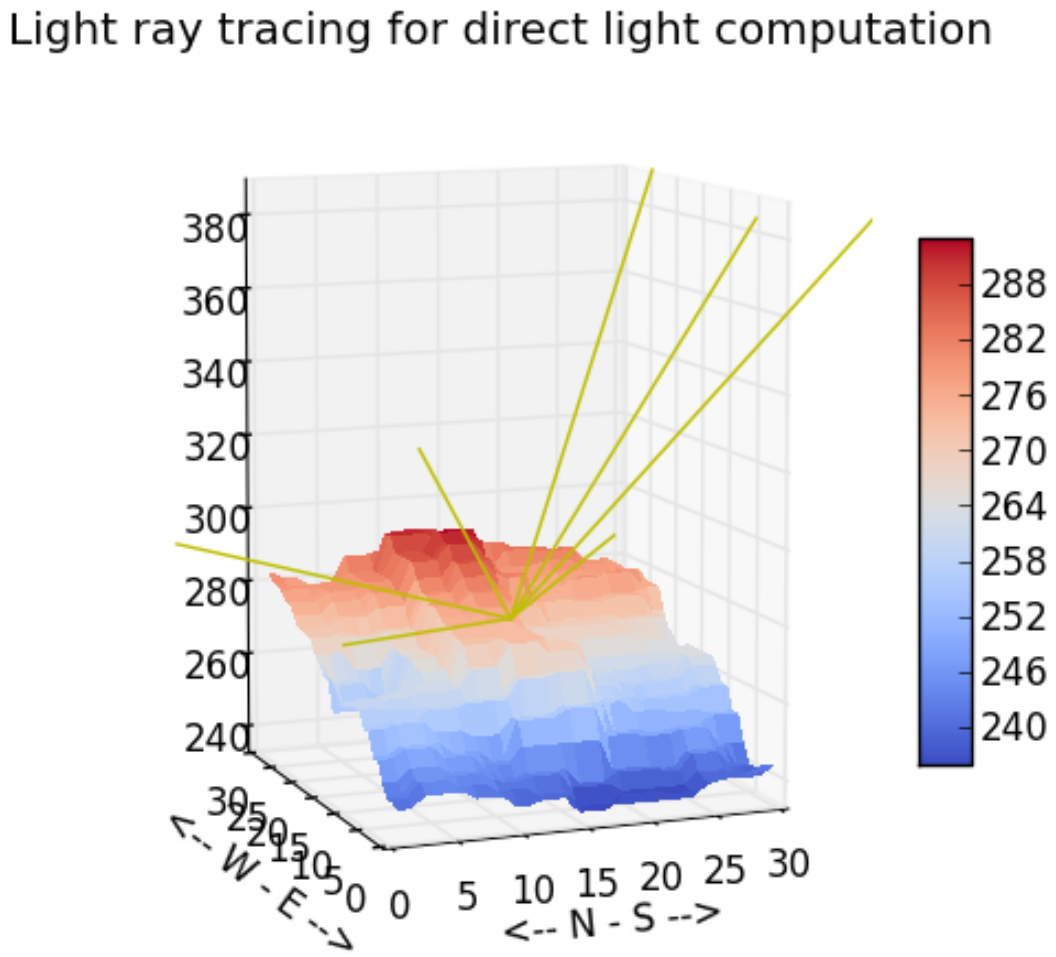

Fig. 2.14: Sun ray tracing for direct light computation from 7 of the 8 primary compass directions at 4 different angles, based on sun location during the growing season. The sun elevation angle is much greater to the SE, S and SW, than to the other directions. The lowest sun elevation angles are experienced from the NW and NE directions. There is no direct light from the N in Siberia. The colorbar symbolizes elevation (m) above sea level.

The annual computation of the light environment is spatially explicit, and has a spatial resolution of 10m x 10m x 1m (plot size x 1m vertical step). This is also the most computationally-expensive subroutine of this single-thread simulation, and has been accelerated using the Numba library (http://www.numba.pydata.org). The computational demand for the 3-D light subroutine increases exponentially with increasing spatial domain. Furthermore, the light ray tracing in complex terrain requires special parameterization. Originally, the light environment was computed within a volume above the complex terrain that was capped at 50m above the highest point on the terrain. In order to not increase the volume through which the light rays are traced above a complex terrain, the light is now computed only within a 50m thick column of the atmosphere above each plot, which may have a different elevation than adjacent or nearby plots. The trees can still shade each other on nearby plots, however, the light ray is capped at 50m above each elevation level. This simplification significantly decreases the computational demands of the light subroutine above simulated hilly or mountainous terrain.

2.1.5 Evapotranspiration

In ZELIG, potential evapotranspiration (PET) was computed via the Thornthwaite-Mather equation (*Thornthwaite and Mather*, 1957) using average monthly temperatures and correction coefficients for each month and latitude. This equation does not consider the available water (land surface limitations on evaporation), and is therefore intended for the calculation of PET only. It is known to underestimate PET by 20-30% (*Fisher et al.*, 2011). Furthermore, the Thornthwaite-Mather equation has not been validated for PET calculations at high latitudes above 50^o N (*Botkin*, 1993), and correction factors are not available for those regions. Fischer *et al.* (2011) recommends a radiation-based or a combination approach for estimating PET in boreal regions. For SIBBORK, a modified Penman equation (*Campbell*, 1977) was selected:

$$PET = \frac{a \times (Temperature + b) \times (Radiation)}{\lambda \times 1000} \tag{2.2}$$

where *a* and *b* are coefficients, with common values of 0.025^oC^{-1} and 3^o C, respectively, and λ is the latent heat of vaporization (2430 Jg^{-1}). Air *Temperature* and *Radiation* in this calculation are plot-wide parameters that change with each month of the year, and are in units of degrees Celsius and Jm^{-2} (converted from WHm^{-2}), respectively. The 1000 factor in the denominator converts PET to cm/month.

Due to the variation in air temperature and radiation input across complex terrain, evaporative demands (PET) are heterogeneous across the landscape. Figure 2.15a compares the annual PET computed via the modified Penman equation utilized in SIBBORK for southern taiga, middle taiga, and treeline locations (average of 10 years) to an overview map of PET for Russia (*Kolosova*, 1982).

The water budget for a single-layer soil was computed in ZELIG via

$$runoff = SoilMoisture + Precipitation - PET \tag{2.3}$$

where the *Soil Moisture* parameter refers to the previous month's soil moisture in a single-layer soil, which can be at field capacity, between field capacity and wilting point, or at wilting point. At the start of the simulation, the soil moisture is equal to field capacity. Any soil moisture at the end of this computation in excess of field capacity is considered runoff (overland flow and gravitational water). In certain regions of central Siberia, PET exceeds precipitation during the growing season. Equation (2.3) overestimates soil dryness, especially in regions underlain by permafrost. To estimate the soil moisture more realistically in SIBBORK, the water balance is computed as follows:

$$runoff = SoilMoisture + Precipitation - AET \tag{2.4}$$

where, *AET* is estimated as a fraction of PET (from equation (2.2)). This fraction, called evapotranspiration coefficient, is estimated at 60-70% in central Siberia (*Olchev and Novenko*, 2011) and 30-50% in the driest region of central Siberia near Yakutsk (*Ohta et al.*, 2008; *Matsumoto et al.*, 2008; *Maximov et al.*, 2008). The actual evapotranspiration depends on the structure and composition of the forest canopy (*Nakai et al.*, 2008), which changes over the course of succession or with altered environmental conditions, but the inclusion of a computation of AET with input from canopy parameters and the estimation of foliage growth based on AET would introduce a circular dependency and increase computational demand. Additionally, there is high interseasonal and interannual variability in the evapotranspiration coefficient (*Matsumoto et al.*, 2008). With the focus on the growing season and the central Siberian region along the Yenisei River meridian, the evapotranspiration coefficient of 0.7 appeared to adequately estimate the $\frac{AET}{PET}$ ratio. Figure 2.15b demonstrates the fit between the AET computed by SIBBORK (10-year average) and Global Evapotranspriation dataset (*Zhang et al.*, 2010; www.ntsg.umt.edu/project/et, spatial resolution 4x8km at 58^oN latitude). Furthermore, the observed moisture coefficient (ratio of precipitation to PET), which varies in the range of 1-2 along the Yenisei River meridian and dips below 1 in southern Siberia, is appropriately simulated by SIBBORK (Figure 2.15c). It is interesting to note that some of the greatest uncertainty in the estimation of PET and AET using modeling and remote sensing approaches is for boreal regions of Siberia and North America (*Zhang et al.*, 2010).

2.1.6 Growing Degrees

There is an optimal temperature range for tree processes, above and below which the rates of photosynthesis, respiration, and related processes are reduced (*Waring and Schlesinger*, 1985). Although the effectiveness of the photosyn-

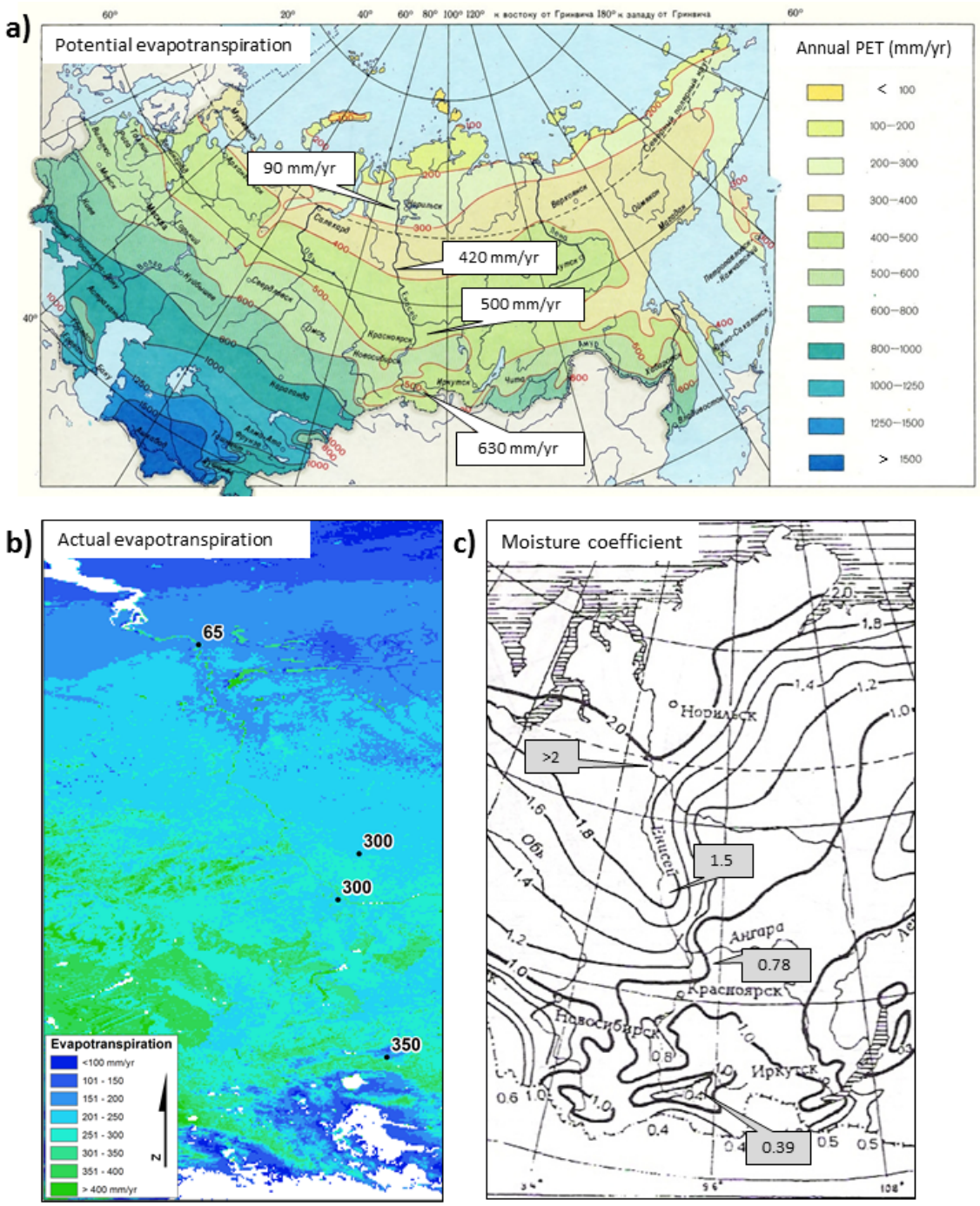

Fig. 2.15: Water budget variables for central Siberia. (a) Potential evapotranspiration is conveyed via the Kolosova (1982) map, with northern treeline, middle taiga, southern taiga, and southern treeline PET quantities (mm/yr) computed for the WMO weather stations of Dudinka, Severo-Enisejske, Enisejsk, and Kyzyl, respectively, and shown via insets oriented north-to-south on map. Note that the PET computed for Kyzyl is on the order of 600mm/yr. Kyzyl is located in an arid basin, surrounded by steppe vegetation. Forested hillsides in the vicinity experience a lower PET (230-500mm/yr), depending on aspect and elevation. (b) Actual evapotranspiration from the Global Evapotranspiration dataset (*Zhang et al.*, 2010) is shown in the background. The AET computed in SIBBORK for the same 4 locations as in (a) are shown via numerical labels (mm/yr). (c) The annual moisture coefficient from a map by Isachenko (1985, background) is compared to the same quantity computed in SIBBORK (grey insets). This ratio is unitless.

thetic process has a temperature dependency (*Atkin et al.*, 2007), temperatures extreme (high) enough to damage the photosynthetic apparatus do not occur in the Siberian boreal forest (*Larcher*, 1995). However, there is a lower limit on the temperatures necessary for photosynthesis. For conifers, this limit is closer to 0^oC, whereas broadleaf trees initiate photosynthesis at temperatures above about 5^oC (*Shugart et al.*, 1992; *Chapman et al.*, 2006). For the purpose of simplification in the model, it is assumed that all trees become photosynthetically active when the air temperature is above 5^oC. For ease of convention, the annual accumulated heat load in the simulation is expressed in growing degree days above the base temperature of 5^oC (*Shugart et al.*, 1992; *Chapman et al.*, 2006; *Shuman*, 2010). Whenever a daily air temperature exceeds this base temperature, growing degrees are accumulated. A day with an average daytime air temperature of 14^oC would accumulate 9 growing degrees (GDD_5) above the base temperature. In the model, daily temperatures are simulated and growing degrees are summed up. Some arboreal species, such as birch, function best in warmer climes and have a low tolerance for frost or cold weather (GDD_5 minimum = 410^oC). Others, such as larch, can grow in very cold locations, and have a low growing degrees requirement (GDD_5 minimum = 300^oC). Growing degrees are accumulated over the course of the year, and can be used to track the amount of heat available for vegetation processes, especially as climate changes.

In previous versions of ZELIG, each of the arboreal species had a minimum requirement of GDD_5, and a maximum heat tolerance (maximum GDD_5), from which a parabolic curve for optimal growing degree days was derived (*Pastor and Post*, 1986). However, Bugmann and Solomon (2000) suggest that a nonlinear response may be the more appropriate parameterization of vegetation response to the accumulated annual GDD_5. Based on empirical evidence, SIBBORK was reparameterized such that trees will not experience stress from accumulated heat over the growing season, if soil moisture is not limiting (*McDowell et al.*, 2011; *Bauweraerts et al.*, 2014; *Wertin et al.*, 2012). However, too little warmth will be limiting to species with a certain growing degree requirement, and the minimum warmth requirement is specified for each species in SIBBORK, as it was in ZELIG.

The parabolic and the nonlinear vegetation response parameterizations to the GDD_5 are shown in Figure 2.16. Historical annual average GDD_5, represented by a dashed line in Figure 2.16, summarizes the temperature conditions over the second half of the 20^{th} century at a WMO weather station in central Siberia. The dashed line labeled "+ 2^oC" denotes what the average GDD_5 sum may be with a 2-degree increase in the annual average temperature. Note that with the parabolic parameterization of heat tolerance, larch (*Larix sibirica*) experiences significantly reduced growth - less than 20% of optimal. In the nonlinear parameterization, none of the three species are affected by heat alone, and growth is not decreased due to an increase in growing degrees, provided soil moisture is not limiting.

Growing degrees can be used to describe a characteristic of the environmental conditions, and the total annual heat load can be the most limiting factor to tree growth at certain locations in some years. Larch has the lowest minimum

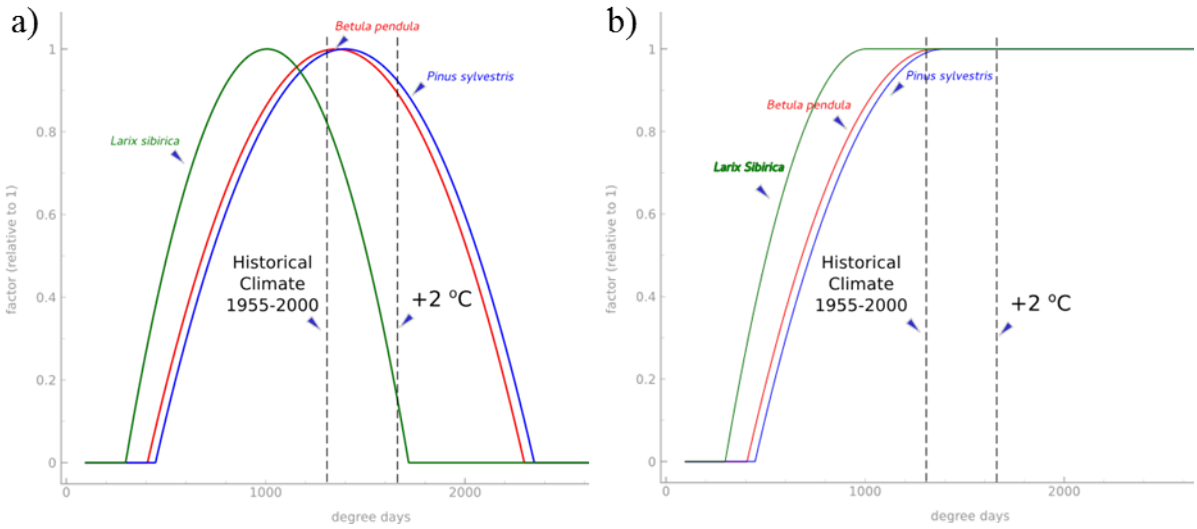

Fig. 2.16: Species response to annual accumulated heat load (GDD_5) as was parameterized in ZELIG (a) and using the new, non-linear parameterization in SIBBORK (b).

GDD_5 requirement of boreal tree species (300^oC). This limit corresponds to the forest-tundra boundary conditions (*Tchebakova and Parfenova*, 2006).

2.1.7 Soil Moisture

Soil moisture in the simulation was parameterized using site-specific field capacity and wilting point for the top meter of soil. Field capacity and wilting point were approximated as one-quarter and one-eighth of total available water capacity (TAWC) specified for site locations in a soils geospatial database (*Stolbovoi and McCullum*, 2002; *Shuman*, 2010). A newer soil moisture parameterization was developed after model testing. This new parameterization uses the soil type (FAO) description in a geospatial database that describes soils for all of Russia (*Stolbovoi and McCullum*, 2002), from which soil texture is determined from the clay, sand, and silt contribution to the soil type. Thereafter, soil field capacity and wilting point are approximated using the soil texture associated with each soil type class (*Saxton and Rawls*, 2006). Although the estimation of field capacity as one-quarter of TAWC in the earlier parameteriation (*Shuman*, 2010) followed the expected trend, with clay soils retaining more moisture against gravity, and sandy soils allowing for more drainage, the wilting point was smaller than one-eighth of TAWC for all soil texture classes. The over-estimation of wilting point may have led to flagging trees for drought-related stress at sufficient soil moisture levels.

FAO soil type	drainage class	TAWC	FC (cm)	WP (cm)	soil texture
cambisols	well-drained	106-180	26.5-45	13.25-22.5	sandy loam
chernozems	well-drained	106-175	25.5-43.75	13.25-21.9	loamy
arenosols	excessively drained	106	26.5	13.25	loamy sand
podzols	moderately well-drained	106-180	26.5-45	13.25-22.5	sandy to loamy
fluvisols	poorly and very poorly-drained	250	62.5	31.25	clay
gleysols	poorly and very poorly-drained	250	62.5	31.25	clay
podzoluvisols	well-drained	162-180	40.5-45	20.25-22.5	sandy, clay, loam
greyzems	moderately well-drained	106-180	26.5-45	13.25-22.5	loamy, silty
histosols	very poorly-drained	250	62.5	31.25	peat
andosols	moderately well-drained	200	50	25	volcanic, fine
leptosols	moderately poorly-drained	13-57	3.25-14.25	1.6-7.1	very shallow
regosols	imperfectly drained	180	45	22.5	sandy, silty
phaeozems	moderately poorly-drained	165-175	41.25-43.75	20.6-21.9	silty, loamy
solonetz	imperfectly drained	165-180	41.25-45	20.6-22.5	clay
calcisols	well-drained	106-180	26.5-45	13.25-22.5	silty
kastanozems	well-drained	106-180	26.5-45	13.25-22.5	loamy
solonchaks	poorly-drained	165	41.25	20.6	silty, clay
planosols	imperfectly-drained	152-162	38-40.5	19-20.25	sandy
sands	extremely well-drained	0	0	0	sand
vertisols	imprefectly-drained	135	33.75	16.9	clay

Fig. 2.17: Soil type and drainage class obtained from Stolbovoi and McCullum (2002). Note: in some locations, podzoluvisols are very poorly-drained, fluvisols are well-drained, and chernozems are moderately poorly-drained. TAWC = total available water capacity. Field capacity and wilting point were estimated as one-quarter and one-eighth of TAWC, as in Shuman (2010). Soil texture class was obtained for each soil type using ISRIC World Soil Information database (isric.org).

soil texture	field capacity (%v)	wilting point (%v)
sand	10	5
loamy sand	12	5
sandy loam	18	8
sandy clay loam	27	17
loam	28	14
sandy clay	36	25
silt loam	31	11
silt	30	6
clay loam	36	22
silty clay loam	28	22
silty clay	41	27
clay	42	30

Fig. 2.18: An alternative soil moisture parameterization includes site-specific field capacity and wilting point approximated from Saxton and Rawls (2006) using the soil texture class associated with each soil type from the geospatial database.

The water budget for the simulation is computed for a single-layer soil as follows:

$$SoilMoisture = SoilMoisture_{prev} + Precipitation - AET - runoff \tag{2.5}$$

where *Soil Moisture* represents the soil moisture available to plants, $SoilMoisture_{prev}$ refers to the total available water remaining in the soil from the previous month, and AET is computed as a fraction of PET.

The model is initialized with soil moisture at field capacity, which is a characteristic of soil type. When soil moisture exceeds field capacity, the excess water is considered as runoff and is removed from the simulation. When soil moisture decreases below zero, the trees reach the wilting point and photosynthesis is inhibited. Field capacity and wilting point are computed as a function of soil type and total available water from a soils database (*Stolbovoi and McCullum*, 2002). For the purposes of simplification and convention, a single wilting point is specified for all species in the simulation. When no soil type information is available, a wilting point of 15 bar is used (*Bonan*, 1988). Figure 2.19 shows the process flow for the soil moisture computation in SIBBORK.

2.1.8 Soil Fertility

Soil fertility exerts a limit on the maximum amount of biomass that can be accumulated on a hectare of land per year at a specified location. It is a cap on the annual productivity at a simulated site. This may be similar to a limit on gross primary productivity (GPP). In SIBBORK, there is no limit to total standing biomass, just to the rate at which it can be accumulated on an annual basis. When the vegetation on a simulated plot approaches this maximum rate of biomass accretion, trees experience suppressed growth scaled by species-specific tolerances to low soil nutrition.

Russian forestry utilizes a site index parameter to describe how different species may perform at a given site (I=good, V=poor). A species that requires a high amount of soil nutrition, e.g. fir, may grow poorly on the same soil on which a species with low nutrition requirements, e.g. pine, may grow well and reach a larger diameter at a younger age. In this case, site index V may be used to describe this location for fir, whereas for pine, the site index may be closer to I or II. In this manner, site index is a species-specific characteristic, but this is very difficult to parameterize for mixed species stands.

For the purposes of simplification and generalizability, soil fertility in SIBBORK is derived from the forestry yield table parameter of Net Growth specified in tons per hectare (biomass) or cubic meters per hectare (biovolume) accumulated per year for monospecies stands of different site indices. Central Siberia is dominated by site index III and IV soils, whereas southern regions of central and western Siberia are dominated by site index II soils for the species that grow there (*Korpachev et al.*, 2010). However, site index III soils with larch may have greater annual productivity than

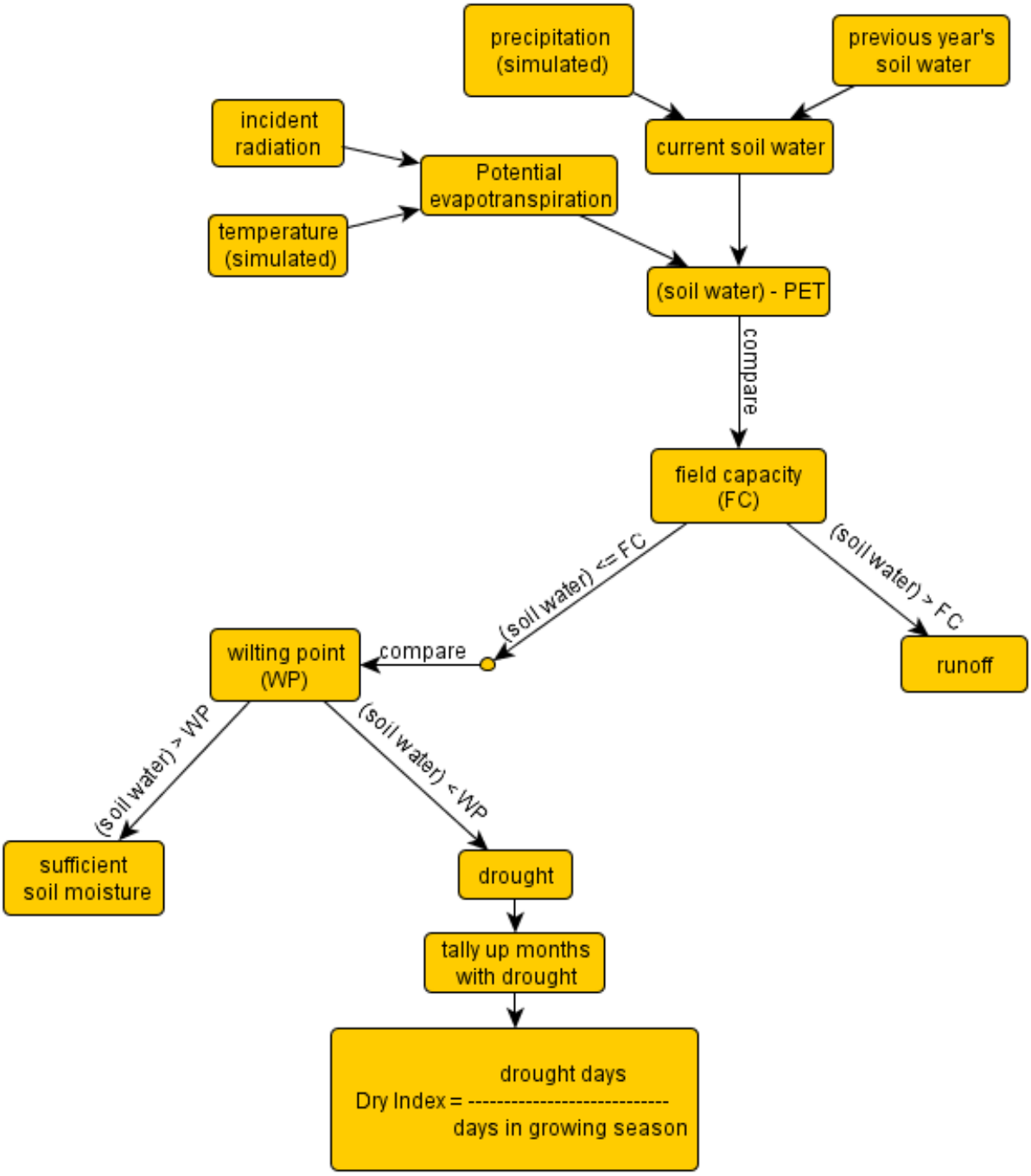

Fig. 2.19: The soil moisture in SIBBORK is assessed as a dryness index, which is computed as a fraction of the growing season with soil water content below wilting point.

SITE INDEX					
Species	I	II	III	IV	V
Abies sibirica ǂ	32 – 36.8 cm	27 – 31.8 cm	22.2 – 26.9 cm	17.2 – 22 cm	12.3 – 17.1 cm
Larix sibirica ǂ	27.4 – 36.7 cm	20.2 – 27.2 cm	15 – 20.1 cm	11.1 – 14.9 cm	8.2 – 11 cm
Betula spp. *	15.5 – 18 cm	12.8 – 15.4 cm	12 – 14.7 cm	7.7 – 10.1 cm	7.8 – 11.1 cm
Picea obovata ǂ	26.4 – 31 cm	23.4 – 26.3 cm	21.3 – 23.3 cm	19.6 – 21.2 cm	17.5 – 23.1 cm
Pinus sibirica	57.3 – 81.6 cm	39.6 – 56.8 cm	27.6 – 39.2 cm	19.2 – 27.3 cm	13.4 – 19 cm
Pinus sylvestris ǂ	31.7 - 39.3 cm	24.6 – 31.5 cm	18.5 – 24.4 cm	13.1 – 18.3 cm	13.4 – 18.2 cm
Populus spp. *	19 – 22.5 cm	15.4 – 18.9 cm	11.7 – 15.3 cm	11.6 – 8.1 cm	8 – 4.5 cm

Fig. 2.20: Site index is estimated for monospecies stands based on average tree height at stand ages of 50 and 100 years. Here, the diameter-height relationship was used to convert the heights to diameters at breast height (DBH), so as to compute the site index - biovolume (function of DBH) relationship for the soil fertility parameterization.

site index III soils with fir. For simulations of monospecies stands, the soil fertility GPP limitation is taken directly from the forestry yield tables (*Shvidenko et al.*, 2006). For simulation of mixed species stands, the site index of the most productive species is used to determine the cap on GPP. For example, in middle taiga, cap levels of 6, 4 and 2 *tons* $ha^{-1}yr^{-1}$, which correspond to biovolume caps of 6, 5, and 4 $m^3ha^{-1}yr^{-1}$, are used for soils with site indices II, III, and IV, respectively.

2.2 Vegetation Processes

2.2.1 Sapling Establishment

Regeneration is a stochastic process affected by the seed rate specified in the driver file for each species in the simulation. Saplings establish up to a maximum per-plot stem density specified in the driver file. ZELIG utilizes a 1 stem/ m^2 maximum stem density, whereas SIBBORK allows the user to specify the stem density, which can exceed 1 stem/ m^2 in order to better represent dense pine forests observed in Siberia. The minimum stem density in SIBBORK is 1 stem/plot, which facilitates the simulation of open canopy forests encountered in northern taiga. When a sapling is established, it is not assigned an explicit x,y position within a plot. Instead, the uncertainty of its location on the simulated landscape is localized to within a specified plot. Saplings are planted with a DBH of $2.5 \pm 0.25cm$. This size may be representative of a 40-year old larch in severely limiting environmental conditions, or a 5-year old birch under favorable conditions for the species. This discrepancy creates difficulty in comparing simulated stands with a specific age structure to observed stands, however, usually, the comparison is good to within a decade (i.e. 40-year old trees in the simulation compare well to 50-year old trees in the field). Saplings are established at the end of the simulation year,

after mortality and growth have been accounted for. Sapling establishment is affected by the environmental factors of ground-level light, growing degrees, and soil moisture.

Some species, notably aspen, birch and spruce, reproduce by stump sprouting. This type of regeneration is currently not included in SIBBORK, although frameworks for this exist in FAREAST (*Yan and Shugart*, 2005) and later versions of ZELIG (*Larocque et al.*, 2006). Inclusion of stump sprouting in the model would likely increase the contribution of aspen and birch to stand composition, especially after disturbances, such as wildfire.

2.2.2 Tree Growth

Annual tree growth is a function of the species type, tree size, and the effects of environmental conditions. An optimal diameter growth increment (OGI) is computed for each tree based on its current size and species type. Estimation of OGI has been modified following methodology described by Bragg (2001, 2003) to account for growth of older, larger trees. Previous parameterization of OGI halted growth at an estimated maximum diameter. However, species-specific maximum diameters are difficult to estimate. The new parameterization utilizes maximum observed growth to determine the actual relative diameter increment (ARI). The potential relative diameter increment (PRI) is computed by fitting a curve with the following form to a subset of the largest observed ARIs for a species:

$$PRI = a \times DBH^b \times c^{DBH} \tag{2.6}$$

The PRI represents optimal diameter increment for a species relative to its current size (DBH). Empirically-derived coefficients *a*, *b*, and *c* are species-specific. OGI is computed via:

$$OGI = PRI \times DBH \tag{2.7}$$

annually for each tree in the simulation. This maximum gain in diameter represents the growth a tree would experience at a given size if it had access to unlimited resources. The OGI is scaled down by environmental constraints representative of the conditions in each year of the simulation and the species-specific tolerances to such resource limitations. The new parameterization for the optimal diameter increment does not constrict tree growth at an arbitrarily assigned maximum diameter, but does significantly reduce vigor for older trees.

Figure 2.21 demonstrates how the optimal growth diameter increment (OGI) is computed in SIBBORK for different species in the simulation. Based on forestry yield table regional averages of DBH at decadal time increments, pine has a larger PRI than birch (a), which means that each year a pine tree has the potential to grow more, relative to its current diameter, than a birch. The peak OGI (b) for birch is larger than pine, but pine continues to grow vigorously,

while birch growth drastically decreases as it approaches a DBH of 40cm. According to this approach, a pine tree with a 40cm DBH could be expected to add a larger tree ring each year than a 40cm birch in non-limiting environmental conditions.

Forestry yield tables (*Shvidekno et al.*, 2006) represent regional averages. Using the Usolsky forestry inventory (*Ershov and Isaev*, 2006), a potential relative increment was computed for pine (c). Note that the PRI is larger for pine in Usolsky than in the yield tables. It is possible that the smaller spatial scale of the Usolsky forest inventory reflects pine growth in microclimates particularly suited for this species. The difference between ZELIG and SIBBORK parameterizations of OGI using Scots pine (*Pinus sylvestris*) as an example is shown in (d). The blue triangles represent the forestry yield table data. Values for older trees are often extrapolated from young tree measurements rather than measured directly. The black line is the ZELIG fit with a user-assigned maximum diameter of 56 cm. This curve fits the yield table data quite well. However, Scots pines diameters in the >1m range have been reported (*Shugart et al.*, 1992a). The blue line is fitted to the yield table data using the curve defined by equation (2.7). The fit is appropriate, and older trees are able to continue growing past 56cm in diameter. Setting the maximum diameter to 100 cm and using the ZELIG parameterization for OGI results in the black dashed line. The Usolsky forest inventory contains averages for smaller areas, although the values in the inventory still represent averages and do not capture maximum growth of individual trees. The green squares represent a subset of the Usolsky inventory for areas where pine exhibited the most annual growth. The green line is the curve fitted to the Usolsky subset using Bragg methodology and equation (2.7). Although the ZELIG and the Bragg estimates based on Usolsky inventory data capture the rapid early increases in growth and the maximum diameter increment experienced by a pine tree without any environmental limitations, the growth experienced by older trees is represented quite differently by the two parameterizations. Expanding the parameterization for growth of older trees is particularly important for simulation of Siberian boreal forests, where more than half of the assessed stands were considered in the mature or over-mature stages in the 1990s (*Krankina et al.*, 1996).

Understanding that yield tables and Usolsky inventory data represent averages, and individual faster-growing trees may be found in the region, the OGI curve was modified to include a 15% increase over the Usolsky-based maximum OGI estimates, which is represented by the red line in Figure 2.21d. The OGI for each species in the simulation is presented in Figure 2.21e, with aspen (*Populus spp.*) showing the largest maximum diameter increment, but all conifers maintaining the potential even as they grow beyond 40cm DBH. Aspen and birch photosynthesis rates have been shown to be more than twice the rate of gas exchange in pine and spruce (*Kobak*, 1988; *Smith and Hinckley*, 1995; *Brooks et al.*, 1997), which supports the relatively fast growth rates of these tree species shown in Figure 2.21e.

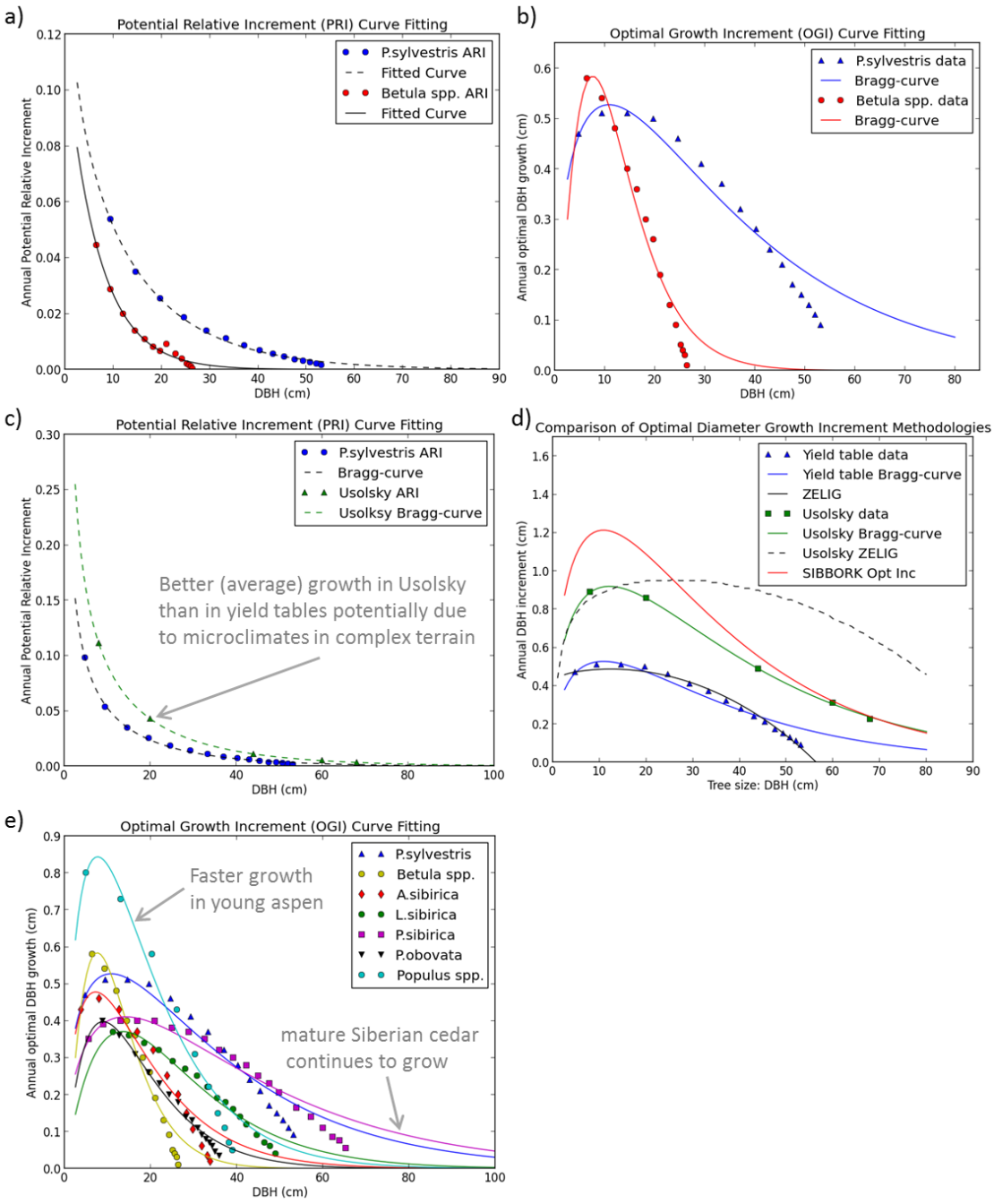

Fig. 2.21: Determining the optimal diameter increment based on species type and tree size. (a) Annual potential relative increment for pine and birch and (b) optimal diameter increment for pine and birch, based on forestry yield tables. (c) Forestry inventories representing a smaller spatial extent may capture greater annual tree growth than the regional averages in yield tables. (d) Comparison of ZELIG and SIBBORK methodologies for determining the annual optimal diameter increment based on species and tree size. (e) Optimal diameter increment for seven boreal species in SIBBORK.

2.2.3 Tree Mortality

Mortality is a stochastic process modeled using a uniform random number generator along with species-specific silvicultural information specified in the driver file. Tree mortality can be from two sources: natural or stress-based. Natural mortality, also known as age-based mortality, is based on the principle that only 1% of individuals within a species survive to the maximum age, and therefore maximum size (max DBH, max height). Stress-related mortality is dependent on environmental conditions and species-specific tolerances to resource limitations. Natural and stress-induced mortality subroutines were retained from ZELIG, however, a new mortality trigger has been added coupled with disturbance triggers. This type of mortality allows the user to specify the species and the sizes of trees that will be removed from the simulation following a disturbance event.

Age-related Mortality

Age-related mortality is based on the principle that only 1% of individuals within a species will survive to the maximum age for that species, and follows the general trend described in the equation (2.8) and Figure 2.22 (*Shugart*, 1984). The important thing to note here, is that the 1% may be an appropriate estimate for forests without disturbances, however, inclusion of disturbances, such as wildfire or insect outbreaks, will significantly reduce the number of individual trees that survive to the species-specific maximum age (*Mielke et al.*, 1978).

$$Probability = 1 - e^{\frac{-4.605}{AGEMAX}} \tag{2.8}$$

Stress-based Mortality

Stress-based mortality is a result of species-specific tolerances to resource limitations. When resources, such as light, soil moisture and soil nutrition, are limited, the tree will not grow at the optimal rate for its size and species type. The annual optimal diameter increment (ODI) is decreased based on the limitations from environmental conditions. In ZELIG, when the actual diameter increment (growth) acquired by an individual in a given year is <10% of the optimal diameter for a tree of its size and species type, a stress flag is activated for that individual. In SIBBORK, species-specific thresholds for percent of ODI needed to induce stress are employed to decrease stress mortality of hardy species that are able to survive multiple consecutive slow growth years (*Keane et al.*, 2001). These thresholds were estimated from forestry yield tables for each species (*Shvidenko et al.*, 2006). Similar to ZELIG, after two consecutive years with a stress flag, the individual in SIBBORK has a 37% chance of dying in each of the subsequent years until the tree dies or until the stress flag is removed. The stress flag is removed when the tree achieves at least 10% of its

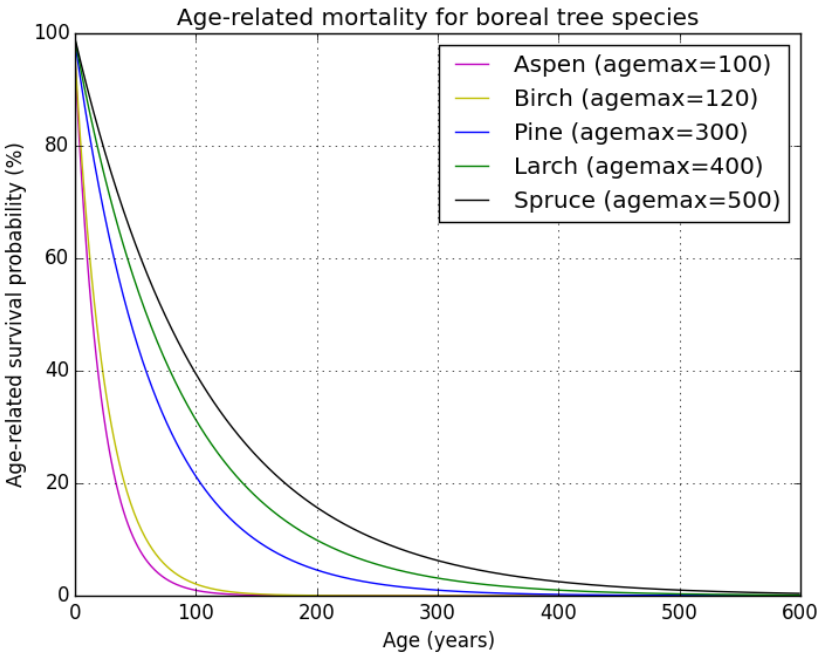

Fig. 2.22: The age-related mortality differs for the boreal trees, based on the estimated maximum age for the species. At each age, a tree has the specified probability of surviving to the next year, such that, for example, a 100-year old pine has a 20% chance of surviving to the next simulation year.

species	stress-flag threshold (%ODI)
Abies sibirica	6%
Larix sibirica	5%
Betula pendula	10%
Picea obovata	8%
Pinus sibirica	8%
Pinus sylvestris	10%
Populus tremula	10%

Fig. 2.23: The species-specific stress-flag thresholds were estimated based on the optimal diameter increment calculations (see Tree Growth section for detail) and the forestry yield table values for decadal diameter increments for mature (>75% of agemax) monospecies stands.

optimal diameter increment within a simulation year. Throughout a tree's lifetime, it may be stressed and released several times, based on environmental conditions and its species-specific tolerances to resource limitations.

SIBBORK is tailored toward the simulation of boreal ecosystems, although the framework is flexible enough to easily re-parameterize it to the simulation of any type of forest ecosystem for which appropriate forestry data are available. Boreal forests are dominated by hardy trees, which can survive in very limiting conditions for decades. Based on forestry yield tables (*Shvidenko et al.*, 2006), mature fir, spruce, Siberian cedar and especially larch can survive for decades while incrementing the DBH by less than 0.1mm per year (on average). To reflect this resilience, the threshold for stress flag assignment, which was 10% for all species in ZELIG, was restructured as a species-specific parameter,

which allows Siberian larches to increase the DBH by as little as 5% of their annual ODI without being flagged for stress-based mortality. Species-specific stress-flag thresholds are listed in Figure 2.23.

2.3 Allometry

Species-specific allometric equations in SIBBORK represent fitted relationships for height, biovolume, above-ground biomass, above- and below-ground biomass, foliage biomass, and leaf area as functions of DBH. These relationships were derived from the regional yield tables for the southern and middle taiga regions of central Siberia listed in Figure 2.24 (*Shvidenko et al.*, 2006). Figure 2.25 conveys species-specific allometric equations employed in SIBBORK. The DBH and base of the canopy are two structure-related state variables tracked by SIBBORK from year to year (Figure 2.1). Other tree dimensions are computed as a function of DBH in post-processing. Some relationships are conveyed as piece-wise functions to preserve realism in tree structure. The equation form for the same variable, i.e. height, may differ from species to species, which presents a significant difference from species-specific parameterizations in ZELIG. This approach provides greater flexibility in using the equation(s) of best fit to describe the allometric relationships for each species.

2.3.1 Height

The height equations in SIBBORK represent curves of best fit derived from yield table data for each species. The form of the equation differs between species. To make sure this is the best approach, height equations from ZELIG, a Monte Carlo gap model FAREAST (*Yan and Shugart*, 2005) and yield tables were compared for all seven species in SIBBORK. The comparison revealed that the previous ZELIG parameterization, which computes tree height via a second-order polynomial with species-specific coefficients based on estimated maximum diameter and height that a tree of a given species can attain, did not always match the form of the height-diameter relationship presented in the yield table data. When a second-order polynomial equation is used to compute height as a function of DBH, height begins to decrease for large trees. This is not the case in nature. SIBBORK predominantly utilizes piece-wise functions to estimate tree height as a function of DBH to reflect fast vertical growth in young stems, and slower growth rate for mature trees. Figure 2.26 presents the comparison between three different parameterizations for height from two different gap models and the forestry yield tables. SIBBORK uses the yield table parameterization, which involves piece-wise functions for all but one species.

Species	Regional forestry yield tables used for deriving allometry
Abies sibirica	Fir stands of mountain ecoregions of the Central Siberian Plateau
Larix sibirica	Larch stands of maximal productivity in Middle Siberia (ecoregions of middle and south taiga); Larch forests of Yenisei Krjazh and south of Krasnoyarskii krai (ecoregions of mountain taiga forests and subtaiga); Larch forests of Angara River basin (ecoregions of middle and south taiga)
Betula spp	Birch stands in south and middle taiga ecoregions of Siberia
Pinus sibirica	Fully-stocked mixed cedar forests of the Central Siberian Plateau; Mixed cedar stands of Central Siberian Plateau
Pinus sylvestris	Fully-stocked pine stands in middle taiga, south taiga, sub-taiga and forest steppe ecoregions of Central and East Siberia
Picea obovata	Fully-stocked spruce forests of Middle Siberia (ecoregions of southern and middle taiga)
Populus spp.	Fully-stocked aspen stands of Central and East Siberia (ecoregions of middle and southern taiga); Aspen stands in south taiga ecoregions of Central Siberia

Fig. 2.24: Regional forestry yield tables used for deriving allometric relationships for different species in SIBBORK.

Height equation used in FAREAST:

$$H = 1.3 + (\frac{H_{max}}{100} - 1.3) \times (1 - e^{\frac{-S \times DBH}{H_{max} - 1.3}}) \tag{2.9}$$

where H_{max} is the estimated maximum height a tree of a given species can achieve, and *S* is the slope of the H-DBH relationship for young saplings.

Height equation used in ZELIG:

$$H = \frac{237 + \frac{2 \times (H_{max} - 137)}{D_{max}} \times DBH - \frac{H_{max} - 137}{D_{max}}}{100} \tag{2.10}$$

where H_{max} and D_{max} are the estimated maximum height and diameter at breast height a tree of a given species can achieve. These maximum height and diameter values are difficult to estimate, and vary based on site conditions.

Species	Height (m)	Biovolume (above-ground) (m^3/tree)	Biomass (above- & below-ground) (t/tree)	Foliage Biomass (t/tree)	Forestry yield table applicability
Abies sibirica	$-0.0049dbh^2+0.9546dbh+1.37$ ($R^2 = 0.9993$)	$0.0001\ dbh^{2.5371}$ ($R^2 = 0.9993$)	$0.00002dbh^3-0.0003dbh^2+0.0039dbh$ ($R^2 = 0.9975$)	*for dbh < 33cm:* $0.015\ dbh^{2.1934}$ *for dbh > 33cm:* $53.975\log(dbh) - 156.59$ ($R^2 = 0.9993$)	south & middle taiga
Larix sibirica	*for dbh < 36cm:* $-0.0152dbh^2+1.3806dbh+1.37$ *for dbh > 36cm:* $6.0278\log(dbh) + 9.6025$ ($R^2 = 0.9675$)	*for dbh < 20cm:* $0.0004\ dbh^{2.3061}$ *for dbh > 20cm:* $0.0013dbh^2 - 0.0074dbh$ ($R^2 = 0.9996$)	$0.0002\ dbh^{2.5568}$ ($R^2 = 0.9999$)	*for dbh < 34cm:* $0.0218\ dbh^{2.0014}$ *for dbh > 34cm:* $69.793\log(dbh) - 220.71$ ($R^2 = 0.9789$)	south & middle taiga
Betula pendula *Betula platyphylla* *Betula pubescens*	*for dbh < 26.5cm:* $1.0389dbh+1.37$ *for dbh > 26.5cm:* $1.3444\log(dbh) + 24.501$ ($R^2 = 0.8455$)	$0.0002\ dbh^{2.5213}$ ($R^2 = 0.9997$)	$0.0002\ dbh^{2.3793}$ ($R^2 = 0.9998$)	*for dbh < 22.4cm:* $0.0492\ dbh^{1.5835}$ *for dbh > 22.4cm:* $6.5771\log(dbh) - 13.672$ ($R^2 = 0.9387$)	south & middle taiga
Picea obovata	*for dbh < 25cm:* $0.0401dbh^2-0.0516dbh+1.37$ *for dbh > 25cm:* $21.928\log(dbh) - 45.405$ ($R^2 = 0.974$)	$0.00006\ dbh^{2.8291}$ ($R^2 = 0.9973$)	$0.00006\ dbh^{2.6887}$ ($R^2 = 0.9992$)	*for dbh < 27.3cm:* $0.0497\ dbh^{1.844}$ *for dbh > 27.3cm:* $13.789\log(dbh) - 23.48$ ($R^2 = 0.8652$)	south & middle taiga
Pinus sibirica	*for dbh < 38.5cm:* $-0.0073dbh^2+0.913dbh+1.37$ *for dbh > 38.5cm:* $0.3544\log(dbh) - 8.4582$ ($R^2 = 0.9731$)	$0.0001\ dbh^{2.514}$ ($R^2 = 0.9986$)	*for dbh < 43cm:* $0.00008\ dbh^{2.5387}$ *for dbh > 43cm:* $2.8067\log(dbh)-9.4117$ ($R^2 = 0.995$)	*for dbh < 33.6cm:* $0.0075dbh^2+0.2328dbh-0.2592$ *for dbh > 33.6cm:* $19.537\log(dbh) - 52.641$ ($R^2 = 0.9976$)	Central Siberian Plateau
Pinus sylvestris	*for dbh < 32cm:* $-0.0105dbh^2+1.1644dbh+1.37$ *for dbh > 32cm:* $12.739\log(dbh) - 16.297$ ($R^2 = 0.9863$)	$0.0003\ dbh^{2.4137}$ ($R^2 = 0.9994$)	$0.0001\ dbh^{2.3922}$ ($R^2 = 0.9993$)	*for dbh < 40:* $0.0298\ dbh^{1.7463}$ *for dbh > 40cm:* $15.907\log(dbh) - 39.909$ ($R^2 = 0.897$)	Central & East Siberia
Populus suaveolens *Populus tremula*	*for dbh < 34cm:* $0.0013dbh^2+0.736dbh+1.37$ *for dbh > 34cm:* $13.358\log(dbh)-19.19$ ($R^2 = 0.9272$)	$0.0001\ dbh^{2.5877}$ ($R^2 = 0.9989$)	$0.0001\ dbh^{2.4599}$ ($R^2 = 0.9992$)	*for dbh < 28.3cm:* $0.0281\ dbh^{1.6509}$ *for dbh > 28.3cm:* $7.6636\log(dbh)-18.632$ ($R^2 = 0.9937$)	south & middle taiga, Central & East Siberia

Fig. 2.25: Species-specific allometric equations derived from regional forestry yield tables.

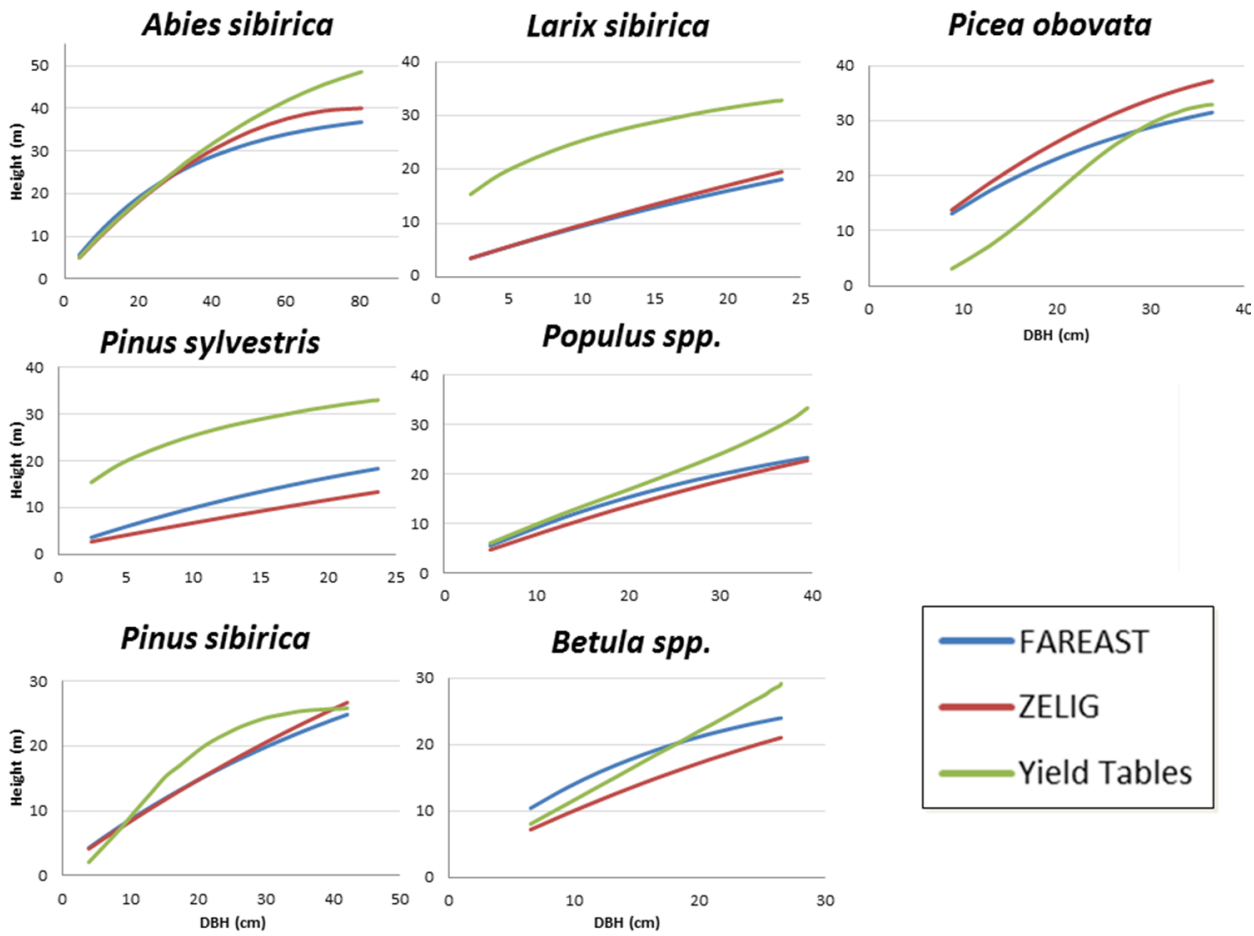

Fig. 2.26: Comparison of height parameterizations across models. SIBBORK is parameterized from forestry yield tables (green line).

2.3.2 Biovolume

Biovolume is a typical forestry survey parameter and represents predominantly the volume of the tree stem. SIBBORK computes biovolume in m^3/tree via a species-specific function of DBH derived from the average DBH, stem density, and average stand biovolume variables presented in the forestry yield tables (*Shvidenko et al.*, 2006). Species-specific equations for computing the biovolume of individual trees are presented in Figure 2.25. These equations represent lines of best fit for the stand biovolume (m^3/ha) divided by stem density (*stems/ha*) and the average DBH (*cm*). Biovolume is not typically computed by gap models, however, as this is the parameter estimated in field surveys, including it in the model facilitates comparison along an additional variable. Furthermore, average DBH, stem density (stems/ha), and biovolume (m^3/ha) are reported within the same forestry yield table for each species, allowing for the direct derivation of an allometric relationship for biovolume as a function of DBH. This is in contrast to the allometric

relationship between biomass (t/ha) and average stand DBH, which is divided between forestry yield tables and tables of biological productivity, which were manually joined along the age variable (Figure 2.27).

2.3.3 Biomass

Biomass measurements are destructive and labor intensive. For this reason, biomass is not typically measured in field surveys, but is instead calculated from field-estimated stem biovolume using wood density. Focus on the tree stem can significantly underestimate the amount of total above- and below-ground biomass associated with each tree, since more than 30% of the biomass may be in the tree crown (*Monserud and Tchebakova*, 1996; *Shvidenko et al.*, 2006), and more than 25% of the biomass may be in the root system (*Schepaschenko et al.*, 1998; *Shvidenko et al.*, 2006). Nonetheless, the common approach is to estimate the tree stem volume and convert it to biomass by multiplying it by the wood density. The wood density can either be assumed the same for all trees (*Krankina et al.*, 1996; *Yan and Shugart*, 2005), or species- and region-specific values may be used to convert biovolume to biomass. There is a lot of variability in species-specific wood density values reported in the literature (*Monserud and Tchebakova*, 1996; *Schepaschenko et al.*, 1998; *Kajimoto et al.*, 1999; *Miao and Li*, 2007; *Falster et al.*, 2015), and the values used for the composition of the yield tables are not specified.

For SIBBORK, species-specific relationships were derived for above-ground biomass as a function of DBH based on the data presented in what were perceived to be overlapping forestry yield tables and tables of biological productivity for a given species and region. Since SIBBORK is an individual-based model, the relationship needs to represent the biomass per tree as a function of DBH. This was achieved by dividing the average stand biomass (*tons/ha*) by stem density (*stems/ha*), and fitting an equation to the relationship between this biomass and average stand DBH (*cm*). This was accomplished using the stem density and DBH values provided in the yield table that corresponds to the same species and ecotone as the biological productivity table. Foliage biomass, as well as the total above- and below-ground biomass, are similarly computed as a function of DBH. Figure 2.28 shows how the contribution of foliage and roots to the total above- and below-ground (AGBG) tree biomass changes over the course of a tree's lifetime.

This process to determining biomass allometry is very error-prone and depends on the yield tables and tables of biological productivity describing the same stands. Although species-specific equations for above-ground, as well as above- and below-ground biomass are included in SIBBORK, the verification and validation of these parameters is problematic, as few studies report above- and below-biomass estimates and the derivation of accurate biomass allometry may not even be feasible using the available forestry tables.

Yield table of fully-stocked (normal) pine stands

1.1. Ход роста полных (нормальных) сосновых древостоев

Возраст, лет / Age, year	Средняя высота, м / Average Height, m	Средний диаметр, см / Average Diametr, cm	Число деревьев / Number of Trees	Сумма площадей сечения, м² · га⁻¹ / Basal Area, m² · ha⁻¹	Запас, м³ · га⁻¹ / Growing Stock, m³ · ha⁻¹	Изменение запаса, м³ · га⁻¹ · год⁻¹ / Net Growth, m³ · ha⁻¹ · year⁻¹: текущее / current	среднее / average	Общая продуктивность, м³ · га⁻¹ / Total volume, m³ · ha⁻¹	Прирост по общей продуктивности, м³ · га⁻¹ · год⁻¹ / Gross Growth, m³ · ha⁻¹ · year⁻¹: текущий / current	средний / average	Отпад, м³ · га⁻¹ · год⁻¹ / Mortality, m³ · ha⁻¹ · year⁻¹
Ib бонитет											
10	5.5	5.1	8277	17.0	57	9.95	5.65	61	11.22	6.15	1.27
20	11.6	10.9	3263	30.4	178	13.51	8.89	205	16.80	10.27	3.29
30	16.9	16.5	1863	39.7	316	13.74	10.53	386	18.80	12.85	5.06
40	21.6	21.7	1245	46.2	448	12.46	11.19	574	18.70	14.36	6.24
50	25.4	26.6	911	50.5	563	10.64	11.27	756	17.47	15.12	6.83
60	28.6	31.0	709	53.4	660	8.77	11.00	922	15.71	15.37	6.95
		35.0	576	55.4	739	7.05	10.56	1070	13.77	15.28	6.72

Table of dynamics of biological productivity of fully-stocked pine stands

1.1. Динамика биологической продуктивности полных сосновых насаждений

Возраст, лет / Age, year	Фитомасса насаждения, т · га⁻¹ / Actual Forest Phytomass, t · ha⁻¹: древостой / Stand by fractions: ствол / Stem	в т.ч. кора / of which bark	древесина кроны / Wood of crown	хвоя (листья) / Foliage	итого надземной / Above ground	корни / Roots	всего / Total	подрост и подлесок / Understory	напочвенный покров / Green forest floor	всего / Total	Общая продуктивность фитомассы, т · га⁻¹ / Total Phytomass Production, t · ha⁻¹	Текущий прирост фитомассы, т · га⁻¹ · год⁻¹ / Net Growth, dm t · ha⁻¹ · year⁻¹: наличного насаждения / Actual Phytomass	по общей продуктивности / Total Phytomass	Углерод фитомассы, т · га⁻¹ / Carbon, t · ha⁻¹: наличного насаждения / Actual Phytomass: всего / Total	в т.ч. ствол / of which stem	по общей продуктивности / Total Phytomass Production: всего / Total	в т.ч. ствол / of which stem	Чистая первичная продукция, г С · м⁻² · год⁻¹ / Net Primary Production, gC · m⁻² · year⁻¹
Ib бонитет																		
10	18.5	2.2	4.3	3.5	26.3	7.6	33.9	0.2	0.7	34.8	42.1	5.64	7.33	17.1	9.2	20.7	10.0	360
20	65.6	4.5	8.5	6.5	80.6	21.7	102.3	0.4	1.1	103.8	143.6	7.62	12.01	51.5	32.8	70.5	35.4	589
40	181.7	7.5	14.2	9.3	205.2	49.3	254.5	0.8	1.9	257.2	429.1	7.14	15.41	128.1	90.9	210.5	107.6	755
60	277.4	9.0	17.3	10.2	304.9	68.6	373.5	1.2	2.6	377.3	736.8	4.91	15.04	187.9	138.7	360.8	179.6	733

Fig. 2.27: The upper table contains the variables of average DBH, stem density, and stand biovolume. This facilitates the derivation of an allometric relationship for computing biovolume for each tree. The lower table contains information regarding biomass of different tree parts and total above-ground, as well as above- and below-ground biomass stand estimates. The common features between the two tables are the titles, which refer to the same species and ecotone, as well as the site index and the stand age.

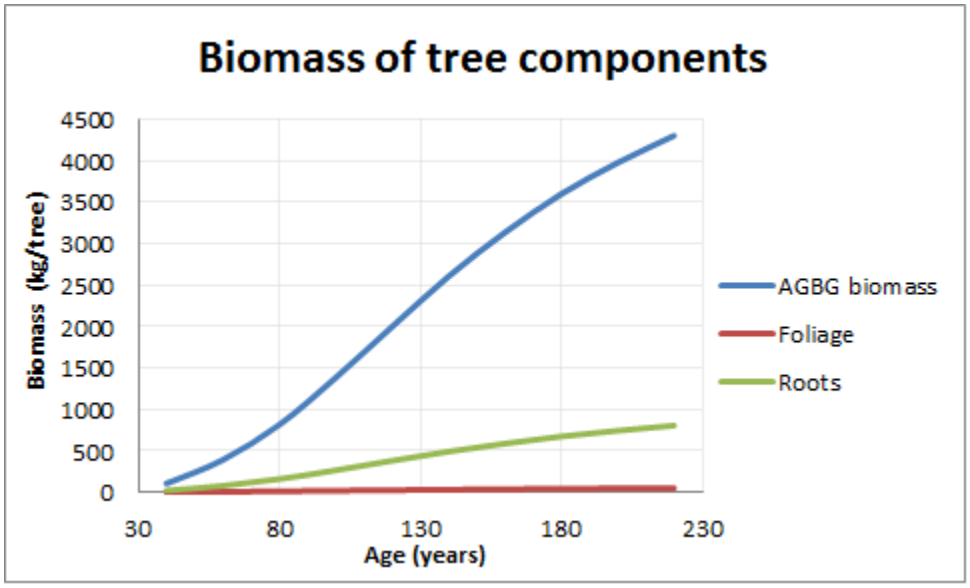

Fig. 2.28: Using Siberian larch as an example, the contribution of different tree components to total above- and below-ground tree biomass is shown for different stages in the tree's lifetime. Data obtained from Shvidenko *et al.* (2006).

2.3.4 Foliage Biomass

Foliage biomass comprises 1-30% of total tree biomass (*Monserud and Tchebakova*, 1996; *Shvidenko et al.*, 2006). According to the table of biological productivity, foliar biomass contributes more to the total biomass in the dark conifers fir, spruce, and Siberian cedar (8-13%). The denser canopy facilitates more light extinction, and this is why these species are collectively referred to as "dark" conifers. In contrast, light conifers - larch and pine - have lighter-colored, less dense canopies, which comprise up to 4 and 6% of total tree biomass, respectively. A larger proportion of young tree biomass is comprised of foliage. As the tree matures, foliage may constitute as little at 1% of total biomass.

Similar to tree biomass, foliage biomass is computed as a function of DBH based on the overlap of forestry yield tables and tables of biological productivity. This calculation is prone to the same errors as the above-ground biomass described in the previous section.

2.3.5 Leaf Area

Canopy leaf area estimates are of interest due to the control that the leaf area exerts on an array of physiological processes, from photosynthesis and respiration (*Asner et al.*, 2003) to water interception and sunlight availability (*Breda*, 2003), and ultimately the biological productivity. Numerous approaches to computing leaf area can be found in the literature, accompanied by several definitions of what should be considered leaf area (*Scurlock et al.*, 2001). For

broadleaf trees, this is fairly simple - the leaf area can represent the area of one side of a leaf or two sides of a leaf. This is referred to as single-sided (projected) or double-sided (total) leaf area. Conifer needles can have cylindrical or triangular prism shapes, of which the latter has three sides. Leaf area can therefore be defined as one-sided (projected), two-sided, or three-sided (total). An additional definition for conifer needle leaf area estimates was suggested by Chen and Black (1992): "half the total intercepting area", also known as hemisurface area (*Gower et al.*, 1999). In stand descriptions, often the leaf area index is used instead, which represents the leaf area per ground area. Much of the literature on leaf area (LA) and leaf area index (LAI) does not specify which definition was used to estimate the leaf area, which makes model parameterization and comparison of model output to published field-based estimates difficult. Furthermore, LA and LAI are site-specific, and are affected by soil nutrition and nitrogen content, soil moisture, and other environmental conditions (*Gower et al.*, 1999). This complicates the derivation of an allometric relationship between DBH and LA that could be applied to a multi-century simulation - a time frame over which environmental conditions could change significantly, especially when climate change is considered.

Leaf area is computed in SIBBORK in order to estimate the light environment throughout and below the canopy, however, no physiological process in the model depends on the leaf area directly. The computed leaf area is allocated evenly along the crown length of the tree (height - crown base) (*Urban*, 1990), and the horizontal extent of each tree's canopy within each 1m vertical step is assumed to be homogeneously distributed across the plot area (*Shugart et al.*, 1988).

The original ZELIG model was created for mixed broadleaf temperate forests, and computed leaf area (m^2) as a function of DBH (*cm*) using the same equation form and coefficients for all species:

$$LA = 0.160694 \times DBH^{2.129} \tag{2.11}$$

A later version of ZELIG (v2.3) computed leaf area as a function of tree diameter and sapwood cross-sectional area at breast height:

$$LA = \pi \times \frac{DBH^2}{2} - \pi \times (\frac{DBH}{2} - r_{sapwood}) \times (Ratio_{\frac{sapwood}{leafarea}}) \tag{2.12}$$

where DBH is in *cm*, $r_{sapwood}$ corresponds to the portion of the tree radius at breast height that represents the sapwood (*cm*), and the $Ratio_{\frac{sapwood}{leafarea}}$ is the species-specific ratio of the sapwood area in the tree stem to the leaf area of the foliage. However, there is a significant difference in the vascular morphology of broadleaf and coniferous trees, and field-based estimates of conducting sapwood area are difficult (*Vertessy et al.*, 1995). In some broadleaf trees, the allometric relationship is observed between the few outer annual rings and leaf area, whereas in other broadleaf trees and in conifers the relationship is observed between the leaf area and the entire cross-sectional area of the sapwood

species	SLA (m^2/kg)	Reference
Abies sibirica	11.6	*Yan et al.*, 2010; *Wang et al.*, 2011
Larix sibirica	22.9	*Eguchi et al.*, 2004
Betula pendula	19.9	*Niinemets et al.*, 2002; *Repola et al.*, 2007
Picea obovata	12.9	*Tjoelker et al.*, 1998; *Hoffman and Usoltsev*, 2002
Pinus sibirica	15.2	*Tjoelker et al.*, 1998; *Hoffman and Usoltsev*, 2002; *Lindroth et al.*, 2008
Pinus sylvestris	13.4	*Tjoelker et al.*, 1998; *Hoffman and Usoltsev*, 2002; *Lindroth et al.*, 2008
Populus tremula	15.9	*Hoffman and Usoltsev*, 2002; *Breda*, 2003

Fig. 2.29: Specific leaf area (SLA) for boreal species obtained from the literature.

(*Albrektson et al.*, 1984; *Breda*, 2003). Even within plant functional types, there is significant variability in LA-sapwood area allometry (*Waring et al.*, 1982, *Breda*, 2003). Calculation of leaf area based on equation (2.12) may thus be appropriate for some tree species in the boreal forest, but not for others.

The FAREAST leaf area calculation is based on the Shinozaki pipe model (*Shinozaki et al.*, 1964) and uses the following equation:

$$LA = D_L \times (DBH \times \frac{H - CrownBase}{H - 1.3})^2 \tag{2.13}$$

where D_L is the ratio of the leaf area to the squared diameter at the base of the canopy crown - a ratio that is the same for all species in FAREAST. Height (*H*) and the distance from the ground to the first branch (*CrownBase*) are both in meters. Although the FAREAST model has been validated for China and Russia based on the ability to reproduce species composition and above-ground biomass, specifically the LA and the LAI calculations have never been validated (*Shugart, personal communication*). Both parameters are used to compute the light environment in the model, however, since FAREAST is a Monte Carlo simulation of independent plots, the light environment is only computed from directly overhead. Due to the differences between the Monte Carlo simulation and the spatially-explicit SIBBORK model, a LA or LAI parameterization that works well in FAREAST may not be appropriate for SIBBORK, where direct and diffuse light is computed along multiple light ray traces.

A method presented in Breda (2003) computes leaf area as a function of foliage biomass:

$$LA = B_f \times SLA \tag{2.14}$$

where B_f is the foliage biomass in kg, and *SLA* represents specific leaf area values for each species in m^2/kg. Published SLA values for boreal tree species are shown in Figure 2.29.

Specific leaf area generally represents the area-to-weight ratio of leaves or needles, but definitions for SLA diverge in the literature (*Gower et al.*, 1999). Broadleaf trees (birch, aspen) generally have higher SLA values than conifers,

and larch exhibits the highest SLA of boreal conifers (*Kloeppel et al.*, 1998). SLA varies widely between stands and seasons (*Araki*, 1972), depends on soil nitrogen and ambient CO_2 concentrations (*Curtis et al.*, 2000), as well as soil moisture and leaf age (*Landsberg and Gower*, 1997; *Ermolova and Utkin*, 1998). Specific leaf area can vary significantly even within the crown of a single tree, with sun leaves thicker and heavier per unit area than the shade leaves (*Araki*, 1972; *Ermolova and Utkin*, 1998; *Asner et al.*, 2003).

However, this approach is attractive, since SLA values for different boreal species can be found in the literature, and the forestry tables of biological productivity specify a foliage biomass estimate for monospecies same-age cohorts (Figure 2.27). The latter creates a potential for deriving an allometric relationship between DBH and foliar biomass, provided the cross-correlation between forestry yield tables and tables of biological productivity is correct. However, it is important to keep in mind that SLA values are species- and site-specific, and can vary widely even within the crown of an individual tree. The SLA values in Figure 2.29 may not be fitting for some simulated sites, and downscaling the allometry from the stand-based tables of biological productivity to the individual trees in the simulation may not be appropriate.

In the simulation, LAI normalizes the sum of leaf areas of all trees on a plot by the area of the plot (100 m^2). This is the parameter used in the exponent of the Beer-Lambert Law (equation (2.1)) for calculation of extinction of solar radiation as it travels through the forest canopy. Numerous approaches for LAI estimates exist in the literature, and some depend on the divergent definitions and measurement methodologies for LA and SLA (*Barclay*, 1998; *Scurlock et al.*, 2001; *Asner et al.*, 2003). LAI depends on time of year, canopy closure, stem density, stand age, and other structural parameters, such as the leaf/needle angle and the degree of damage experienced by a crown from disturbances such as fire or defoliators (*Chen and Black*, 1992; *Chen*, 1996; *Scurlock et al.*, 2001). Typical LAI indices for forests range 3-19, with highest LAI values reported for boreal coniferous forests, and values less than 6 in broadleaf and mixed stands (*DeAngelis et al.*, 1981; *Schulze*, 1982; *Chen*, 1996; *Asner et al.*, 2003). LAI values in the teens reported for boreal and mixed forests may be a result of measurement methodologies or adjustments between definitions (*Barclay*, 1998). According to one of the definitions, LAI relates the one-sided leaf area to the ground area below the canopy, i.e. the shade cast by the canopy of a tree when the sun is directly overhead (*Barclay*, 1998). Asner *et al.* (2003) conducted a global survey of LAIs reported for different biomes, and estimated that the average LAI for boreal deciduous and evergreen forests are 2.6 and 2.7, respectively, although this analysis under-represents Russian forests and accounts for only one site in southeastern Siberia. Large scale average LAI values of less than 3.5 appear to characterize the middle and northern taiga ecotones, while LAI of 3.5-4.5 is estimated for the southern taiga region from a remote sensing and modeling-based product (*Asner et al.*, 2003). Furthermore, LAI values reported in the literature often represent area averages (ha^{-1}) and do not represent the variability in LAI across the terrain or at point locations. A gap model, however, computes LAI for much smaller areas, and greater variability in LAI is expected on a plot by plot basis. The

divergence in LAI values reported for boreal forests complicates the validation of the LAI calculations in the model, however, all SIBBORK-simulated LAI values fall within the broad range of LAIs reported in the literature for boreal species.

The SLA parameterization from equation (2.14) was adapted in SIBBORK. Model testing revealed that this approach may overestimate total leaf area and the leaf area index, with mature conifer forests exhibiting LAIs in the teens and even the lower 20s. Although the lower side of this range may agree with some of the values reported in the literature (*Chen et al.*, 2002; *DeRose et al.*, 2010) with adjustment factors for conifer needles and clumping of 1.5-2 (*Barclay*, 1998; *Scurlock et al.*, 2001), the LAI values at the higher end of this range are rarely found in the literature, but have indeed been measured in some forests (*DeAngelis et al.*, 1981). Moreover, the simulated stand structure and composition, both of which depend on the light environment computed using LAI, have been verified and validated for southern, middle and northern taiga locations on flat terrain, as well as in complex terrain at the southern extent of the boreal forest.

To determine the most appropriate leaf area parameterization for the boreal ecosystem, each of these four approaches should be used to compute LA and LAI for a stand under the historical climate conditions, and model output compared to published values of LAI for different monospecies stands. It will also be important to assess that the structure and composition of the stands are appropriately simulated with each of the four parameterizations. However, this involves scripting four different versions of the model, and conducting verification and validation testing with each version. This falls outside of the scope of this dissertation project, however, highlights an area for further refinement of the SIBBORK model. At this point, the framework of SIBBORK has been designed to allow for species-specific equations for the LA calculation, so that the most appropriate approach can be selected and employed for each species in the simulation.

A simpler, short-term solution to LAI overestimation could be a quality control check implemented to correct any plot-wide LAI of greater than a certain maximum threshold to a reasonable value in the lower teens. This approach has not been implemented, because within the simulated 3-D light environment, there is not much difference in the amount of light available in the lower portions of the canopy with an LAI of 15 or 22. Most of the light below a canopy with LAI of 15 is extinguished, which prevents shade-intolerant saplings from establishing in the subcanopy of dense coniferous trees, preserving realism in the simulation.

2.4 Environmental Effects on Vegetation Processes

Vegetation processes of sapling establishment, growth, and mortality are affected by environmental forcings. In ZELIG (*Urban*, 1990; *Urban et al.*, 1993; *Weishampel et al.*, 1996), the growth response of trees to the environmental factors of light availability, soil moisture, ambient temperature, expressed as growing degree days, and soil fertility, expressed as maximum biomass per plot, were parameterized as in Figure 2.30.

In SIBBORK, the environmental factors of growing degree days, soil moisture, soil fertility, permafrost, ground-level available light, as well as available light throughout and below the canopy are generated for the simulation area based on climatological record (*NCDC*, 2005a, 2005b) and lapse rates from DEM, hydrologic modeling based on DEM, soil datasets (*Stolbovoi and McCallum*, 2002; *Stolbovoi and Savin*, 2002), permafrost datasets (*Brown et al.*, 2002), and the Area Solar Radiation calculator based on DEM (*Fu and Rich*, 2002), respectively. The degree to which each species is affected by the presence or limited quantity of each factor is based on species-specific tolerances, which were obtained from the literature (*Shugart et al.*, 1992a; *Yan and Shugart*, 2005; *Larocque et al.*, 2016).

2.4.1 Available Light Factor

Available light is arguably the most important environmental constraint on vegetation growth and establishment (*Purves et al.*, 2008; *Purves and Pacala*, 2008), especially in environments with harsh and complex light regimes, such as the high-latitude boreal forests. In the absence of shade, trees are able to achieve optimal growth, provided other environmental factors are not limiting. In the shade, the growth rate diminishes until a species-specific compensation point is reached. At the compensation point, the energy gained from photosynthesis equals the energy expended on metabolism and respiration. Foliage and branches that are shaded to the point of acting as a drain on the plant's overall carbon budget are self-pruned. For example, shade-intolerant species may prune branches and foliage that receive less than 9% of above-canopy light, whereas shade tolerant species may be able to maintain foliage down to 5% of above-canopy light (Figure 2.30a).

Following the approaches in other gap models (ZELIG, FAREAST), a shade tolerance class 1 (shade-tolerant) through 5 (shade-intolerant) is assigned to each species in the simulation based on literature descriptions (*Shugart et al.*, 1992a; *Smith and Hinckley*, 1995; *Yan and Shugart*, 2005; *Shuman*, 2010). The compensation point is computed based on equation:

$$ALF = C_1 \times (1 - e^{-C_2 \times (AL_h - C_3)}) \tag{2.15}$$

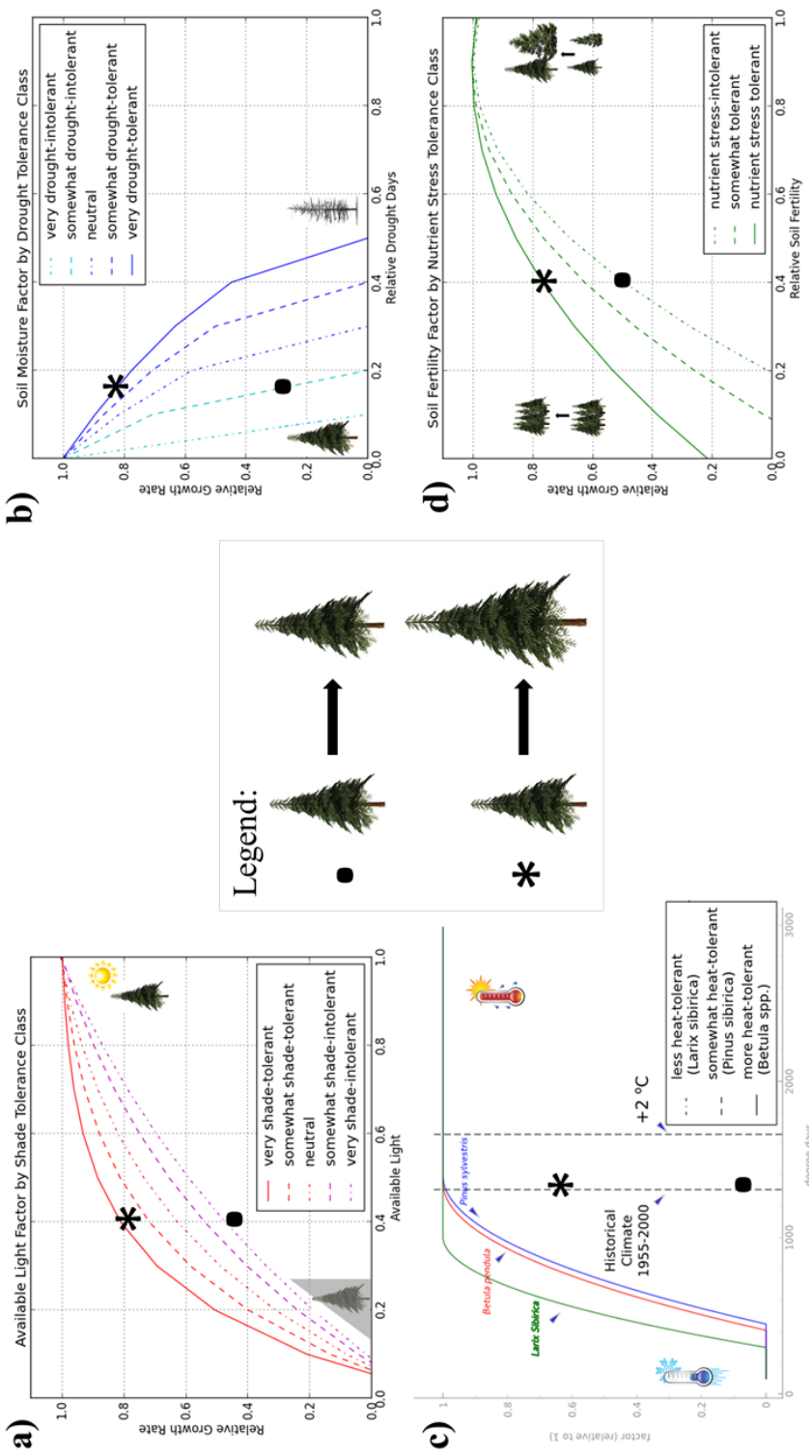

Fig. 2.30: Each simulated tree interacts with the surrounding environment based on species-specific tolerances to resource limitations. Growth responses are shown for (a) 5 shade tolerance classes to light limitations, (b) 5 drought tolerance classes to soil moisture limitations, (c) species-specific heat tolerance, reformulated from Pastor and Post (1986) based on Bugmann and Solomon (2000) and Bugmann (2001), and (d) 3 nutrient deficiency tolerance classes to nitrogen limitations. The * in each case denotes the more tolerant species.

Tolerance class	C_1	C_2	C_3
1 (very shade tolerant)	1.01	4.62	0.05
2	1.04	3.44	0.06
3	1.11	2.52	0.07
4	1.24	1.78	0.08
5 (very shade intolerant)	1.49	1.23	0.09

Fig. 2.31: The shade tolerance class coefficients and compensation points were retained from ZELIG (Urban, 1990).

where *ALF* is the Available Light Factor with a value of 0 to 1, while C_1, C_2 and C_3 are coefficients specific to the shade tolerance class. Specifically, C_2 reflects the degree to which growth is affected by a decreasing amount of light, and C_3 represents the compensation point for the specific shade tolerance class (Figure 2.31). AL_h is computed using Beer-Lambert Law (equation (2.1)) and LAI, and represents the fraction of above-canopy light available at each 1-meter vertical step through the canopy.

2.4.2 Growing Degree Days Factor

The growing degree days factor (*GDDF*) is used to determine whether plant growth is limited by inadequate warmth over the course of the growing season. As in ZELIG, this function is initially generated as a parabola based on the maximum and minimum growing degrees that confound the species range (*Botkin et al.*, 1972a) via:

$$GDDF = \frac{4 \times (TY - min) \times (max - TY)}{(max - TY)^2} \tag{2.16}$$

where *GDDF* is the degree days factor with a value of 0 to 1, *TY* is the current year's growing degrees (GDD_5) in the simulation, and *min* and *max* correspond to the maximum tolerated and minimum required growing degrees for the species. Generally, the maximum corresponds somewhat to the southern boundary of the geographical range the species inhabits. The left half of the parabola limits tree growth whenever not enough growing degrees are accumulated during the growing season. It is important to note that no growth occurs at the GDD_5 minimum for a species, and very few representatives of the species may be found for several kilometers equatorward (or downslope) of this GDD_5 isoline in pockets of favorable microclimates. If all other environmental factors are not limiting, some trees of the species of interest may be found in locations experiencing annual GDD_5 sums of 100^o C or more above the GDD_5 minimum for the species. The right half of the parabola in SIBBORK has been modified to a non-linear function and extended at the non-limiting value (1.0), based on evidence that plant growth is not limited by heat alone, when enough soil moisture is available (*Bugmann and Solomon*, 2000). The effects of GDDF on tree growth are shown in Figure 2.30c.

2.4.3 Soil Moisture Factor

Each species in the simulation is assigned to one of five drought tolerance classes (1 = very drought-intolerant, 5 = very drought-tolerant). Even the most drought-tolerant species require plant available water during at least 50% of the growing season (Figure 2.30b). The fraction of dry days during the growing season is compared to species-specific thresholds via the following equation:

$$SMF = \sqrt{\frac{(Tol/10 - DRT)}{(Tol/10)}} \tag{2.17}$$

where *SMF* is the Soil Moisture Factor with a value of 0 to 1, *Tol* refers to the species-specific drought-tolerance class (1 to 5), and *DRT* represents the minimum of $\frac{Tol}{10}$ and the fraction of the growing season with no plant available water (soil moisture below wilting point).

2.4.4 Soil Fertility Factor

Although arboreal tree species inhabit regions with very slow decomposition rates and low soil nitrogen, even within these harsh conditions boreal species require different levels of soil nutrition for optimal growth. In SIBBORK, species are assigned to one of three nutrient stress tolerance classes (1 = very intolerant, 3 = very tolerant to poor soils). Just like the other environmental factors, the soil fertility factor (*SFF*) ranges from 0 to 1 (Figure 2.30d). The species-specific SFF is computed based on relative soil fertility (equation (2.19)) and the amount of biovolume that potentially could be accumulated on a plot during each simulation year based on limitations of the other environmental factors:

$$SFF = C_1 \times N + C_2 \times N \times sf + C_3 \times N \times sf^2 \tag{2.18}$$

where C_1, C_2, and C_3 are regression constants (Figure 2.32) based on the species-specific tolerance to nutrient stress, N is the assigned nutrient stress tolerance class (1 to 3), and sf is the normalized soil fertility based on the soil fertility value specified for this region in the simulation and the amount of biovolume that could be accrued on the plot this year:

$$fertility_{relative} = \frac{SoilFertility}{BiovolumeIncrement_{optimal}} \tag{2.19}$$

In ZELIG, the optimal biomass increment is computed based on the optimal diameter increment and represents non-limiting conditions. In SIBBORK, the maximum possible biovolume increment is computed based on the limitations on growth exerted by the *ALGF* and *GDDF*. In this manner, the actual growth that could be attained is downscaled,

Tolerance class	C_1	C_2	C_3
1 (very intolerant)	-0.6274	3.6	-1.994
2	-0.2352	2.77	-1.55
3 (very tolerant)	0.2133	1.789	-1.014

Fig. 2.32: The regression coefficients for the different tolerance classes to poor soil nutrition were retained from ZELIG (Urban, 1990).

Growth on permafrost / permafrost presence	Present	Absent
Cannot grow on permafrost	0	1
Can grow on permafrost	1	1

Fig. 2.33: Boolean limitation of tree establishment and growth on permafrost based on species-specific tolerances to this environmental parameter.

rather than the optimal growth:

$$fertility_{relative} = \frac{SoilFertility}{BiovolumeIncrement_{MaximumPossible}} \tag{2.20}$$

2.4.5 Permafrost Factor

The permafrost parameterization is greatly simplified in SIBBORK. The permafrost presence (1) or absence (0) is specified for each plot, similar to elevation or soil fertility. Each species in the simulation is assigned to one of two groups based on whether it is capable of growing on permafrost (1) or not (0), and the permafrost factor is computed based on the site and species specifications (Figure 2.33). Of the 7 species in the simulation, Siberian larch (*Larix sibirica*), Siberian pine (*Pinus sibirica*) and spruce (*Picea obovata*) are able to grow on permafrost (*Shugart et al.*, 1992a; *Tchebakova et al.*, 2009a). As much as 80% of Siberia is underlain by permafrost - a factor that significantly affects species composition in those areas (*Kotlyakov and Khromova*, 2002; *Tchebakova et al.*, 2009a). The presence of permafrost for a region of interest can be obtained from the National Snow and Ice Data Center (http://nsidc.org/data/gdd600.html; *Kotlyakov and Khromova*, 2002). Alternatively, similar to the site index, the presence or absence of permafrost can be specified by the user for each plot.

The parameterization of permafrost can be expanded to include interaction with soil moisture and soil fertility, following the approaches in Bonan (1988).

2.4.6 Overall Growth Factor

The overall growth factor used to scale down annual tree ring growth is computed using all five environmental factors. The *Leibig's Law of the Minimum* is applied to below-ground effects (soil fertility, soil moisture, permafrost), to avoid

unrealistically small annual growth. Regardless of whether soil moisture or soil fertility conditions are limiting, if a species is not able to grow on permafrost and the presence of permafrost has been specified for the plot, that species will not be able to establish on that plot. A multiplicative effect is assumed to occur from the limitations of the above-ground environmental factors (available light, growing degrees) and the minimum of the below-ground factors.

$$GrowthFactor = ALGF \times GDDF \times min(SMF, SFF, Permafrost) \tag{2.21}$$

Using solely the environmental conditions as the limiting factor on species establishment and growth, SIBBORK simulates appropriate species composition for forests in northern, middle, and southern taiga, and even at the southernmost boreal forest boundary in the complex terrain of Altay-Sayan mountains, without an explicit specification of species ranges in the driver.

The model source code is available at http://www.github.com/sibbork/SIBBORK

CHAPTER

THREE

MODEL CALIBRATION AND TESTING

"The gap between theory and practice is a lot smaller in theory, than it is in practice." - YogiBerra

Abstract

Climate change is altering forests globally, some in ways that may promote further warming at the regional and even continental scales. In order to predict how forest ecosystems might adapt to a changing climate, it is important to understand the resilience and vulnerabilities that each species within that current ecosystem might have to a modified future environment. Complex systems that occupy large spatial domains and change slowly, on the order of decades to centuries, do not lend themselves easily to direct observation. A simulation model is often the more appropriate and attainable approach toward understanding the inner workings of large, slow-changing systems, and how they may change with imposed perturbations. We report on a new, spatially-explicit dynamic vegetation model SIBBORK developed for the purpose of investigating the effects of climatological changes on the long-term dynamics, structure and composition of the Siberian boreal forest.

3.1 Introduction

There is uncertainty in forecasts of how global forests will be affected, but we know that changes in forest extent, type and structure have the potential to feedback to the atmosphere and intensify climate change at the regional, continental and even global scales (*Bonan et al.*, 1995; *Pielke and Vidale*, 1995; *Woodwell et al.*, 1995; *Cox et al.*, 2000; *Bonan*, 2008; *Jackson et al.*, 2008; *Hollinger et al.*, 2010; *Groisman et al.*, 2013; *Kuusinen et al.*, 2014). Moreover, changes in vegetation structure and composition can reduce or accelerate the rate of carbon exchange between the atmosphere and the biosphere in boreal ecosystems (*Kolchugina and Vinson*, 1995; *Krankina et al.*, 1996; *Betts et al.*, 2000; *Kumala et al.*, 2004; *Randerson et al.*, 2006; *Ma et al.*, 2012). In order to understand what changes

may be expected in a forest based on changes in environmental conditions, we have developed a new ecological model, called SIBBORK, that is robust and easily parameterized to represent dynamics of different forest ecosystems using publicly available datasets, such as the World Meteorological Organization (WMO) temperature and precipitation records, and information routinely collected in forestry surveys and reflected in forestry yield tables. The purpose of SIBBORK development rests in the desire for (1) better understanding of forest response to climate change based on tree process responses to the surroundings and (2) more explicit parameterizations of environmental conditions, which depend on the tree's position on the landscape at the smaller scale. Few gap models incorporate effects of surroundings some distance away (20-100m) on tree processes. SIBBORK can be used to investigate biome shifts and successional trajectories in forest ecosystems, to understand the likely compositional and structural changes a forest may experience with climate change, to test potential mitigation approaches, such as introduction of new species and expansion of timber plantations, assist with planning for habitat changes or shifting the economy to/from the timber sector, and assessing ecosystem services. We focus here on describing this new model, the functionality that provides advances over other models, and the testing of the model output against multi-dimensional time-series data.

3.2 Methodology

SIBBORK was developed to tease out the dependencies and interactions between trees and environmental conditions. We are interested in understanding the internal forest processes and their potential responses to disturbances, because forest structure and composition have a significant effect on how energy and carbon are cycled through the ecosystem (*Bonan et al.*, 1995; *Liu et al.*, 2005; *Bonan*, 2008; *Ashton et al.*, 2012). Due to the large extent, recent climatological changes, and potential large (spatial scale) forcings that the Eurasian boreal forest can exert on the global climate, we focused specifically on this ecosystem. Like many individual-based gap models, SIBBORK simulates the establishment, growth and mortality of individual trees on plots approximately the size of a crown of a canopy dominant tree ($100m^2$). Canopy size of each tree is limited by the plot size. However, unlike Monte Carlo type simulations of independent plots (e.g. FAREAST, *Yan and Shugart*, 2005), the plots in SIBBORK are arranged in a grid and connected to each other. Trees on each plot can interact with trees on adjacent and nearby plots through shading. The shadow of a typical canopy dominant from central Siberia (22-24m, *Simard et al.*, 2011) can extend up to 100m, depending on foliage density and sun elevation angle. Trees within a plot also interact with each other via shading of diffuse light from directly overhead as a function of cumulative leaf area above each 1m vertical level. In contrast, the shading capacity of a tree on an independent plot in FAREAST is limited to the plot size ($500m^2$). Environmental conditions are computed and specified at the plot level and reflect the edaphic, hydrologic, and climatological gradients associated with relief. Since trees do not have explicit x,y position on the landscape, the uncertainty of a tree's location on the

terrain is limited to a specific plot. Certainly, it is possible to give each tree an assigned location within the simulated domain and get rid of plot designation, however, the plots are retained for specification of environmental conditions and stem density at the plot level and for ease of aggregating stand characteristics at different spatial scales. The horizontal resolution of environmental conditions and vegetation structure is 10m X 10m, and the vertical resolution of the light environment and canopy structure is 1m. Species-specific parameterizations and generation of climate conditions synthesize our current knowledge of boreal ecosystems, climatology, and numerical modeling. This model highlights important progress in ecological modeling via simulation of 3-dimensional space above a real landscape. The model simulates the environmental conditions at the plot level, and the vertical and horizontal distribution of vegetation across a 3-dimensional landscape. This renders the model fit for the application toward simulation of what has already been observed as heterogeneous changes in temperature and precipitation across the spatial and temporal domains, and the associated response of vegetation to this spatially and temporally heterogeneous climate change.

3.2.1 Development from ZELIG

ZELIG was derived from FORET (*Shugart and West*, 1977), which is a more generalized version of JABOWA (*Botkin et al.*, 1972). It was originally developed for temperate forests of North America (*Smith and Urban*, 1988; *Urban et al.*, 1991; *Weishampel et al.*, 1996), but has since then been used in investigations of coastal forest (*Urban et al.*, 1993), dry tropical forest in Puerto Rico (*Holm et al.*, 2012), upland and bottomland forests in the arid Midwest of the U.S. (*Holcomb*, 2001), northern hardwood forests (*Larocque et al.*, 2006, 2011), and Amazonian forests (*Holm et al.*, 2014) . Like JABOWA, ZELIG is based on the assumption of landscape homogeneity at the plot level and within the simulation domain. ZELIG, however, presents one of the first departures from the standard gap model by introducing the idea of simulating several adjacent plots to represent a transect on a landscape. We substantially expanded the functionality of ZELIG (*Urban* 1990, 2000; *Urban et al.*, 1991, 1993) through modification to the 3-D light subroutine, simulation of canopy architecture and terrain representations, species-specific parameterization and specification of the simulation area and plot size. We modified the governing equations for soil hydrology and climate, and introduced species-specific allometry. The optimal diameter increment in SIBBORK is computed based on observed maximum annual diameter increments from the yield tables (*Shvidenko et al.*, 2006) and the Usolsky timber enterprise inventory (*Ershov and Isaev*, 2006), using methodology described by Bragg (2001, 2003). This is in contrast to the JABOWA-based calculation employed in ZELIG (*Botkin et al.*, 1972), which depends on a set maximum age for each species - a variable that depends on environmental conditions and is difficult to estimate. Soil hydrology in SIBBORK utilized the modified Penman equation, which incorporates solar radiation and air temperature inputs and is more appropriate for high latitude environments. Soil fertility in SIBBORK acts as a cap on gross primary productivity (GPP), and annually limits actual biomass accumulation rather than maximum potential biomass

accumulation based on optimal diameter increment computed in ZELIG (*Urban*, 1990). Soil fertility is specified at the plot level for each location based on soil type (*Stolbovoi and McCullum*, 2002) and a map of biological productivity for Russia (*Isachenko*, 1985). We built on the plasticity of ZELIG with simplified re-parameterization to different site and species characteristics using georeferenced matrices as input files for plot-level specification of environmental conditions (radiation, elevation-based temperature adjustment, soil fertility) for enhanced portability to simulation of other ecosystems.

As in ZELIG, the simulated trees in SIBBORK are fully coupled to the light environment and soil moisture (*e.g.* light affects trees, trees affect light), partly coupled to the soil fertility (soil fertility affects trees, but trees don't affect soil fertility), and uncoupled from (do not affect) air temperature. SIBBORK differs from ZELIG via modifications to how the spatial domain of the simulation is specified, the ability of the light regime to be computed above varied terrain, the computation of soil hydrology, the inclusion of permafrost and several parameterizations for tree growth and environmental conditions. SIBBORK simulates heterogeneous landscapes and different environmental conditions at the resolution of the plot, and builds more plasticity into the specification of environmental conditions and aggregation of results at different spatial scales. The enhanced simulation of the environmental conditions allow for wider application of SIBBORK, including the study of boreal forests with complex light and soil moisture regimes.

The simulation inputs include allometric equations and species-specific tolerances to environmental conditions, as well as initialization conditions, maximum stem density, climatological trajectory (stable or changing), and simulation duration. Additionally, the user specifies the simulation domain using a georeferenced digital elevation model (DEM) file. This can be artificial user-created terrain for testing purposes (*e.g.*, flat or N- and S-facing slopes along an E-W ridge), or real terrain, such as from ASTER DEM (*METI and NASA*, 2011). During pre-processing, the DEM will need to be resampled at the desired plot size. Using the DEM and environmental lapse rates, temperature is computed for each plot that is at a different elevation than the reference weather station. The ArcGIS Area Solar Radiation tool (*Fu and Rich*, 2002) is used to compute monthly incident solar radiation, and includes published cloud fraction and direct-to-diffuse radiation fraction for the simulated region, where available. Potential evapotranspiration (PET) is computed as a function of monthly temperature and solar radiation for each year of the simulation. In this manner, environmental conditions are either specified at the start or computed within the simulation at the plot level. This allows us to resolve variability in conditions associated with topographic gradients, simulate transition zones, and aggregate output at different spatial scales or via masks by terrain features, *e.g.* slope aspect or elevation.

The model can be initialized from bare ground or an initial stand conditions. Bare ground symbolizes the complete absence of any trees on the landscape and represents the conditions following a disturbance, such as an intense wildfire, clear-cutting, or a landslide. Establishment of trees into the disturbed area is assumed to occur from seeds from nearby stands. Stump-sprouting and regeneration by layering are not currently parameterized in SIBBORK. Alternatively, to

begin the simulation with a stand of a given structure and composition, initial stand conditions, including stand density and average diameter at breast height (DBH) for each species, can be specified. The establishment of saplings can be turned on or off for all or individual species, allowing the user to track the evolution of a given stand for comparison to forestry yield tables or field data. Following pre-processing and initialization, each simulated year in the simulation proceeds as follows:

1. Generate monthly average temperature and monthly precipitation sums from a Gaussian distribution based on historical monthly averages and standard deviations recorded at the nearest WMO weather station(s). Then, quality control check that the simulated monthly average temperature does not fall outside the range bound by the absolute maximum or minimum temperatures observed for the region, and flush all negative precipitation values to zero. Temperature and precipitation are simulated at a monthly time step.

2. Calculate growing degree days (GDD) from the simulated average monthly temperatures with a growing degree base of 5^oC. Compute thermal effects for each species in the simulation based on species-specific tolerances and user-specified parabolic (*Botkin et al.*, 1972) or non-linear (*Bugmann and Solomon*, 2000) response curves. GDDs use temperatures simulated at a monthly time step, and are evaluated at annual time steps.

3. Compute PET via a modified Penman equation using simulated average monthly temperature and radiation inputs. Next, estimate soil moisture based on precipitation inputs, actual evapotranspiration outputs (70% of PET for boreal, *Olchev and Novenko*, 2011), field capacity and wilting point. Runoff is computed as gravitational water above field capacity. PET, runoff, and soil moisture are computed at monthly time steps. Thereafter, determine effect of available soil moisture on growth based on species-specific drought tolerances at an annual time step.

4. Implement age-related and stress-related mortality. Individuals stressed for at least two consecutive years have a 37% chance of mortality in each subsequent year of stress (*Shugart*, 1984). Dead trees are removed at the beginning of each simulation year.

5. Determine optimal diameter increment for each species in the simulation. Optimal diameter increment represents maximum growth without environmental constraints. The optimal diameter increment for each tree is determined at the end of each simulation year based on tree size and species.

6. Compute soil fertility limitations based on a combination of the potential annual biovolume accumulation, the amount of new biovolume that can be supported by the soil quality on each plot, and species-specific soil nutrition requirements. When the annual biovolume increment exceeds the annual GPP that can be supported by the soil conditions, growth of all species on the plot is downscaled, but some species are more sensitive to this limitation. This is computed at an annual time step.

7. Determine available light for each grid block in the simulated environment above the terrain using Beer-Lambert law extinction as a function of leaf area index (LAI). Compute incident direct radiation from seven compass directions (no direct light from the north in extratropical northern hemisphere) and solar elevation angles. Assess diffuse radiation along two angles from each of eight compass directions and from directly overhead. Adjust crown base of each tree crown based on light extinction through the canopy and species-specific shade tolerances. Estimate shade-related growth limitations for each individual tree based on available light averaged across the entire crown length. The light environment is computed at the end of each simulation year.

8. Compute the realized DBH increment for each individual tree in the simulation based on the optimal diameter increment scaled down by the multiplicative effect of species-specific tolerances to environmental effects of growing degree days, available light, and the minimum of the below-ground factors (soil moisture, soil fertility, permafrost). Tree size is incremented at an annual time step.

9. Flag for possibility of stress-related mortality the individuals not realizing a species-specific threshold (%) of their optimal growth in the current simulation year due to environmental limitations. Remove stress flags from previously-stressed individuals that realize growth above a species-specific threshold (%) of their optimal growth.

10. Compute ground-level light at the plot scale based on leaf area index and light extinction through the canopy from multiple directions for direct and diffuse light. Ground-level light is computed at the end of each simulation year.

11. A "seedbank" is generated based on relative viable seed availability for species in the simulation (*e.g.*, more for Scots pine than for aspen). Using a uniform random number generator, saplings are selected from the seedbank for establishment up to a maximum stem density, which is specified at the plot level. New saplings are sprouted from the seeds selected from the species-specific relative seed bank based on species-specific ground-level light requirements and an accumulation of species-specific number of climatologically favorable years. New saplings with a DBH of $2.5cm \pm 0.25cm$ are planted within the $100m^2$ plot, without an explicit (x, y) location within the plot. New saplings are planted at the end of each simulation year.

The state variables of DBH, height of crown base, and stress flags for each individual in the simulation are carried over from year to year. Environmental forcings affect how much of the optimal diameter increment is realized each year by each individual tree. See Figure 3.1 for a conceptual diagram of the model.

I further developed the algorithm for light-ray tracing (*Weishampel*, 1994) for compatibility with independent and interactive simulation modes. Figure 3.2 shows the configuration of simulated plots on the ground for the 1-D and 3-D simulations of the light environment and the associated ray traces. To provide continuity in the generation of the 3-D

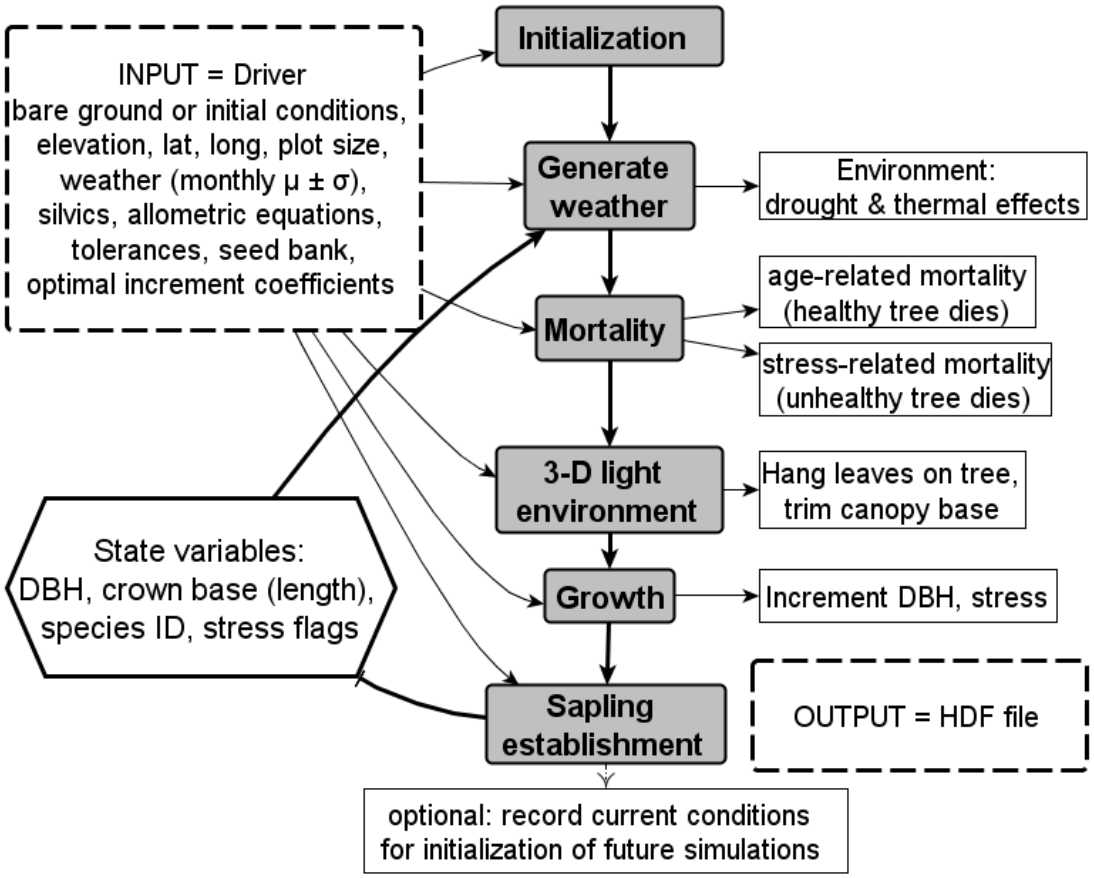

Fig. 3.1: Conceptual diagram of process flow in SIBBORK. Pre-processing includes analysis of climatological, radiation and edaphic factors for the location of interest and generation of topography and associated gradient matrices using ArcGIS. Weather is generated at the monthly time step. State variables are updated annually. HDF output file contains a record of state variables at user-specified increments. Height (m), basal area (m^2), biovolume (m^3), foliar biomass (t), above-ground biomass (t), above- and below-ground biomass (t), and leaf area (m^2) are computed at the individual level from DBH during post-processing, and aggregated at the user-specified scale.

light environment in the interactive simulation mode, the westernmost edge of the simulation grid is wrapped around to the easternmost edge, and the southernmost edge of the grid is wrapped around to the northernmost edge, creating a torus. In this manner, edge effects are eliminated and a tree located in the westernmost plot, for example, can still cast shadows to the southwest, west, and northwest by wrapping this shadow around to the easternmost edge of the simulation grid (Figure 3.3). To avoid numerical instability during edge-to-edge wrapping, the user should specify a spatial domain wider and longer than the maximum shadow length during the growing season at the latitude of interest. In contrast, in the 1-D simulation mode, independent plots are collocated and the light ray is not wrapped around. The light is only computed from directly overhead, which limits the shade cast by the canopies to the plot they are on. However, light is arguably the most important driver of forest dynamics (*Purves et al.*, 2008; *Purves and Pacala*, 2008). SIBBORK is able to resolve the spatial interaction between light and vegetation, including height-structured

competition, via this 3-D light subroutine. SIBBORK is therefore the logical model for simulation of boreal forest, which has a unique light regime.

The 3-D light environment is comprised of a 50m-thick slice of the atmosphere above the grid of plots. Light is diminished through shading by (1) terrain and (2) surrounding canopy. On a landscape, higher south-facing slopes receive more light than north-facing slopes and valley bottoms throughout the growing season due to terrain shading. Furthermore, SIBBORK computes direct and diffuse radiation as light travels through and below the canopy within the simulated space above the simulation grid. The 3-dimensional light computation is spatially-explicit, as the light environment at each location in the canopy is affected by foliage density and forest structure at adjacent and nearby locations within the canopy, both vertically and horizontally. The shading effect is computed based on the cumulative 3-D canopy of all trees on one plot, however, the cumulative leaf area and its vertical distribution on a plot $100m^2$ in size is mostly determined by 1-2 canopy dominant trees. Within a forest, light along a ray trace is likely to diminish due to LAI before reaching the distance of maximum shadow length.

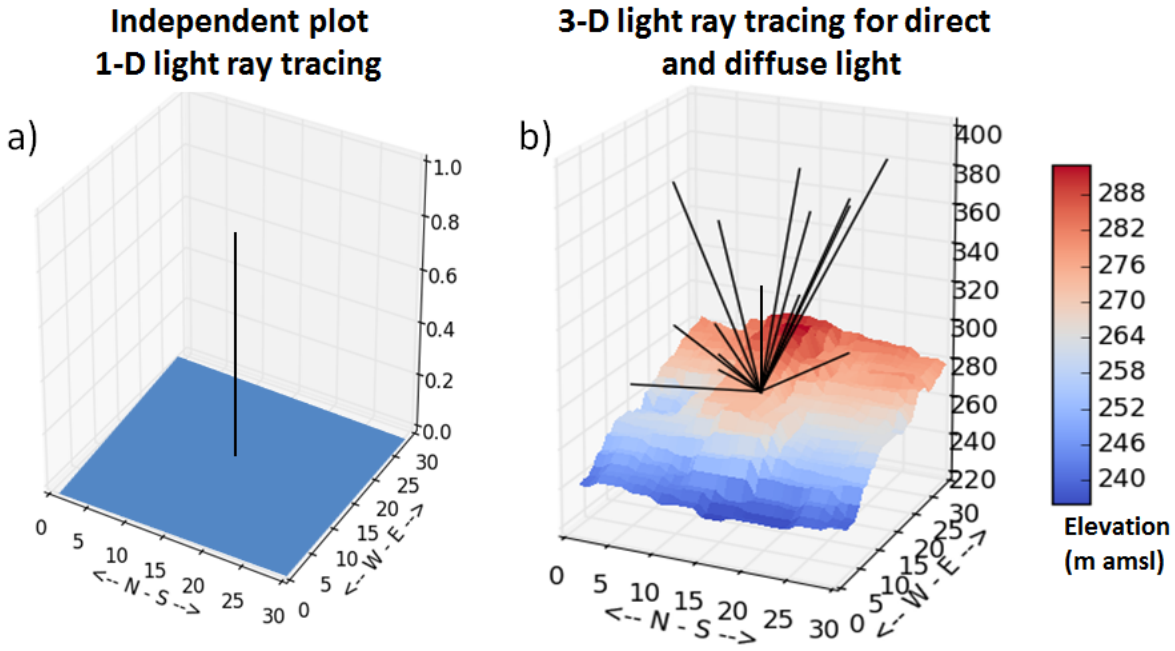

Fig. 3.2: Comparison of 1-D and 3-D light subroutines in dynamic vegetation models. (a) In non-spatially-explicit simulations, such as the 1-D mode of SIBBORK or Monte Carlo style simulations of independent plots at point locations, the light is only computed from one direction - directly overhead. (b) In our spatially-explicit simulation, the direct light is computed from 7 compass directions (no light directly from the north in the northern hemisphere), and the diffuse light is computed from an isotropic sky from 8 compass directions and from directly overhead.

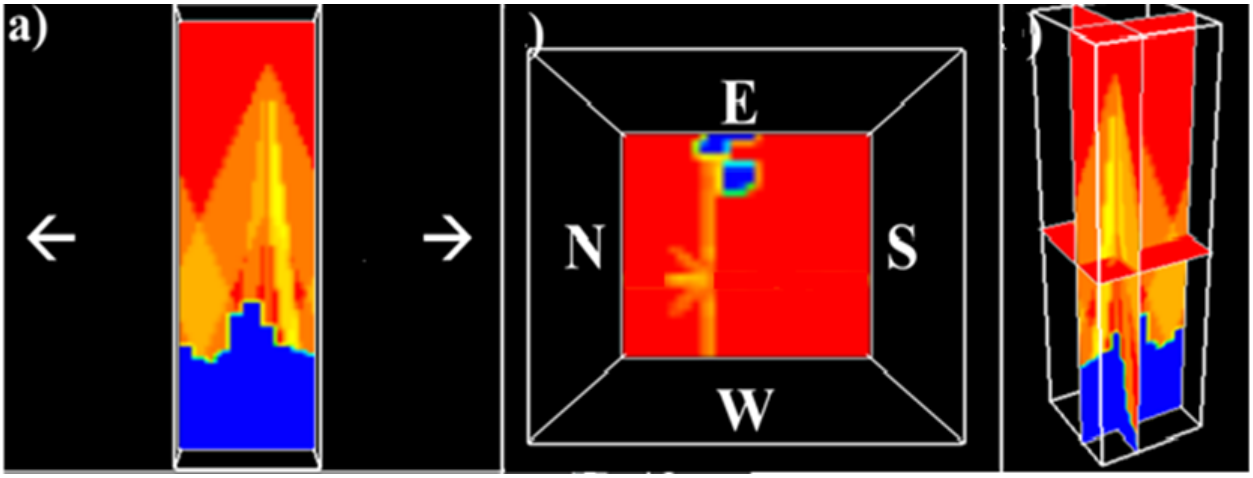

Fig. 3.3: Over the course of the growing season, a single 20m tree casts a shadow in different directions. The shadows to the northeast, north, and northwest are generally shorter than the shadows to the east and west, because the solar angle in the southwest, south, and southeast is greater. (a) A slice through the E-W plane. Full (100%) light (red), no light in the regions below terrain (blue), and varying degrees of shade (yellow, orange) from a single 20m tree along the direct light ray traces. Edge wrapping eliminates edge effects, here from E to the W edge. (b) View from above: shade along 7 directions and wrap-around of shade that the tree casts to the E and W. The shadows to the southeast and southwest are not significant during the growing season, so only 5 significant shadows (yellow) are seen from above. The shadows cast to the east and west are similar in length, however, due to the positioning of the tree within the simulation grid, the shadow to the west should extend past the westernmost edge of the simulation domain. The remainder of this shadow is wrapped around to the easternmost edge and enters the simulation space from the east, in this case, overlapping with the shadow cast by the tree to the east. (c) Synthesis of (a)-(b) for a 3-D view of the terrain and light environment above the simulation area.

The annual optimal diameter increment has been modified following methodology in Bragg (2001, 2003). Annual diameter increment (ADI) curves were fitted for each species in the simulation using equation form presented in (3.1)

$$OI = a \times DBH^b \times c^{DBH} \tag{3.1}$$

where OI is the optimal diameter increment (cm), DBH is in cm, and a, b, and c are species-specific coefficients. The approximation of the optimal ADI in ZELIG (*Urban*, 1990) and JABOWA (*Botkin et al.*, 1972) individual-based gap models is based on the assumption of a maximum tree age, which is difficult to estimate. Additionally, the formulation assumes no tree growth occurs past the maximum age. The Bragg formulation does not constrict tree growth to an estimated maximum age, but does significantly reduce vigor for older trees. Removing the maximum tree age assumption allows for trees in favorable environmental conditions to continue growing and accumulating carbon, as supported by Luysseart *et al.* (2008). Figure 3.4 compares the Bragg and JABOWA-based formulations.

For each species, the ADI curves based on Usolsky inventory reflect an annual increment approximately double the magnitude of the ADI from forestry yield tables. Yield table values represent regional averages. The Usolsky inventory reports averages from smaller areas, some of which may be representative of microclimates, in which some species

experience enhanced productivity. We assumed that the optimal ADI, not affected by environmental factors, will be greater than even the maximum observed ADI from the Usolsky forest. The adjustment coefficient between largest observed ADI reflected in the forestry yield tables and the ODI in SIBBORK was determined iteratively for each species and varied between 1.2 and 5.0.

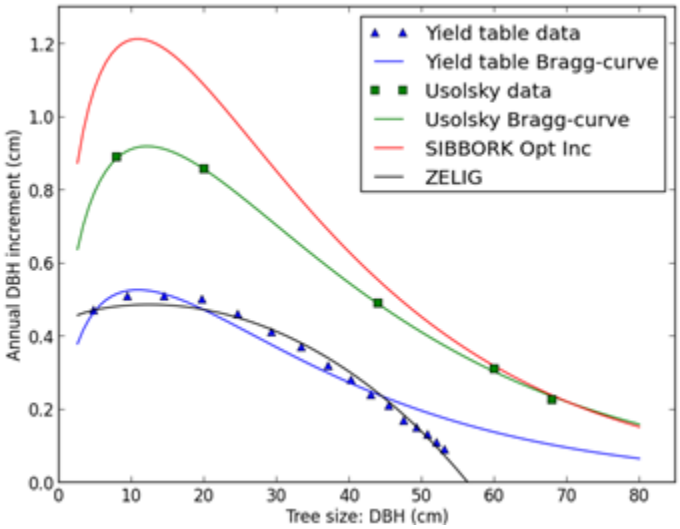

Fig. 3.4: The difference in parameterization of the annual ODI in ZELIG and SIBBORK is demonstrated by the black and blue lines, respectively. Here, *Pinus sylvestris* growth is shown as an example. The black triangles and a fitted Bragg-curve (blue) show the average observed ADI, as represented in regional forestry yield tables. The green squares and the fitted Bragg-curve (green) denote the maximum observed diameter increments in Usolsky. These values are averaged across a smaller area, and may capture some pockets of microclimates where Pinus sylvestris has achieved greater annual growth. The red line represents the annual ODI parameterized in SIBBORK based on iterative adjustment of a multiplier coefficient for the ADI from the yield tables.

Species-specific allometric equations in SIBBORK represent fitted relationships for height, biovolume, and biomass as functions of DBH (shown for Siberian fir in Figure 3.5). Some relationships are conveyed as piece-wise functions to preserve realism. In ZELIG, allometric equations for each species followed the same form and no piece-wise equations were used.

In contrast to the ZELIG estimation of leaf area as a function of DBH, the leaf area calculation in SIBBORK utilizes species-specific conversions from foliage biomass to leaf area following the method described by Breda (2003):

$$LA = B_f \times SLA \tag{3.2}$$

where *LA* is leaf area (m^2), B_f is foliage biomass (kg), and *SLA* represents published specific leaf area values for each species ($m^2 kg^{-1}$). Foliage biomass was empirically-derived as a species-specific function of DBH based on forestry yield tables.

Species	Height	Above-ground biomass (t/tree)	Biovolume (m^3/tree)
Abies sibirica	For DBH $\leq$ 30cm: $-0.0081dbh^2+1.0456dbh+1.37$ ($R^2 = 0.9967$) For DHB $>$ 30cm: $5.7405\ln(dbh)+7.85$ ($R^2 = 0.9929$)	$0.0001dbh^{2.3813}$ ($R^2 = 0.9975$)	$0.0001dbh^{2.5371}$ ($R^2 = 0.9993$)

Fig. 3.5: Species-spSpecies-specific allometric equations in general follow polynomial or exponential forms for each species, but piece-wise functions describe growth better for structural forms of some species and include logarithmic functions for older trees. Species-specific allometric equations were derived by fitting lines of best fit to regional yield table data from Shvidenko *et al.* (2006).

Finally, in ZELIG, PET was computed via the Thornthwaite-Mather equation (*Thornthwaite and Mather*, 1957). However, the Thornthwaite equation has not been validated for the calculation of PET at high latitudes above 50^oN (*Botkin*, 1993), and correction factors are not available for those regions. For this reason, a modified Penman equation (3.3) was utilized for the computation of PET in SIBBORK for the boreal forest:

$$a \times (T_a + b) \times \frac{S_t}{\lambda} \tag{3.3}$$

where λ is the latent heat of vaporization (2430 Jg^{-1}), a and b are coefficients with typical values of 0.025^oC^{-1} and 3^oC, respectively, T_a is the average monthly air temperature (^oC) and S_t is the solar radiation (Wm^{-2}) computed in GIS at the plot level (*Campbell, 1977*). This approach allows for representation of hydrological gradients in SIBBORK based on terrain slope and aspect.

Specific regional forestry yield tables for the southern taiga ecotone in central Siberia were utilized for parameterization of SIBBORK (Figure 3.6). Species-specific equations for (above-ground) biovolume were derived from the regional forestry yield tables with greatest productivity (*i.e.*, site index I), as it is expected that the tree growth in the model will be throttled back by resource limitation during simulation on less productive sites. Allometric equations for computation of foliage biomass, above-ground biomass, as well as above- and below-ground biomass were derived from forestry tables of biological productivity.

Species in Simulation			Regional forestry yield table used for parameterization	Reference (within *Shvidenko et al.*, 2006)
Latin name	Common name	Species Code		
Abies sibirica	Fir	ABSI	Fir stands of mountain ecoregions of the Central Siberian Plateau	Falaleev et al., 1975
Larix sibirica	Larch	LASI	1) Larch stands of maximal productivity in Middle Siberia (ecoregions of middle and south taiga); 2) Larch forests of Yenisei Krjazh and south of Krasnoyarsk kray (ecoregions of mountain taiga forests and subtaiga); 3) Larch forests of Angara River basin (ecoregions of middle and south taiga)	Semechnkin, 1990; Falaleev et al., 1975
Betula spp	Birch	BEPE	Birch stands in south and middle taiga ecoregions of Siberia	Goncharuk et al., 1997
Pinus sibirica	Siberian cedar	PISI	1) Fully-stocked mixed cedar forests of the Central Siberian Plateau; 2) Mixed cedar stands of Central Siberian Plateau	Semechnkin, 1990
Pinus sylvestris	Scotts Pine	PISY	Fully-stocked pine stands in middle taiga, south taiga, subtaiga and forest steppe ecoregions of Central and East Siberia	Motovilov, 1966; Falaleev & Polyakov, 1969; Falaleev et al., 1975; Kozlovsky & Pavlov, 1967
Picea obovata	Spruce	PIOB	Fully-stocked spruce forests of Middle Siberia (ecoregions of southern and middle taiga)	Falaleev et al., 1975; Goncharuk et al., 1997
Populus spp.	Aspen	POTR	1) Fully-stocked aspen stands of Central and East Siberia (ecoregions of middle and southern taiga); 2) Aspen stands in south taiga ecoregions of Central Siberia	Falaleev et al., 1975; Falaleev et al., 1976

Fig. 3.6: Description of regional forestry yield tables used for the parameterization of SIBBORK. Whenever multiple yield tables are listed, the tables with maximum productivity were used to derive the allometric equations for the species.

3.2.2 Model Testing

Following a stand-replacing disturbance, numerous saplings regenerate on bare ground. This stage in succession corresponds to a rapid increase in biomass accumulation. As the saplings grow, peak biomass is attained before the competition for space, light and other resources results in natural thinning and a decrease in stand biomass via mortality of trees from the initial cohort. As new gaps in the canopy open up due to tree mortality, new saplings regenerate in the gaps. Eventually, equilibrium is reached between regeneration and mortality, resulting in the stabilization of stand biomass, basal area, and biovolume - this defines the mature or equilibrium forest. Figure 3.9 shows this behavior for biovolume of a larch stand initialized from bare ground. During model testing, we assessed SIBBORK's ability to reproduce these stand dynamics via verification and validation tests.

Verification of the model involves the comparison of model output to the data on which it was "trained" - which was used for parameterization of the model and creation of input files for the simulation. Verification assesses how well the numerical model aligns with the conceptual model (*Cale et al.*, 1983). In this case, the conceptual model includes the assumptions that tree establishment, growth, and mortality depend on the light environment, climate and soil conditions. This simplified model quantifies the dependencies of each species on these four environmental factors, and adjusts growth based on species-specific tolerances to resource limitations.

Conversely, a model can be validated by comparing the model output to an independent data set, information from which was used to initiate the model, but which was not employed in parameterization. Validation tests the accuracy of the concept map and how well the model can be generalized to new scenarios, environments and locations. The model may need to be revised several times in order to achieve the desired accuracy and realism in representation of forest growth and responses, and to better match the computer simulation to the concept map of the forest processes, feedbacks, and interactions (*Cale et al.*, 1983).

Usually, model verification and validation are conducted by comparing model output from a given year of simulation (or a time-average) to a dataset that represents a "snapshot" of the forest conditions at a given time. A stronger test is the comparison of model output to data that represents a timeseries and reflects how the structure of a stand changes over time (*Bugmann*, 2001). Verification and validation of SIBBORK employed this stronger test. SIBBORK output was evaluated against multi-dimensional empirical timeseries. Plot-level output was spatially averaged across a 9-ha simulation domain and compared to field data at specific time increments. Averaging across 150 independent simulation replicates enhanced statistical validity of model output (*Bugmann et al.*, 1996). Only flat terrain was simulated for model calibration and testing.

Model Verification

The forestry yield tables used for verification contain species-specific data on regional average DBH (cm), height (m), stem density (stems/ha), basal area ($m^2 ha^{-1}$), biovolume ($m^3 ha^{-1}$), and biomass (t/ha) at decadal or 5-year increments, for 100-300 years of tree growth. Mature forests and old growth are generally not represented in forestry yield tables, so this dataset could only be used to verify relatively young forest structure, for stands that have not yet peaked or stabilized in biomass (see Figure 3.9). The "young stands" column in Figure 3.7 corresponds to the time frame used for verification comparison between model output and forestry yield table data for each species. The model was initialized from the same initial conditions (average DBH, stem density) as the first record in the yield table for the species (Figure 3.8). Thereafter, estimated growth of individual trees was compared to observed growth at 5- or 10-year increments, depending on data record, using linear regression on the three variables that represent forest structure: average DBH, height, and stem density. Stand aggregate basal area, biovolume, and biomass are functions

Species	Young stands	Maximum bio-volume	Stabilized bio-volume	Maximum age for species (1% survive to this age)
(units)	(age in years)	(years in sim)	(year in sim)	(age in years)
Abies sibirica	< 80	100-110	> 270	300
Larix sibirica	< 50	70-80	> 240	400
Betula pendula	< 30	35-45	> 100	120
Picea obovata	< 60	80-90	> 280	500
Pinus sibirica	< 60	75-85	> 210	400
Pinus sylvestris	< 70	90-100	> 240	300
Populus tremula	< 30	40-50	> 80	100

Fig. 3.7: Timeframe definitions for "young" stands and "mature" stands were obtained from monospecies simulations of 1000 years in duration. Between young and mature stands, a peak in biovolume is observed in the simulation and in natural forests, however, this peak is not represented in forestry yield tables likely due to management practices, and is only specified here for simulated dynamics. Mature stands are those with stabilized biovolume, biomass, and basal area. This timeframe was used for model verification against the Usolsky forest inventory. :math:'*' Maximum species age values were obtained from Nikolov and Helmisaari (1992).

of DBH and stem density, so if the structure of the forest is simulated appropriately, the stand aggregate information is more likely to also compare well to observations.

species	Initial DBH	Initial stem density
(units)	(cm)	(stems per ha)
Abies sibirica	3.8	7300
Larix sibirica	11.3	2200
Betula spp.	6.5	2400
Picea obovata	8.8	900
Pinus sibirica	9.8	2700
Pinus sylvestris	4.8	13500
Populus spp.	5.0	7800

Fig. 3.8: Initial conditions from the first year of record of the forestry yield tables (*Shvidenko et al.*, 2006) used to initialize model for verification testing.

Model validation

To assess that the predictive capability of the simulation continues from young into mature forests, simulated and observed biovolume from mature forest stands were compared using linear regression. Model validation employed an independent dataset from the Usolsky forest enterprise (*Ershov and Isaev*, 2006), containing average age, DBH, height, and biovolume for polygons with homogeneous canopy composition (*i.e.*, same dominant species). Space-for-time substitution was used to generate a timeseries dataset for quantitative evaluation of the simulated mature boreal forest characteristics. The Usolsky forest is managed, and the histories of the stands within the enterprise are not known (*i.e.*, thinning, logging schedule, natural disturbances).

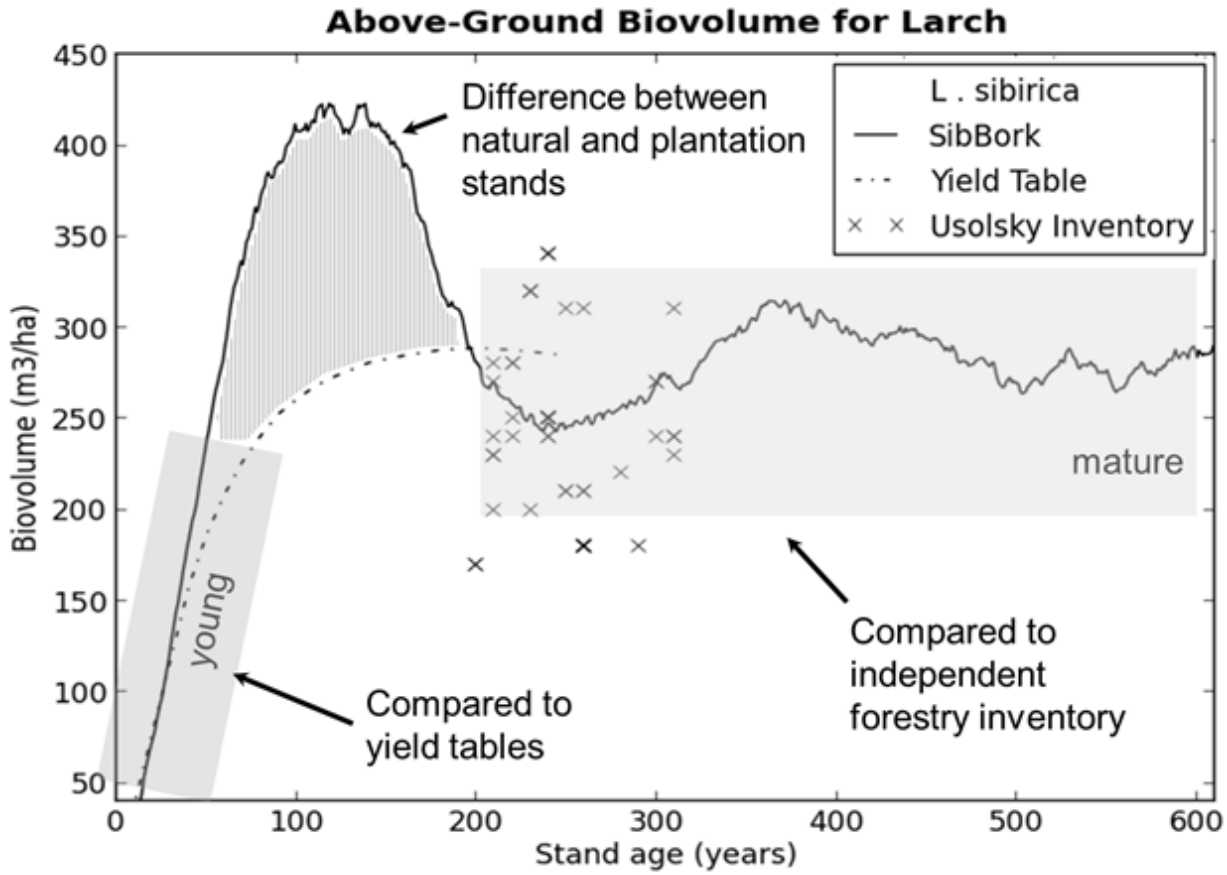

Fig. 3.9: Typical biovolume accumulation pattern after a stand-replacing disturbance, here for Larix sibirica, is shown here via the solid line, and was obtained by spatially averaging output from 900 plots in the simulation domain and across 150 independent model runs initialized from bare ground. Dash-dot line represents biovolume accumulation presented in a forestry yield table for larch. "Young" stands were defined as stands at less than 30% of the maximum age for the species. This timeframe is shaded in a tilted rectangle along the left side of the figure, labeled "young". Stand structure characteristics (DBH, height, stem density) of young stands were verified against forestry yield tables via linear regression. Equilibrium stands were defined as those with stabilized basal area and biovolume. This time frame is shaded in a rectangle along the right side of the figure, labeled "mature". Stand structure (DBH, height, stem density) and aggregate (basal area, biovolume) characteristics of mature stands were validated against an independent dataset from the Usolsky forest timber enterprise via non-parametric Smirnov-Kolmogorov test and linear regression. The region shaded under the peak denotes the difference in biovolume accumulation patterns between natural and managed plantation stands.

For each monospecies simulation, the model was initialized from bare ground. Sapling establishment was turned on only for the species of interest. Spatially averaged (across the simulation area of 9-ha) biovolume was recorded at ten year intervals during the "mature" timeframe from 150 independent replicate model runs and assessed against biovolume records from the Usolsky forest inventory for areas with corresponding dominant species and average age.

The more interesting analysis, of course, is for mixed forest. Records of mixed forest characteristics are available for several species combinations in the yield tables, Usolsky inventory, and in the literature (*Petrov and Ponomareva*, 1977; *Reimers*, 1990; *Shugart et al.*, 1992a; *Roser et al.*, 2002; *Schulze et al.*, 2005; *Chen et al.*, 2005). For each comparison, only the species present in the observed forests were included in the simulation. Whenever initial conditions were provided, the model was initialized from those initial conditions. Otherwise, the model was initialized from bare ground. The timing and magnitude of successional transitions from pioneer to equilibrium species was qualitatively evaluated. The basal area, biovolume and biomass of simulated forests at decadal increments were quantitatively evaluated against available data.

Model Generalizability

The model's generalizability was tested using observations from three types of forest stands at a middle taiga site, which is located outside the calibration region and has different soil characteristics, climate and radiation budget than the southern taiga ecotone represented in forestry yield tables or the Usolsky forest. Antonio *et al.* (2007) suggest that allometric relationships are not affected by stem density, climate, or site index, therefore, these relationships were left unchanged in SIBBORK for the generalizability test, however, there is new evidence that the allometric relationships are changing in regions of Siberia (*Lapenis et al.*, 2005), and the static allometry may be a limitation of the model when it is applied to investigate stands outside of the calibration region or to climate sensitivity analysis. Site characteristics are reported in the bottom row of Figure 3.10.

The observed forest types at the middle taiga location include a birch-dominated 50-year old stand, a mixed forest with an estimated age of 250 years, and a 400-500 year old forest dominated by 200-year old fir. The mixed forest contains fir, birch, spruce, Siberian cedar, and species from the *Sorbus* genus. The latter, are not parameterized in the model, as mountain ash, rowan, and other species of the *Sorbus* genus are not considered economically viable and are, therefore, not represented in forestry yield tables or forest inventories. The model was initialized from bare ground, with regeneration turned on for all the species present in the mixed forest described by Roser *et al.* (2002). We evaluated the projections of average DBH, height, stem density, basal area, and species composition for each of the three types of stands.

Characteristic	middle/southern taiga	middle taiga
Lat. (N)	57.6	61.0
Long. (E)	95.4	89.5
Alt. (m amsl)	180	180
Plot size (m^2)	100	100
Mean Monthly Temperature (^oC)	-21.1 to +18.6	-23.2 to +18.5
Mean Monthly Precipitation (mm)	13.03-62.29	30.9-84.2
Soil Field Capacity (cm)	41.0	62.5
Soil Wilting Point (cm)	20.5	31.25
Mean Monthly Radiation (Wm^{-2})	115	115
Mean Monthly Radiation (Growing Season) (Wm^{-2})	176	166
Relative Direct : Diffuse Solar Radiation (Growing season) (%)	47:53	45:55

Fig. 3.10: Site parameters for the Usolsky forest (southern taiga), located near the confluence of the Angara and Yenisei Rivers in southern Krasnoyarsk Region, Russia, and the climatological and radiation parameters for the middle taiga site described by Roser et al. (2002), used to test model generalizability. The climate parameters were computed based on data from the Yenisejsk and Turukhansk World Meteorological Organization stations, respectively. Ranges represent monthly low and high averages. Soil characteristics were obtained from Stolbovoi and Savin (2002). Field capacity was computed as Œ of Total Available Water Capacity (cm), and wilting point corresponds to œ of field capacity (cm) in the top 1 meter of soil, using methodology from Shuman (2010). The radiation parameters were computed using Area Solar Calculator in ArcGIS (Fu and Rich, 2002) and validated against World Radiation Data Centre datasets from Vanavara (60° 12' N, 102° 10' E) and Ekaterinburg (56° 29' N, 60° 23' E) stations. These environmental parameters represent the difference between the simulation of southern and middle taiga in central Siberia.

3.2.3 Site Descriptions

The region's continentality, extensive snow cover, unique light regime, and the influence of the Siberian semi-permanent high pressure system and the continental arctic air masses facilitate the extreme cold winter temperatures. The rest of the year, continental temperate and continental tropical air masses bring little precipitation to the region (*Lydolph*, 1977; *NCDC*, 2005a, b). Annual PET demands regularly match and in some regions exceed annual precipitation (*Shugart et al.*, 1992a; *Yamazaki et al.*, 2004). In general, throughout the short growing season, there is either not enough heat or moisture, or both, to support most arboreal species, resulting in a floristically-simple ecosystem dominated by frost-hardy trees.

Training Region

Shvidenko *et al.* (2006) present a compilation of several hundred yield tables for natural, fully-stocked, managed and unmanaged, single-species and mixed-species forests across various regions of Eurasia. The yield tables are applicable for specified regions where the terrain can be described as flat or nearly-flat (less than 20o slope). Highest productivity yield tables for each species predominantly for the southern taiga ecotone were used for parameterization of the model.

Validation Site

The validation site (57° 36' N, 95° 23' E) is within the boundaries of the Usolsky Forest Enterprise located in southern taiga, at the confluence of the Yenisei and Angara rivers (*Ershov and Isaev*, 2006). This site will from hence forth be referred to as the Usolsky forest or the southern taiga location. The topography of the Usolsky forest is representative of the lower slopes of the central Siberian uplands, with elevation ranging from 95 to 460m amsl.

A continental climate with short, warm, dry summers, and long, dry, cold winters characterizes this region of central Siberia. Mean annual air temperature is -1^oC. The average annual precipitation is 410 mm, with a minor wet season occurring in June-August (WMO data analysis, *NCDC*, 2005a, b). Annual evapotranspiration rates are in the range of 500-700 mm (*Yamazaki et al.*, 2004; MOD16 Global Terrestrial Evapotranspiration dataset) and exceed average growing season precipitation, indicating that soil thaw and the thawing of the active permafrost layer are important sources of soil moisture in central Siberia. Areas of insular permafrost underlay southern taiga, however, no detailed information is available regarding presence of permafrost at the validation site within the Usolsky forest. Figure 3.10 lists additional site parameters.

The Usolsky forest inventory was collected in 1992 by an East-Siberian Forest Inventory Enterprise and compiled into a GIS dataset, which includes average age, DBH, height, and dominant species for over 120,000 irregularly-shaped polygons ranging in sizes from $34m^2$ to tens of hectares. Polygons are grouped by dominant species, so that each polygon represents only one canopy dominant species. Subcanopy species are recorded for some polygons. The vegetation in the Usolsky forest varies based on the logging rotation, with significant areas of closed-canopy taiga. Ten primary arboreal species within six genera comprise the forest: Betula *spp*. and Populus *spp*. are found along higher elevation slopes and in areas of recent disturbance; *Picea obovata*, *Abies sibirica*, and *Pinus sibirica* generally occupy the moist soils on north-facing slopes, and along rivers and stream drainages; while *Larix sibirica* and *Pinus sylvestris* are found on poor soils at higher elevations. The minimum average DBH recorded is 2cm. At the time of inventory, the stem densities ranged 3,000-10,000 stems/ha, with maximum stem densities observed in stands dominated by Abies sibirica. The basal area in Usolsky ranged from 16 to 320 m^2ha^{-1}. When only canopy dominant trees were considered, the average tree age in the Usolsky forest was 107 years, the average height was 20.3m, and the average DBH was 24cm. The average tree age on each polygon was reported to the nearest 5 years, average DBH - to the nearest centimeter, and average height - to the nearest meter. Biovolume was specified for < 20% of the polygons in the survey. In 1992, the average biovolume within Usolsky was 183 m^3ha^{-1}, with up to 510 m^3ha^{-1} of above-ground biovolume accumulated on the most productive sites along river banks in stands dominated by old growth (>100 years old) *Pinus sylvestris*.

New Location Site

We tested the generalizability of the model by applying it to the simulation of vegetation at a location 600km north-northeast of the Usolsky forest without additional tuning of model parameters. This site experiences colder winters, and a similar, though wetter, growing season regime compared to the Usolsky forest. Figure 3.10 reflects the differences in climate, radiation budget, and soil characteristics between this middle taiga site and the Usolsky forest location.

3.3 Results

3.3.1 Verification

Figure 3.11 and Figure 3.12 summarize the significant agreement between observed early stand development in Siberia and the evolution of the young monospecies stands in the simulation over the course of several decades. The stand structure, assessed through DBH, height, and stem density, is accurately projected, with high Pearson correlation coefficients for the linear regression on all three variables (range: 0.93-0.99) for the seven species in the simulation. Regression slopes for the major stand structure variables approached unity (μ±s for DBH: 0.92 ± 0.1; height: 0.96 ± 0.05; stem density: 0.95 ± 0.05). Regression line intercepts were close to zero for height and DBH, and 19.3 for stem density. The intercept for stem density is not expected to be close to zero, since the model simulation for this comparison was not run long enough to have all trees in the simulation die. The simulated self-thinning process and the associated decrease in stem density as the stand matures compared well to the forestry yield table data.

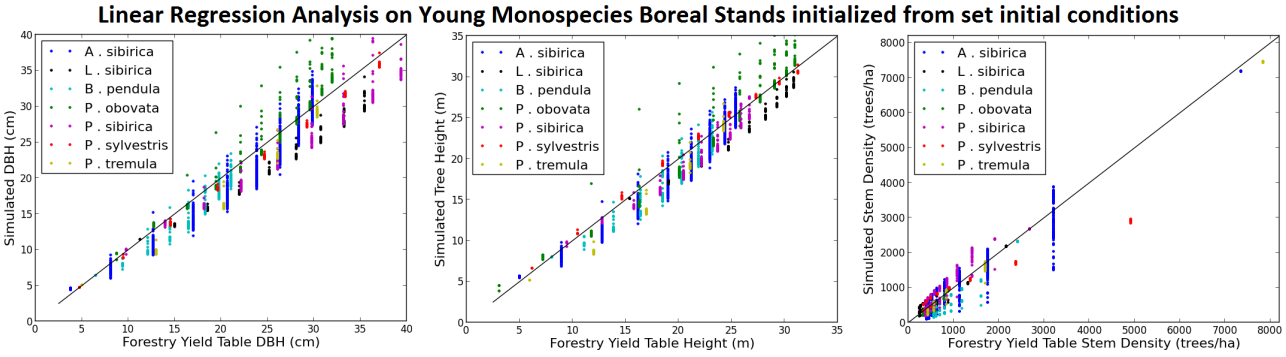

Fig. 3.11: The model reproduced biovolume accumulation patterns for thousands of trees of different species with reasonable accuracy

species	DBH	Height	Stem density
Abies sibirica	R^2=0.955, N=1350, RMSE=1.8	R^2=0.96, N=1350, RMSE=1.35	R^2=0.98, N=1350, RMSE=288
Larix sibirica	R^2=0.99, N=1062, RMSE=0.59	R^2=0.97, N=1062, RMSE=0.7	R^2=0.97 N=1062, RMSE=94
Betula spp.	R^2=0.96, N=1200, RMSE=0.89	R^2=0.96, N=1200, RMSE=0.9	R^2=0.946 N=1200, RMSE=117
Picea obovata	R^2=0.94, N=363, RMSE=2.0	R^2=0.96, N=363, RMSE=1.9	R^2=0.95, N=256, RMSE=39
Pinus sibirica	R^2=0.962 N=350, RMSE=2.6	R^2=0.97, N=350, RMSE=0.9	R^2=0.925, N=350, RMSE=203
Pinus sylvestris	R^2=0.998, N=450, RMSE=0.5	R^2=0.997, N=450, RMSE=0.4	R^2=0.97, N=450, RMSE=641
Populus spp.	R^2=0.97, N=350, RMSE=1.5	R^2=0.97, N=350, RMSE=1.27	R^2=0.999, N=350, RMSE=73

Fig. 3.12: Results of linear regression on the main stand structure variables show a high correlation between output from 150 model replicates and observed values (from forestry yield tables). The Pearson correlation coefficients are for regression not forced through the origin. The sample size varies between species due to different stem densities specified in the initial conditions.

3.3.2 Validation

The range and overlap of the biovolume distributions demonstrate that the structures of the simulated monospecies stands were very similar to the observed mature stands (Figure 3.13). As the generalizability of the model should not be sacrificed to obtain a perfect match with a single validation dataset, we evaluated the robustness of the simulation via linear regression on simulated, spatially-averaged biovolume against observed monospecies stands in Usolsky forest (Figure 3.13h). The model reproduced biovolume accumulation patterns for thousands of trees of different species with reasonable accuracy (average R2=0.83, RMSE=30 $m^3 ha^{-1}$, slope=0.97, intercept=20).

In the assessment of dynamics in a mixed stand containing larch, fir, Siberian cedar, and birch (*Semechkin*, 1990, in *Shvidenko et al.*, 2006), simulated forest composition changed from a birch-dominated forest to one dominated by pine over the course of three centuries (Figure 3.14 top panel). The same successional transition was reproduced by SIBBORK using two approaches: (1) starting with the same initial conditions as the first year of record in the forestry yield table, and (2) starting from bare ground. Throughout the simulation, fir and larch consistently contributed 5-15%

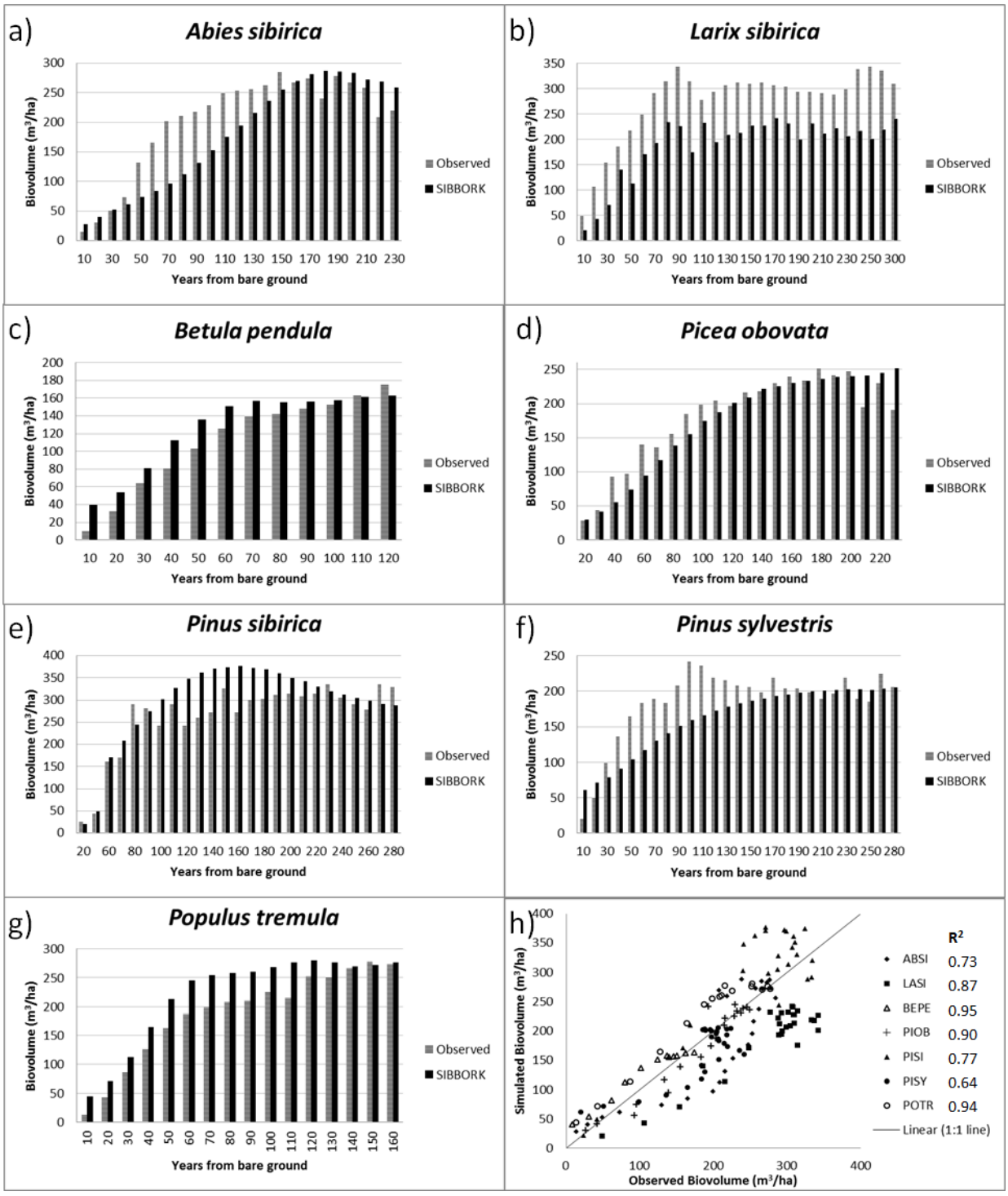

Fig. 3.13: (a-g) Simulated and observed biovolume distributions for the seven major species included in the SIBBORK simulation of central Siberian boreal forests. Good overlap of distributions is more important than differences identified by the Smirnov-Kolmogorov test, as the model is not intended to simulate just the test site, but needs to be generalizable across the broader region of Siberia. (h) Linear regression analysis reveals a strong relationship between simulated and observed timeseries of biovolume for mature stands at decadal time steps, with slope near unity and R^2 > 0.64 for all seven monospecies stands.

to the overall biomass of the forest. Presented in Figure 3.14 are the averages from 150 replicates, however, even a single model run reproduces the successional transition along the appropriate pathway and at appropriate times. The simulated structure of this mixed stand closely tracks the observed structure of the stand: average height of 25m and 24m, basal area of $44m^2ha^{-1}$ and $40m^2ha^{-1}$, and biomass of 280t ha^{-1} and 260t ha^{-1} during the timeframe of 250-300 years from disturbance for observations and simulation output, respectively, on site index III soils, which have an approximate GPP of $7m^3ha^{-1}yr^{-1}$.

The most interesting feature of the SIBBORK model is the ability to simulate heterogeneous stands of mixed-age mixed-species forests. In the 7-species mixed forest simulation, the environmental conditions and species-specific tolerances to resource limitations dictated which species established when, if at all. The successional trajectory, reflected through biomass changes for different species, is depicted in Figure 3.14 (middle panel) and compares well to literature descriptions of the forests at different stages of succession in the same region (*Petrov and Ponomareva*, 1977; *Reimers*, 1990; *Schulze et al.*, 2005). The realism of biomass dynamics and successional transitions in a 1000-year simulation was assessed using potential natural vegetation of the central Siberian region. The transition between pioneer and equilibrium species in the simulation occurred at the appropriate time from disturbance (*Roser et al.*, 2002; *Shvidenko et al.*, 2006), as shown in Figure 3.14. Initially, birch dominated the simulated landscape (180m amsl, flat), as expected. Starting around the sixth decade of the simulation, birch is gradually superseded by larch and pine. Thereafter, a mixed broadleaf/conifer forest existed briefly one and a half centuries post disturbance. By year 200, the forest was comprised predominantly of larch and pine. Larch in Siberia coexists predominantly with pine (*Pinus sylvestris*), because the foliage of both species is light enough to facilitate coexistence of these two shade-intolerant species. The larch/pine forest is replaced by dark conifers (Siberian cedar, fir, spruce) three centuries post disturbance. Canopy structure of dark conifers facilitates the trapping of light, so the forest floor is dark and pioneer species are not able to return until large enough gaps are formed (mortality of dominant trees on several adjacent plots). Sufficient mortality of dark conifer species is observed approximately four centuries post disturbance, and the larch/pine forest returns, with few birches growing in areas with particularly large gaps. Over the course of the 1000 year simulation, two cycles of larch/pine forest replacement with dark conifers occurred in the current version of SIBBORK, which does not include disturbance.

Total biomass was computed using biovolume and species-specific and, where available, region-specific bulk density values from the literature (*Curtis et al.*, 2000; *Yatskov et al.*, 2003; *Seedre et al.*, 2013). Total biomass of mature mixed forest averaged across 150 replicates and across five levels of soil nutrition (site indices) was 104.3 ± 30.1 (t ha^{-1}), which compares well with 99.61 ± 48.53 (t ha^{-1}) reported for the region near the confluence of the Angara and Yenisei Rivers (*Houghton et al.*, 2007) and represents the variety of soil conditions observed in the region (*Stolbovoi and McCullum*, 2002). Structural and compositional agreement between simulated and observed stand dynamics

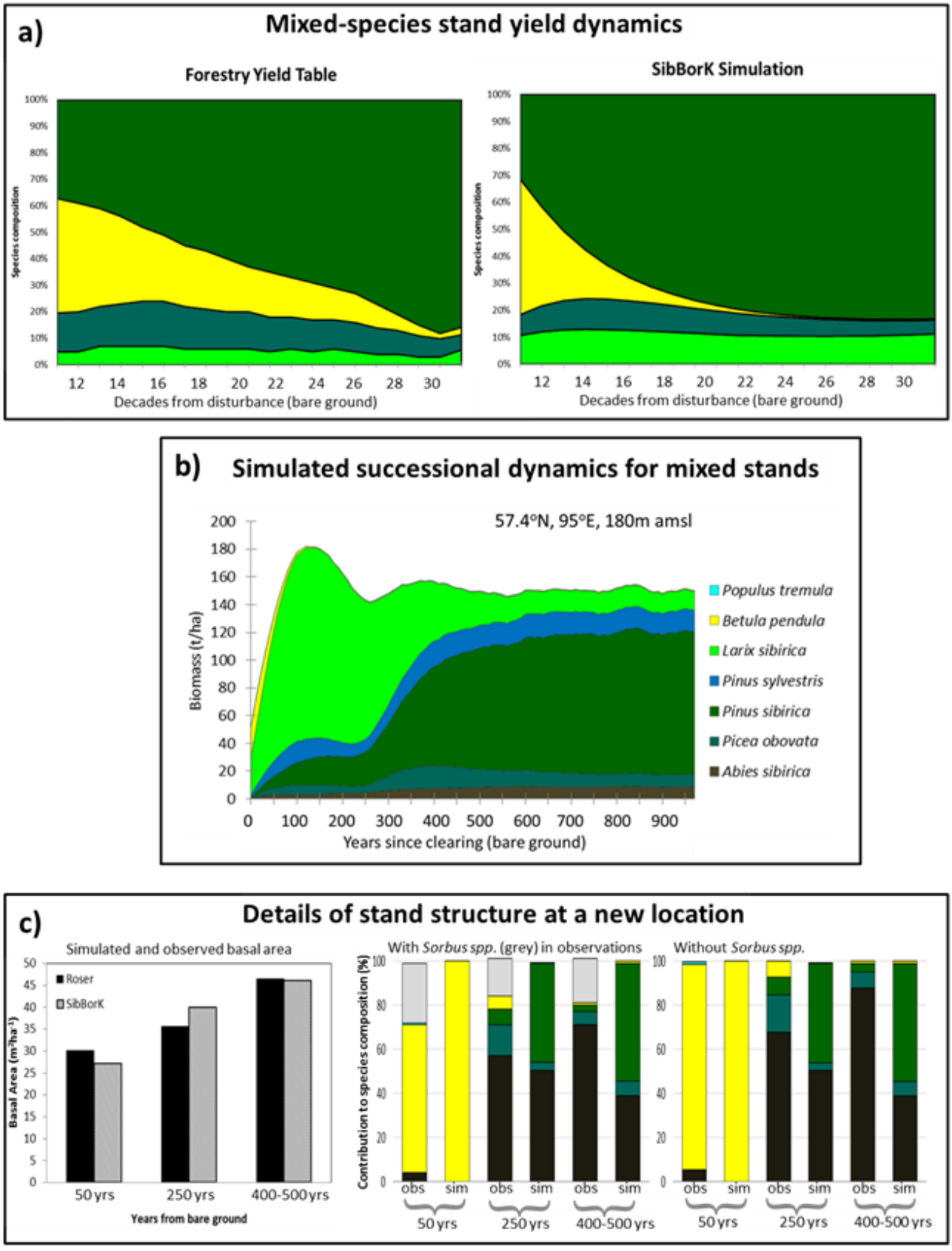

Fig. 3.14: [Caption on next page]

of multi-species boreal forest over the short (decades) and long (centuries to millennia) time scales provide further support for validation of SIBBORK.

Figure 3.14 Results of multi-dimensional model testing are presented in three panels. The same color-coded legend for species shown in the middle panel applies to all subsets, except the lower leftmost bar graph. (a) SIBBORK output is compared to forestry yield table records (*Shvidenko et al.*, 2006) for secondary succession dynamics in a mixed broadleaf-conifer forest comprised of four species: *Pinus sibirica*, *Betula pendula*, *Picea obovata*, and *Larix sibirica*. Observed shifts in species composition are reproduced by a simulated secondary succession trajectory over the course of 300 years from stand-replacing disturbance (bare ground). (b) Successional dynamics in a 1000-year simulation appropriately represent the transition from a short-lived birch-dominated (Betula *spp*.) community, to co-dominance by larch and pine (*Larix sibirica*, *Pinus sylvestris*), to a dark conifer forest comprised of fir (*Abies sibirica*), spruce (*Picea obovata*) and Siberian cedar (*Pinus sibirica*), with few instances of larch and pine. Similar successional stages and transitions are described in the literature for southern and middle taiga forests (*Reimers*, 1990; *Shugart et al.*, 1992a; *Schulze et al.*, 2005). (c) The order of bars in all three graphs is the same: observed (*Roser et al.*, 2002) (left bar) and simulated (right bar) for each age group. Simulation of stand structure at a new location revealed the robustness of SIBBORK in reproducing forest stands outside of the model verification region. The leftmost figure demonstrates that the observed and simulated basal area of 50, 250, and 400-500 year old forest stands at a middle taiga site are very close. This figure represents the average per hectare basal area from 150 independent replicates of the model simulation. Each model simulation represents a 9-ha area, divided into 900 plots. The standard deviation was obtained from each simulation. The standard error of the means, computed as the standard deviation divided by the square root of the number of samples is on the order of $0.01 - 0.1 m^2 ha^{-1}$ for each time step in the simulation. For clarity, these error bars were omitted from the figure. Errors or variability in the field observations were not reported by Roser *et al*. (2002). The two right-most figures in this panel show the observed and simulated species composition, with the presence of Sorbus *spp*. in the observation dataset (center), and with Sorbus *spp*. contribution removed (right) and the species composition for the observations normalized to the total stems without Sorbus *spp*. The simulation does not include Sorbus *spp*., which comprises a group of trees and shrubs in the Rose family and is not valuable for the timber industry.

3.3.3 Generalizability

The results of the generalizability test (Figure 3.14, lower panel) demonstrate the flexibility of the model with regards to application to a different region of the Siberian boreal forest without the need for tuning model parameters for tree growth and tree responses to the surrounding environment. The simulated structure and composition are comparable

to stand characteristics from three different stands at a middle taiga site (*Roser et al.*, 2002). The youngest of the three is an even-aged 50-year old birch-dominated stand with the main canopy height of 15m, stand density of 4600 stems/ha, and basal area of 30.2 m^2ha^{-1} (*Roser et al.*, 2002). Around the 50th year of the simulation, the birch stand exhibits an average height of 18.5m (for stems with DBH > 6.0cm), stem density of 1300-1400 stems/ha (for stems with DBH > 3.0cm), and the basal area peaks at 28 m^2ha^{-1}. The transition from birch to fir dominance occurs over the years 90-130 in the simulation, which compares well to the transition at stand age 100-150 years at this middle taiga site. The mixed forest during the transition period contains birch, fir, spruce, and a small contribution from Siberian cedar. Approximately 200-400 years post stand-replacing disturbance (in the model: from bare ground), a mixed coniferous forest develops. Aside from lack of silvicultural information of the Sorbus genus, which is not represented in the model, the species composition in the simulation matches closely the observed composition of the 250-year old mixed coniferous forest. The simulated mixed forest exhibits an average height (for stems with DBH > 6.0cm) of 20-21m, stand density of 2200 trees/ha (including all stems with DBH > 3.0cm), and basal area of 38.5 m^2ha^{-1}. Field observations from the mixed reflect forest structure with a mean height of 22m, stem density of 2467 stems/ha, and basal area of 35.7 m^2ha^{-1}. The 200-year old fir-dominated forest occurs 400-500 years post disturbance. At this point in the simulation, the forest is co-dominated by fir and Siberian cedar, with spruce comprising a smaller fraction, and only a few isolated old growth birches. This is comparable to the fir-dominated forest described by Roser *et al.* (2002), except in the observations spruce contributes somewhat more to stand composition than Siberian cedar. The reported stand characteristics include a mean canopy height of 22m, stem density of 1056 stems/ha, and basal area 46.5 m^2ha^{-1}. The simulation produces fir-dominated stands with mean canopy height of 21-23m, stem density of 1050-1150 stems/ha, and basal area 46-47 m^2ha^{-1}. Only stems with DBH greater than 6cm were used in calculating mean canopy height and stem density to avoid skew of the average height by the presence of a multitude of smaller stems. Roser *et al.*, (2002) did not report what size trees were included in the stem density estimate, so we retained stems with DBH > 3.0cm for the comparison. The close match between simulated and observed stem densities at different stand ages reflects the models ability to realistically balance sapling establishment and stem mortality rates. SIBBORK simulates successional transitions similar to those reported by Roser *et al.* (2002), which further demonstrates the model's robustness and generalizability to regions outside those used for model training and validation.

3.4 Discussion

Ecologists develop vegetation models for the prediction of specific features, such as timber yield or canopy processes. These models predict the specific characteristic(s) that defines the model's purpose. In predicting the long-term changes in forest dynamics, especially with changes in climatological parameters, it is important to test the model's

predictive ability against a diverse, multi-scale timeseries of observations (*Bugmann*, 2001). It is important to understand whether the computations of some parameters are dominated by a single "key" parameter. Qualitative and quantitative tests should include the evaluation of multiple outputs for monospecies and mixed stands, as well as for even- and mixed-age stands. Quantitative evaluation of SIBBORK model functionality has involved the comparison of field observations against multiple model outputs (DBH, height, basal area, biovolume, species composition) at different stages in succession. It is important to test the model in these multiple dimensions. Most often, model output for one or a couple of parameters is compared to field observations or remote sensing data that represent a "snapshot" of forest structure at a specific time. For a stronger test, we compared SIBBORK model output from several centuries of simulation to multiple timeseries of field data, as this approach allowed us to see whether the internal stand processes of the forest are simulated well over time.

Multi-dimensional testing of the SIBBORK model included qualitative and quantitative evaluation of model output for simulated stands at different points from bare ground, without fitting to each stage in secondary succession. Individual process formulations (tree growth, mortality, light extinction through the canopy, *etc*.) and overall stand dynamics were evaluated against multiple datasets from within the calibration region (southern taiga) and outside of this region (middle taiga). The model quantitatively and qualitatively reproduces the structure and dynamics of young and mature stands in monospecies and mixed forest. SIBBORK simulates the correct structure and appropriately-timed successional transitions, whether initialized from a set of initial conditions or from bare ground, where the latter represents succession following a stand-replacing disturbance, which are common in this boreal region. Multiple combinations of species have been tested, including all of the arboreal species whose ranges overlap the validation sites and for which we were able to obtain forestry yield table data. In each case, SIBBORK model output produced realistic combinations of species at each stage in succession, and matched fairly closely to the observed stand structure and total biovolume. Moreover, SIBBORK output matched the evolution of species composition, stand structure, and biovolume over the course of several centuries. Although the match is not perfect, model output from a given year of simulation closely matches observed structure of stands whose age is within 10 years of the simulation year. It is important to remember here that when SIBBORK introduces saplings into the simulation, they are planted at approximately 2.5cm DBH. For some species and under some growing conditions, this may be representative of a 40 year old tree, *e.g.* larch under very limiting environmental conditions, whereas for other species and environmental conditions, the 2.5cm DBH may be more representative of a 4-5 year old tree, *e.g.* birch in favorable conditions. Therefore, if the simulated forest is compared year by year to the observed forest, the successional transitions in the simulated forest are likely to occur in earlier years than observed. When the birch saplings are establishing in the first decade of the simulation, the stand structure is more representative of a birch stand in its 2^{nd} decade from bare ground.

The random and systematic errors of the data presented in the regional forestry yield tables are estimated at 4-7% (*Shvidenko et al.*, 2006). The uncertainty associated with the Usolsky forest inventory, as well as the histories of the observed stands with regards to management and natural disturbances are not known. The match of model output to verification and validation datasets may well be within the uncertainty of these datasets. Additionally, approximately 2% of the middle and southern taiga forest area are dominated by arboreal species not of interest to the timber industry (*Shvidenko and Nilsson*, 2002) and not represented in the yield tables. These species (*e.g.*, Sorbus *spp*.) are not represented in SIBBORK, which may contribute to the uncertainty of model estimates.

The 3-D character of the SIBBORK model facilitates the simulation of successional processes that are not explicitly parameterized, such as regeneration of shade-intolerant species in gaps the size of multiple large tree crowns. These multi-scale processes are not captured in non-spatially-explicit simulations of independent plots. Upon conducting the multi-level tests, it is evident that some of the internal forest processes, such as competition for light and space, and the transition of trees from the subcanopy to the main canopy, are represented in the simulation although not explicitly parameterized. When the model captures a multitude of stand characteristics at different stages post disturbance, we can utilize the model to further our understanding of how forest ecosystems operate and the consequences of changes to edaphic and climatological conditions at different points along a successional trajectory. This gives us greater confidence in applying the model toward the simulation of boreal forest with shifts in temperature and precipitation regimes that are likely to accompany climate change in Siberia.

SIBBORK brings a multitude of advantages to the table that are not represented by other classical gap dynamics models, such as FAREAST (*Yan and Shugart*, 2005), or spatially-explicit forest dynamics models, such as FORMIX3 (*Huth et al.*, 1996) and FORMIND (*Kohler and Huth*, 1998). Dynamics and patterns on scales larger than the size of a plot are not resolved by models of independent plots, such as FAREAST. The average landscape dynamics in FAREAST are obtained from an average of 200 independent plots. However, since FAREAST is not spatially explicit, trees on each of the independent plots do not interact with trees on other simulated plots and the average dynamics are extrapolated to the landscape scale from the plot scale ($500m^2$). In contrast, SIBBORK simulates a continuous landscape, with the spatial domain of the simulation tested up to 81 hectares, and environmental conditions specified at the plot-level. Extrapolation of stand dynamics to the landscape scale may be more appropriate from simulations that encompass a larger spatial domain and more explicitly represents the varying conditions on the terrain.

Similar to FORMIND, SIBBORK does not assign an exact location for each tree on the landscape, and does not explicitly include space-based competition, aside from limitation to stem density and maximum annual GPP cap at the plot-level. In contrast to FORMIND, however, species-specific parameterization allows for resolution of interspecific competition in SIBBORK, and does not limit the species range to associations with vegetation from the same plant functional type. This allows for new species assemblages to emerge as environmental conditions change, which is in

accordance with what has been observed through pollen records and other vegetation history reconstruction studies (*West et al.*, 1981; *Webb and Bartlein*, 1992; *Shugart et al.*, 1992a). In post-processing, trees can be grouped into similar-age, similar-DBH cohorts or analyzed individually. Additionally, SIBBORK has finer horizontal and vertical resolution in the 3-D light environment computation, compared to FORMIX3, wherein the plot size is larger (20m X 20m) and the light is computed for 5 canopy layers, each several meters thick. SIBBORK is more similar to FORMIND with regards to the vertical resolution of the light environment and foliage distribution, which are computed in 1m vertical increments. SIBBORK contains a more complex mortality subroutine, which includes species-specific age-related mortality, as well as stress-related mortality based on species tolerances to resource limitations. However, SIBBORK does not spatially-resolve Chablis-type events, and dead trees are removed from the simulation without damage to the surrounding trees. This lack of damage from tree-fall may be appropriate for lower-density boreal forests where mortality often results in standing snags, but may need to be refined before SIBBORK can be applied to study tropical forests with significantly greater stem density. FORMIND and SIBBORK can be used for similar applications, including investigation of the effects of logging practices and other disturbances on forest dynamics and composition.

A model such as SIBBORK, verified to this extent, may present a unifying theory for the internal organization of Siberian boreal forests and the adaptive behavior of individual trees within the landscape-scale forest dynamics. SIBBORK simulation includes complicated dynamics not expressed in other models, such as regeneration of pioneer species in gaps the size of multiple tree crowns, early and mature forest structure and dynamics without spin-up, and strong coupling to local environmental conditions that reproduce species ranges without external limitation to where each species can grow. No one model is best at simulating every process, structure, and pattern within the complex forest ecosystem, but SIBBORK does represent individual-level and landscape-level characteristics and dynamics in a way that is consistent with observed patterns. At this stage, SIBBORK may be in a "Medawar zone" described by Grimm *et al*. (2005) - a functional balance between the model's ability to compute dynamics and still possess a degree of realism in the structure and composition of the forest. The ability to simulate forest structure dynamically opens the possibility for furthering our understanding of how the boreal ecosystem operates and how its function, and especially its role as a sink for atmospheric carbon, may change with already-occurring temperature and precipitation regime shifts (*Kharuk et al.*, 2007, 2009, 2013; *Soja et al.*, 2007; *Tchebakova et al.*, 2011). SIBBORK-based predictions of forest structure and dynamics can be utilized for testing the effects of mitigation approaches geared toward maintaining the boreal forests' role as a carbon sink (*Krankina and Dixon*, 1994; *Ashton*, 2012), such as viability of new plantations on abandoned agricultural lands, the replacement of low-productivity broadleaf stands with conifers, or understanding which species are more likely to retain productivity under changing climatological conditions. Additionally, the 3-dimensional nature of the SIBBORK can be utilized for generation of synthetic data of foliage distribution in forests

under different environmental conditions, which can be used to facilitate novel approaches for driving future development of new remote sensing instrumentation and developing algorithms for analyzing remote-sensing data from current systems for a multitude of environmental conditions.

3.5 Conclusions

SIBBORK presents a new approach to modeling the boreal forest. We have demonstrated the application of SIBBORK to simulation of young and steady-state boreal forest structure and behavior, as well as successional dynamics in a mixed forest under historical climate (1950s-2000). The model has been calibrated to southern taiga in Krasnoyarsk region of central Siberia, and tested on independent datasets from within that region. Generalizability of the model was tested by simulating forest stands at a site in the middle taiga ecotone, located 600km north-northwest of the calibration region, without fitting. The model accurately simulates the structure and dynamics of mixed and monospecies boreal stands across a simulation area of up to 81-ha over multiple time scales. SIBBORK is particularly suited to address the heterogeneous response of vegetation to changing temperature and precipitation regimes due to its ability to explicitly resolve spatial characteristics of landscape and forest at a fine resolution.

CHAPTER

FOUR

STRUCTURE AND DYNAMICS IN COMPLEX TERRAIN AND IN A CHANGING CLIMATE

"A new tool does not merely increase the number of ways to attack old problems, but also changes the nature of these existing problems, and, in an extreme case, may reveal whole new classes of problems to systematic inquiry." - E. Di Paolo, J. Noble, and S. Bullock (2000)

Abstract

To understand how the Siberian boreal forests may respond to near-future climate change, we employed a modeling approach and examined thresholds for significant and irreversible changes in forest structure and composition that are likely to be reached by mid-21st century. We applied the new spatially-explicit gap-dynamics model SIBBORK toward the understanding of how transition zones, namely treelines, which are notoriously undersampled and difficult to model, may change in the near future. We found that a 2^oC change in annual average air temperature significantly altered the structure, composition, and productivity of boreal forests stands both in the northern and the southern treeline ecotones. Treeline migration occurs at smaller temperature changes. Based on the current (1990-2014) observed warming trends, a 2^oC increase in annual average temperature compared to historical climate (1961-1990) is likely to be experienced at the northern treeline by 2040 and at the southern treeline by 2050. With regards to the forest biome, the most significant warming to date has been predicted and observed in Siberia. A 2^oC increase in annual average temperature compared to the second half of the 19th century is smaller than the predictions of even the most conservative RCP2.6 climate change scenario (*IPCC*, 2013), and has previously been assumed to not likely result in dramatic changes to ecosystems or biome shifts. We show that at a $+2^oC$ change, biome shifts from forest to steppe are likely to occur across a large area in southern Siberia. These changes in land cover will inevitable result in changes in the biodiversity, carbon storage, and the ecosystem services provided by the boreal forests of southern Siberia.

4.1 Introduction

Boreal forests contain approximately half of the terrestrial carbon (*Gower et al.*, 2001), which is mostly stored in soils and permafrost (*Strauss et al.*, 2013). However, changes in boreal forest vegetation structure, composition and productivity can affect how the below-ground carbon is exchanged with the atmosphere (*Betts et al.*, 2000; *Kumala et al.*, 2004; *Bonan*, 2008; *Hollinger et al.*, 2010; *Ma et al.*, 2012; *Groisman et al.*, 2013; *Kuusinen et al.*, 2014). For example, increased tree mortality from wildfires, insect outbreaks, and other disturbances, release carbon to the atmosphere. It additionally leads to albedo changes and more exposed soils, which can facilitate further release of carbon from soils and permafrost (*Krankina et al.*, 2005). Simultaneously, a warmer environment may facilitate increased productivity, especially in forests where precipitation and air temperature increase concurrently.

There is uncertainty in how these changes in forest structure and composition will affect the role of Russian boreal forests in the global carbon cycle. To understand how the boundaries of the Siberian boreal forest may shift in the near future and to provide a rigorous test for a new gap dynamics model, we applied the SIBBORK vegetation model to the investigation of potential changes at the northern and southern treeline transition zones in central Siberia, which has some of the fastest recorded warming rates (*Gruza et al.*, 2015). These shifts in temperature regimes are likely to drive change in forest structure in the near future, in as little as decades. This will likely have a significant effect on how carbon is cycled between the boreal ecosystem and the atmosphere.

Modeling allows us to synthesize field data, to understand forest processes, and to extrapolate for conditions not currently observed, such as future climate. Any model is based on simplifications and assumptions, which carry with them a certain level of uncertainty. Our study employs a new spatially-explicit gap dynamics model, SIBBORK, which has been validated for forest composition and structure for southern- and middle-taiga ecotones (*Brazhnik and Shugart*, 2015). SIBBORK does not include chilling requirements for growth and regeneration that could drive especially the southern boundary of species ranges, or frost tolerance that may limit the northward distribution. The species ranges in SIBBORK are reproduced based on interspecific competition in combination with species-specific tolerances to limitations on four environmental factors deemed of primary importance for forest vegetation processes (*Pastor and Post*, 1986; *Urban*, 1990): available light, soil moisture, soil fertility, and growing degree days. The model explicitly considers the fully-coupled 3-dimensional light-environment including the effect of available light on tree growth, and the feedback with the amount of foliage affecting available light throughout the canopy. The model does address the multitude of other ways in which vegetation potentially affects the local microclimate. The current version of SIBBORK does not include permafrost or disturbances, whereas changes in both have been forecast for the near future in Siberia and may contribute to current treeline location and future migration. Nonetheless, SIBBORK contains several strengths that render it the appropriate model for this investigation. For example, SIBBORK utilizes species-specific

parameterizations, which include tolerances to environmental stressors and reflect differences in vascular and root structure (*e.g.* larch is more drought-tolerant than spruce due to difference in root structures (*Babushkina et al.*, 2010), and pine is more drought-tolerant than broadleaf species due to differences in vascular structure (*Bauweraerts et al.*, 2014). Furthermore, SIBBORK does not require or assume landscape homogeneity, which allows for heterogeneous landscapes and associated gradients to be simulated. Vegetation responds to the environmental conditions on the landscape, and we are therefore able to resolve the differential responses of vegetation, which include differences in stand structure and composition, based on the simulated conditions on the landscape. Application of SIBBORK to the simulation of transition zones and the response of vegetation in these ecotones to changes in the thermal regime presents a rigorous test of this model's capabilities.

4.2 Methods

SIBBORK is an individual-based gap model, which tracks the establishment, growth, and mortality of individual trees on 10m x 10m plots, which are arranged in a grid along user-specified terrain (*Brazhnik and Shugart*, 2015). Tree location on the terrain is resolved at the plot scale for a maximum stand density. Since it retains plots and specifies environmental conditions at the plot-level resolution, SIBBORK is not a continuous space model sensu Grimm and Railsback (2005) for competition and other interactions. The governing equations in SIBBORK address tree growth, the interactions among trees through shading, and the interactions between trees and their environment. The four environmental factors explicitly parameterized are growing degrees days above a base temperature of 5^oC (GDD_5), soil moisture as a function of precipitation, evapotranspiration and runoff, available light throughout the canopy as a function of foliage density, and soil fertility, which caps the annual gross primary productivity. The environmental conditions (incident radiation, air temperature, soil fertility) are specified at the plot-level, which significantly enhances the resolution of the conditions on the landscape and allows for simulation of vegetation response to changes in those conditions.

In a transition zone simulation, environmental conditions change along a transect or across a region. Artificially compressed gradients (i.e. radiation, temperature) can be imposed within the simulation domain. At the southern boreal treeline in central Siberia, the transition is along a steepened gradient due to the presence of complex terrain. On mountain slopes, transitions between ecotones occur along 100s of meters, whereas similar transitions occur along 100s of km on flat terrain (*Holtmeier*, 2005; *Soja et al.*, 2007; *Kharuk et al.*, 2010a). Using the ASTER GDEM (*NASA and METI*, 2011) resampled at 10m x 10m resolution, the incident radiation is computed using the Area Solar Calculator (*Fu and Rich*, 2002) in ArcGIS (*ESRI* v10.2, 2014). An environmental lapse rate of 6.5^oCkm^{-1} is applied to extrapolate the temperature from the nearest weather station to the simulated landscape based on elevation

(*Polikarpov*, 1986). Downscaling of precipitation to the resolution of several meters is poorly understood, therefore, in the model, the entire simulated region receives the same monthly precipitation. Soil fertility, field capacity, and wilting point are specified for each plot based on soil type using data and soil nomenclature from Onuchin (1962) and Stolbovoi and Savin (2002).

A treeline is a transition between a region dominated by arboreal vegetation and one with a general absence of trees (*Stevens and Fox*, 1991). These transitions occur at the northern or southern edge of tree dominance, or on a more local scale, such as along an elevational gradient or along the boundary of a body of water. The drivers of northern treeline are poorly understood, but likely include a combination of the following: the distribution of continuous permafrost (*Kryuchkov*, 1973), the average position of the polar front (*Bryson et al.*, 1970; *Pielke and Vidale*, 1995), the $10-12^oC$ July isotherm (*Arctic Atlas*, 1985; *Anuchin et al.*, 1986; *MacDonald et al.*, 2000), the length of the growing season (*Stevens and Fox*, 1991), incident radiation during the growing season (*MacDonald et al.*, 2000), winds (*Holtmeier and Broll*, 2005), the balance between precipitation (P) and potential evapotranspiration (PET) (*Hogg and Hurdle*, 1995), and other components of the local climate (*Woodward*, 1987; *Körner*, 1998; *Esper and Schweingruber*, 2004; *Dulamsuren et al.*, 2005b; *Kharuk et al.*, 2006; *Sun et al.*, 2011). In contrast, the southern treeline of the boreal forest experiences a large degree of climatic continentality, and has different potential drivers, which may include a combination of the local temperature/precipitation regimes (*Savva et al.*, 2003; *Dulamsuren et al.*, 2005a; *Chytry et al.*, 2008), the $19-20^oC$ July isotherm (*Arctic Atlas*, 1985; *Anuchin et al.*, 1986), the P-PET balance (*Kharuk et al.*, 2013b), winds (*Kullman and Kjallgren*, 2006; *Holtmeier and Broll*, 2010), fire regime (*Tchebakova et al.*, 2009; *Ivanova et al.*, 2010), and competition with shallow-rooted grasses, which may be better at utilizing the meager amounts of precipitation received during the growing season than deep-rooted, large-structured trees (*Stevens and Fox*, 1991). Additionally, the microclimates associated with complex terrain, as well as resource and vegetation patchiness, can promote tree establishment and growth even when the surrounding conditions are not favorable to arboreal vegetation. Not all of these environmental factors are captured by SIBBORK, however, the simulation of transition zones, such as treelines, provides a rigorous test for the strength of SIBBORK in simulating 3-dimensional terrain and associated gradients, and the resulting heterogeneous response of vegetation to the conditions on the landscape.

We selected the relatively data-rich northern treeline ecotone in the Krasnoyarsk Region of central Siberia for simulation with SIBBORK to better understand how the structure and dynamics of this vegetation may change with shifts in temperature and precipitation regimes. The topography at northern treeline is relatively flat (Figure 4.1a), with poor drainage and low soil fertility on gleyzem soils (*Stolbovoi and Savin*, 2002) underlain by continuous permafrost (*Kotlyakov and Khromova*, 2002). Along the Yenisei River meridian, the treeline is observed between the World Meteorological Organization (WMO) weather stations of Dudinka (#23074, 69.4^oN, 86.18^oE, 19m above mean sea level or amsl) and Turukhansk (#23472, 65.47^oN, 87.56^oE, 32m amsl), 440 km to the south. Average monthly temperatures

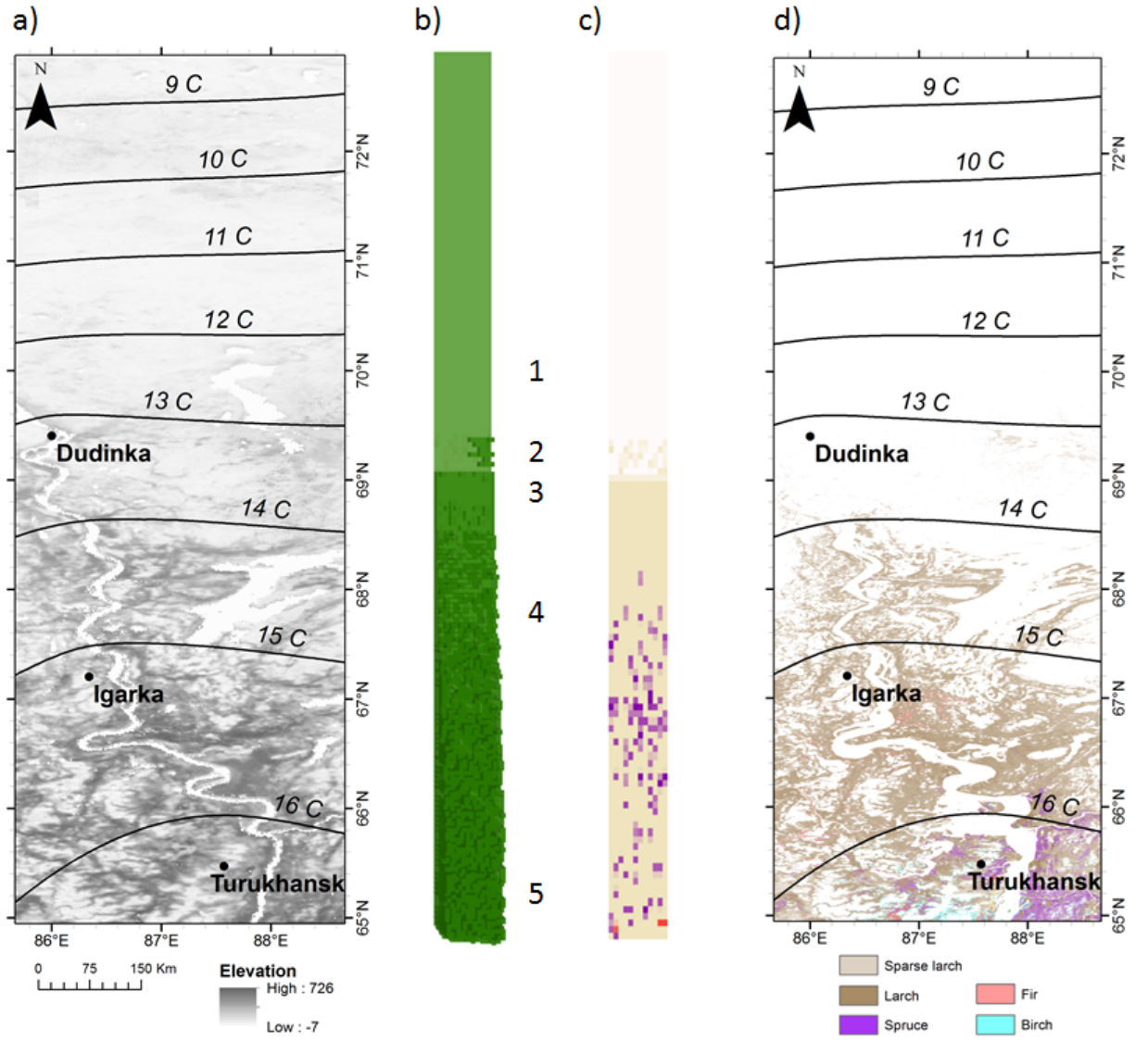

Fig. 4.1: Northern treeline. (a) Map showing average July temperature isotherms (^oC) in the vicinity of the northern treeline. The steepened temperature gradient in the simulation captures the transect between 7^oC and 16^oC July isotherms, which corresponds to a 700km transect along the Yenisei meridian. The topography at the northern treeline, near Dudinka, is relatively flat, compared to regions farther south, where trees begin to occupy low-lying terrain along stream banks. In the simulation, only flat terrain was used. (b) The simulated forest structure along the compressed temperature gradient under a historical climate (1961-1990). The spatial domain of the simulation is 12x181 plots (~22ha). 1 – denotes tundra, where no arboreal vegetation is observed. 2 – denotes a region of individual trees or small clusters of larches beyond the treeline. 3—denotes a uniform block of newly-established saplings. SIBBORK establishes saplings with 2.5±0.25cm diameter at breast height (DBH), which makes these newly-established saplings appear as a block. Within the first decade following establishment, stress levels will determine whether these saplings will remain in the simulation as viable trees. However, during this first decade, new saplings are generally considered an artifact of the inseeding subroutine. 4 – denotes the transition between open canopy and closed canopy larch forest. 5 – denotes closed canopy forest. (c) The simulated species composition along the compressed temperature gradient under a historical climate (1961-1990). The color legend is same as in (d), light pink denotes the tundra. The treeline and open canopy forest are dominated by larch. Further south, the closed canopy forest is dominated by larches (*Larix sibirica*) with a small admixture of spruce (*Picea obovata*). (d) Observed species composition along the 700km transect from the tundra to Turukhansk. The tundra and unvegetated areas (e.g. river) are denoted in white. The northern treeline is irregular, and depends highly on local topographic, edaphic, and climatological conditions.

and precipitation totals were computed for these two stations using the meteorological record from 1936-1990 (*NCDC* 2005a, b). The climates at the two stations set the conditions for the southern and northern edges of the simulated transect, with a linear interpolation of monthly temperatures in between to specify the thermal regime at the plot-level. The ArcGIS Area Solar Calculator (*Fu and Rich*, 2002) was used to compute monthly radiation at the plot-level for Igarka (#23274, 67.28^oN, 86.32^oE, 30m amsl), located between Dudinka and Turukhansk, which was then validated against observations from the nearest World Radiation Data Centre (wrdc-mgo.nrel.gov) station in Olenek (68.30^oN, 112.26^oE). The northern treeline is discontinuous, dominated by larch (*Larix sibirica*), with a maximum productivity of up to 100 m3 ha-1 (wood volume) found along the river and stream banks (*Bartalev*, 2010; *Bartalev et al.*, 2011; *Huttich et al.*, 2014). Environmental conditions specified in SIBBORK simulation of northern treeline are listed in the top row of Figure 4.2.

Lat.°N Long.°E Alt. (m)	Plot Size (m^2)	Mean Monthly Temperature (C°)	Mean Monthly Precipitation (mm)	Soil Field Capacity (cm)	Soil Wilting Point (cm)	Mean Monthly Radiation (W m^{-2})	Mean Monthly Radiation (Growing Season) (W m^{-2})	Relative Direct and Diffuse Solar Radiation (Growing season) (%)
69.4 86.4 19.0	100	-27.7 to +13.5	30-59	62.5	31.25	191	251	0.33/0.67
51.4 94.2 100-3000	100	-30.1 to + 19.9	3-47	26.5	13.25	285	303	0.5/0.5

Fig. 4.2: Environmental conditions at northern and southern limits of the boreal forest in central Siberia. *Top row*: climatological and edaphic conditions at Dudinka, near northern treeline. *Bottom row*: climatological and edaphic conditions near Kyzyl, in southern Alay-Sayan mountain region.

Site	**Winter**	**Spring**	**Summer**	**Autumn**
units	(°C/yr)	(°C/yr)	(°C/yr)	(°C/yr)
Northern treeline	0.02	0.1	0.03	0.02
Southern treeline	0	0.055	0.045	0.028

Fig. 4.3: Observed warming trends by location and season during 1990-2014 from *Gruza et al.* (2015).

In contrast, the southern taiga treeline occurs in the complex terrain of the generally east-west-oriented Altay-Sayan mountain system (*Ivanova et al.*, 2010) and mountain ranges of northern Mongolia. Treelines are found for both the lower and higher elevational limits of forest. Although north-western Altay-Sayan receives considerable precipitation on windward slopes (up to 1600 mm/yr; *Chytry et al.*, 2008), the south-central Altay-Sayan region, and specifically the

Tannu-Ola, Sengilen, and Obruchev ranges are characterized by high continentality, with average July temperatures exceeding 20^oC in the valleys and basins, annual precipitation of 200-500mm and PET of 150-300 mm/yr (*Samoilova*, 1973; *Ivanova et al.*, 2010). Both slopes are in a rain shadow, but the south-facing slopes receive more insolation, which drives higher PET demands and results in drier soils and vegetation dominated by grasses rather than trees.

The distribution of vegetation differs based on elevation and slope aspect, with coniferous forests dominating the north-facing slopes, and steppe and hemiboreal forests prevalent on south-facing slopes, called "expositional forest-steppe" (*Sedel'nikov*, 1979; *Wilmking et al.*, 2004; *Dulamsuren et al.*, 2005b; *Kulagin et al.*, 2006; *Chytry et al.*, 2008; *Kharuk et al.*, 2009, 2010a, b; *Timoshok et al.*, 2014). Species composition differs among the different sub-regions within the Altay-Sayan Mountains. Although there is variability between individual mountain ranges, on average the south-facing slopes below 1500m amsl are dominated by the steppe ecotone. An alpine belt, containing larch (*Larix sibirica*), Siberian fir (*Abies sibirica*), and Siberian cedar (*Pinus sibirica*, also called Siberian pine or Siberian Stone pine) stands is found 1500-2000m, above which alpine tundra dominates. Along north-facing slopes, dark taiga, comprised of Siberian fir, Siberian spruce (*Picea obovata*), and Siberian cedar, extend up to 1750m, with the subalpine belt found 1750-2100m, and tundra above that (*Isachenko et al.*, 1988; *Gorchakovsky and Shiyatov*, 1978; *Istomov*, 2005; *Chytry et al.*, 2008; *Kharuk et al.*, 2013b), although in some locations the transition to tundra is found higher, at 2200-2400m (*Ovchinnikov and Vaganov*, 1999). The variability of vegetation belts along the Altay-Sayan mountain ranges is often on the order of 300-500m and can be up to 1000m (*Monserud and Tchebakova*, 1996).

To simulate the southern treeline, an artificial digital elevation model for an idealized 3000m tall "mountain" with south- and north-facing slopes was generated. This DEM was used to compute the incident radiation in ArcGIS and the elevation-based temperature adjustment from the nearest WMO weather station located in Kyzyl (#36096, 51.4^oN, 94.23^oE, 629m amsl) using the 6.5^oCkm^{-1} lapse rate (*Polikarpov et al.*, 1986). GIS-generated monthly radiation was validated against observations from the nearest World Radiation Data Centre station in Irkutsk (51.16^oN, 104.21^oE). PET and GDD_5 were computed along the mountain slopes using plot-level monthly temperature and radiation input, and simulation-wide precipitation (200-500 mm/yr; *Samoilova*, 1973; *NCDC* 2005b). I did not adjust the precipitation received on the north- versus the south-facing slope of the idealized mountain in the simulation, and focused more on the average conditions representative of the Tannu Ola and Sengilen ridges, which are most proximal to the southern treeline in the Krasnoyarsk region (Figure 4.4).

A soil fertility gradient was generated based on description of mountain soils in that region, with more fertile soils along the foothills, and shallower, less fertile soils toward the top of the ridge (*Samoilova*, 1973; *Chytry et al.*, 2008; *Chlachula and Sukhova*, 2011). Soil fertility in SIBBORK is specified as a cap on gross annual productivity (GPP). Simulated plots along the lower slopes were assigned a GPP cap of 6 t $ha^{-1}yr^{-1}$, whereas GPP in plots at the top of the ridge was capped at 1 t $ha^{-1}yr^{-1}$. The GPP limit was estimated based on the correlation between site index

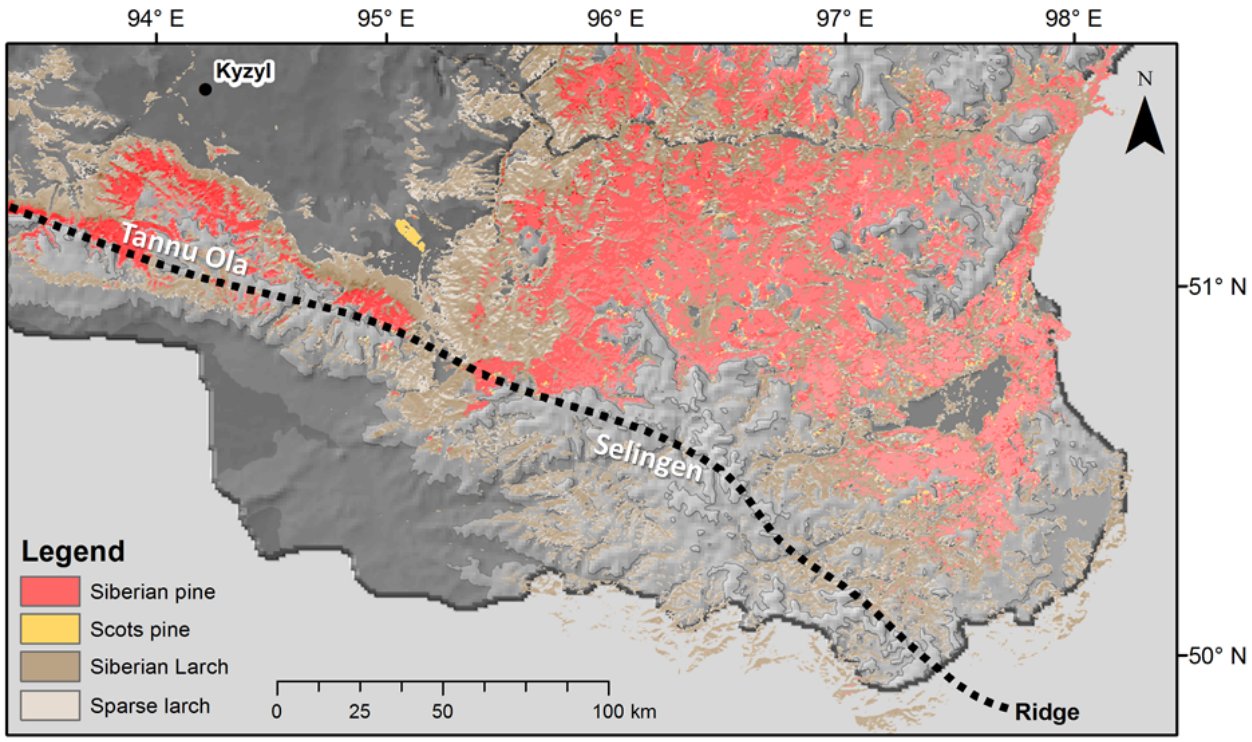

Fig. 4.4: Southeastern Altay-Sayan mountain region. The Tannu-Ola and Selingen ridges are denoted by the dashed line. Only the Russian territory is shown. Vegetation distribution along the north- and south-facing slopes of the Selingen and Tannu-Ola ranges is comprised of Siberian pine (*Pinus sibirica*), Siberian larch (*Larix sibirica*), and small patches dominated by Scots pine (*Pinus sylvestris*), as shown here using the Hybrid Biomass and Land Cover Map for Central Siberia (*Bartalev*, 2010; *Bartalev et al.*, 2011; *Huttich et al.*, 2014), which is based on satellite and field observations. In general, thin ribbons of larch stands are observed on south-facing slopes, and dark taiga is observed on north-facing slopes, with steppes in the basins and tundra above a certain elevation on the ridges.

and forest productivity in forestry yield tables (*Shvidenko et al.*, 2006). Soils in these mountains are mostly well draining cambisols, with kastanozems in the arid valleys where arboreal vegetation is generally absent (*Samoilova*, 1973; *Stolbovoi and Savin*, 2002; *Ivanova et al.*, 2010). Field capacity and wilting point were computed from a georeferenced database of soils (*Stolbovoi and Savin*, 2002) for the average cambisols found on Sayan mountain slopes. Environmental conditions specified in SIBBORK simulation of southern treeline are specified in the bottom row of Figure 4.2.

To minimize computational expense, the spatial domain of the northern treeline simulation was limited to 2km x 120m (22ha). A compressed thermal gradient was created via temperature adjustment to each row of plots within this swath of landscape. The generated July temperature gradient is shown in Figure 4.1a, and stretches between 7 and 16^oC. This temperature gradient corresponds to an approximately 700 km-long transect along the Yenisei meridian, as determined from temperature interpolation between the Dudinka, Igarka, and Turukhansk WMO weather stations. Conversely, for the simulation of the southern treeline, an idealized 100-3000m amsl mountain was created (6km x 120m, 70ha), with half of the area on the north-facing and the other half on the south-facing slopes. Elevation-based

adjustment to air temperature was applied, but the thermal gradient was not compressed, so the distances and elevation within the simulation represent actual distances and elevation gradients.

For all simulations, the historical climate, which is described by monthly average temperatures and precipitation sums, was defined by the WMO pre-1990 record, as in *Gruza et al.* (2015). Simulations were initialized from bare ground (no trees, but seeds available), with inseeding turned on for all species of interest to the timber industry in the Krasnoyarsk Region. The start year of the simulation was assigned based on the average age of the forest reported for each region, which is based on the mean fire return interval for the region of interest: ~100 for northern treeline (*Pautova*, 1976; *Mitrofanov*, 1977; *Deyeva*, 1985, 1987; *Esper and Schweingruber*, 2004; *Kharuk et al.*, 2005, 2006), 60-80 years for southern Siberian mountains (*Onuchin*, 1986; *Houghton et al.*, 2007; *Buryak et al.*, 2009; *Ivanova et al.*, 2010). In this manner, we initialized the simulation so as to obtain a forest of approximately the observed age by the beginning of pronounced warming in 1990 (100 years, *Kharuk et al.*, 2005). Wildfire and other disturbances rarely occur at northern treeline, so the average age of the stands can be in excess of 100 years (*Esper and Schweingruber*, 2004). In contrast, frequent disturbances, such as annual ground fires on the dry south-facing slopes (*Ivanova et al.*, 2010), significant variability in crown fire frequency over the 20th century, and an increased occurrence of insect outbreaks (*Kondakov*, 2002) in the Altay-Sayan mountains maintain a younger forest, but the more moist north-facing and upper slopes have some old trees in excess of 400 years (*Ovchinnikov and Vaganov*, 1999; *Istomov*, 2005).

To approximate the stand age in the simulation, the first year of the simulation was initialized from bare ground corresponding to the calendar year 1890 and 1910, in the simulation of the northern and southern treeline ecotones, respectively. In the year 1990, warming trends were applied as seasonal linear monotonic increases to the simulated monthly temperature based on the observed seasonal warming trends for each region (*Buermann et al.*, 2014; *Gruza et al.*, 2015). Both, historical and warmed air temperatures were adjusted at the plot-level for elevation relative to the nearest weather station. The historical climate parameters and the warming trends are specified in Figure 4.2 and Figure 4.3, respectively. Model output from 150 replicates was recorded at 5 year increments. The height, biovolume, and species of the dominant tree on each plot were averaged across the replicates, and raster maps of the most frequently dominating species (mode), as well as Lorey's height and biovolume, were generated at plot-level resolution. (Note: biovolume is a field-estimated parameter commonly reported in forestry yield tables and field surveys. This is in contrast to biomass, measurements of which require destructive sampling, and is often computed from field-estimated biovolume using bulk wood density, instead.) The precipitation regime was not altered alongside warming during these simulations, as no appreciable changes in growing season precipitation were observed in the Altay-Sayan mountains since the 1970s (*Kharuk et al.*, 2013; *Gruza et al.*, 2015), and although annual precipitation has somewhat increased at the northern treeline, this transition zone is not water limited and increase in soil moisture is not likely to significantly affect the arboreal vegetation growing there.

4.3 Results

Based on very simple parameterization of climatological and environmental conditions, in which the plots receive an enhanced temperature adjustment based on the distance from the nearest weather station, creating a steepened temperature gradient across the northern treeline ecotone, equal receipt of precipitation on each plot, and GIS-based incident radiation for the latitude of interest, SIBBORK generates annual PET and GDD_5 at the plot level. In this simulated environment, SIBBORK plants saplings and grows trees based on species-specific tolerances and silvicultural information. In this case, SIBBORK planted and grew predominantly larches, the height, biovolume and density of which decreased to the north. North of a certain point along the air temperature gradient, no saplings established. This constitutes the northern forest limit – the treeline – in the simulation (Figure 4.1 b and c).

In the simulation, the treeline coincides with where the 12^oC July isotherm and the 30cm/yr PET isoline occur on the simulated landscape. These conditions are similar to those observed at the northern treeline (*Kolosova*, 1982; *Malysheva*, 1993). Trees become stunted north of $500^oC\ GDD_5$. The established larch saplings are stressed due to insufficient heat during the growing season and succumb to stress-related mortality within the first few decades of life north of $400^oC\ GDD_5$, and are not able to establish north of $300^oC\ GDD_5$. This latter cutoff is in agreement with the Sayan Mountain model (*Monseud and Tchebakova*, 1996), which also draws a division between tundra and taiga vegetation at $300^oC\ GDD_5$. Moreover, this is congruent with reported minimum $300 - 400^oC\ GDD_5$ requirements for Siberian larch (*Osawa et al.*, 2010). South of $500^oC\ GDD_5$, canopy dominant larch trees achieve 20-24m in height, with average biovolume of $102 \pm 39 m^3 ha^{-1}$, and an admixture of spruce begins to appear. This compares well to observed biovolume of $75 - 100 m^3 ha^{-1}$ in larch stands between the 14^oC and 15^oC July isotherms, reported in a georeferenced database of stand biovolume and composition by Bartalev and his colleagues (*Bartalev*, 2010; *Bartalev et al.*, 2011; *Huttich et al.*, 2014). Furthermore, this compares well with the observed average biovolume of $40 - 120 m^3 ha^{-1}$ reported for northernmost stands of Siberian larch in central Siberia (*Osawa et al.*, 2010). The likely reason the simulated biovolume appears at the higher part of this range is because the small saplings are not excluded from the biovolume calculation. Bartalev (2010) does not report the minimum DBH used for biovolume calculation in his database.

The structure and composition of the simulated forest along these thermal transitions are shown in Figure 4.1 b and c. If there are no disturbances and the forest is allowed to grow for several centuries, spruce plays a more dominant role south of $500^oC\ GDD_5$ by year 400 (this corresponds to region 5 in Figure 4.1 b and c). To the south of that, mixed dark conifer taiga prevails. In the simulation of the northern treeline, trees essentially stop growing where they are supposed to. Species ranges are not specified in SIBBORK. Species stop growing whenever the environmental conditions are not favorable to seedling establishment, or where the trees are too stressed to obtain >10% of age- and

species-specific optimal diameter growth and succumb to stress-related mortality, as is the case north of the treeline. To the south, species (*e.g.*, larch) may be outcompeted by other species (*e.g.*, spruce), for which the site conditions are more favorable. GDD_5 is not the only driving factor for the northern treeline and species distribution, but here provides a systematic way to describe the orientation of stands of different structures and composition along a (compressed) thermal gradient. The simulated species distribution closely resembles the observed species distribution between the tundra and Turukhansk, and simulates the location of the northern treeline very close to the observed treeline along the Yenisei River meridian, as shown in Figure 4.1 c and d.

Within the first few decades of warming corresponding to year 1990-2020, the sparse, unstable, severely stunted larch saplings at the northern treeline are able to establish farther north, up to the new $400^oC\ GDD_5$ isoline, with unstable saplings extending north to the new $300^oC\ GDD_5$ isoline. Colonization to the north appears almost immediate, on the order of years to decades, as conditions change to allow regeneration. This is an artifact of the sapling establishment subroutine, which plants trees at a DBH of $2.5 \pm 0.25cm$. Siberian larch of this diameter can be 4.7-6.4m tall and 16-40 years old, depending on site index, which makes it seem as though trees, not saplings, appear beyond the treeline mere years after the warming trend is applied. This rapid response could be delayed through modification to the inseeding subroutine or if spatially-explicit dispersal processes were included in the model (*Kharuk et al.*, 2006). However, not enough data are available on small saplings with DBH less than 2.5cm in this region for validation of a new sprouting subroutine. With regards to vegetation responses in the spatial and temporal domains, regeneration of larches has been observed >3km from the nearest treeline (*Kharuk et al.*, 2006), and rapid treeline equilibration with environmental conditions is seen in some paleoecological as well as in more recent records (*Clark*, 1998; *Kullman and Kjallgren*, 2006), thus, the limit on seed dispersal may not need to be as stringent. As warming continues over the course of 150 years, however, the treeline in the simulation does not continue to advance northward. Instead, the stands south of the treeline accrue biomass, and a gentle decrease in maximum tree height is observed between what used to be the treeline under the historical climate, where full mature trees now grow, and the new treeline.

For the simulation of the southern boreal boundary, SIBBORK computes PET and GDD_5 on each plot based on temperature at the WMO station elevation and radiation computed for the north- and south-facing slopes of a given steepness. Slopes of both aspects receive the same amount of precipitation. SIBBORK appropriately simulates a drier environment on the south-facing slope and a 12^oC July isotherm around 2000m amsl on the north-facing slope. Because of differential environmental conditions, different species are able to establish and become dominant at different elevations on the two opposite slopes. On the south-facing slope, no trees occur in the simulation up to 1400m. Between 1400 and 2200m, larches dominate, with stunted and stressed larches occurring close to the lower (1400-1500m) and upper (2100-2200m) elevational treelines. Larches at the lower tree line are stressed by insufficient soil moisture, whereas at the upper timberline they are stressed by insufficient heat. Above 2200m no arboreal vegetation

is simulated. On the north-facing slope, the vegetation is starkly different – dark conifers (fir, spruce, Siberian cedar) dominate the slope up to 1800m. The Lorey's height of the mixed conifer forest reaches 22-24m at lower elevations, and gradually decreases to 5m at 1800m. Above 1800m, larches gain dominance, but these trees are significantly shorter ($3.7 \pm 0.7m$) than the stands observed on the south-facing slope at the same elevation. Above 2040m the larch populations are unstable, severely stunted, and stressed by insufficient GDD_5. No arboreal growth occurs in the simulation above 2180m on the north-facing slope. The simulated elevational distribution of boreal vegetation is remarkably similar to observed vegetation belts in the Altay-Sayan mountain system (Figure 4.5).

Source	Tundra	Subalpine belt	Forest belt	Steppe
Samoilova, 1973	In west & central: >1900-2000m In south & eastern: >1400-1500m	1000-1900m		S:300-1000m
Polikarpov et al., 1986	S: >1600m N: > 1400m	S: 600-1600m	N: 300-1400m	S: <600m N: <300m
Gorchakovsky and Shiyatov, 1978	>1500-2200m	–	–	–
Isachenko et al., 1988	S: >2000m N: >2100m	S: 1500-2000m N: 1750-2100m	S: none S: <1750m	S: <1500m N: none
Rakovskaya and Davydova, 1990	S: >2200-2400m N: >1200-2000m	S: 800-2200m N: 800-2000m	S: 700-1800m N: 200-1400m	S: <700m N: < 200m
Ovchinnikov and Vaganov, 1999	S: >2200m N: >2000-2200m	–	–	–
Moiseev, 2000	>1600m	1300-1600m	< 1440m	-
Chytry et al., 2008	S: >2000m N: > 1600-1750m	600-1950m		< 600m
Kharuk et al., 2010a	>1800m	1600-1800m	400-1700m	< 300m
Kharuk et al., 2010b	>2310-2570m	S: 2000-2300m N: <1800-2200m		–
Kharuk et al., 2013b	1350-1500m	1100-1350m	600-1100m	S: <600m
SIBBORK (simulated)	**S: 2200 N: 2100**	**S: 1340-2000m N: 1800-2000m**	**S: none N: <1800m**	**S: <1500m N: none**

Fig. 4.5: SIBBORK model output (bottom row) compared to descriptions of vegetation belts by aspect and elevation in the Altay-Sayan mountain region found in the literature. Note that aspect is not always specified in descriptions of vegetation belts, and so may include the highest and lowest elevations observed for certain vegetation, describing a larger range than may be encountered on a slope of a given aspect. Each article describes different regions within the Altay-Sayan mountain region, and it is understandable that the climate at the same aspect and elevation on various mountain ranges is likely to be different due to local conditions, location of the mountain range within the mountain system, differences in local lapse rates, and the location of this elevation band relative to the overall mountain height (*Kammer et al.*, 2002). "None" signifies no arboreal vegetation at the specified elevation and aspect.

Within the first few decades of warming (this corresponds to 1990-2030), the lower treeline on the south-facing slope retreats uphill up to 2000m. Larches are able to establish sparsely at 1600-2000m, but they are drought-stressed and do not survive more than a few decades. Meanwhile, on the north-facing slopes, the larch stands grow taller, and the admixture of spruce in the 1600-2000m belt increases. As warming continues over the course of 150 years (this corresponds to years 2110-2150), the spruces almost completely replace the larches on the north-facing slope, while on the south-facing slope the lower treeline retreats to 2000m. By the year 2100, the upper treeline advances to 3000m, which is the highest elevation simulated.

4.4 Discussion

Overall, the SIBBORK simulation of the environmental conditions, as well as vegetation structure and composition in the northern and southern boreal treeline ecotones match field observations.

Larch dominates the northern treeline in central Siberia. The treeline is not a continuous wall of forest, but rather a gradual decrease in stand density from south to north, until just a few individual trees or clumps of trees are surrounded by tundra (*Aksenov et al.*, 2002; *Holtmeier*, 2005). In the simulation, the northernmost stands are sparse and stunted, with tree height and biovolume increasing southward along the simulated transect. Just to the east of Dudinka, along the lower slopes of the Putorana Plateau, stands with average heights of 6.2m and biovolume of $4 - 33 m^3 ha^{-1}$ have been observed, albeit for birch stands. In our simulation, northern treeline is comprised of larch stands with Lorey's height of $7.2 \pm 2.6 m$, and biovolume of $6 - 10 m^3 ha^{-1}$. Biovolume for larch-dominated treeline along the Yenisei River meridian is not available, and often only described as "sparse larch" (*Bartalev*, 2010; *Bartalev et al.*, 2011; *Huttich et al.*, 2014).

The gradual decrease in stand density is appropriately simulated by SIBBORK, with few individual trees separate from the low density open canopy forest (region 2 in Figure 4.1b), and biovolume increasing from $7 \pm 1.3 m^3 ha^{-1}$ near the treeline to $45.9 \pm 14.2 m^3 ha^{-1}$ at the $14^o C$ July isotherm. Spruce is not encountered until the transition from very poorly drained gleyzems soils to moderately well drained podzolic soil, 200-300km south of the northern treeline along the Yenisei River (*Stolbovoi and Savin*, 2002; *Bartalev*, 2010; *Bartalev et al.*, 2011; *Huttich et al.*, 2014). Spruce begins to appear just north of the $16^o C$ July isotherm in the simulation, and dominates stands south of the $16.3^o C$ July isotherm that are more than 400 years old. Spruce in 200-year old simulated stands have a biovolume of $104 \pm 78 m^3 ha^{-1}$ (not shown). In younger stands (< 200-years old), spruce appears as an admixture just north of the $16^o C$ July isotherm, where at least 600 GDD_5 are accumulated annually. Simulated spruce admixture agrees well with observations of 100-200-year disturbance regimes (predominantly fire) that maintain younger, larch-dominated stands (*Pautova*, 1976; *Mitrofanov*, 1977; *Deyeva* 1985, 1987; *Esper and Schweingruber*, 2004; *Kharuk et al.*, 2005;

Kharuk et al., 2006). Moreover, the presence of spruce to the south is also supported by field-based estimates - spruce stands with an average biovolume of $100 - 125 m^3 ha^{-1}$ have been observed at the northernmost range of spruce along the Yenisei River (*Bartalev*, 2010; *Bartalev et al.*, 2011; *Huttich et al.*, 2014), which is situated near the 16^oC July isotherm.

Although Monserud and Tchebakova (1996) examined the thermal requirements for the tundra, subalpine taiga, montane taiga, and dark-needled montane taiga in southern Siberia, the thermal limits for the ecotones are also likely to be valid for the northern treeline thermal gradient. They found that tundra generally exists in regions where the total thermal accumulation is less than $300^oC\ GDD_5$, sparse and subalpine vegetation is found between 300 and 550^oC GDD_5, and dark taiga occurs in regions that acquire at least $750^oC\ GDD_5$ during the growing season. The transitions between no arboreal vegetation and sparse larch stands occur in the simulation around the $300^oC\ GDD_5$. The stands, dominated by larch, just as in the subalpine taiga ecotone, become thicker and taller between 300 and 500^oC GDD_5, at which point a small admixture of spruce (a dark needle-leaf conifer) begins to occur, with almost complete spruce and mixed dark taiga dominance south of the 16.3^oC July isotherm, which is approximately collocated with the $750^oC\ GDD_5$ isoline. The model simulation appropriately reproduces the observed species distribution along a thermal gradient. Field observations from the northern treeline ecotone in Siberia reveal that individual trees can establish few (*Kharuk et al.*, 2006) to tens of kilometers (*MacDonald et al.*, 2000) from the nearest tree stand. These observations facilitate the interpretation of fast (decades) colonization of the tundra upon warming in our simulations, which do not include a spatially-explicit seed dispersal subroutine.

Northward expansion of sparse larch stands into the tundra, and the increasing density and crown closure of what used to be sparse stands near the northern treeline have been observed in various regions of northern Siberia, with rates of treeline advancement of 3-10 m/yr near Khatanga (*Kharuk et al.*, 2006; *Sun et al.*, 2011), 1-4 m/yr in the Polar Urals (*Devi et al.*, 2008), 4-14 m/yr in the Polar Urals (*Kharuk et al.*, 2003), and comparable rates at numerous sites between those two locations (*Esper and Schweingruber*, 2004), with likely increase in colonization rate as climate warms and as the new young treeline individuals reach reproductive maturity (*Kharuk et al.*, 2006) and are able to provide a more sheltered environment for establishment of new saplings. If the reproductive processes are temperature controlled, rapid advance of the northern treeline is likely (*Grace et al.*, 2002). Saplings that have established north of the 19th century treeline have experienced slow growth, often growing no more than 4m tall in 50 years (*Esper and Schweingruber*, 2004). SIBBORK also simulates slow growth of northernmost saplings, which reach $5.3 \pm 1.0 m$ over the same time frame. Increasing crown closure has been observed near the historical northern treeline (*Kharuk and Fedotova*, 2003; *Kharuk et al.*, 2006), and SIBBORK appropriately simulates an increase in foliage density in trees located at the historical northern treeline following a period of warming.

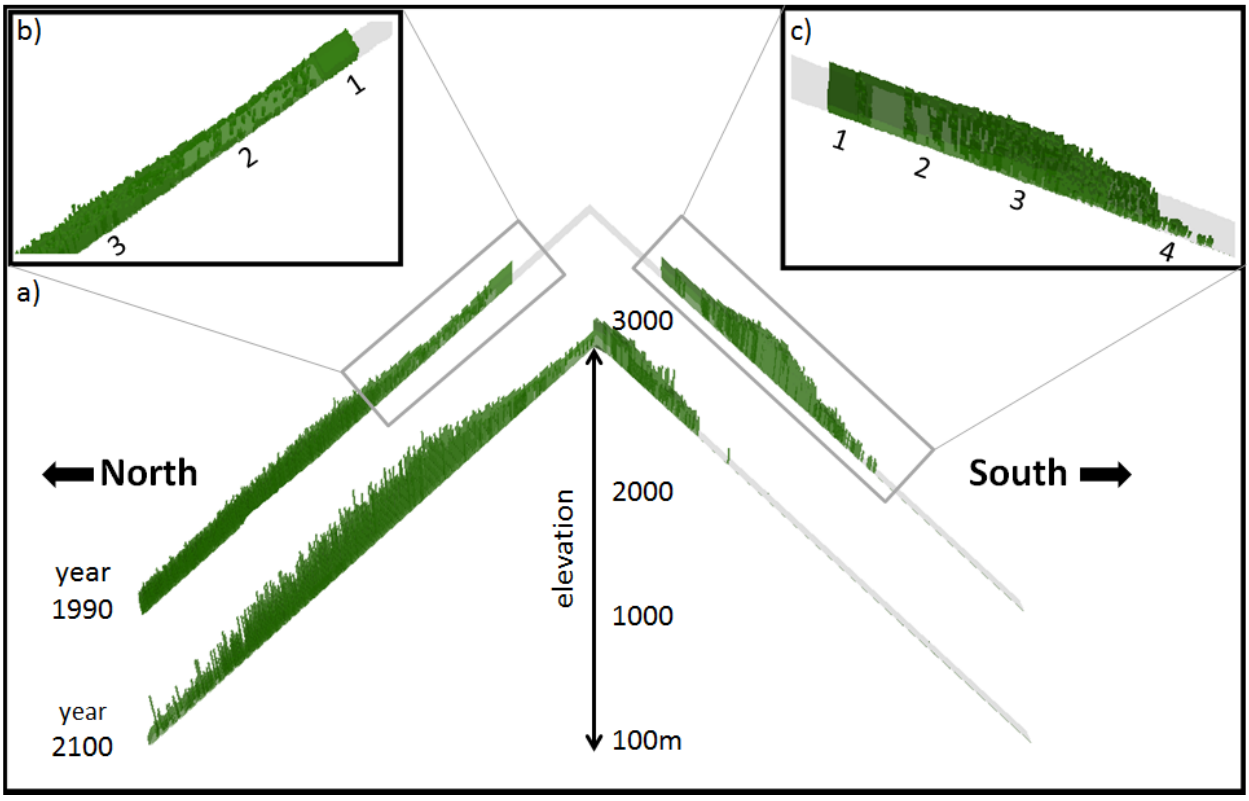

Fig. 4.6: The simulated distribution of arboreal vegetation along south- and north-facing slopes on an idealized 3000m tall mountain is visualized here using a green pillar to symbolize the largest tree on each 10m X 10m plot. The spatial domain of the simulation is 12x581 plots (~70ha). (a) The historical treeline. The upper mountain profile shows forest structure for the year 1990, which was grown using the historical climate (1961-1990). The lower mountain profile shows forest structure for the year 2100, following 110 years of warming using observed, average 1990-2014 seasonal warming trends for the region (*Gruza et al.*, 2015). The upper timberline shifted upslope by almost 1000m over the course of 110 years of warming. The lower timberline on the south slope receded above 2000m within the same time frame. (b) Detail of upper north-slope forest structure. 1 – denotes a block of new saplings. SIBBORK establishes saplings with 2.5±0.25cm diameter at breast height (DBH), which makes these newly-established saplings appear as a block. Within the first decade following establishment, stress levels will determine whether these saplings will remain in the simulation as viable trees. However, during this first decade, new saplings are generally considered an artifact of the inseeding subroutine. Above the block of new seedlings, arboreal vegetation is absent. This region corresponds to alpine tundra. 2 – denotes sparse tree stands akin to the structure of the forest-tundra ecotone or the Subalpine Taiga/Golets Taiga ecotones described by Monserud and Tchebakova (1996). 3 – denotes closed forest dominated by fir, spruce, and Siberian cedar. This vegetation belt resembles the Dark-needled Chern Taiga described by Monserud and Tchebakova (1996). (c) Detail of south slope forest and treeline structure. 1 – denotes a block of new saplings, same as on the north-facing slope. 2 – denotes individual trees and small stands of larch, akin to the Golets Taiga ecotone described by Monserud and Tchebakova (1996). 3 – denotes closed forest, dominated by larch, similar to the Montane Taiga described by Monserud and Tchebakova (1996). 4 – denotes stunted individual and clustered larch trees, similar in structure and composition to the Light-needled Subtaiga, Forest-Steppe, and lower on the slope – the Dry Larch Taiga peristeppe ecotones described by Monserud and Tchebakova (1996). Lower down the slope, arboreal vegetation is absent. This corresponds to the Montane Steppe ecotone, where the soils are too dry to support tree growth. Simulated vegetation distribution corresponds well with observed vegetation belts in the southeastern Altay-Sayan mountains, which is shown in Figure 4.4. In simulation and observations, south-facing slopes have patchy vegetation mid-slope, whereas arboreal vegetation on north-facing slopes extends to 1800-2000m. Many south-facing slopes do not have arboreal vegetation and correspond to the steppe ecotone.

The mountains of southern Siberia stretch for over 1,065,000 km^2 and include the Altay-Sayan ranges, as well as the Zabaikal'e region to the south and east of Lake Baikal, where forests and forest-steppe cover 80% of the territory (*Samoylova*, 1973). Along the southern boundary of the boreal forest, ribbons of forest appear predominantly on north-facing and upper slopes in the Altay-Sayan mountain region. The forest belt, thus, has a lower treeline limit on south-facing slopes dictated by soil moisture conditions, and an upper timberline on slopes of all aspects driven by temperature (*Samoilova*, 1973; *Dulamsuren et al.*, 2005a).

In SIBBORK, it is possible to monitor which environmental factor exerts the greatest limitation on growth of each individual tree. In the simulation, the trees along the upper treeline are most limited by insufficient growing degree days, whereas the growth of trees along the lower treeline on the south-facing slope is most severely limited by insufficient plant available water and too great of a fraction of growing season spent in drought, where soil moisture is below the wilting point.

Larch dominates both the lower and upper treeline on south-facing slopes, with occasional admixtures of pine (*Pinus sylvestris*) and birch (*Betula spp.*) (*Babushkina et al.*, 2010). Stand density and tree height near and at the forest boundary are smaller than in the middle of the forest belt (*Samoilova*, 1973), and our simulations appropriately reproduce this observed patchiness near the upper and lower treelines (Figure 4.6). The larch stands at the lower treeline are stressed, and this boundary is likely to recede as temperatures warm without corresponding increases in precipitation (*Dulamsuren et al.*, 2008, 2010). A 300-m upward retreat of the lower treeline due to increased tree mortality was recently observed in the Altay mountains in just 6 years (*Kharuk et al.*, 2013b). Germino and colleagues found that higher sunlight, such as may be available at the upper or lower treelines on south-facing slopes, compared to north-facing slopes or flat terrain, in combination with warm temperatures and water stress, inhibit the growth of Picea and Abies saplings in montane regions (*Germino et al.*, 2002). These species are generally not found on south-facing slopes in the Altay-Sayan mountains, and in the Zabaikal'e region just to the east (Figure 4.4). In our simulations, these species are appropriately absent from south-facing slopes, which are dominated by larch, with small patches of pine and birch (Figure 4.6). Lorey's height for northern-aspect mid-slope forests in the simulation exhibit a range of 7-17m (mean$\pm$std: $9.9 \pm 2.2m$), which compares well with observed heights in birch-fir-pine forests in the Khamar-Daban mountains of the Zabaikal'e region, just to the east of the Altay-Sayan complex (range: 7-14m, mean$\pm$std: $10.8 \pm 3.6m$) in 40-60 year old stands (*Onuchin*, 1986). Additionally, simulated forest biovolume on south- (range: $8 - 150m^3ha^{-1}$) and north-facing (range: $7 - 49m^3ha^{-1}$ for 80-year old stands; $100 - 181m^3ha^{-1}$ for 200-year old stands when plots with young saplings regenerating in recently-formed gaps with biovolume of less than 1kg/-plot are excluded from calculation) slopes correspond well with observed biovolume in the Selingen range (range: N $100 - 175m^3ha^{-1}$; S sparse-$150m^3ha^{-1}$; sparse denotes $< 100m^3ha^{-1}$, *Bartalev*, 2010; *Bartalev et al.*, 2011;

Huttich et al., 2014). Figure 4.6 represents the simulated species distribution along south- and north-facing slopes in the mountains of southern Siberia.

In the early 1990s, forests of the Krasnoyarsk region were assessed to be a weak sink for atmospheric carbon (*Krankina and Dixon*, 1994), however, with increasing air temperatures not accompanied by any significant changes in precipitation in the southern part of this region, forest vegetation is likely to be stressed from temperature-induced drought, especially in southern Siberia (*Allen et al.*, 2010), and the increased mortality is likely to shift the role of these forests into sources of atmospheric carbon. As warming forces forests to recede higher uphill (migration of the lower timberline), but the upper timberline advances at a slower rate, there is the likelihood of significantly decreasing forest cover in this region. It has been hypothesized that increasing PET demands as a result of increasing air temperatures accompanied by only meager, if any, increases in precipitation, will stress and decrease the productivity of the boreal forests in Siberia (*Briffa et al.*, 1998; *Knorre et al.*, 2006; *Allen et al.*, 2010), Europe (*Dirnbock et al.*, 2003), Canada (*Hogg and Hurdle*, 1995; *Ma et al.*, 2012), and Alaska (*Bonan and Shugart*, 1989; *Barber et al.*, 2000), and potentially result in biome shifts (*Stitch et al.*, 2008; *Buermann et al.*, 2014).

Regeneration and advancement of arboreal alpine vegetation in continental montane areas may be more sensitive to changes in the soil moisture than to the thermal regime (*Holtmeier and Broll*, 2005), and as the climate in southern Siberia becomes warmer and drier, grasses may significantly outcompete tree saplings, especially on dry soils (*Ivanova et al.*, 2010). Others have forecast the rapid (decades to centuries) upslope migration of the lower and upper treelines (*Tinner and Kaltenreider*, 2005), as well as the migration of the southern boreal forest boundary northward over the next few decades (*Tchebakova et al.*, 2009). The upward retreat of the lower treeline on the south-facing slopes in the Altay-Sayan mountains has been observed in the last decade, most pronounced on south- and southeast-facing slopes, where forest receded upslope by over 200m in just 7 years (*Kharuk et al.*, 2013b). Similarly, increased drought-induced mortality of birch was observed in the forest-steppe region on south-facing slopes in Transbaikalia mountains to the east of Lake Baikal and only a few hundred kilometers east of the simulated region (*Kharuk et al.*, 2013a), effectively shifting the lower treeline upslope by 22-40m within the first decade of the 21st century. Increased drought-induced mortality has been observed in aspen (*Populus tremuloides*) stands in the Rocky Mountains in the U.S. (*Anderegg et al.*, 2012; *Huang and Anderegg*, 2012) and Canada (*Hogg et al.*, 2008) with similar rates of retreat.

With regards to the upper timberline, a shift of 160m since the 1890s has been noted (*Istomov*, 2005), which expands on the shift of 100m observed in the Western Sayan Mountains between 1976 and 2000 (*Kharuk et al.*, 2010a), with the greatest regeneration above treeline observed on north- and northwest-facing slopes. Other field studies report similar rates of upward timberline migration in the latter half of the 20th century along the southern boundary of the boreal forest in Russia ($63 \pm 37m$ in 42 years; *Kharuk et al.*, 2010b) and Scandinavia ($165 \pm 20m$ in 50 years; *Kullman*, 2000, 2001, 2004). In addition to the treeline shifts, there are also shifts of species ranges along the slopes, with

SIBBORK appropriately reproducing the upward shift in Siberian cedar and fir populations, the beginnings of which have already been observed in Altay (*Moiseev*, 2000). Shifts in optimum elevation of plant species, which focuses on the center of distribution range, rather than just the upper or lower montane limit, of 2.94 ± 1.09 m/yr have been observed in the mountains of western Europe since 1971 (*Lenoir et al.*, 2008), showing that the observed warming with no appreciable change in precipitation regime affects the entire range of species, and not just the range boundaries. Furthermore, increased stand density and crown closure has been observed at the upper alpine treeline, sometimes in addition to, and sometimes in lieu of pronounced upslope timberline advance (*Kullman*, 2005). This change in stand structure has also been appropriately simulated by SIBBORK.

Previous modeling studies have suggested that a significant loss of forest is likely to occur in mountain areas with a $+2^oC$ change in average annual temperature in Europe (*Dirnbock et al.*, 2003) and North America (*Chapin et al.*, 2004), especially when the precipitation regime does not concurrently change or becomes drier. The $+2^oC$ also appears as an important threshold for the substantial decrease in forest-covered area along the simulated mountain slopes of southern Siberia in our study. The area occupied by pine-larch forests in Tuva (southern Sayan) has decreased by 70% since 1990, due to increased tree mortality and fire activity, and decreased regeneration post disturbance (*Buryak et al.*, 2009; *Ivanova et al.*, 2010). Retreat of forests from the simulated southeastern Altay-Sayan region (Tuva basin) has been forecast based on observations of warming and drying conditions in the region (*Tchebakova*, 2006). The replacement of forest-steppe with steppe at the lower treeline has already been observed following fire and permafrost retreat (*Monserud and Tchebakova*, 1996). This ecotone shift is likely to persist with warming and an increase in drought mortality and fire frequency in the coming decades, and is simulated appropriately by SIBBORK, even though the simulation does not include explicit parameterizations of disturbances and permafrost.

Numerous environmental factors that may affect treeline location, such as permafrost, winds, snowpack, and seed dispersal, are not included in this version of SIBBORK, so it is entirely possible that the northern treeline, which appears to be a function of air temperature in the simulation, may have completely other drivers. The model essentially simulates the theoretical treeline, based on environmental conditions, and as those conditions change, the colonization of areas that become favorable or retreat from regions that become no longer favorable may occur significantly faster than observed in nature, as the model does not address the increased susceptibility of young sapling to stress, compared to mature individuals, and does not explicitly represent seed dispersal.

Crawford and colleagues suggested that the northern treeline in Siberia may actually retreat south with warming due to increased soil and permafrost melt resulting in paludification (*Crawford et al.*, 2003). Since permafrost is not included in the current version of SIBBORK, the possibility of this feedback is not represented in our simulations. Increases in stand density and canopy closure have been observed at the upper timberline in southern Siberia (*Kharuk et al.*, 2010a, b). In SIBBORK, however, the maximum stand density limit is specified in the model driver. Although the simulation

can contain less than the maximum number of stems per plot due to unfavorable conditions, the possibility of future environmental conditions facilitating denser stands is not accommodated by the static limit on maximum stand density. Wind is an important factor in maintaining not only the northern forest boundary, but also the upper timberline (*Resler et al.*, 2005; *Kullman and Kjallgren*, 2006), and lack of parameterization for this factor may result in establishment of saplings in sheltered areas on the terrain not due to shelter from the wind, but rather due to decreased incident radiation and, therefore, PET demands, again, missing the exact combination of driving factors for the location of the treeline, but getting the gist of it with the limited environmental factors that are explicitly resolved in the simulation.

The model does not consider the differences in allometric relationships observed between trees within a forest compared to those on the exposed treeline edge (*Hogg and Hurdle*, 1995). It is assumed that the environmental conditions along the treeline edge will differ from those within the closed canopy, and the growth of treeline trees will be adjusted in the simulation based on the stress those individuals experience. Kharuk and his colleagues (*Kharuk et al.*, 2013a) have found that in areas with increased tree mortality from temperature-induced drought stress, vegetation underlain by patches of permafrost was not adversely affected by increased temperatures, because the thawing of the permafrost active layer provided sufficient soil moisture throughout the growing season. The simulation can be improved to reflect this heterogeneous response using a spatially-explicit parameterization for permafrost and associated soil processes. Additionally, with more local precipitation data available from field sites in southern Siberia (*Monserud and Tchebakova*, 1996; *Kharuk et al.*, 2009, 2010c, 2013b), it will be possible to adjust precipitation by elevation and slope aspect, which would improve the resolution of local environmental conditions and the associated vegetation response to changes in these conditions. Disturbances, such as wildfire and insect outbreaks, are not included in this version of the SIBBORK model. An increase in the frequency and extent of these disturbances has already been observed across the Eurasian boreal forest (*Buermann et al.*, 2014), and their incidence is expected to continue to increase. Presence of disturbance shifts the forest age structure to a younger forest, with greater dominance by pioneer species, such as birch and pine. Repeated fires inhibit regeneration of arboreal species, promote dominance of grass species (*Kukavskaya et al.*, 2013), and expedite the shift from a forest to a grassland or steppe biome (*Kukavskaya et al.*, 2014).

4.5 Conclusions

The SIBBORK dynamic gap model keeps track of the establishment, growth, and mortality of millions of trees across tens of hectares of artificial or real terrain, and simulates heterogeneous response of vegetation to the conditions on the landscape. SIBBORK appropriately reproduces transition zone vegetation, with the structure and composition closely approximating the observed forests at the northern and southern boreal forest limits, including the upper and lower elevational treelines in the complex terrain of southern Siberian mountains. The ability to appropriately simulate

vegetation distribution in central Siberia (*Brazhnik and Shugart*, 2015) and at the transition zones, not only provides a rigorous test of the model's capabilities, but also helps us understand the potential response of these ecosystems with continued warming. Alarmingly, the loss of forest at the southern treeline far exceeds the rate and amount of forest gained at the northern and upper elevational treelines, however, this is consistent with observations from Siberia, Scandinavia, and North America. A spatially-explicit gap dynamics model that is able to simulate forest structure and composition across ten of hectares provides a strong platform for understanding what near-future changes in forest vegetation and the associated carbon cycling are likely in different regions of the Siberian boreal forest.

Observed warming trends in the Siberian boreal forest exceed predicted trends for this time period (*IPCC*, 2013; *Gruza et al.*, 2015). It is likely that not only will the forest vegetation be responding to larger climate changes than predicted, especially in mountainous southern Siberia (*Tchebakova*, 2006), but also that the rate of response may be faster than anticipated. Boreal forests in Siberia have experienced significant decline, both in the wood stock ($m^3 ha^{-1}$) and area covered since 1980s (*Shvidenko and Nilsson*, 2002). The observed increase in wildfires and insect outbreaks in recent decades, which has resulted in the dieback of millions of hectares of forest in southern Siberia (*Soja et al.*, 2007) makes this investigation particularly pertinent. Furthermore, Hansen and colleagues have found that during the first decade of the 21st century, the ratio of forest loss to forest gain was 2.1 for boreal forests, with Russia experiencing greatest forest loss compared to the rest of the globe (*Hansen et al.*, 2013). This forest dieback has occurred with less than $+2^oC$ increase in annual average temperature, demonstrating that the boreal forest ecosystems may be much more sensitive to warming than previously anticipated.

CHAPTER

FIVE

MODEL SENSITIVITY

"The most important challenge for ecologists remains to understand the linkages between what is going on at the level of the physiology and behavior of individual organisms and emergent properties such as the productivity and resiliency of ecosystems." - S. Levin (1999)

Model sensitivity refers to a range of conditions for which model output is realistic, which may be limited by the underlying assumptions of vegetation responses to environmental forcings or by the computational domain selected. The model, thus far, has been implemented with $100m^2$ plots and spatial domains of at least 9 hectares. It is possible that computations on smaller or larger plots may not yield output that compares well to observed stand structure and composition, or that simulation of smaller areas using edge-to-edge wrapping results in numerical instability or periodicity in the available light that is an artifact of the model algorithm rather than simulated terrain or vegetation. Although the SIBBORK model has been verified and validated against several multi-dimensional datasets, model structure and functionality warrants further examination. Verification and validation were only conducted on a few variables, predominantly limited by available data. Additionally, the biomass simulated by the model has not been verified or validated due to lack of information on the conversion factors between field-estimated biovolume and reported biomass, and an error-prone approach of manually joining forestry yield and productivity tables. SIBBORK has appropriately reproduced observed vegetation in the southern, middle, and northern taiga ecotones, demonstrating the generalizability of the model algorithms within central Siberia, but it is important to understand how certain user-specified parameters may affect model output. Moreover, does spatial explicity enhance predictive capabilities? Does model simulation using 1-D light versus 3-D light yield different results? How does the spatial resolution (plot size) affect model output? Furthermore, model application toward understanding how the central Siberian boreal forest may respond to climate change and how this response is different in the 1-D and 3-D modes are explored in this chapter.

5.1 Does spatial-explicity matter?

Simplification of many ecological models includes simulation of vegetation on flat terrain, on one or several independent plots with the same environmental conditions, and consideration of light only from overhead. SIBBORK takes this several steps further, through the explicit simulation of terrain and the associated environmental gradients, light ray tracing in 3-dimensions, and variable foliage density with height. Vegetation processes depend on air and soil temperature, both of which vary significantly with topographic position (*Dixon*, 1986). The amount of photosynthetically active radiation (PAR) available to plants varies based on terrain elevation, aspect, slope steepness, and surrounding topography. Whether the trees on plots within the simulation interact across the spatial domain or not, the representation of terrain and associated gradients may facilitate a more realistic vegetation response through structure and composition.

Classical gap dynamics models simulate independent plots approximately the size of the crown of a canopy dominant tree or the size of the estimated zone of influence of a canopy dominant (*Urban and Shugart*, 1992; *Yan and Shugart*, 2005; *Larocque et al.*, 2006, 2011). The patch dynamics simulated on each plot are averaged across several model runs to obtain average landscape dynamics. SIBBORK differs from these models by the ability to run in the independent *and* interactive plot mode. ZELIG also could be run in the independent plot mode, however, individual plots in the simulation were then collocated in space and always experienced the same input parameters and environmental conditions in any given year of the simulation. In contrast, the 1-D mode in SIBBORK retains the plot position on the landscape, allowing for different environmental conditions to be specified at the plot level, and simply not permitting the trees on the plots to interact (e.g. shade trees on adjacent and nearby plots). The ability to simulate the same spatial domain with plot-level environmental conditions in 1-D and 3-D modes allows for a direct assessment of whether the spatially-explicit interactions expand the model's predictive capabilities.

1-D vs 3-D on Flat Terrain

For the initial comparison, the simulation was maximally simplified by utilizing only flat terrain, and generating an environment that is minimally limiting to boreal tree growth. These conditions are representative of some of the most productive forest stands in middle and southern taiga of central Siberia (*Houghton et al.*, 2007), in the vicinity of the Usolsky forest (validation site, *Ershov and Isaev*, 2006). Two batches of 20 simulations each were initialized from bare ground, with all species contributing to the seed bank, and all plots in the simulated grid experiencing the same initial environmental conditions. Maximum stem density was capped at 1000 stems/ha. The simulations were run for 600 years with a non-random historical climate (i.e., random number generator seed set for both simulation modes) across a 9 hectare spatial domain. One batch of simulations was run in the 1-D light mode, whereas the other

was run in the 3-D interactive mode. Model output was spatially averaged across all 900 plots in the simulation. Model output was further averaged across replicate runs. The successional trajectories from both types of simulation were qualitatively evaluated. The timeseries distributions of average stand DBH, Lorey's height, basal area, and biovolume were quantitatively compared using the nonparametric Smirnov-Kolmogorov test. Stand aggregate basal area, biovolume and biomass for mature forest (>300 years from bare ground) were compared between simulation modes using ANOVA. Each species' contribution to stand aggregate basal area was used to compute the species composition at 10 year intervals. The comparison between forest structure simulated with 1-D and 3-D light modes is shown in Figure 5.1, Figure 5.2 and Figure 5.3.

In the 1-D light simulation, diffuse light extinction is computed from directly overhead, scaled down via Beer-Lambert law (equation 2.1) and overhead LAI. The highest LAI achieved in this simulation is 20. This is realistic for dark conifers spruce, fir and cedar, but not for birch (*DeAngelis et al.*, 1981; *Chen et al.*, 2002; *Stenberg et al.*, 2013), for which LAI also peaks at 20 in the 1-D simulation. Similarly high LAI values have been observed in densely planted young birch and aspen stands (*Johansson*, 1989), when the saplings were less than 3m in height. In the model, the saplings are planted at a $2.5 \pm 0.25cm$ average DBH, and such small saplings do not occur, nor does the stand density reported in this study (50,000-90,000 stems/ha). During the time of birch dominance, the stem density in the simulation is approximately 200 stems/ha. Pine and larch, which have fluffy canopies, peak at LAI of 9 and 5, respectively, which is a little bit higher than observed values (*Gower and Richards*, 1990; *Wirth et al.*, 1999; *Shibistova et al.*, 2002; *Lindroth et al.*, 2008; *Stenberg et al.*, 2013). MODIS-based LAI estimates for a coniferous forest just to the north of Usolsky (57.3^oN, 91.6^oE) fall in the range of 4-6.5 (*Chen et al.*, 2005) and could vary as much as 30% over the course of the summer (*Chen et al.*, 1999). These estimates are known to underestimate LAI for these types of forests, so values greater than 6.5 are still reasonable. The field-based estimates of LAI from the same study were slightly greater than 7. Compared to field observations, the LAI simulated in the 1-D light mode for birch is too high, but falls within the realistic range for the conifers in the simulation.

The overall stand structure exhibits shorter heights and smaller DBHs across all species in the 1-D mode, compared to the 3-D model output, as can be seen in Figure 5.1 - a snapshot from the year 500. Pine appears to persist as the canopy dominant in the 1-D simulation starting around 150 years from bare ground and throughout the rest of the simulation. In the 3-D simulation, pine and larch co-dominate the canopy in a mature forest, with spruce transitioning from the subcanopy to the top of the canopy toward the end of the 5th century from bare ground. Pine and larch play a greater role in the mature forest in the 3-D mode than in the 1-D mode. Fir contribution to stand composition is similar in both simulation, but since the 1-D simulation results in significantly lower aggregate stand basal area, the proportional contribution of fir is much smaller in the 3-D simulation mode. The evolution of stand composition as a function of contribution to total stand basal area by each species is shown in Figure 5.3.

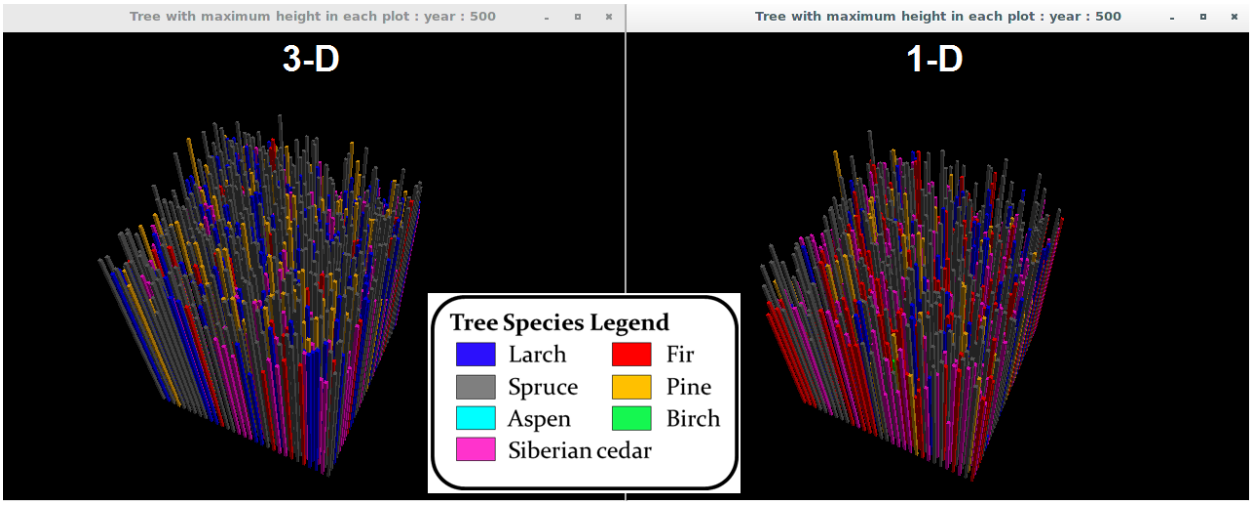

Fig. 5.1: The stand structure is conveyed via color-coded pillars by species. Each pillar represents the tallest tree on the plot. Although the subcanopy and understory are not represented in this visualization, the heterogeneity in the top of the canopy is easily observed in both simulations. Even the largest, tallest trees in the 1-D simulation are smaller than in the 3-D mode.

MIXED FOREST: MODE	1-D	3-D
DBH (cm)	cedar: 15.4(0.4)	cedar: 20.9(0.7)
Lorey's height (m)	pine: 26.3(0.6)	larch: 28.1(0.6)
LAI	20	4.4
stand basal area (m2/ha)	15.4(0.4)	34(0.9)
species-specific basal area(m2/ha)	cedar: 6.0(0.2)	cedar: 14.3(0.7)
biovolume (m3/ha)	137(8)	404(17)
species-specific biovolume (m3/ha)	cedar: 37(3)	cedar: 127(14)
biomass (t/ha)	102(6)	298(11)

Fig. 5.2: The maximum average DBH and LAI, maximum species-specific basal area and biovolume, stand aggregate basal area and stand aggregate biovolume normalized to per hectare, as well as maximum Lorey's height, are shown for the mature mixed forest (>300 years old) simulated using 1-D and 3-D light regimes. Although the height of canopy emergents is comparable between two different simulation modes, the 1-D simulation produces significantly smaller stems, with lower stand biomass, biovolume, and basal area. Average values are presented with standard deviations in parentheses. All variable values are statistically significantly different at the 0.05 level (ANOVA) between the 1-D and the 3-D simulation modes.

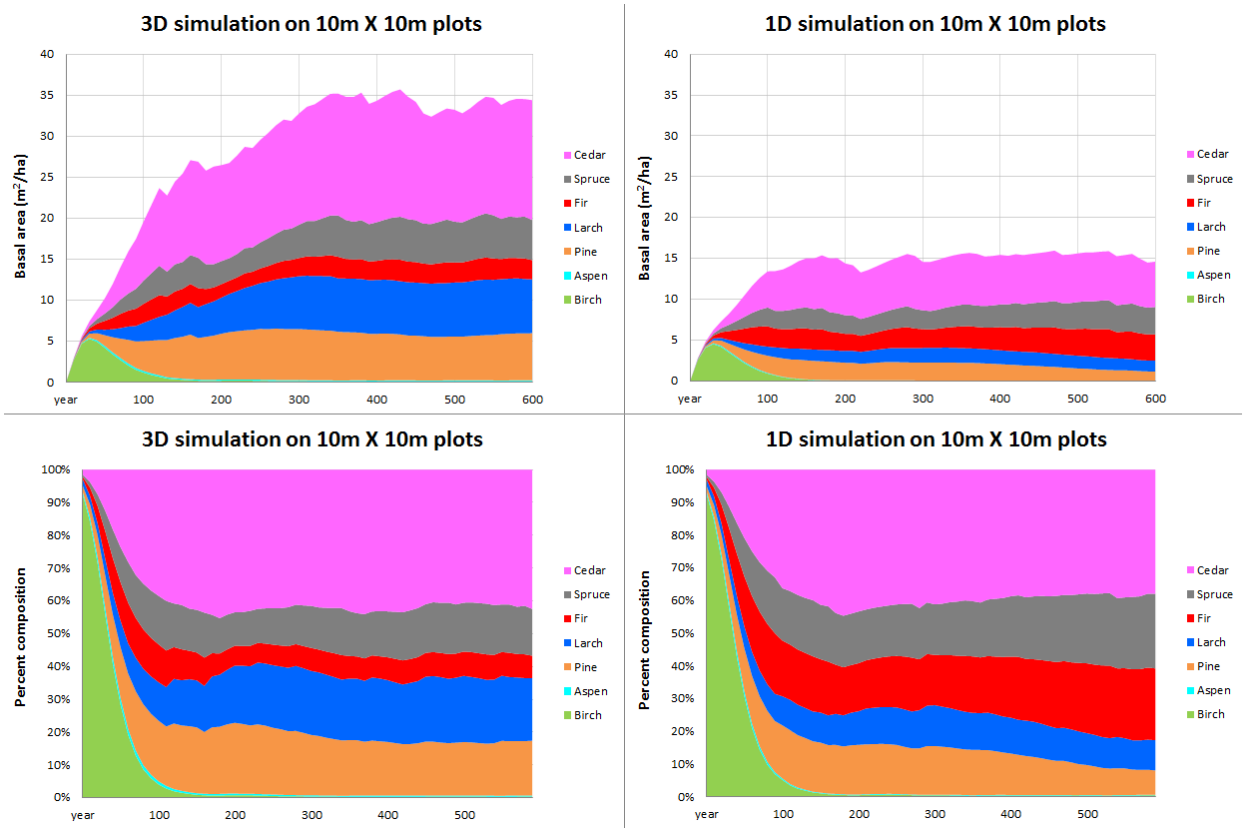

Fig. 5.3: The evolution of stand composition is conveyed for 1-D and 3-D simulations based on each species contribution to total stand basal area. When climate is held constant, the average basal area across model replicates responds to the same occasional limitations in environmental conditions (3 occurrences of drought during the 600-year simulation). The average of the model replicates is therefore jagged, and these 3 drought events do not get averaged out. To better assess the average stand evolution, climate was allowed to vary randomly around the mean. This produces much smoother curves, as each simulation has its own years of drought that are not necessarily coincident in model replicates.

Forest biovolume in Russian forests, averaged for young, middle-aged and mature/overmature stands is in the range of $99.85 \pm 44.35 m^3 ha^{-1}$ (*Alexeyev*, 1998; *Forest Fund of Russia*, 1995). Parsing the same dataset into young, middle-aged, and mature/overmature stands, the average biovolume estimates in each age class are 27.5, 100.2-140.4, and 131.3 $m^3 ha^{-1}$. This is averaged across all of Russia, all types of soils and environmental conditions. The biovolume from the 1-D simulation of mature forest does correspond well with average observed values in mature/overmature stands. These types of stands comprise over 50% of the Siberian boreal forest (*Alexeyev*, 1998; *Krankina and Dixon*, 1994). The higher end of the productivity spectrum, however, is not represented by these average values, and is not captured in the 1-D simulation mode.

Multiple estimates of average forest biomass are reported in the literature for boreal stands that represent different ecotones and age structure groups, which are often not clearly defined. In one summary of average biomass estimates (*Houghton et al.*, 2007), above-ground biomass range of 80.6-223 t/ha is reported. Stand biomass values of $99.61 \pm$

48.53 t/ha (*Houghton et al.*, 2007) and 43.3-245.2 t/ha (*Krankina et al.*, 2005) have been reported for Usolsky forest and central Siberia in general, respectively. Field observations from a site in central Siberia (60.75^oN, 89.38^oE) report 107 t/ha biomass for a stem density of 450 stems/ha, which is half the stand density in this simulation (*Wirth et al.*, 1999; *Shibistova et al.*, 2002). Although biomass does not scale linearly with stem density, it may be possible to estimate that a stand at this site with a stem density of 1000 stems/ha, as in the simulation, may exhibit biomass closer to 200 t/ha. Carbon storage in above-ground biomass at another study site (60.73^oN, 89.15^oE), just to the north of Usolsky, was estimated in the range of 100-200 tC/ha (*Schulze et al.*, 2002). As carbon makes up approximately half of the tree's biomass (*Ajtay et al.*, 1979; *Kobak*, 1988; *Patenaude et al.*, 2004), we can estimate that the above-ground biomass at this study site is in the range of 200-400 t/ha. Furthermore, a coefficient of 0.4 tC/m^3 (*Yan and Shugart*, 2005) can be used to backwards-compute the stand biovolume, which then falls in the range of $250 - 500 m^3 ha^{-1}$. A coefficient of 0.516 tC/m^3 is also sometimes used to estimate carbon stocks from forest biovolume (*Krankina et al.*, 1996). This can be used to backwards-compute a biovolume for the forest studied by Schulze and colleagues, which results in a range of $194 - 386 m^3 ha^{-1}$. A more recent space-based LIDAR estimate of carbon contained in the boreal above-ground biomass in Siberia is in the range of 27.6-65.6 tC/ha (*Neigh et al.*, 2013), which can be used to estimate the above-ground biomass: 55.2-131.2 t/ha, and the above-ground biovolume: $69 - 164 m^3 ha^{-1}$ or $53.4 - 127 m^3 ha^{-1}$, depending on which conversion factor is used.

Modeled biomass from both simulation modes falls within the wide range of field-estimated values, however, I was trying to simulate the most productive stands, and the biomass from the 1-D simulation is comparable either to the middle of the range or the lower end of some estimates, more representative of average stand conditions. In contrast, biomass and biovolume from the 3-D simulation more appropriately align with the higher end of the reported ranges of above-ground biomass and biovolume from stands in central Siberia. When all site indices (soil productivity ranges) are represented in the simulation, or when the average soil fertility (site index III) is used, the 3-D simulation output is also comparable to the middle of the ranges reported in the literature (:math:104.3pm30.1t ha^{-1}‘, Chapter 3). Note that biomass is a questionable calculation in SIBBORK based on the uncertainty associated with linking forestry yield tables to tables of stand productivity (see Section 2.3.3).

With regards to the successional trajectory, both simulation modes appropriately simulate a birch stand initially, followed by a mixed birch-pine forest approximately 50-100 years from bare ground (*Houghton et al.*, 2007), with co-dominance of the two species in the main canopy and other shade-tolerant conifers coming up in the understory. Aspen contributes very little to stand composition in both simulation modes, which is in accordance with observations (*Krankina et al.*, 2005). Starting with 100 years from bare ground, a mixed conifer forest exists, with contributions from larch and pine in the main canopy, and fir, spruce and cedar in the subcanopy, regardless of simulation mode. Stand composition determined from how much each species contributes to total basal area differs somewhat between

the 1-D and 3-D simulation modes, with larch and pine playing a greater role in the 3-D simulation ($36 \pm 1\%$), whereas the dark conifers contribute more to stand composition ($78 \pm 4\%$) in the 1-D mode. The most stark difference is that in the 1-D light mode, the stand basal area is less than one half of what is simulated in the 3-D light mode (Figure 5.3).

1-D versus 3-D in Complex Terrain

For the second comparison, the southern boundary of the boreal forest in the Altay-Sayan mountains was simulated using 3-D and 1-D light subroutines, and non-random historical climate for 200 years. Complex terrain was simulated following the idealized mountain approach from Chapter 4. Almost 7000 plots were simulated in a 70-ha spatial domain that included a south-facing slope and a north facing slope extending from 100m to 3000m amsl. Simulations were initialized from bare ground. Plot-level environmental conditions varied based on elevation and aspect, with south-facing slopes receiving more radiation throughout the growing season and, therefore, experiencing higher PET demands. Temperature was extrapolated from the Kyzyl WMO station (51.4^oN, 94.23^oE) using the standard atmospheric lapse rate of $6.5^oC/km$. Soil nutrition was highest along the lower slopes, and poorest above 2000m. All environmental conditions and species-specific parameterizations were the same across the two simulations. The only difference was the ability of trees on a plot to shade trees on adjacent and nearby plots in the 3-D simulation, and the computation of the light environment from different angles versus only from directly overhead.

In the 1-D simulation, birch and larch were more prevalent in the main canopy on the north-facing slopes, interspersed with fir. Larch occupied the subcanopy, while pine, aspen and birch sprouted and persisted in the understory in a fir-dominated forest - un unlikely position for any of these shade-intolerant species (*Shugart et al.*, 1992). In the 3-D simulation, the north-facing slopes were dominated by fir, with Siberian cedar and spruce coming up in the understory and subcanopy, which matches field observations (*Gorchakovsky and Shiyatov*, 1978; *Isachenko et al.*, 1988; *Istomov*, 2005; *Chytry et al.*, 2008; *Bartalev*, 2010; *Bartalev et al.*, 2011; *Kharuk et al.*, 2013b; *Huttich et al.*, 2014) and other modeling studies (*Monserud and Tchebakova*, 1996). The upper north-facing slopes were dominated by a belt of larches in both simulation modes, however, the 3-D mode output also contains an admixture of spruce, which is in accordance with observations from the Altay-Sayan mountain region (*Polikarpov et a.*, 1986; *Monserud and Tchebakova*, 1996; *Kharuk et al.*, 2009; *Bartalev*, 2010; *Bartalev et al.*, 2011; *Huttich et al.*, 2014; *Timoshok et al.*, 2014). At the timberline on the north-facing slope, both modes appropriately simulate sparse canopy cover and stunted larches.

The simulated biovolume was six times smaller in the 1-D mode, mostly comprised of larch and fir, with greater contribution from birch and cedar (on a percent of composition basis) than in the 3-D simulation. The latter also has mostly larch and fir, but with a greater admixture of spruce (Figure 5.4 and Figure 5.5). This difference is likely due to the light regime and the resulting LAI. When the light is only computed from overhead, it doesn't matter

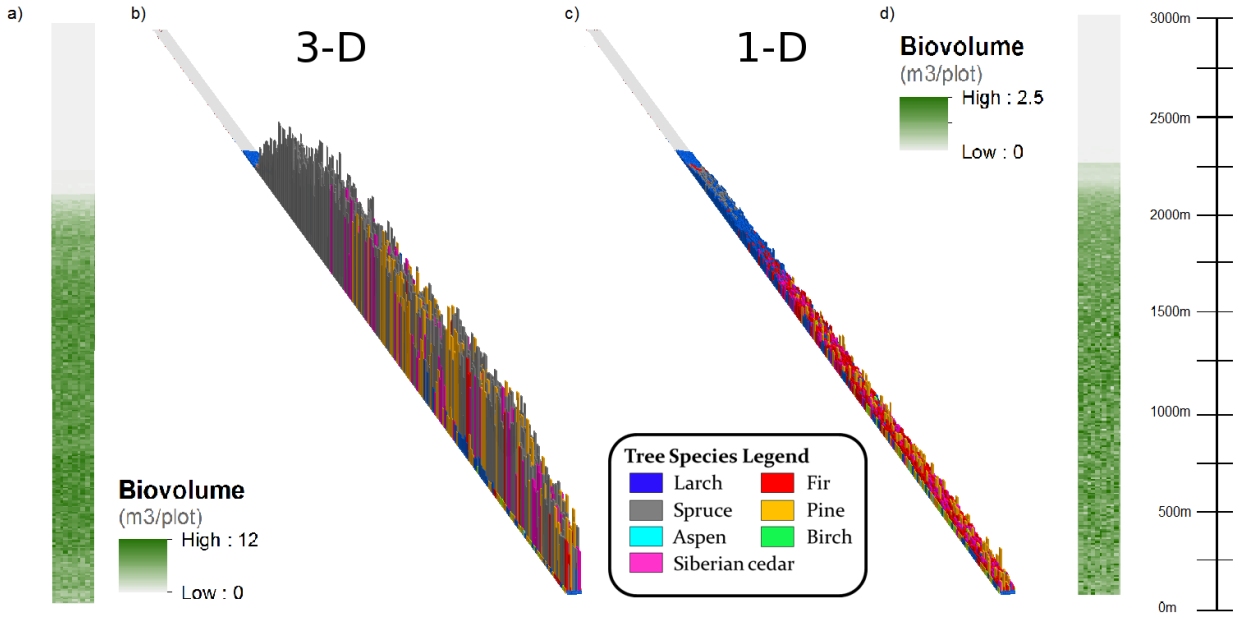

Fig. 5.4: Stand structure and composition of 200 year old forest on north-facing slopes near the southern extent of the boreal forest are shown using 1-D and 3-D model output. The stand composition is conveyed via color-coded pillars by species. Each pillar is scaled to represent the aggregate biovolume on each plot, not tree height. In the 3-D simulation, (a) the biovolume can reach $12m^3/plot$, and (b) stand composition contains significantly more spruce. In the 1-D simulation, (c) the biovolume in the 1-D simulation is about six times smaller, and (d) the forest is mostly comprised of larch, fir and cedar. The scale bar on the right denotes elevation above mean sea level (amsl). The slope extent is 100m-3000m amsl.

MIXED FOREST: MODE	1-D	3-D
DBH (cm)	7	11-12
Lorey's height (m)	19	18
LAI	18	5
maximum biovolume (m3/plot)	2.5	12
average biovolume (m3/plot)	0.91(0.28)	6.5(2.44)

Fig. 5.5: The output from the complex terrain simulation is spatially explicit, as each plot has its own environmental conditions based on its location on the terrain. Spatial averaging or aggregation of this output doesn't make sense. This table only reports the maximum average DBH and LAI, maximum and average plot-aggregate biovolume (standard deviation in parentheses), as well as maximum Lorey's height simulated along the slopes of the idealized 3000m tall mountain for 200 year old mixed forest using 1-D and 3-D light regimes. The values were obtained from raster analysis for each variable.

what the surrounding forest is like, and one may assume that the surrounding forest contains similar structure as the independent plot simulated. In a 3-D light regime, however, the light environment is affected by the canopies upslope and downslope, which are higher or lower by virtue to elevation differences. The trees in the 3-D simulation, therefore, are able to receive more light throughout the canopy, as the canopies are staggered on the terrain, and this affects light penetration to the subcanopy and the understory. In this manner, the effective LAI is significantly smaller in the 3-D mode, and the trees, especially in the subcanopy and understory, are able to achieve more growth each year.

Both simulations appropriately simulate south-facing slopes mostly without arboreal vegetation, with a narrow belt mid-slope dominated by larch (*Tchebakova et al.*, 2001). The trees are stunted at the upper and lower timberlines. The evolution of the stands is very similar in the first 200 years, with mature trees occurring in the upper half of this elevation belt. However, in the 3-D simulation, there are more mature larch trees, whereas in the 1-D simulation higher mortality is experienced due to stress from shading, and the mature larch stands are more sparse. The average available light factor experienced by trees in the 3-D simulation varied between 0.1 and 0.5 in the 1-D mode, with greatest shading experienced by the understory (trees <6m tall), compared to 0.4-0.7 in the 3-D mode. Additionally, the larch elevation belt was routinely wider in the 1-D mode (1300-2500m amsl) than in the 3-D mode (1500-2350m amsl), as a result of more unstable larch sapling populations generated in the 1-D mode. In both simulations, the treed zone on the south side was simulated within the observed range of elevations: lower timberline $717 \pm 372m$, upper timberline $1883 \pm 297m$ (*Samoilova*, 1973; *Polikarpov et al.*, 1986; *Isachenko*, 1988; *Rakovskaya and Davydova*, 1990; *Chytry et al.*, 2008; *Kharuk et al.*, 2010a, 2013b).

The primary advantage of the 1-D light regime is the faster runtime, since the light computation is significantly simplified. For a 600-year simulation with 7 species on 9-ha of flat terrain, runtimes for the 1-D mode are on the order of 3.6 ± 0.1 minutes, compared to 5.4 ± 0.1 minutes for the 3-D mode. For the 200-year simulation with 7 species on 70-ha of complex terrain, the runtimes were on the order of 15 minutes and 24 minutes, for the 1-D and 3-D modes, respectively. The variability in the runtime depends on how many trees are present in the simulation. The 1-D light regime and independent plot mode might be an appropriate simplification for the simulation of flat terrain, large spatial domains, or multiple point locations across the Eurasian boreal forest, as the output falls within the published average stand biomass and biovolume ranges. However, if the investigation focuses on a specific ecotone, transition zones, regions of complex terrain, or where the resolution of environmental gradients across the spatial domain is a particularly important driver for stand structure and successional trajectories, the 3-D light mode is more appropriate and does not increase the computation time significantly. In either case, much more time is spent on analysis of model output than running the model. Spatial explicity, thus, does appear to increase realism in the simulation and has better predictive capabilities. Furthermore, as disturbances become greater in extent and frequency with global climate changes, the ability to simulate stand dynamics at scales larger than one patch (plot) is desirable to more realistically simulate the effects of disturbances of various sizes on forest structure, composition and dynamics.

5.2 Model sensitivity to spatial resolution

In gap dynamics theory, the forest is comprised of a mosaic of patches of stands at different stages of succession, resulting in heterogenous age structure. In previous gap models (JABOWA, FOREST, FAREAST, ZELIG), the plot

size approximated the canopy of a dominant tree within the ecosystem of interest. The reason for this, is that the gap dynamics are driven by the availability of light through the opening created in the canopy when this dominant tree dies and falls to the ground. The availability of light and other resources below the canopy and at the ground level that facilitate growth of previously suppressed trees and the establishment of new saplings changes based on the size of the gap created (*Bradshaw*, 1992). Plot sizes of $1000m^2$ and $400m^2$ were utilized for simulations of temperate and tropical forests in ZELIG, respectively (*Urban*, 1990; *Garman et al.*, 1991; *Holm et al.*, 2014). Application of ZELIG toward simulation of northern hardwood forests in Canada included an assessment of model sensitivity to plot size, and although for monospecies forests different plot sizes were optimal depending on the species crown shape and size, a plot size of $400m^2$ was estimated to best approximate the average crown size and zone of influence of dominant trees in the mixed hardwood forest ecosystem (*Larocque et al.*, 2006; *Larocque et al.*, 2011). The FAREAST Monte Carlo simulation has been used for investigation of dynamics within mixed species (coniferous and hardwood) temperate and boreal forests in China and Russia, and employs circular $500m^2$ plots (*Yan and Shugart*, 2005). In all of these simulations, collocated individual plots of the specified size were simulated, and the dynamics across 100-200 independent replicate runs were averaged to estimate average stand dynamics.

SIBBORK simulation model has been calibrated, verified and validated using $100m^2$ plots, based on the estimate that boreal trees have smaller crowns than temperate or tropical trees. To understand the effect that the size of the smallest spatial unit (plot) has on the spatially-explicit simulation of stand composition and structure, plot size, which is a user-specified parameter, was systematically modified and model output from the simulation of (1) a monospecies broadleaf forest, (2) a monospecies conifer forest, and (3) a mixed hardwood-conifer forest were compared. Square plots $100m^2$, $400m^2$, and $900m^2$ in size were tested using both the independent (1-D grid) and interactive (3-D grid) modes. The idea is that the plot size should represent the size of a canopy dominant tree. In the simulation, the canopy size is limited by the plot size, as a tree's canopy is not allowed to extend outside the boundaries of the plot it is on. When a dominant tree dies and falls, a gap is created in the canopy. Following gap dynamics and plot size limitation on crown size, the size of canopy gaps created by mortality of dominant trees should be congruent with the plot size. In actuality, on a $100m^2$ plot, the canopy is dominated by 1-2 trees, and when one of these succumbs to mortality, a gap opens up in the canopy allowing light to penetrate deeper into the subcanopy and the understory. On a $900m^2$ plot, there may be half a dozen or more canopy emergents, so when one of those dies, no real gap is opened up in the simulated canopy. Instead, the LAI is decreased homogeneously across the plot, and the gain in light at lower levels in the canopy is minimal.

Variation in gap size is likely to change the light environment in the forest, and systematic variation in plot sizes revealed some of this sensitivity in the model. The light environment is computed based on leaf area (LA), which is divided by the plot area to compute the leaf area index (LAI). The LAI is then employed in the exponent of the Beer-

Lambert Law computation of light extinction through the canopy (Figure 2.1). When a dominant tree on a plot dies and falls over, a gap the size of the plot develops in nature, however, in the simulation, the effects may be portrayed quite differently. The larger the plot size - the larger should be the gap simulated. This would change the light environment not only on the plot in focus, but also on adjacent and nearby plots. In a simulation, however, the gap formation depends on the number of dominant trees on a plot. On a $100m^2$ plot, there may be 1-2 dominant trees, but on a $900m^2$ plot there may be half a dozen or more canopy dominants, so the mortality of a single canopy emergent on a $900m^2$ plot doesn't open a gap in the simulation, but rather incrementally decreases the LAI.

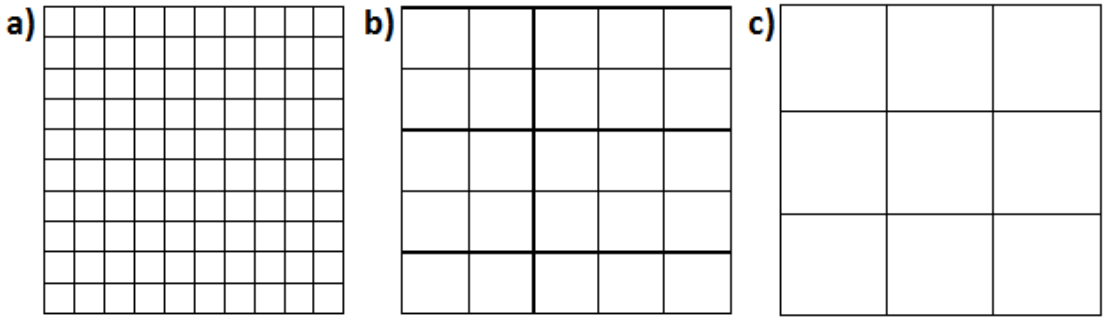

Fig. 5.6: The simulation spatial domain was kept the same, but it was divided into plots of different sizes: $100m^2$, $400m^2$ and $900m^2$ for (a), (b) and (c), respectively. Within a 9-ha simulation area, there are (a) 900 10m X 10m plots, (b) 450 20m X 20m plots, and (c) 300 30m X 30m plots.

To minimize variability between the simulations, the weather subroutine was initialized with the same seed for the random number generator, the stands were initialized with saplings at an initial DBH of $2.5 \pm 0.25cm$ at a maximum stem density of 1000 stems/ha. For the monospecies broadleaf and mixed forest simulations, the model was initialized with birch saplings; for the monospecies conifer forest, the model was initialized with spruce saplings. The spatial domain of the simulation was kept the same (9-ha), however, this represented a different number of plots, based on the plot size specified (Figure 5.6). Soil fertility is specified at the plot level, and exerts a cap on accrual of annual biomass in units of $kgha^{-1}yr^{-1}$. The average DBH, Lorey's height, and biovolume were compared at decadal increments. These stand structure variables for a mature forest (>300 years from bare ground) were statistically compared using an ANOVA, with α at the 0.05 level. In the mixed forest simulation, species composition was assessed via contribution of each species to the total basal area, also at decadal time steps. All stochasticity was removed from the model, including sapling establishment and mortality. The difference in stand structure between simulations with different plot sizes was apparent. However, this produces identical output between model replicates. In order to be able to compute the confidence interval for model output, random climate, inseeding and mortality were activated. Since flat terrain with same environmental conditions on all plots was simulated, model output was spatially averaged across the simulation domain. Twenty model replicates were averaged together, and this average output was compared between simulations with different plot sizes. Optimally, 150 independent model replicates would be used for this analysis (*Bugmann et al.*,

BIRCH: PLOT SIZE	10m X 10m	20m X 20m	30m X 30m
plot area (m2)	100	400	900
plots in simulation	900	225	100
maximum stems per plot	10	40	100
DBH (cm)	$9.4(0.1)^a$	$9.9(0.1)^b$	$9.9(0.7)^b$
Lorey's height (m)	$18.6(0.1)^a$	$19.2(0.1)^b$	$18.9(0.7)^{a,b}$
LAI	$3.6(0.05)^a$	$4.2(0.06)^b$	$4.2(0.58)^b$
basal area (m2/ha)	$8.9(0.15)^a$	$10.7(0.2)^b$	$10.4(1.6)^b$
biovolume (m3/ha)	$96.4(1.8)^a$	$118(2.3)^b$	$113.7(18.6)^b$
biomass (t/ha)	$64.7(1.1)^a$	$78.8(1.5)^b$	$76.1(12.1)^b$

Fig. 5.7: Birch stands varied in structure across multiple plot sizes. Averages are presented for mature stands (>300 years old) with standard deviations in parentheses. Variable values with the same letter are not statistically significantly different at the 0.05 level (ANOVA).

1996), but in the interest of resource and time allocation, 20 independent replicates each containing several hundred plots were considered sufficient replication. Plto size effect on model output was tested using the 3-D interactive grid mode.

Monospecies birch stand

Birch is a pioneer, shade-intolerant species that is somewhat tolerant to stress from inadequate soil nutrition, and is drought-intolerant. The simulation was initialized with birch saplings at an initial DBH of $2.5 \pm 0.25cm$ and a maximum stem density of 1000 stems/ha, and run for 600 years. Figure 5.7 summarizes the initialization and model output information for the mature simulated birch stand conditions. All other species were turned off in this simulation. In the mature birch stand, the stem number oscillates around 900 stems/ha, 970 stems/ha, and 1000 stems/ha, in the $100m^2$, $400m^2$, and $900m^2$ plots, respectively. The canopy height structure becomes highly heterogeneous by the end of the first century from bare ground.

Regardless of plot size, the thermal and soil moisture conditions were not limiting throughout the simulation, with values of 0.99-1.0 and mostly 1.0, respectively. Soil fertility was also not limiting, with factor values close to 1. On the $100m^2$ plots, the birches experienced an average overall growth factor of 0.6, with the available light factors for canopy emergents around 0.7, subcanopy - 0.64, and understory - 0.53. On the $400m^2$ plots, the birches experienced an average overall growth factor of 0.7, with the available light factors for canopy emergents around 0.75, subcanopy - 0.7, and understory - 0.6. On the $900m^2$ plots, the birches experienced an average overall growth factor of 0.7, with the available light factors for canopy emergents around 0.75, subcanopy - 0.7, and understory - 0.6. Trees at all three canopy levels were more suppressed by the light environment on the $100m^2$ plots.

The differences in stand structure and LAI are minimal and not statistically-significantly different between the $400m^2$ and $900m^2$ plots. Although the average plot-wide LAI is smaller, the available light factor experienced by trees on the

SPRUCE: PLOT SIZE	10m X 10m	20m X 20m	30m X 30m
plot area (m2)	100	400	900
plots in simulation	900	225	100
maximum stems per plot	10	40	91
DBH (cm)	$21.1(0.5)^a$	$21.1(0.5)^a$	$16.8(3.5)^b$
Lorey's height (m)	$28.2(0.7)^a$	$28.4(0.7)^a$	$24.2(2.4)^b$
LAI	$16.2(0.4)^a$	$17.0(0.4)^b$	$12.5(3.9)^c$
basal area (m2/ha)	$40.7(2.3)^a$	$43.1(2.3)^b$	$28.2(9.1)^c$
biovolume (m3/ha)	$531(44)^a$	$565(45)^b$	$329(116)^c$
biomass (t/ha)	$327(25)^a$	$375(26)^b$	$206(72)^c$

Fig. 5.8: Spruce stands varied in structure across multiple plot sizes. Averages are presented for mature stands (>300 years old) with standard deviations in parentheses. Variable values with the same letter are not statistically significantly different at the 0.05 level (ANOVA).

$100m^2$ plots is slightly more than on the bigger plots. This results in slightly different stand structure on the $100m^2$ plots, with statistically significantly less biovolume and biomass accrued in the mature birch stands (Figure 5.7).

Monospecies spruce stand

Spruce is a late successional, shade-tolerant species that is somewhat tolerant to stress from inadequate soil nutrition, and is quite drought tolerant. This conifer species was selected in contrast to birch, to assess how plot size may affect the growth trajectory for dark conifer species. The simulation was initialized with spruce saplings at an initial DBH of $2.5 \pm 0.25cm$ and a maximum stem density of 1000 stems/ha. All other species were turned off in this simulation. Figure 5.8 summarizes the initialization and model output information for the mature simulated spruce stand conditions. In the mature spruce stand, the stem number oscillates around 900 stems/ha, 950 stems/ha, and 980 stems/ha, in the $100m^2$, $400m^2$, and $900m^2$ plots, respectively. The canopy height structure becomes highly heterogeneous by the end of the first century from bare ground.

Regardless of plot size, the thermal and soil moisture conditions were not limiting throughout the simulation, with values of 1.0 for both factors, except during 3 years when soil moisture was limiting due to a one-year drought each time. Soil fertility was also not limiting, with factor values around 0.95 in the simulations using the smaller plots. Interestingly, the soil fertility, as well as the DBH, basal area, biovolume, and biomass showed greatest variability over the course of the simulation, and even in the mature stands, on larger $900m^2$ plots. On the $100m^2$ plots, the spruce experienced an average overall growth factor of 0.8, with the available light factors for canopy emergents around 0.87, subcanopy - 0.83, and understory - 0.8. On the $400m^2$ plots, the spruce experienced an average overall growth factor of 0.8, with the available light factors for canopy emergents around 0.9, subcanopy - 0.85, and understory - 0.8. On the $900m^2$ plots, the spruce experienced less suppression, with an average overall growth factor of 0.85-0.9, and the available light factors for canopy emergents around 0.95, subcanopy - 0.94, and understory - 0.9.

MIXED FOREST: PLOT SIZE	10m X 10m	20m X 20m	30m X 30m
plot area (m2)	100	400	900
plots in simulation	900	225	100
maximum stems per plot	10	40	91
DBH (cm)	cedar: 18.4(1.2)	cedar: 20.8(1.1)	cedar: 23.0(0.6)
Lorey's height (m)	larch: 28.2(0.7)	cedar: 24.9(0.5)	larch: 28.6(0.4)
LAI	cedar: 4.5(0.1)	cedar: 5(0.1)	larch,cedar: 5(0.4)
basal area (m2/ha)	$35.8(1.8)^a$	$37.3(1.8)^b$	$41.2(2.8)^c$
biovolume (m3/ha)	$531(44)^a$	$442(19)^b$	$520(26)^c$
biomass (t/ha)	$327(25)^a$	$344(9)^b$	$384(17)^c$

Fig. 5.9: Keeping the total simulation area (9-ha) and maximum stem density (1000 stems/ha) the same, the plot size was systematically varied. Changes in plots size necessitate changes in some plot-level inputs in order to maintain the average per hectare values the same across all simulations. The input parameters that different between the simulations are shown for all plot sizes assessed. The maximum average DBH and LAI, maximum species-specific basal area and biovolume, stand aggregate basal area and stand aggregate biovolume normalized to per hectare, as well as Lorey's height, are shown for the mixed forest simulations, with standard deviations in parentheses. Variable values with the same letter are not statistically significantly different at the 0.05 level (ANOVA).

The differences in maximum DBH and Lrey's height are minimal and not statistically significantly different between the $100m^2$ and $400m^2$ plots. However, the LAI, stand aggregate basal area, biovolume and biomass are statistically significantly different between the simulations with $100m^2$ and $400m^2$ plots. On the $900m^2$ plots, there is greater variability in stand structure and light availability throughout the canopy. The stand structure on the $900m^2$ plots is statistically significantly different from the simulated structure on the smaller plots (Figure 5.8).

Mixed boreal forest

Five boreal conifer species (larch, pine, spruce, cedar, and fir) and two broadleaf genera (birch and aspen) were used in the mixed boreal forest simulation. All runs were initialized with birch saplings with an initial DBH of $2.5 \pm 0.25cm$ and a maximum stem density of 1000 stems/ha. The annual cap on GPP was set at $4m^3ha^{-1}yr^{-1}$. The goal was to simulate very productive stands that are minimally-limited by environmental conditions. The mixed boreal forest simulation was run with a random historical climate for 600 years on flat terrain.

Spatial averaging across the 9-ha simulation area was conducted, in addition to averaging across 20 model replicates. Average landscape dynamics were assessed through the basal area and biovolume changes observed over time on each of the three types of simulated landscapes. Stand structure was assessed through stem density, maximum average DBH, and maximum Lorey's height on a per-species basis, as well as aggregated across the simulation (Figure 5.9). These stands are representative of some of the most productive stands observed in the Usolsky forest (validation site), with biomass values in the 300s of tons per hectare, and biovolumes near $500m^3ha^{-1}$ ($510m^3ha^{-1}$, *Ershov and Isaev*, 2006).

3-D visualization of the simulated stands facilitated qualitative assessment of stand structure and composition at decadal time intervals. Stand evolution is shown at 100-year intervals on $100m^2$, $400m^2$ and $900m^2$ plots (Figure 5.10). This simplified visualization represents the tallest tree on each plot with a pillar that is color-coded to the tree species. It provides a fast qualitative assessment of the composition of canopy emergents in a stand and the canopy geometry as viewed from above. The tallest tree is also likely to contribute the most biomass, biovolume, and basal area to plot aggregate values of those variables. However, it is also possible, and has been observed in the simulation, that the tallest tree is only "tallest" by a few centimeters, in which case, this representation can be somewhat deceptive of the structure of the main canopy on each plot.

At 100 years from bare ground, the stand biodiversity is much greater in the simulation with smaller plots. Some pioneer species trees have died and conifers represent the tallest trees on some plots. In the larger plots, however, birch (green) and pine (yellow) persist as dominants in the canopy much longer. Birch completely disappears from the canopy by the year 200, regardless of plot size. Pine and larch (blue) dominate the canopy two centuries post disturbance on the $900m^2$ plots, with spruce (grey) taking a stronger hold starting at this time. This is in contrast to stand evolution on the $100m^2$ plots, where cedar (pink), fir (red), and spruce can be the tallest trees on the plot even at the end of the first century from bare ground. A mixed conifer forest persists on the smaller plots for several centuries, with spruce progressively contributing more to stand composition.

Regardless of plot size, the tallest trees in a mature forest were pine and larch, reaching 28m. Siberian cedar trees had the largest average DBH and greatest number of stems. This resulted in cedar having the greatest cumulative species-specific basal area: $18 - 25m^2ha^{-1}$. The aggregate per hectare basal area and biovolume showed greatest variability, and maximum values on the largest plots. The evolution of basal area and biovolume on the plots varied, with smaller plots ($100m^2$ and $400m^2$) experiencing more gradual increase in both variables across 600 years, while the accumulation on the larger plots followed a logarithmic profile, with fast growth in the first 200 years, and leveling off in the last several centuries (Figure 5.11). LAI differed slightly across plot sizes, with higher LAI on larger plots. This makes sense, as to maintain the same per hectare stem density, more stems are allowed to inseed on the larger plot. LAI accumulated from more canopies is likely to be higher. Slightly more shading was experienced throughout the canopy on the smaller plots. This is likely due to the light ray trace traversing more plots, and traveling through more leaf layers, than in simulations of larger plots. If the shadow of a 20m tree can extend up to 100m, this equates to 10 plots in the $100m^2$ plot simulation, compared to just over 3 plots in the $900m^2$ parameterization. Accumulation of LAI along the ray trace that may cross 10 plots with an average LAI of 4.4 will result in greater light extinction than along a similar ray trace that only crosses 3 plots with an average LAI of 5.5.

During the course of the 600 year simulation, species in the simulated environment were generally not stressed by lack of soil moisture. Aspen experienced greatest limitation from insufficient heat, with a GDDF of 0.9. The rest of

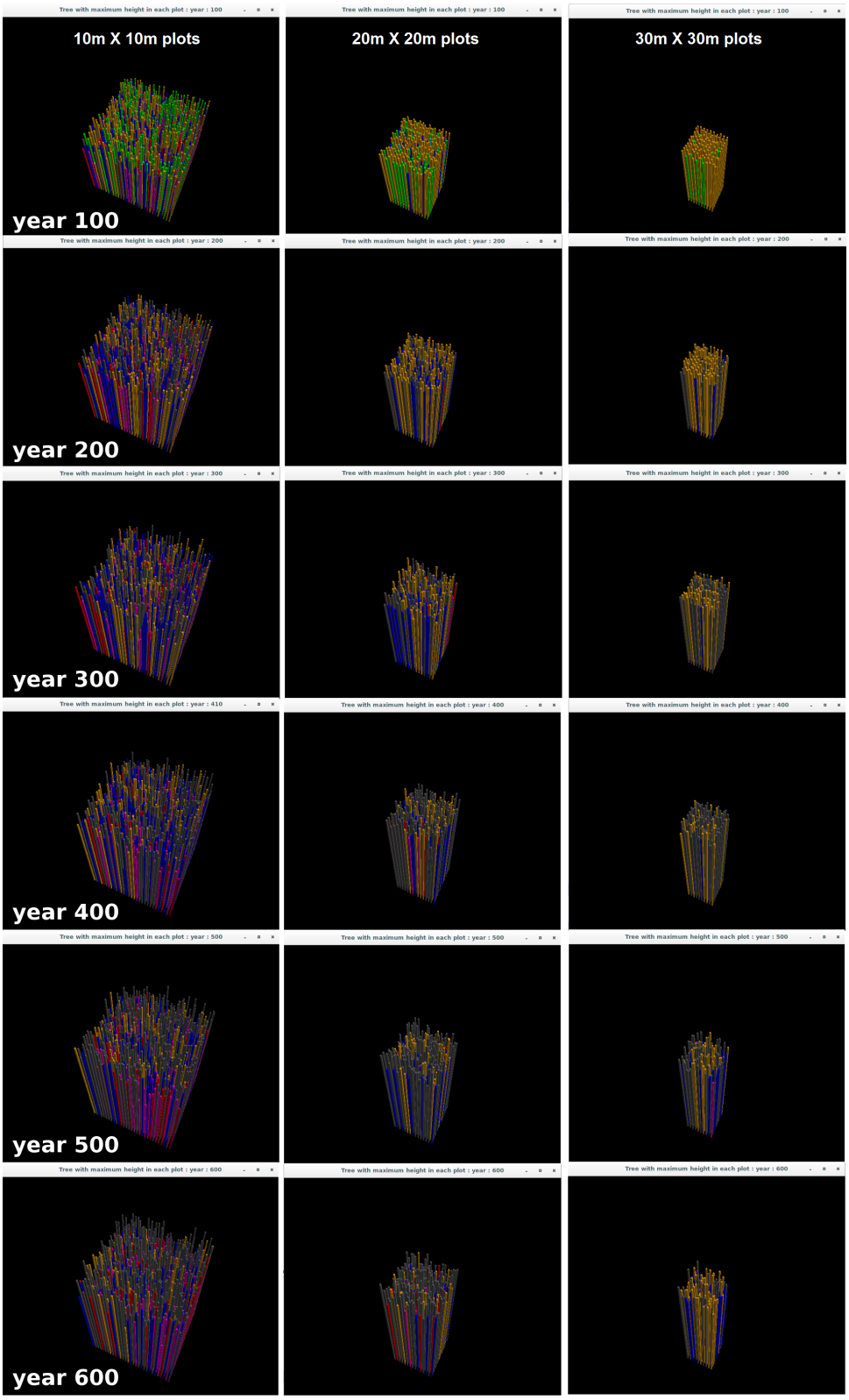

Fig. 5.10: A single tallest tree on each plot is used to represent stand structure via color-coded pillars at 100-year intervals. The spatial domain is the same, but appears smaller simply because fewer trees are used to represent stand structure in the simulation with $900m^2$ plots versus $100m^2$ plots. Legend is the same as in Figure 5.1.

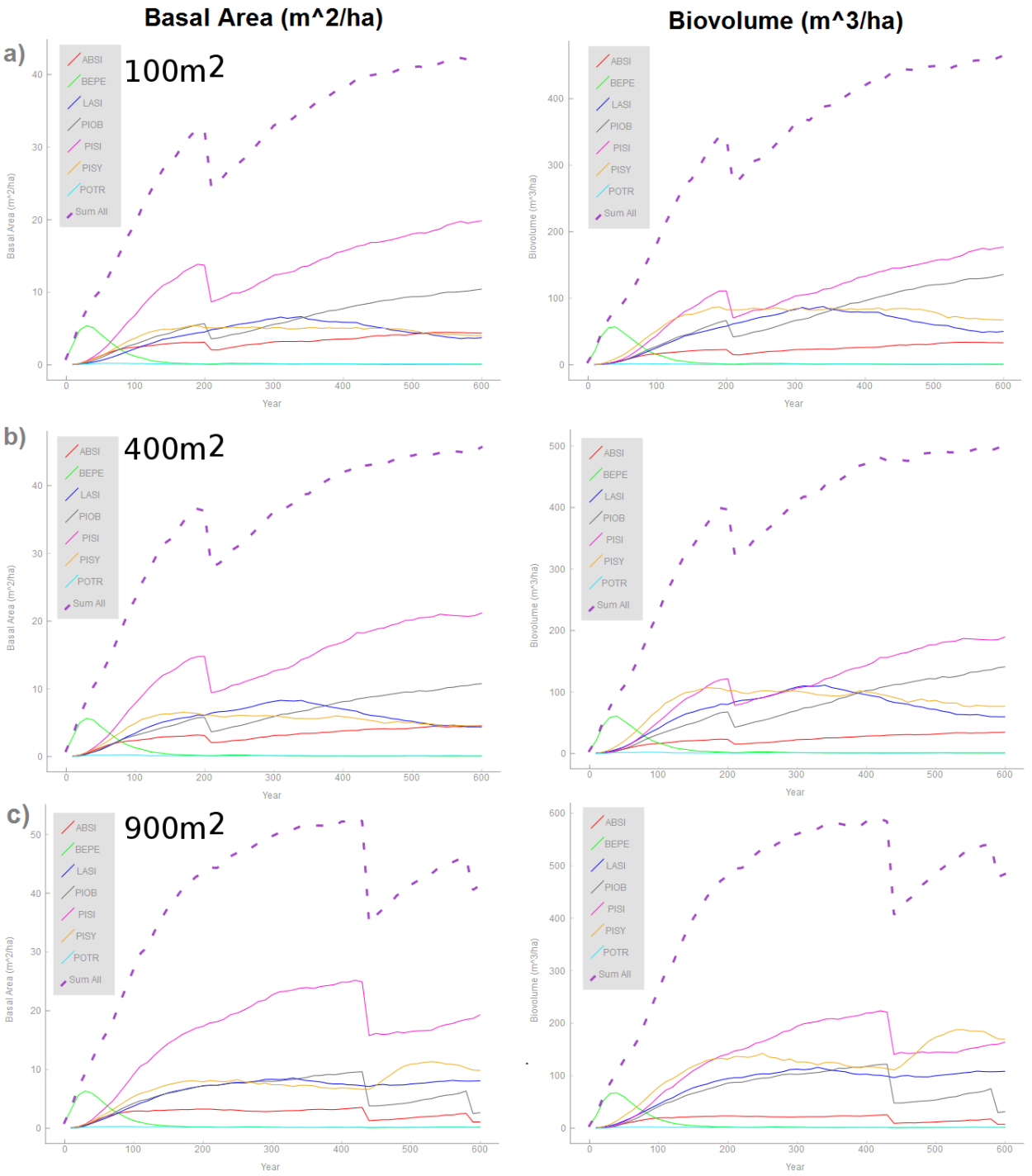

Fig. 5.11: Evolution of basal area and biovolume, normalized to per hectare, shown for (a) $100m^2$, (b) $400m^2$, and (c) $900m^2$ in minimally-limiting thermal, soil moisture and soil fertility conditions over the course of a 600 year simulation. The dashed line represents the aggregate stand sum for each variable normalized to per hectare. Model output presented from a single replicate for each plot size, with fixed climate.

PLOT SIZE	10m X 10m	20m X 20m	30m X 30m
overall growth factor	0.46-0.8	0.5-0.8	0.55-0.85
available light factor (ALF)	0.4-0.88	0.55-0.95	0.55-0.94
soil fertility factor (SFF)	0.88-0.95	0.8-0.95	0.7-0.9
growing degree days factor (GDDF)	0.85-1	0.85-1	0.85-1
soil moisture factor (SMF)	mostly 1	mostly 1	mostly 1

Fig. 5.12: The effects of the growing degrees, soil moisture, and soil fertility are computed for each species on each plot. Available light factor is computed for each individual tree on each plot, as two trees of the same species can experience different light environments within a plot based on the size and the location of the canopy. Plot size has no effect on growing degrees and soil moisture. Within the simulated stands, the average overall growth factor for each tree and the individual environmental effects, varied slightly but not significantly with plot size.

the species have sufficient thermal environment for growth, with GDDF values 0.98-1.0. In general, these are not very limiting above-ground conditions, typical of central Siberia (Figure 5.12).

The soil conditions in these simulations are representative of the more productive stands in central Siberia, with a GPP cap of 4 $m^3 ha^{-1} yr^{-1}$. It was anticipated that the manner in which soil fertility and the light environment affect tree growth will differ between simulations on plots of different sizes. The most nutrient stress intolerant species, such as fir, were most affected by a decrease in soil nutrition as the stand matured, but even that limitation was not very significant, and varied only slightly between different-sized plots. On $100m^{2}$‘ plots, fir was most stressed, with SFF values in the range of 0.88-0.9, while other species were less limited and had SFF values around 0.95. On $400m^2$ plots, fir was most stressed, with SFF values in the range of 0.84-0.86, while others had SFF values around 0.93. On $900m^2$ plots, fir was most stressed, with SFF values near 0.7, while others had SFF values around 0.85.

Species most suppressed by the light environment in a mature forest were birch and aspen, regardless of plots size. Spruce were least suppressed in the closed canopy mature forest environment, regardless of where these trees occurred within the canopy. For the analysis of how light affects trees of each species, the stand was divided into canopy emergents (height > 18m), subcanopy (6m > height > 18m), and understory (height < 6m). The understory experienced the greatest variability in available light over the course of the simulation, regardless of plot size. The average light factors for each species based on the tree's location within the canopy are shown in Figure 5.13.

Although several plot sizes were evaluated, from $100m^2$ to $900m^2$, which encompasses the range of plot sizes used in other gap models (ZELIG, FAREAST, FORMIND, LANDIS), cedar attained the largest average DBH and vied for canopy dominance (Lorey's height) with larch in a mature forest in all simulations. The trees on these plots were similarly affected by their environment. Some trees on the smaller plots experienced more suppression, with the slowest growth 10% smaller than on the larger plots, but the stand structure, assessed through DBH, height, and stem density, did not differ all that much between simulations with different plot sizes.

PLOT SIZE	10m X 10m	20m X 20m	30m X 30m
available light factor (ALF)			
canopy emergents (> 18m)			
aspen	0.62	0.78	0.78
birch	0.55	n/a	n/a
pine	0.64	0.79	0.79
larch	0.59	n/a	n/a
cedar	0.79	0.9	0.9
fir	0.87	0.94	0.94
spruce	0.88	0.95	0.94
subcanopy (6m < height < 18m)			
aspen	0.58	0.72	0.71
birch	0.51	0.72	0.71
pine	0.58	0.77	0.76
larch	0.51	0.77	0.76
cedar	0.75	0.89	0.89
fir	0.84	0.94	0.94
spruce	0.84	0.94	0.94
understory (< 6m)			
aspen	0.45-0.55	0.55-0.7	0.55-0.7
birch	0.4-0.5	0.55-0.65	0.55-0.65
pine	0.5	0.6-0.7	0.6-0.7
larch	0.45	0.6-0.7	0.6-0.7
cedar	0.7	0.8	0.8
fir	0.68-0.78	0.8-0.9	0.8-0.9
spruce	0.8	0.9	0.9

Fig. 5.13: The available light factor is computed for each individual tree on each plot. Thereafter, the light factor experienced by all trees of the same species were averaged based on the tree's location in the canopy. Larch and birch did not appear in the tallest tree category on 20m X 20m and 30m X 30m plots. Trees on smaller plots experienced slightly more shade at all levels in the canopy, but overall plot size appeared to have minimal effect on light limitation.

Sensitivity analysis on plot size and, hence, model resolution, is an important step in model development, because a 9-ha simulation using $900m^2$ plots runs much faster, 2.0 ± 0.4 minutes compared to 6.8 ± 0.9 minutes for the same spatial domain using $100m^2$ plots. Fewer plots decrease the computational time of the light subroutine, which has the largest processing requirements. If shorter simulation times can be achieved by reducing resolution without sacrificing the realism of the results, this is a simple and attractive approach for runtime optimization. However, potentially due to smaller canopy sizes observed in the boreal forest, the simulated biovolume and basal area on $100m^2$ plots closer resemble observed values, than simulations on $400m^2$ and $900m^2$ plots. For these reasons, the spatial resolution of 10m X 10m x 1m has been retained in SIBBORK. At this point, analysis of model output takes significantly longer than running the model.

5.3 Climate Sensitivity Analysis: spatially-explicit forest responses to climate change in central Siberia

The boreal forest, like any forest, sequesters CO_2 from the atmosphere through photosynthesis and stores carbon in above-ground and below-ground biomass. Although boreal vegetation exhibits lower productivity and stores less carbon than tropical or temperate forests (*Bonan*, 2008), it constitutes over 20% of total forested areas (*Krankina et al.*, 1996) and serves as a gate-keeper to the vast carbon stores in boreal soils and permafrost. Soils acquire carbon from litterfall and tree detritus. Decomposition rates are slow in the cold thermal regime of the boreal forests. However, as climate warms, structural and compositional changes in the boreal forest may lead to local and regional amplification of warming through the albedo feedback, as warm-loving dark conifers have a significantly lower albedo year round, compared to cold-loving deciduous larches. Changes in vegetation cover could lead to greater regional warming than would be expected from atmospheric CO_2 concentrations alone (*Randerson et al.*, 2006; *Shuman et al.*, 2011). A shift in boreal forest composition to dark conifer dominance will likely increase the local and regional air temperatures and, therefore, soil temperatures, leading to an increase in decomposition rates and accelerating release of CO_2 to the atmosphere. Additionally, vast regions of the boreal forest are underlain by permafrost, which is also rich in carbon. Some published estimates of carbon stored in the permafrost are more than double the amount of carbon already in the atmosphere (*Schuur et al.*, 2015). Vegetation above the permafrost layer can affect the active layer depth (the depth to which the soil thaws during the growing season) and the release of permafrost carbon into the soil layer and, eventually, into the atmosphere.

For example, larches dominate the region between the Yenisei and Lena rivers in central Siberia. Larches are a deciduous conifer, and lose their foliage in the fall. During the winter, the incoming radiation is reflected by the snow-covered forest floor, keeping the region severely cold (absolute minimum winter temperature -71^oC), which facilitates the maintenance of permafrost. The presence of the semi-permanent Siberian High pressure over this region of Siberia also facilitates a colder climate as clear nighttime conditions are conducive to radiative loss of terrestrial energy to space (*Lydolph*. 1977). When in leaf, the albedo of larch foliage is 0.2, which is almost double of other conifers (*Hollinger et al.*, 2010). In this manner, over the course of the year, larches facilitate a colder climate, which is conducive to shallow depths of thaw during the growing season and freezing of the ground during the winter. If larches were replaced by dark conifers, such as spruce, with a year-round albedo of 0.08 (*Hollinger et al.*, 2010), more solar radiation would be absorbed by the forest canopy through all seasons, facilitating local warming of the air and soil temperatures, deeper depths of thaw, less soil freezing in the winter and, therefore, greater decomposition rates and carbon release from the soils and the permafrost (*Kobak*, 1988; *Kharuk et al.*, 2007; *Shuman et al.*, 2011). Interestingly,

Season	Winter	Spring	Summer	Autumn	Year Average
Trend (C/decade)	0.15	0.58	0.42	0.50	0.42

Fig. 5.14: These warming trends are spatially averaged across all of Russia for each season and represent the average seasonal trends observed during 1990-2014. The lower warming rate during the winter season is misleading. According to Roshydromet Office, wintertime warming trend of 0.44 C/decade was observed during 1976-2009, but following the transition in the North Atlantic Oscillation to the negative phase, winter temperatures have actually been decreasing, especially along south-central Russia, where the observed trend for 1976-2010 was -0.54 C/decade and more recently (1994-2014) -2.0 C/decade.

recent remote sensing analyses demonstrate greater impacts of warming on the productivity and composition of larch forests in Siberia than any other forests in Eurasia (*Bunn et al.*, 2007; *Goetz et al.*, 2007). These findings make the analysis of the response of the denser central Siberian middle taiga forests to climate change, explored in this chapter, all the more pertinent.

Understanding the dynamics of compositional changes in the boreal forest accompanying shifts in thermal and precipitation regimes will help us estimate the rate of subsurface carbon release to the atmosphere, as well as the capacity of this ecosystem to serve as a sink for atmospheric carbon. Previous modeling studies estimate that the boreal belt is expected to decrease in areal extent with climate warming (*King and Neilson*, 1992; *Tchebakova et al.*, 2009b).

5.3.1 Observed and Forecast Climatological Changes

According to the Intergovernmental Panel on Climate Change (IPCC's) Fifth Assessment Report (AR5) report, global annual average near-surface air temperatures have increased approximately 0.88^oC during the 20th century (*IPCC*, 2013). Air temperatures over land have increased at approximately double the rate of those over the oceans. High-latitude areas have warmed more than mid-latitude and equatorial regions, and locations with greater continentality have experienced steeper warming trends than regions with maritime climates. According to the Russian Hydrometeorology Office, the annual average temperature across Russia has been increasing at a rate of $0.42^oCdecade^{-1}$ during 1976-2014 (*Gruza et al.*, 2015), which significantly exceeds the global average of $0.12^oCdecade^{-1}$ for the same time period (*IPCC*, 2013). The warming trends vary by season, as shown in Figure 5.14 for the time frame of 1990-2014 compared to the base historical period of 1961-1990.

The daily air temperature does not necessarily have significant effects on vegetation processes, but the accumulated heat load over the course of the growing season, as summarized with growing degree days (GDD_5), does affect tree growth and evapotranspiration demands. The monthly anomalies for the year 2014 are shown in Figure 5.15 for the Russian Federation (reproduced from *Gruza et al.*, 2015). Considering the year 2014 as a recent example, I estimated the monthly positive and negative anomalies, adjusted the historical monthly average temperatures for the region

(based on WMO records for 1955-2000), and calculated the growing degree days for a WMO station (Dzerzhinskoe #29481) just south of the Usolsky forest used for model validation. A significantly greater amount of growing degree days was accumulated in 2014: 1330, compared to 1267^oC based on the historical average (1955-2000). This warming has not been accompanied by any appreciable changes in precipitation in central Siberia (*Vaschuk and Shvidenko*, 2006; *Gruza et al.*, 2015) and, for this reason, effects of changes in precipitation regime were not examined in this study.

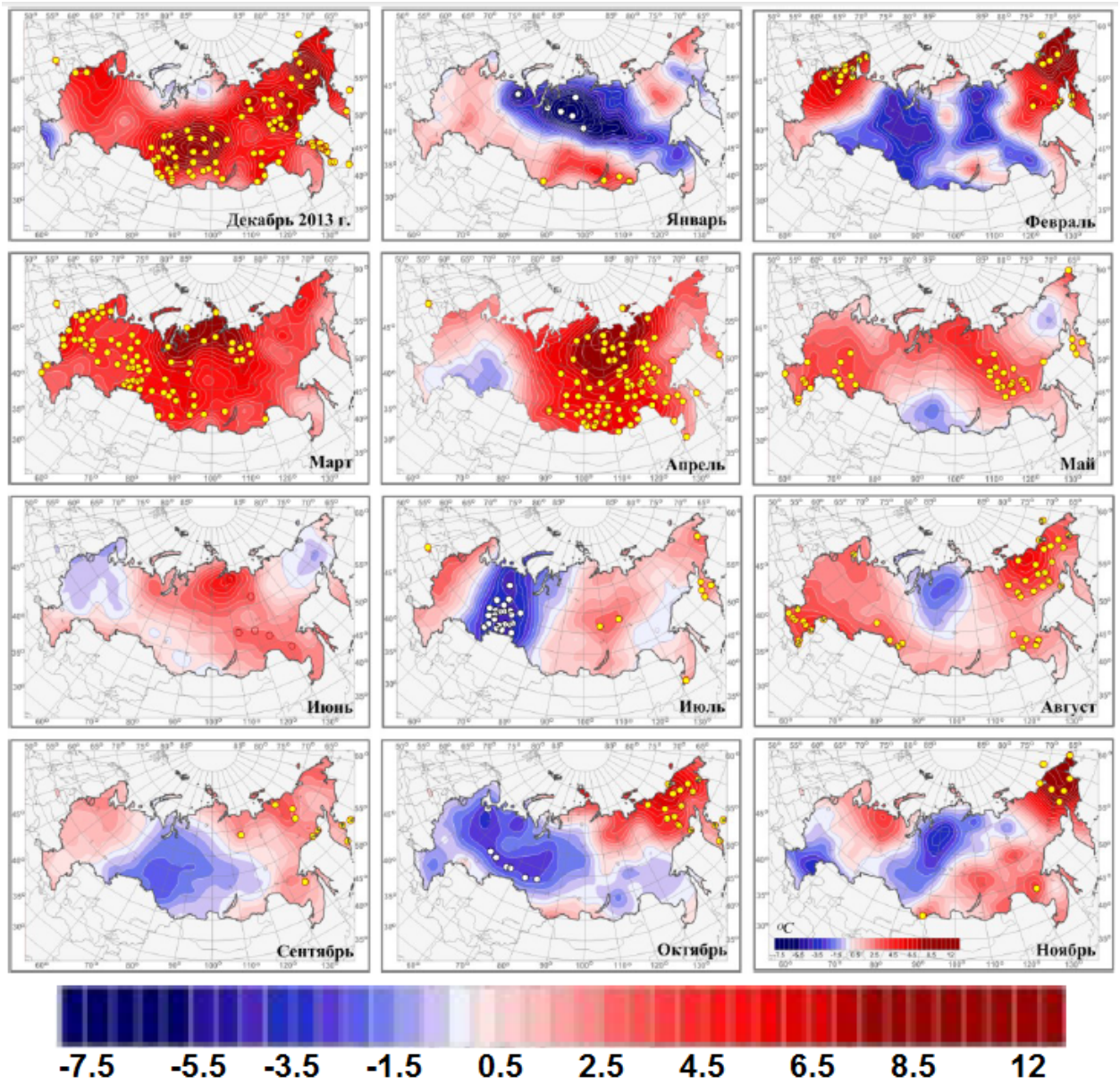

Fig. 5.15: [Reproduced from Figure 1.3 from Gruza *et al.* (2015).] Starting with December of 2013 in the upper left, and moving across to January, February, etc., monthly anomalies are shown in degrees Celsius. Note the heterogenous distribution of the anomalies, both in the spatial and temporal domain.

Forest composition affects the canopy albedo, because different species absorb and reflect different amounts of solar radiation based on canopy geometry and photosynthetic ability (*Betts*, 2000). Changes in forest structure also affect canopy albedo, because canopies of different geometries interact with incoming light differently (*Monsi et al.*, 1973; *Oker-Blom*, 1986; *Betts*, 2000; *Larocque et al.*, 2006). Modifications to the surface (here, canopy) albedo affect heat storage and transfer within the canopy (*Betts*, 2000; *Barlage et al.*, 2005; *IPCC*, 2013). Furthermore, forest structure and composition have a direct effect on the regional water budget, because broadleaf trees respire only during the growing season and at lower rates than coniferous trees, and forests with greater leaf area have greater potential for evapotranspiration, if soil moisture is not limiting (*Kobak*, 1988; *Gower and Richards*, 1990; *Smith and Hinckley*, 1995). For all of these reasons, it is important to understand how the structure and composition is likely to change with the observed and forecast shifts in temperature and precipitation regimes, and to understand the thresholds and tipping points for irreversible compositional changes and biome shifts.

5.3.2 Vegetation response to climate change in 1-D and 3-D modes

Under the historical climate (1955-1990, *NCDC*, 2005a,b; *Gruza et al.*, 2015), the forests in central Siberia, in the vicinity of Usolsky, were not drought-stressed. The 3-D mode best approximated the most productive sites (*Ershov and Isaev*, 2006), while the 1-D simulation mode predicted stand biovolume and biomass close to the average conditions on the landscape (*Houghton et al.*, 2007). For the simulation of the historical climate, monthly average temperature and precipitation sums were generated as in Chapter 4 using a gaussian distribution about an observed mean (*NCDC*, 2005a, 2005b). Climate change in this region was simulated using observed seasonal warming trends (Figure 5.14, *Gruza et al.*, 2015) starting in simulation year 1990. The simulation was initialized in the year 1800, so that by the application of climate change, the forest reaches the average stand age reported in the Usolsky forest inventory (107 years, *Ershov and Isaev*, 2006). The simulation was set up identically to Section 5.1, with flat terrain, a maximum stem density of 1000 stems/ha, and a cap on GPP of $4m^3ha^{-1}yr^{-1}$.

In the 3-D simulation, the entire simulated stand died out suddenly between the years 2070 and 2080 due to insufficient soil moisture. This die-off is reproducible between multiple simulation replicates with random climate. The droughts become more frequent and prolonged after the year 2040, and the region remains in almost continuous drought starting in 2090 and through the end of the simulation (year 2200). Starting with the year 2110, more than 60% of the growing season is in drought. These environmental conditions flag all species, even the most drought-tolerant, for stress-related mortality. The rapid decrease in basal area, biovolume and biomass (Figure 5.16) begins between the years 2030 and 2080 and is very abrupt. Figure 5.16 shows average stand behavior from 20 replicates for each mode. The averaging dampens the apparent rate of collapse. Within a single simulation, the collapse occurs over the course of 1-2 decades.

A few trees remain standing thereafter, but succumb to stress-related mortality within a decade or two. Although some larch and occasional birch saplings try to establish in the decades that follow, they all succumb to mortality from drought-stress and, thereafter, no saplings are able to establish for the remainder of the simulation. Note that saplings of each species require a certain number of years with a favorable environment before they can establish in the simulation at an average DBH of $2.5 \pm 0.25cm$. Those years represent the timeframe when the saplings have a DBH of less than $2.5cm$.

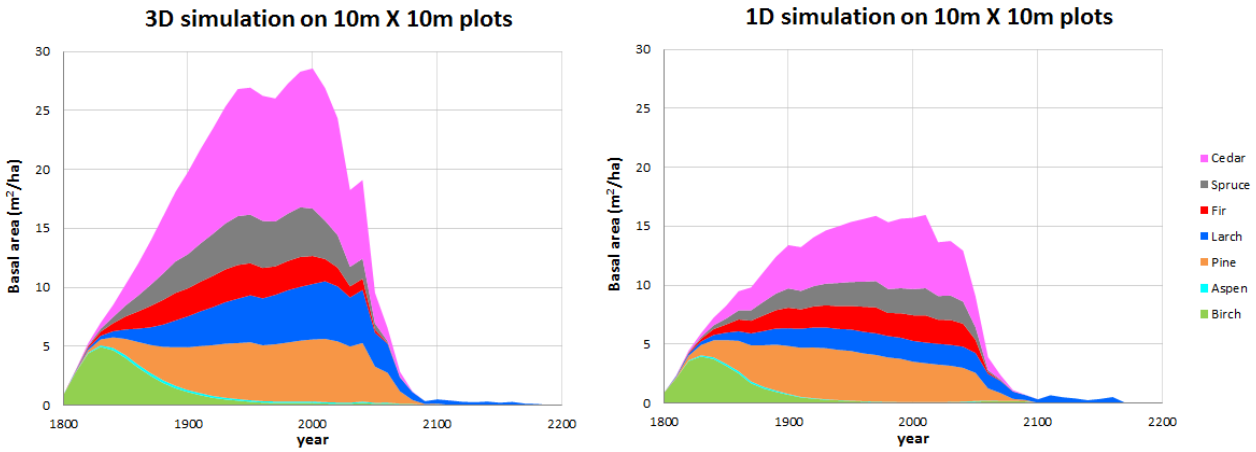

Fig. 5.16: Central Siberian boreal forest response to observed temperature trends extrapolated forward to the year 2200. A significant decrease in live vegetation occurs mid-21st century, a shown through species-specific and stand aggregate basal area.

In the 1-D simulation, the abrupt collapse is also observe within a similar timeframe. However, the stand structure prior to the collapse and attempted regeneration that follows differ from the 3-D simulation. Pre-collapse, the simulated stands in the 1-D simulation are smaller, with approximately one half the basal area of the stands simulated in the 3-D mode, yet three times the LAI (16 compared to 3-4). The pre-collapse forest is of smaller stature and tree growth is more suppressed (as in Section 5.1). There are more birches and pines in the main canopy, and Siberian cedar plays a greater role in the stand composition. Post-collapse, a strong release signal is apparent in the available light factors for main canopy, subcanopy and understory trees, which is absent in the 3-D simulation. Larch, birch, and pine saplings are evident in regeneration in the late 21st century. Pine is generally absent from regeneration in the 3-D mode. Furthermore, larch regeneration appears more intense post-collapse in the 1-D mode, which may be due to higher LAI (3-8 in the regenerating stands, compared to <1 in the 3-D mode), resulting in less light at the ground level and, thus, lower PET demands than in the 3-D simulation.

It is difficult to say which of the two modes more appropriately simulates the vegetation response to climate change. The responses are quite similar across the two modes, and occur within the same time frame and with a similar rate. Spatial-explicity does appear to play a significant role in simulating stands of appropriate structure and composition in

a specified environment. Both simulations modes, however, capture the dramatic decrease in growth rate and increase in stress-related mortality near the same temperature thresholds. Rapid decrease in biomass occurs following a 2^oC increase in annual average temperature (year 2060), collapse occurs with a 2.5^oC increase (year 2080), regeneration by the species in the simulation is no longer successful following a 3^oC increase (year 2090), and conditions are no longer favorable for germination with a 6^oC increase (year 2160). The year estimates in parentheses were obtained using a linear extrapolation of the seasonal trends summarized in Figure 5.14 observed during the 1990-2014 timeframe. However, these trends are likely to change, especially as local changes in vegetation structure and composition become more significant drivers of accelerated climate change in the region, and the listed thresholds are, thus, likely to be reached sooner. The 16-model CMIP3 ensemble of Global Circulation Models predicted that if the IPCC A2 scenario (*IPCC*, 2007) is sustained, an increase of $4 - 6^oC$ in annual average temperature is likely during the 21st century in central Siberia (*Meleshko et al.*, 2008). This GCM-predicted rate is greater than the extrapolation of observed seasonal warming trends used in the SIBBORK simulation.

These results are in contrast to the findings by Gustafson *et al.* (2010) and Shuman and Shugart (2009), who used the LANDIS-II and the FAREAST models, respectively. In the FAREAST simulation, a gradual 2^oC increase in annual average temperature over the course of 200 years, without changes in precipitation, did not result in statistically significant changes in stand biomass across multiple sites in Eurasia. A 2^oC increase over the course of 2 centuries represents a much slower rate of warming than reported by Gruza *et al.* (2015) for the period of 1990-2014. In the LANDIS-II study, Gustafson and his colleagues parameterized the model according to species and site conditions from an area just east of Usolsky (58.9^oN, 103.0^oE), and increased the temperature by 5^oC over the course of a century, alongside a 20% increase in precipitation. They observed no significant changes in biomass or stand composition due to changes in climate alone. It is possible that a very gradual warming rate would not change stand dynamics in SIBBORK either, or that an increase in temperature accompanied by an increase in precipitation would not result in the dramatic forest collapse toward the end of the 21st century. These analyses were not conducted. Instead, actual observed seasonal warming trends were employed to modify temperature at an observed rate alongside no change in the precipitation regime, since none has been observed in the region, and a collapse of forest structure was observed with a 2.5^oC warming in central Siberia. This particular result is not unique to SIBBORK. Further investigation by Shuman and her colleagues using the classical gap dynamics model FAREAST observed a collapse in forest biomass following a comparable increase in annual average temperature in central Siberia (*Shuman et al.*, 2011). Climate change was simulated as a linear increase of historical annual average temperature by 4^oC over the course of 500 years, and a collapse in larch-dominated stands was observed at year 175, which corresponds to 1.4^oC increase. However, at that point in their simulation, birch and pine were still able to establish and a forest with new composition quickly developed. This type of regeneration was not observed in SIBBORK following the collapse of forest vegetation with

a 2.5^oC increase in annual average temperature and no change in precipitation in central Siberia. Sudden changes in vegetation structure and biome shifts have been observed in the past, such as at the end of the Pleistocene (*Chapin et al.*, 2004), and so are likely to occur in the future, especially as the current rate of warming in Siberia seems to have surpassed most time periods in the paleontological record. The outlook is grim, however, SIBBORK can be used to assess the feasibility of mitigation efforts, including selection of species that are most likely to thrive under the probable new growing conditions in southern and central Siberia in the 22nd century.

CHAPTER

SIX

CURRENT AND FUTURE DEVELOPMENTS

"Sometimes the questions are complicated and the answers are simple." - Dr. Seuss

6.1 Disturbances and Mitigation

Eurasian boreal forests represent half of the global boreal forest, constitute nearly a quarter of global forested area (*Anonymous*, 1990; *Conard et al.*, 2002), and comprise a significant area for the exchange of carbon between the atmosphere and the terrestrial biosphere. As atmospheric CO_2 concentrations increase, and the growing global population exerts greater pressures on land use and timber products, it is important to understand how current and potential future disturbance regimes may affect the role of the Eurasian boreal forest in the global carbon cycle. In recent decades, likely due to increasing disturbances, the loss of forest biomass has exceeded biomass accumulation in these forests (*Krankina and Dixon*, 1994; *Krankina et al.*, 1996; *Krankina et al.*, 2005). Similarly, Canadian boreal forests have also experienced greater loss of biomass to timber harvest, stress-induced stand mortality, insect outbreaks, fires, and other disturbances than accumulation of live biomass (*Kurz et al.*, 1995b; *Kurz and Apps*, 1999; *Ashton et al.*, 2012). Equally vital is the understanding of how climate change and the associated shifts in disturbance regimes may affect the structure and composition of the Eurasian boreal forests and their ability to sequester and store carbon, and provide the raw materials for the timber industry. This chapter explores the possibility of including three of the most prominent forest disturbances - fire, insect outbreaks and timber harvest - in the SIBBORK model, and assesses the necessary parameterizations and likely changes to model output from this inclusion.

6.1.1 Inclusion of disturbance alters model output

In SIBBORK, saplings are established and grow into trees. The trees are subjected to species-specific intrinsic mortality, which assigns equal probability of mortality in a given simulation year to all trees of a given species, regardless

of age. Under the current SIBBORK parameterization for age-related mortality, 1% of trees survive to their species-specific maximum age in the absence of environmental stressors (*Shugart*, 1984). This assumption is only valid in stands without disturbances. If disturbances are considered in observed stands and in the simulation, fewer than 1% of individuals would be expected to survive to the species-specific maximum age (*Mielke et al.*, 1978; *Keane et al.*, 2001). Trees are additionally subjected to stress-related mortality, which depends entirely on the environmental conditions and each individual tree's tolerance to these conditions based on species and position in the canopy. Inclusion of disturbance - an event that affects the stress level and mortality of multiple individuals within one year - would shift the forest structure toward a younger forest, and forest composition - toward greater prevalence of pioneer species (*Goetz et al.*, 2007). Dense stands of birch and aspen would become more prominent, and transition to a dark conifer forest may not be reached between disturbances.

Different disturbances affect the forest structure, composition, and dynamics in different ways, and therefore require different parameterizations within a simulation model. I do not have a goal of explicitly simulating different forest disturbances in SIBBORK, as this would require me to become an expert in fire modeling, meso-scale (winds) meteorology modeling, and population dynamics modeling with a focus in entomology. Needless to say, numerous fire and insect propagation models already exist. Rather, I am interested in modeling the *effect* of these different disturbances on forest vegetation processes, which would include parameterizations in the establishment, growth, and mortality subroutines that incorporate species-specific effects of these agents. Wildfires, insect outbreaks, logging, windthrow, landslides differ significantly in their spatial and temporal domains. Their effects on vegetation processes and the rate of carbon release to the atmosphere also differ, depending on the disturbance (*Krankina et al.*, 1996). For example, intense crown fires result in a large flux of carbon into the atmosphere during the disturbance event, whereas low-intensity fires, windthrow and insect outbreaks result in standing and fallen detritus (dead biomass) that continue to release carbon to the atmosphere over the course of several decades following a disturbance (*King and Neilson*, 1992; *Wirth et al.*, 2002; *Kashian et al.*, 2006; *Goetz et al.*, 2007; *Dore et al.*, 2008). Inclusion of parameterization for the effects of disturbances on mortality and sapling establishment subroutines is likely to result in different stand structure and composition for surviving stands, and in different successional pathways for stands recovering from stand-replacing disturbances.

Fire

Millions of hectares of boreal vegetation is destroyed by wildfires annually (*Conard et al.*, 2002). Wildfires affect an ecosystem through a multitude of processes, including a large carbon pulse to the atmosphere, decreased surface and (charred) vegetation albedo in the short-term (years, *Gerard et al*, 2003) followed by increased albedo in the long-term (decades, *Goetz et al.*, 2007), an increase in forest floor decomposition rates and the availability of soil nutrients or loss of forest floor, increased amount of light reaching the ground, as well as modified hydrology and radiation

budgets (*Kasischke and French*, 1995; *Liu et al.*, 2005). The wildfire pattern in boreal ecosystems is a driving factor in the landscape-scale stand structure and diversity (*Bonan and Shugart*, 1989). The intensity of the effect of fire on forest vegetation depends on the expanse and type of fire. Wildfires are generally classified into three categories based on intensity: crown (most intense), ground (moderate intensity), and surface (low intensity) (*Wirth*, 2005). There is significant interannual variability in the area burned each year, and the degree of damage to the forest stands (*Conard et al.*, 2002; *Soja et al.*, 2007). As much as 80% of the burned area may experience low-intensity surface fires, while in intense fire years, 50% of the burned area may suffer high-intensity crown fires (*Conard et al.*, 2002; *Gustafson et al.*, 2010). Different arboreal species have different tolerances to fires, with pines and larches able to survive most medium-severity surface fires due to thicker bark (*Wirth*, 2005), while aspen and birch experience complete mortality even in low-severity fires (*de Groot et al.*, 2013). In the lowest intensity category, mostly the forest floor/litter and some of the smaller saplings are destroyed. Moderately-severe ground fires kill most of the understory. These two categories represent the vast majority of fires reported for Russia and are most common in pine and larch forests (*Conard et al.*, 2002; *de Groot et al.*, 2013). Crown fires are intense enough to kill all vegetation (*Kukavskaya et al.*, 2013), and are more commonly observed in dark conifer forests (*de Groot et al.*, 2013). Frequencies of occurrences for each of these three types of fires has a significant effect on long-term forest dynamics. The recovery trajectory after a fire may be significantly different from the successional pathway that resulted in the pre-burn forest structure and composition, especially if it occurs under different climatological conditions (*Viereck et al.*, 1986; *Kukavskaya et al.*, 2013; *Johnstone et al.*, 2004; *Goetz et al.*, 2007).

Wildfires can occur in a forest of any age, structure and composition. Ignition is often facilitated by lightning (*Kharuk et al.*, 2011), although over 80% of fires in Siberia are likely anthropogenic in origin (*Korovin*, 1996; *Valendik*, 1996; *Mollicone et al.*, 2006; *Gustafson et al.*, 2010). The type of fire, the amount of fuel load and the wind conditions determine the intensity and rate of spread (*Hely et al.*, 2001; *Gustafson et al.*, 2010). Climatic changes affect the amount of moisture in vegetation and, therefore, the likelihood of ignition (*Balzter et al.*, 2005). Forest composition can also facilitate or suppress development of crown fires, such as by high crown moisture content in broadleaf and larch canopies versus highly flammable dark conifer needles (*Cvetkov*, 2002; *Chapin et al.*, 2006 a,b; *de Groot et al.*, 2013), and mediate, to an extent, the amount of carbon released to the atmosphere (*Goetz et al.*, 2007).

Recent studies show that following a fire, not all trees die and fall over. Some remain standing and continue to grow minimally in a very stressed state following fire damage. During this time, which can be upward of 40 years, the forest acts as a source of atmospheric carbon (*King and Neilson*, 1992; *Kashian et al.*, 2006; *Kurz et al.*, 2008). The standing snags do not facilitate regeneration to the same degree that an area with fallen trees would. Regeneration also differs post fire, depending on fire size and intensity. Stand structure and, therefore, light geometry, will differ significantly following a ground fire versus a stand-replacing crown fire. Some trees will be able to survive low-intensity ground

fires, and the regeneration that follows is likely to facilitate establishment of shade-tolerant coniferous saplings. After a stand-replacing, high-intensity crown fire, however, sufficient light environment will likely facilitate sprouting of shade-intolerant broadleaf or deciduous conifer (larch) species (*Nikolov and Helmisaari*, 1992; *Goetz et al.*, 2007). High-intensity crown fires are often followed by regeneration of even-aged cohorts of shade-intolerant species (birch, aspen, larch), whereas low-intensity ground fires allow regeneration of cohorts of shade-tolerant (dark conifers) and somewhat-shade-tolerant species (pine) in the understory (*Gustafson et al.*, 2010). Stand productivities along these two trajectories are vastly different, with shade-tolerant conifers exhibiting lower productivity and lower albedo than broadleaf stands.

Vegetation subject to fires less than 50-ha in size are often replaced by the same species that grew in the area pre-fire, whereas following larger fires, regeneration is delayed, but all species whose range overlaps the burned area are likely to be represented in the new growth (*Buryak et al.*, 2009). Fire facilitates the sprouting of larch due to the heat necessary to open up the serotinous cones (*Chapin et al.*, 2004). Spruce, which regularly reproduce by seed, stump sprouting or layering (vegetative regeneration through roots), predominantly undergo regeneration by layering following a surface fire. Regeneration of some boreal species is delayed following a fire (*Buryak et al.*, 2009). To realistically represent the effects of wildfire on tree growth, mortality and regeneration, species-specific tolerances to fire damage and enhancements to seed bank need to be incorporated. The current version of SIBBORK only addresses reproduction by seed. Some species, such as spruce, birch and aspen, also reproduce vegetatively via stump sprouting. Stump sprouting is currently not represented in SIBBORK, but may become more important in capturing post-fire forest regeneration dynamics and appropriately representing aspen and birch regeneration following a surface fire.

Parameterization of effects of wildfire on vegetation simulated in SIBBORK will need to include fire periodicity and fire intensity, as well as a fire tolerance for each species in the model. The fire tolerance will determine the likelihood that a tree will be killed in a fire of a given intensity. The inseeding rates of species that are facilitated or suppressed by wildfire can also be modified. Figure 6.1 summarizes the data on fire frequency (*Onuchin*, 1986; *Shvidenko and Nilsson*, 2000; *Kharuk et al.*, 2005; *Soja et al.*, 2006; *Houghton et al.*, 2007; *Buryak et al.*, 2009; *Ivanova et al.*, 2010; *Kharuk et al.*, 2011) and area burned (*Furyaev et al.*, 2004) for northern, middle, and southern taiga ecotones. The fire return intervals in Figure 6.2 are presented as a function of the type of fire, classified by fire intensity level. Figure 6.3 assimilates species-specific fire tolerances and the effect of fire on regeneration for boreal species in Siberia (*Nikolov and Helmisaari*, 1992; *Wirth*, 2005; *de Groot et al.*, 2013).

Together with an undergraduate student Charlie Henley, a simple, probabilistic fire subroutine, which kills all trees on plots with fire in a given simulation year, has been developed for SIBBORK. The subroutine is similar to the parameterization used for exogenous mortality in early gap dynamics models (*Prentice et al.*, 1993). The process flow for this subroutine is shown in Figure 6.4. A simple linear model (equation (6.1)), is used to scale the random

ecotone	% burned annually	fire return interval
southern taiga	0.25	60-80 years
middle taiga	0.16	65-100 years
northern taiga	0.13	130-350 years

Fig. 6.1: In the simulation the fire return interval can be used to set the probability of fire on each plot for each year of the simulation. It would be up to the user to specify the correct probability in the driver for the cotone simulated, since "ecotone" is not a variable in the simulation. The percent of area burned can be used to validate the fire probability subroutine by comparing the area burned in the simulation, averaged across 150 replicates, to the observed annual average value. This type of comparison would not work for simulations of independent plots, and would only make sense for 3-D grid simulations with spatial domains of several hectares. Fire return intervals obtained from the literature for southern (Onuchin, 1986; Houghton et al., 2007; Buryak et al., 2009; Ivanova et al., 2010), middle (Kharuk et al., 2005; Soja et al., 2006), and northern taiga (Shvidenko and Nilsson, 2000; Kharuk et al., 2011) .

intensity	fire return interval
low	< 50 years
moderate	50 - 100 years
high	> 100 years

Fig. 6.2: The fire return interval varies based on the type of fire, classified by intensity.

species	Fire tolerance (code)	Fire plant functional type	fire return interval
Abies sibirica	intolerant (1)	Avoider	167 years
Larix sibirica	very tolerant (4)	Resister	59 years
Betula pendula	somewhat intolerant (2)	Invader	57 years
Picea obovata	intolerant (1)	Avoider	167 years
Pinus sibirica	intolerant (1)	Avoider	167 years
Pinus sylvestris	tolerant (3)	Resister	36 years
Populus tremula	intolerant(1)	Endurer	57 years

Fig. 6.3: Species-specific fire tolerances can be used together with fire intensity to assign stress flags or kill trees in the event of a fire disturbance on a plot. Fire tolerance rank (1 = intolerant, 4 = very tolerant) can be used similar to the shade-tolerance classification, to determine the effect of a fire event on each tree on the plot. Each species has a different strategy for survival in an ecosystem where wildfires are a regular disturbance, which focuses either on the survival of the mature tree or the enhanced dispersal/germination of seeds following a fire. Dark conifers are fire avoiders - their flammable canopies result in rapid spread of wildfires and significant damage and mortality of these species in a fire. Larch and pine have thick bark, and are able to resist most low- and moderate-intensity fires. Birch seeds are wind-dispersed, and readily colonize burned areas. Aspen and some species of birch readily stump- or root-sprout following a fire, and are classified as endurers. Due to the species-specific adaptations to fire disturbances and the manner in which species modify their environment, the fire return interval varies based on the fire plant functional type of the dominant species (Wirth, 2005).

probability of fire based on the mean fire return interval (MFRI) by a drought trigger that can induce additional fire events in years with a specified portion of the growing season in drought (soil moisture below wilting point).

$$FireProbability = \beta_0 + \beta_1 \times DroughtFireRiskCoefficient \tag{6.1}$$

where β_0 represents the MFRI ($years^{-1}$) and β_1 represents the fire probability if the entire growing season is in drought. The *DroughtFireRiskCoefficient* will need to be estimated based on how much greater the observed fire activity is during particularly dry years in each ecotone. Initial testing using a β_0 value of 0.012 (MFRI=82 years) and a β_1 of 0.01 (drought increases the chance of fire by 1%) demonstrated that over the course of a 500 year simulation there was a strong correlation between drought and fire occurrence on a plot.

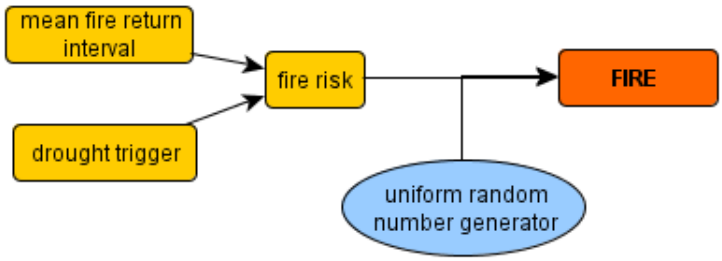

Fig. 6.4: The process flow for the probabilistic fire subroutine with a drought trigger.

Using the MFRI for central Siberia (82 years, Figure 6.1), stand conditions were simulated under a fixed historical climate starting from bare ground, and model output was compared to simulation without fire. The specified MFRI in the simulation means that each plot has a chance of burning once every 82 years. The burning of the plots in this probabilistic fire subroutine is not synchronized, so some plots in the 9-ha simulation burn each year. This suppresses the stand aggregate biovolume and shifts forest composition toward a higher contribution from birch, larch and pine (Figure 6.5). The shift toward shade-intolerant species likely occurs due to the decrease in LAI, which peaks at 7.6 in the simulation without fire, but does not exceed 3.1 in between fire events. Regeneration in both simulations followed a similar pattern following a year with a significant drought (year 200), with a pulse of larch and birch saplings in the understory. This severe drought increased stress-related mortality and triggered more fires than other years, which resulted in gaps the size of multiple plots and significantly more light available in the understory and ground level. The available light factor was 0.6 for aspen, birch and pine in the understory following the drought-stress and drought-triggered fire mortality events, compared to 0.5 just before the drought and in the simulation without fire. The available light factor for birch, aspen, larch, and pine in the subcanopy increased by 5%. Simulation without fire experienced the same drought and stress-based mortality, but this did not open up as many gaps, and the enhancement to the available light factor for the shade-intolerant species in the subcanopy was on the order of 2-3%. Even the shade-intolerant

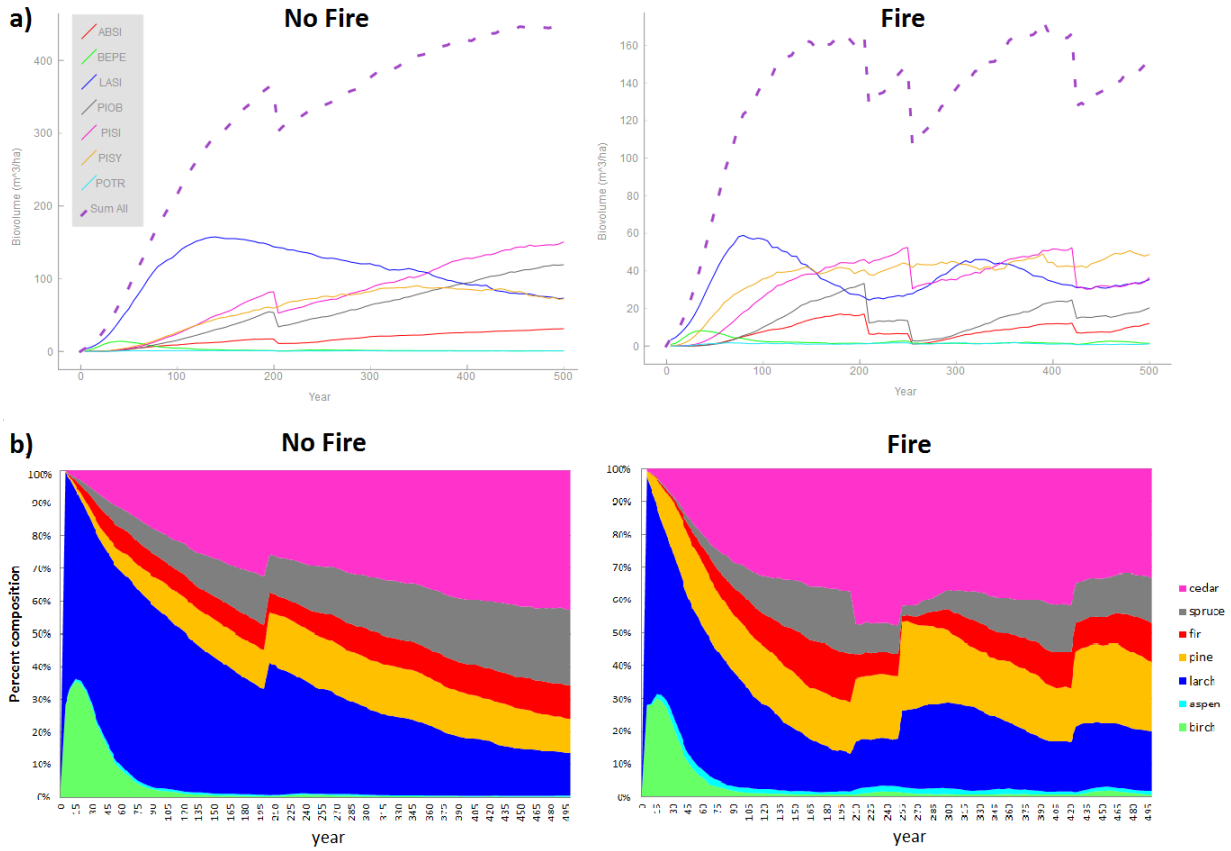

Fig. 6.5: A comparison of (a) simulated biovolume and (b) species composition with and without a probabilistic drought-triggered fire subroutine. When triggered, the fire kills all trees on a plot, which underestimated stand biovolume, however, the change in species composition with the inclusion of the fire disturbance is realistic.

species in the main canopy experienced release with a 5% boost in the available light factor following the drought and the associated fires. There were additional, smaller pulses in larch and cedar regeneration following years in which fire events were more numerous, which were not observed in the control simulation without fire. However, because the plots that burned each year were not necessarily next to each other, only small gaps were created on an annual basis by the death of all trees on the burned plots, and regeneration of pioneer, shade-intolerant species, such as birch and aspen, following probabilistic fire (without drought) was not observed.

This fire subroutine allows the fire trigger to kill all trees on the plot and does not account for different fire intensities, which may leave certain larger and tolerant trees standing. The reduction in biovolume from this approach is exaggerated. The area burned each year in the simulation is slightly larger than observed values, which are $0.48 \pm 0.18\%$ and 0.16%, respectively, potentially due to the rough estimation of the MFRI. When an MFRI of 100 years is used, the area burned each year is decreased to $0.4 \pm 0.14\%$. Further development will include tuning the MRFI to better capture the area burned each year and modification of mortality preferentially assigned to the fire-intolerant species.

The effect of fires on the carbon balance can be estimated by using the accumulated above- and below-ground biomass to estimate the amount of carbon sequestered from the atmosphere, and published estimates for emissions from fires (*Shvidenko and Nilsson*, 2000; *Conard et al*, 2002; *Wirth*, 2005), both in units of $kgCm^{-2}$ or *t* ha^{-1}. For example, Conard and her colleagues estimated that 22.5 tC are emitted for each hectare burned in Eurasia via a high-intensity crown fire, $8.6tCha^{-1}$ emitted in moderate-intensity ground fires, and $2.3tCha^{-1}$ are emitted in low-intensity surface fires (*Conard et al.*, 2002). These emission estimates can be used to convert area annually burned in the simulation to the amount of carbon released to the atmosphere during the associated simulation year.

The fire subroutine could be developed in one of two modes - probabilistic and spatially-explicit. The probabilistic approach simply specifies the fire probability in the driver file, which can optionally be enhanced by a drought trigger. A random number is generated and compared to the fire probability. If the random number is smaller than the probability, a fire event "occurs" on the plot. This fire could kill all trees on the plot or implement differential mortality based on species-specific fire tolerances. This approach is salient in its simplicity and allows for ease of validation against average percent of area burned reported for the different ecotones of Siberia (Figure 6.1). Conversely, the spatially-explicit approach would adjust the fire probability on each plot based on whether a fire has occurred on an adjacent plot, as well as based on topography and/or wind information. This approach is iterative and would require significant computational expense, similar to the light subroutine, however, modules that simulate the spread of fire across the landscape exist (*e.g.*, LANDIS: *Yang et al.*, 2004; *Sturtevant et al.*, 2008; *Scheller and Domingo*, 2012) and can be used as a reference framework.

Insect outbreaks

Insect outbreaks can have a significant effect on the structure and composition of boreal forests at the patch and landscape scales (*Shugart et al.*, 1992a). Examples of this include the spruce beetle outbreak in the Rocky Mountains of the United States (*Bentz et al.*, 2010), the Siberian silkmoth outbreaks in southern and central Siberia (*Kharuk et al.*, 2004; *Ershov and Isaev*, 2006), the mountain pine beetle outbreak in western Canada (*Kurz et al.*, 2008), and the spruce budworm in southern Canada (*Morris*, 1963; *Dymond et al.*, 2010). The insects are always present in a forest, but in healthy stands, the populations are manageable and do not spread. Insects prefer to invade already-weakened stands. As the temperatures in central and southern Siberia continue to increase without an appreciable concurrent increase in precipitation (*Gruza et al.*, 2015), forests become stressed by temperature-induced drought and are likely to be more susceptible to insect outbreaks. Insect outbreaks result in widespread tree mortality and a shift in the ecosystem function to a source of atmosphere carbon, often for decades after the outbreak (*Kurz et al.*, 2008). The impacts of insect outbreaks on carbon dynamics in boreal forests can be comparable in magnitude to the effects of forest fires (*Kurz et al.*, 2008).

species	**Defoliator tolerance** (code)
Abies sibirica	intolerant (1)
Larix sibirica	tolerant (2)
Betula pendula	tolerant (2)
Picea obovata	intolerant (1)
Pinus sibirica	intolerant (1)
Pinus sylvestris	intolerant (1)
Populus tremula	tolerant (2)

Fig. 6.6: Defoliator tolerance rank (1 = intolerant, 2 = tolerant) can be used similar to the shade-tolerance classification, to determine the effect of a defoliator outbreak event on each tree on the plot.

Insect outbreaks affect tree growth, tree mortality, and the light environment (*Kharuk et al.*, 2004). Using the outbreak frequency information for forest-damaging insects in Siberia, the probability of an insect outbreak on a plot in a given simulation year can be set, similar to fire probability. Focusing on the defoliators from the *Lepidoptera* order, which predominantly affect conifers and represent the majority of defoliators in Siberia, the analysis can be simplified to represent average defoliator effects on boreal forest dynamics. In western, southern, and central Siberia, the frequency of outbreaks ranges from 2 to 10 events per century, with more frequent outbreaks in middle taiga than in the southern mountainous regions (*Kharuk et al.*, 2004), and no outbreaks in northern taiga north of 60^oN (*Kharuk et al.*, 2003). Instead of removing the affected species from the simulation, as in the fire subroutine, this subroutine would assign stress flags to all individuals of the affected species on the plot. For example, if the insect outbreak is of a Siberian silkmoth (*Dendrolimus superans sibiricus*), which preferentially destroys conifers (*Kharuk et al.*, 2004; *Valendik et al.*, 2004a,b; *Ershov and Isaev*, 2006), all larches, pines, spruces, and firs on the plot can be flagged for stress-induced mortality. Stress-based mortality gives a 1% chance of the individual surviving 10 consecutive years of stress. As the tree awaits mortality, it is still affecting the light environment on the plot, although to more appropriately simulate the effect of defoliator insects, the annual DBH increment and, therefore, the leaf area of stressed individuals can be downsized significantly. This representation differs from the effects of fire, because the affected trees are allowed to remain standing on the plot and continue to affect the light environment, suppressing regeneration of shade-intolerant broadleaf species. The regeneration trajectory following an insect outbreak that leaves behind standing snags would therefore be different than regeneration following a stand-replacing fire that results in fallen or completely burned trees (*Shugart*, 1987). Figure 6.6 presents species-specific rankings of susceptibility to defoliation. Note that larches, birches and aspens are able to survive defoliation due to their deciduous habit (*Kharuk et a.*, 2004; *Gustafson et al.*, 2010) and are, therefore, labeled tolerant.

The insect outbreak subroutine could be developed in two modes - probabilistic and triggered. The probabilistic mode, similar to the fire disturbance, would simply compare a generated random number to the annual probability of outbreak, which could be averaged for Siberia or specified based on the ecotone simulated. For example, the outbreak recurrence interval observed in central Siberia near the boundary between south and middle taiga ecotones is 15-30

years (*Kondakov*, 1974), so an average annual probability of 0.05 could be used to compare to the random number generated to assess whether an outbreak will occur in a given year of simulation. If the random number is less than the probability, an outbreak "occurs" on the plot, in which case all susceptible species on the plot are flagged for eventual stress-based mortality. Conversely, in a triggered mode, the probability of an outbreak would be assessed or enhanced if a certain threshold in environmental conditions is surpassed, i.e. GDD_{10} (growing degrees above a base temperature of 10^oC) exceeds 1400^oC. The triggered mode eliminates the need to consider or specify the ecotone simulated, as the climatological conditions would be specified through monthly average temperatures in the driver file. Furthermore, utilizing the spatially-explicit nature of SIBBORK, the probability of an insect outbreak on a plot may be affected by an outbreak "occurring" on an adjacent plot. This is a more complex, computationally-expensive approach, but a potential framework for reference already exists in the budworm/forest model (*Clark et al.*, 1979).

Timber management

The timber sector is an important component of the Russian economy, with significant growth in the middle of the 20th century during a push to industrialize Siberia, as well as after the fall of the USSR, when foreign interests began to invest in timber operations. Logging practices have been developed to increase timber yields, and often do no include sustainability or carbon budget considerations. Furthermore, due to corruption in recent decades, illegal harvesting has been increasing in Siberian boreal forests (*Kukavskaya et al.*, 2013). Although remote sensing facilitates monitoring of forest loss (*Hansen et al.*, 2013), data on biovolume of wood harvested illegally is not available. Forests in European Russia and central Siberia represent the hub of Russian timber activity (*Cuevas-Gonzales et al.*, 2009). Current forestry management practices, together with wildfire disturbances, have shifted the European boreal ecosystem toward acting as a source of atmospheric carbon (*Krankina and Dixon*, 1992). The southern half of the Krasnoyarsk Region in central Siberia is also heavily timbered. This coincides with the area that is likely to experience the most drastic changes, especially on south-facing slopes, as forests become stressed by temperature-induced drought and succumb to increased mortality rate, fires and insect outbreaks. Although these changes have been forecast by SIBBORK (Chapter 5) and others (*Scholze et al.*, 2006; *Tchebakova*, 2006; *Sitch et al.*, 2008; *Tchebakova et al.*, 2009a), increased tree mortality and insect outbreaks have already been observed in this region over the last several decades (*Kondakov*, 2002; *Soja et al.*, 2007; *Buryak et al.*, 2009; *Ivanova et al.*, 2010; *Buermann et al.*, 2014). The frequency and expanse of fires have also been increasing (*Goetz et al.*, 2007). Furthermore, not all management practices are equal, and some may even increase carbon storage in managed forest stands (*Kurz and Apps*, 1999; *Winjum et al.*, 1992; *Krankina et al.*, 2005) by as much as 2 Petagrams (*Krankina et al.*, 1996). Assessment of different forest management practices, especially planting and stand thinning, is especially important as pressures on this resource are increased with increasing global population.

The effect of current and proposed timbering practices (*Krankina and Dixon*, 1994) on carbon storage in Eurasian boreal forests can be evaluated using simulation models, such as SIBBORK. Development of management practices based on a simulation output could help determine the approach that increases the carbon sequestration and carbon storage within the forest, and shifts the managed stands to act as sinks for atmospheric carbon. One suggestion is the reforestation of timbered and fallow lands capable of sustaining tree growth (*Winjum et al.*, 1992). As millions of hectares of timber plantations are currently without tree cover (*Krankina and Dixon*, 1994), the use of a vegetation model can facilitate selection of species for planting that would result in the largest rate of carbon accumulation on these unvegetated lands. Furthermore, using the model, the long-term survival of multiple arboreal species can be simulated with consideration of a changing climate, so that the most appropriate species are selected based on environmental resource limitations, fire resistance, and resistance to the prevalent insects in the region. Another suggestion is the replacement of overmature broadleaf (aspen, birch) stands with conifer stands, for increased long-term productivity. SIBBORK can be used to assess what the short- and long-term biomass accumulation patterns are likely to be on the specific soils and under the specific climate of those sites. Planting of coniferous species following clear-cutting has also been suggested. The effect of this approach can be tested by allowing natural inseeding to occur following a timber harvest, and comparing the output to simulations in which the inseeding for all broadleaf species has been turned off, so that following timber harvest, only coniferous species are allowed to inseed. The relationship between species composition and carbon storage can be computed using species- and age-specific ratios of carbon in biomass (*Isaev et al.*, 1995).

A timber subroutine in SIBBORK could be implemented using two modes - a set periodicity for timber harvest or a timbering threshold, such as when a certain percentage of stems for the species of interest reach a specific DBH (*e.g.* 80% of Scots pine have greater than 20cm DBH). An assessment of optimal timber harvest frequency was conducted for tropical forest by Huth *et al.* (1998), and a similar assessment for central Siberian boreal forest would be useful. Previous studies found that longer harvest rotations, more than 50 years in length, result in greater carbon sequestration over the long term (centuries) (*Krankina and Dixon*, 1994; *Huth et al.*, 1998). Furthermore, selective harvesting options can be simulated and compared to the effects of clear-cutting approaches on biomass accumulation and carbon storage.

6.2 Landscape Fragmentation and Edge Effects

Fragmentation refers to the decrease of forested area and the transition from a continuous forested landscape to a landscape with “islands” of forest amidst non-forest vegetation or other terrain (steep slopes, roads, rivers). The result of fragmentation is that the edge-to-area ratio is increased. Edges along the perimeter of the remaining forest can occur

as a result of land use change, timber harvest, fires, landslides, windthrow, and other forest disturbances that result in a sharp boundary between forests and unforested areas. "Edge effects" represent the effect of being near an edge of a forest stand versus in the interior of a forest. Numerous edge effects occur along the perimeter and can extend as far as 2400m into the undisturbed forest (*Laurance et al.*, 2002; *Broadbent et al.*, 2008). The effects include changes in microclimates and environmental conditions, as along the edge greater diurnal and seasonal temperature variability will be experienced, together with increased light, which results in greater PET and, therefore, AET, thus decreasing the soil moisture and potentially increasing drought-induced stress in trees within a certain distance from the edge. As the area of the forest fragment decreases, the proportion of the remaining forested area that experienced edge effects increases (*Laurance*, 2008), and for small fragments it is possible that no area within the forested fragment has retained the characteristics of a forest interior. Fragmentation and edge effects alter the biodiversity, gap dynamics, productivity, radiation budget, nutrient cycling, hydrology and carbon storage of a forest stand (*Angelstam*, 1992; *Bradshaw*, 1992; *Chen et al.*, 1992; *Ferreira and Laurance*, 1997; *Laurance et al.*, 2002; *Laurance*, 2008).

Fragmentation and edge effects have been observed in tropical and temperate forests, and include changes in the environmental conditions experienced by the species within a certain distance of the forest edge. This results in alteration of stand structure and species composition, as some species, especially canopy dominants (*Laurance et al.*, 2000) and those less adapted to edge conditions, experience increased mortality, whereas growth and regeneration of other species may be enhanced by the conditions near the forest edge (*Collinge*, 1996). The gap dynamics experienced along a forest edge are very different from those in the undisturbed forest (*Ferreira and Laurance*, 1997; *Broadbent et al.*, 2008). On the other hand, the light regime near the forest edge facilitates regeneration of shade-intolerant pioneer species. Increased light increases the PET and AET, and can therefore result in drier conditions and lower soil moisture near the forest edge than within the forest interior (*Laurance et al.*, 2002). Changes in the soil moisture regime along the edge can lead to changes in the frequency of fire disturbances (*Cochrane et al.*, 1999; *Laurance et al.*, 2002; *Broadbent et al.*, 2008; *Laurance*, 2008), while increased temperature variability and changes in the hydrology and radiation budgets along the edge facilitate greater decomposition rates, with the result of a shift in the role the forest plays in the carbon cycle from a possible sink to a source of atmospheric carbon.

Specific short-term (years) effects of fragmentation on forest structure that have been observed in tropical and temperate forest ecosystems include a decrease in canopy cover and stem density and, therefore, stand basal area (*Chen et al.*, 1992). The decreases in canopy cover and stem density were due to an increased mortality rate experienced by drought-intolerant tree species that prefer the forest interior forest habitat (*Chen et al.*, 1992; *Laurance et al.*, 2002). On the other hand, increased regeneration of shade-intolerant species resulted in the longer-term (decades) changes in stand density and species composition. In this manner, the fragment area experiencing edge effects first undergoes deterioration of stand conditions and gap dynamics, followed by regeneration that shifts species composition

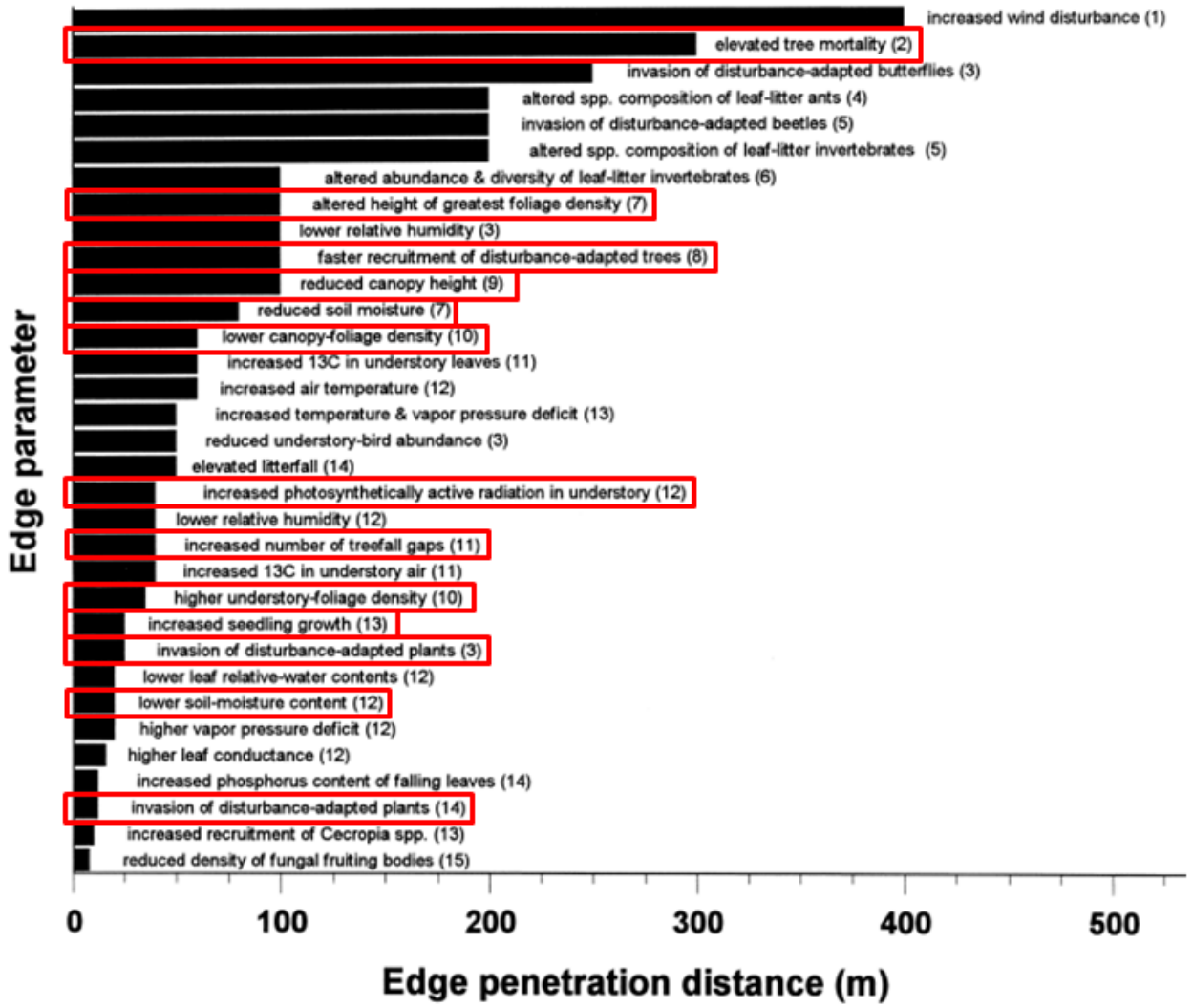

Fig. 6.7: Reproduced from Laurance *et al.* (2002, Figure 3). An array of edge effects and their spatial extent into the forest that have been assessed by Laurance and colleagues or gathered from the literature for Amazonian tropical forests are shown with black bars. Red rectangles denote the characteristics that could be assessed using SIBBORK for Siberian boreal forest ecosystems.

towards dominance by early successional species, shifting the age structure toward younger, less productive stands with decreased carbon storage capacity (*Angelstam*, 1992; *Bradshaw*, 1992; *Chen et al.*, 1992; *Laurance et al.*, 2002).

A spatially-explicit model, such as SIBBORK, can be used to assess the fragmentation and edge effects for boreal forest ecosystems. Due to increased disturbance regimes and timber harvest pressures, the Siberian boreal forest is becoming more and more fragmented (*Aksenov et al.*, 2002). The effects of the disturbances are not limited to the disturbed areas, however, as the edge effects have been measured up to 2400m into the forest (*Laurance et al.*, 2002) and could extend up to 10km into the forest interior (*Broadbent et al.*, 2008). Plant and animal species composition depends on fragment size (*Wegge et al.*, 1992; *Shugart*, 2007). As fragments become smaller and more numerous, more forested area is subject to edge effects. In tropical ecosystems, it was found that the smaller fragmented forest areas were more "vulnerable to stochastic effects" and effects of climate change (*Laurance et al.*, 2002; *Laurance*, 2008). SIBBORK could be used to test the severity of edge effects, their extent into the forest, their effect on the structure and composition of the forest, as well as their effect on the ecosystem response to climate change. To assess the edge effects, the edge-to-edge wrap-around in SIBBORK could be turned off, and spatial domains of different sizes can be simulated. The trees along the edge of the simulation grid would receive full light, which will affect the PET and, therefore, the AET and the soil moisture on the plots with increased light. Since the light and soil moisture conditions are computed at the plot level, SIBBORK will likely be able to resolve the magnitude and extent of the edge effect on environmental conditions on each plot. Tree species establish, grow, and die on the plots based on environmental conditions and stresses due to resource limitations, such as drought-induced stress. SIBBORK will likely be able to reflect the changing structure and composition on plots near the edge compared to plots near the interior of the simulation grid. The high latitude light regime may result in significantly different type and extent of edge effects compared to tropical and temperate ecosystems. Figure 6.7 shows in red rectangles the potential edge effects that may be captured in the SIBBORK simulation. The limitations on the interpretation of the results from this approach include the lack of consideration of the landscape matrix within which the forest fragment is simulated. The matrix often has effects on the regeneration and disturbance regimes experienced along the edge (*Laurance*, 2008), however, for the purposes of simplification of the model, and since the model only simulates arboreal vegetation, the effects of the matrix may need to be ignored.

6.3 Synthetic data generation for Synthetic Aperture Radar calibration and validation

Unlike imagery in the visible or infrared (IR) ranges, including LIDAR (LIght Detection And Ranging), which can be limited by cloud cover, nighttime or weather conditions, air- and space-borne Synthetic Aperture Radar (SAR) uses radio frequencies to acquire high resolution imagery based on signal return strength and duration between pulse and echo return. Signal return depends on the wavelength used: X-band is reflected from leaves, C-band can penetrate through the canopy and is reflected from twigs and branches, L-band is reflected by the branches and small trunks, and P-band penetrates through the smaller parts of the trees and is reflected by large branches and trunks. Previous space-borne estimates of biomass based solely on leaf area yielded great uncertainties. Inclusion of other tree parts in the estimates, and also using polarized SAR to obtain information on the 3-dimensional structure of the forest (*Le Toan et al.*, 1992), facilitates better estimates of carbon storage in global forests, as well as monitoring of changes in forest structure and biomass due to climate change and disturbances. The 3-D structure of the forest also provides information on habitat structure and complexity, which can be used as a proxy for assessment and monitoring of ecosystem biodiversity. NASA is currently working on the calibration and validation of algorithms for SAR signal interpretation for the planned NISAR mission, which will have the L-band and the S-band SAR onboard. The L-band has previously been used to estimate stem volume in boreal (*Fransson*, 1999), temperate (*Beaudoin et al.*, 1994) and tropical (*Englhart et al.*, 2011) forest ecosystems. In the past, LIDAR data has been used to calibrate the SAR signal interpretation (*Englhart et al.*, 2011), however, this necessitates collection of LIDAR data, which is entailed and expensive. The light ray tracing subroutine in SIBBORK, which considers the leaf area, LAI, and foliage biomass along its multiple ray paths, can be particularly useful for the calibration and validation process by generating synthetic data and estimating the expected signal profiles for different ecosystems. SIBBORK can be used to simulated forest stand structures under different environmental conditions and can be easily re-parameterized to simulate temperate and tropical ecosystems using global climate, elevation, and soil datasets, and forestry yield tables or inventory data. SIBBORK can thus be used to generate productive and stressed stands, under an array of environmental conditions, including current and near-future climates, for broad spectrum training of the SAR signal interpretation algorithms.

CHAPTER

SEVEN

CONCLUSIONS

Global forests are changing across multiple spatial and temporal scales. To understand and prepare for the potential near-future changes, we need tools that synthesize forest processes and their responses to changing environmental conditions. The new 3-D spatially-explicit model SIBBORK was created with this purpose in mind. It has enhanced our understanding of the inner workings of forest ecosystems, and how their role in the global carbon cycle may be altered by imposed perturbations, such as near-future climate change. SIBBORK simulates forest structure dynamically, which includes complicated dynamics not expressed in other models without spin-up. This includes strong coupling to local environmental conditions that reproduce species ranges without external limitation to where each species can grow. SIBBORK has been calibrated on forestry yield tables from southern taiga in central Siberia, and validated against field data from southern, middle, and northern taiga ecotones. Furthermore, SIBBORK application has been tested in prediction of the location of current and future northern, southern, and elevational treeline locations. SIBBORK-based simulation of biomass allocation and species shifts can be used to inform management and mitigation in a region currently experiencing the most rapid climatological changes.

SIBBORK was created with flexibility in mind. This tool has been calibrated and tested on the boreal forests of central Siberia, but can be used to simulate other ecotones with minimal re-parameterization, enhancing the infrastructure for research and education. The Siberian boreal forest was selected as a test ecosystem, but the model can be used to simulate forest dynamics for other types of forests. In order to parameterize SIBBORK to a forest ecosystem of choice, climate, soils, and species information is necessary. These datasets are publicly available (*e.g.*, World Meteorological Organization, FAO soils databases, forestry yield tables). Furthermore, it is important to select the plot size that best approximates the size of the crown of the canopy dominant trees in the selected ecosystem. Model sensitivity analysis demonstrated that gap dynamics are most appropriately simulated when there is congruency between the size of the simulated plots and the canopy cross-section of the dominant trees. If the selected plot size is too small, the light computation is complicated by too thick of a canopy, which results in stunted growth and decreased regeneration of

saplings. Converselly, when the selected plot size is too large, the death of a canopy dominant tree does not open a gap in the simulated canopy, but rather decreases the foliage density in the upper canopy layer. This does not facilitate enough light to reach the subcanopy or the ground level to simulate sufficient regeneration. The user can also select to simulate a 1-D or 3-D light environment. Both approximate large-scale biomass dynamics and average species composition, but the 3-D simulation more accuratey reflects local and regional forest dynamics, which becomes increasingly important for investigation of changes in transitional ecotones.

No one model is best at simulating every process, structure and pattern within the complex forest ecosystem, but SIBBORK does represent individual-level and landscape-level characteristics and dynamics in a way that is consistent with observed patterns across a broad range of ecotones in central Siberia. SIBBORK-based predictions of forest structure and dynamics can be utilized for testing the effects of changing natural and anthropogenic disturbance regimes, and the appropriateness of mitigation approaches geared toward retaining forest productivity under changing climatological conditions. Model applications simulating the vegetation response to climate change revealed significant and irreversible changes in forest structure and composition, which are likely to be reached by mid-21st century. These changes in land cover will inevitably result in changes in the biodiversity, carbon storage, and the ecosystem services provided by the Siberian boreal forest. A model such as SIBBORK, verified to this extent, may represent a unifying theory for the internal organization of Siberian boreal forests and the adaptive behavior of individual trees within the landscape-scale forest dynamics. At this stage, SIBBORK may be in a “Medawar zone” - a functional balance between the model’s ability to compute dynamics and still possess a degree of realism in the structure and composition of the forest.

The source code, user manual and all associated files for this new ecological model are open source and freely available at www.github.com/sibbork/sibbork. Moreover, the simulation model can be used as an educational tool in biology and ecology courses to facilitate participation of students and non-scientists in investigation of perturbation effects on forest processes.

CHAPTER

EIGHT

REFERENCES

Acevedo, M. F., Urban, D. L. and H. H. Shugart (1996). Models of forest dynamics based on roles of tree species. *Ecological Modelling*, 87, 267-284.

Acevedo, M. F. (2013). *Simulation of Ecological and Environmental Models*. CRC Press, Taylor & Francis Group, New York.

Ajtay, G. L., Ketner, P., & Duvigneaud, P. (1979). Terrestrial primary production and phytomass. *The Global Carbon Cycle*, *13*, 129-182.

Aksenov, D., Dobrynin, D., Dubinin, M., Egorov, A., Isaev, A., Karpachevskiy, M., Laestadius, L., Potapov, P., Purekhovskiy, A., Turubanova, S., and Yaroshenko, A. (2002). *Atlas of Russia's intact forest landscapes*. Russian NGOs Forest Club, Moscow, Russia. Available at http://www.forest.ru/eng/publications/intact/ [accessed 4 February 2015]

Albrektson, A. (1984). Sapwood basal area and needle mass of Scots pine (*Pinus sylvestris* L.) trees in central Sweden. *Forestry*, *57* (1), 35-43.

Alexeyev, V.A. (1998). Forest health status in Russia. In: *Proceedings of the International Symposium of the USDA Forest Service*. General technical report PSW-GTR-166, USDA Forest Service, Pacific Southwest Research Station, Berkeley, CA, USA, 267-270.

Allen, C. D., Macalady, A. K., Chenchouni, H., Bachelet, D., McDowell, N., Vennetier, M., et al. (2010). A global overview of drought and heat-induced tree mortality reveals emerging climate change risks for forests. *Forest Ecology and Management*, *259* (4), 660-684.

Allison, S. D., & Treseder, K. K. (2008). Warming and drying suppress microbial activity and carbon cycling in boreal forest soils. *Global Change Biology*, *14* (12), 2898-2909.

Anderegg, W. R. L., Kane, J. M., and L. D. L. Anderegg (2012). Consequences of widespread tree mortality triggered by drought and temperature stress. *Nature Climate Change*, DOI: 10.1038/nclimate1635.

Angelstam, P. (1992). Conservation of communities-the importance of edges, surroundings and landscape mosaic structure. In: *Ecological principles of nature conservation*. Springer US. p 9-70.

Anonymous (1990). *Forest Fund of the USSR*. State Committee for Forestry, Moscow, Russia 1-2. (in Russian)

Antonio, N., Tome, M., Tome, J., Soares, P., & Fontes, L. (2007). Effect of tree, stand, and site variables on the allometry of Eucalyptus globulus tree biomass. *Canadian Journal of Forest Research*, *37* (5), 895-906.

Anuchin, N.P. (1986). *Forest Encyclopedia*, Vol II. Soviet Encyclopedia, Moscow, USSR. p455-457. (in Russian)

Araki,M. (1972). The Studies on the Specific Leaf Area of Forest Trees (II). *Japanese Forestry Society*, *54* (6), 184-191.

Arctic Atlas. (1985). USSR Academy of Sciences, Leningrad. (In Russian)

Ashcroft, M. B., Chisholm, L. A., & French, K. O. (2009). Climate change at the landscape scale: predicting fine-grained spatial heterogeneity in warming and potential refugia for vegetation. *Global Change Biology*, *15* (3), 656-667.

Ashton, M. S., Tyrrell, M. L., Spalding, D., & Gentry, B. (Eds.). (2012). *Managing forest carbon in a changing climate*. Springer Science & Business Media.

Asner, G. P., Scurlock, J. M., & A Hicke, J. (2003). Global synthesis of leaf area index observations: implications for ecological and remote sensing studies. *Global Ecology and Biogeography*, *12* (3), 191-205.

Atlas of USSR. (1983). USSR Academy of Sciences, Leningrad. (In Russian)

Atkin, O.K. et al. (2007). Respiration as a percentage of daily photosynthesis in whole plants is homeostatic at moderate, but not high, growth temperatures. *New Phytologist*, *174*, 367-380.

Babushkina, E. A., Knorre, A. A., Vaganov, E. A., & Bryukhanova, M. V. (2010). Transformation of climatic response in radial increment of trees depending on topoecological conditions of their occurrence. *Geography and Natural Resources*, *32* (1), 80-86. (in Russian)

Baldocchi, D., Kelliher, F. M., Black, T. A., & Jarvis, P. (2000). Climate and vegetation controls on boreal zone energy exchange. *Global Change Biology*, *6* (S1), 69-83.

Balzter, H., Gerard, F. F., George, C. T., Rowland, C. S., Jupp, T. E., McCallum, I., ... & Schmullius, C. (2005). Impact of the Arctic Oscillation pattern on interannual forest fire variability in Central Siberia. *Geophysical Research Letters*, *32* (14), .

Barber, V. A., Juday, G. P. and B. P. Finney (2000). Reduced growth of Alaskan white spruce in the twentieth century from temperature-induced drought stress. *Nature*, *405*, 668-672.

Barchenkov, A. P. (2010). Changes in morphology of regenerating organs of Siberian larch along the River Yenisei. *Conifers of the Boreal Zone*, *27* (1-2), 36-42. (in Russian)

Barclay, H. J. (1998). Conversion of total leaf area to projected leaf area in lodgepole pine and Douglas-fir. *Tree Physiology*, *18* (3), 185-193.

Barlage, M., Zeng, X., Wei, H., & Mitchell, K. E. (2005). A global 0.05^o maximum albedo dataset of snow-covered land based on MODIS observations. *Geophysical Research Letters*, *32* (17).

Bartalev, S. (2010). Hybrid Biomass and Land Cover Map for Central Siberia.

Bartalev, S. A., V. A. Egorov, D. V. Ershov, A. S. Isaev, E. A. Loupian, D. E. Plotnikov, and I. A. Uvarov. 2011. The Vegetation Mapping over Russia Using MODIS Spectroradiometer Satellite Data. *Contemporary Earth Remote Sensing From Space*, *8*, 285-302. (in Russian)

Basilevich, V.I. (1986). Biological productivity of soil vegetation formations in the USSR. *Izvestiia Akademii nauk SSSR - Geography*, *2*, 49-66.

Bauweraerts, I., Ameye, M., Wertin, T. M., McGuire, M. A., Teskey, R. O., & Steppe, K. (2014). Water availability is the decisive factor for the growth of two tree species in the occurrence of consecutive heat waves. *Agricultural and Forest Meteorology*, *189*, 19-29.

Beaudoin, A., Le Toan, T., Goze, S., Nezry, E., Lopes, A., Mougin, E., ... & Shin, R. T. (1994). Retrieval of forest biomass from SAR data. *International Journal of Remote Sensing*, *15* (14), 2777-2796.

Bentz, B. J., Regniere, J., Fettig, C. J., Hansen, E. M., Hayes, J. L., Hicke, J. A., ... & Seybold, S. J. (2010). Climate change and bark beetles of the western United States and Canada: direct and indirect effects. *BioScience*, *60* (8), 602-613.

Betts, A. K., & Ball, J. H. (1997). Albedo over the boreal forest. *Journal of Geophysical Research*, *103*, 28-901.

Betts, R. A. (2000). Offset of the potential carbon sink from the boreal forestation by decreases in surface albedo. *Nature*, *408*, 187-190.

Bhatti, J. S., Van Kooten, G. C., Apps, M. J., Laird, L. D., Campbell, I. D., Campbell, C., ... & Banfield, E. (2003). Carbon balance and climate change in boreal forests. In: *Towards Sustainable Management of the Boreal Forest*, p799-855. National Research Council Research Press, Ottawa. ON.

Blunden, J., Arndt, D. S., Achberger, C., Ackerman, S. A., Albanil, A., Alexander, P., et al. (2013). State of the Climate in 2012. *Bulletin of the American Meteorological Society*, *94* (8), S1-S238.

Boisier, J. P., de Noblet-Ducoudre, N., & Ciais, P. (2013). Inferring past land use-induced changes in surface albedo from satellite observations: a useful tool to evaluate model simulations. *Biogeosciences*, *10* (3), 1501-1516.

Bolin, B. (1986). How much CO_2 will remain in the atmosphere. In: B. Bolin, B.R. Doos, J. Jager, and R.A. Warrick (editors), *The Greenhouse Effect, Climate Change, and Ecosystems*. John Wiley, Chichester. p93-155.

Bonan, G. (1988). Dissertation: Environmental Processes and Vegetation Patterns in Boreal Forests. University of Virginia, Charlottesville, Va.

Bonan, G. B. (1988). A simulation model of environmental processes and vegetation patterns in boreal forests: test case Fairbanks, Alaska. Working Paper WP-88-63. International Institute for Applied Systems Analysis, Laxenburg, Austria. 63 pp.

Bonan, G. B. and H. H. Shugart (1989) Environmental Factors and Ecological Processes in Boreal Forests. *Annual Review of Ecology and Systematics*, *20*, 1-28.

Bonan, G. B., Shugart, H. H. and D. L. Urban. (1990). The sensitivity of some high latitude boreal forests to climatic parameters. *Climatic Change*, *16*, 9-31.

Bonan, G. B., Pollard, D. and S. L. Thompson. (1992). Effects of boreal forest vegetation on global climate. *Nature*, *359*, 716-718.

Bonan, G. B., Chapin III, F. S., & Thompson, S. L. (1995). Boreal forest and tundra ecosystems as components of the climate system. *Climatic Change*, *29* (2), 145-167.

Bonan, G.B. (2008) Forests and climate change: Forcings, feedbacks, and the climate benefits of forests. *Science*, *320*, 1444-1449.

Bond-Lamberty, B., Fisk, J. P., Holm, J. A., Bailey, V., Bohrer, G., & Gough, C. M. (2015). Moderate forest disturbance as a stringent test for gap and big-leaf models. *Biogeosciences*, *12* (2), 513-526.

Botkin, D. B., Janak, J. F. and J. R. Wallis. (1972a). Rationale, limitations, and assumptions of a Northeastern forest growth simulator. *IBM Journal of Research and Development*, *16*, 101-116.

Botkin, D. B., Janak, J. F. and J. R. Wallis. (1972b). Some ecological consequences of a computer model of forest growth. *Journal of Ecology*, *60*, 849-872.

Botkin, D. B. (1993). Forest Dynamics: An ecological model. Oxford University Press, Oxford, UK.

Bradshaw, F. J. (1992). Quantifying edge effect and patch size for multiple-use silviculture - a discussion paper. *Forest Ecology and Management*, *48* (3), 249-264.

Bragg, D. C. (2001). Potential relative increment (PRI): a new method to empirically derive optimal tree diameter growth. *Ecological Modelling*, *137* (1), 77-92.

Bragg, D. C. (2003). Optimal diameter growth equations for major tree species of the Midsouth. *Southern Journal of Applied Forestry*, *27* (1), 5-10.

Brazhnik, K., and H.H. Shugart (2015). SIBBORK: New Spatially-Explicit Gap Model for Boreal Forest in 3-Dimensional Terrain. *Ecological Modelling*, in review.

Breda, N.J. (2003). Ground-based measurements of leaf area index: a review of methods, instruments and current controversies. *Journal of Experimental Botany*, *54* (392), 2403-2417.

Briffa, K. R., Schweingruber, F. H., Jones, P. D., Osborn, T. J., Shiyatov, S. G., & Vaganov, E. A. (1998). Reduced sensitivity of recent tree-growth to temperature at high northern latitudes. *Nature*, *391* (6668), 678-682.

Broadbent, E. N., Asner, G. P., Keller, M., Knapp, D. E., Oliveira, P. J., & Silva, J. N. (2008). Forest fragmentation and edge effects from deforestation and selective logging in the Brazilian Amazon. *Biological Conservation*, *141* (7), 1745-1757.

Brooks, J. R., Flanagan, L. B., Buchmann, N., & Ehleringer, J. R. (1997a). Carbon isotope composition of boreal plants: functional grouping of life forms. *Oecologia*, *110* (3), 301-311.

Brooks, J. R., Flanagan, L. B., Varney, G. T., & Ehleringer, J. R. (1997b). Vertical gradients in photosynthetic gas exchange characteristics and refixation of respired CO_2 within boreal forest canopies. *Tree Physiology*, *17* (1), 1-12.

Brown, J., Ferrians Jr, O. J., Heginbottom, J. A., & Melnikov, E. S. (2002). Circum-Arctic Map of Permafrost and Ground-Ice Conditions, version 2. National Snow and Ice Data Center, Boulder.

Bryson, R.A., Baerreis, D.A., and W.M. Wendland. (1970). The character of late-glacial and post-glacial climate changes. In: Dort, W., and J.K. Jones (eds.), Pleistocene and Recent Environments of the Central Great Plains. University Press of Kansas, Lawrence. pp.53-74.

Buchman, R. G., Pederson, S. P. and N. R. Walters (1983) A tree survival model with application to species of the Great Lakes region. *Canadian Journal of Forest Research*, *13*, 601-608.

Buermann, W., Parida, B., Jung, M., MacDonald, G. M., Tucker, C. J., & Reichstein, M. (2014). Recent shift in Eurasian boreal forest greening response may be associated with warmer and drier summers. *Geophysical Research Letters*, *41* (6), 1995-2002.

Bugmann, H., Fischlin, A., & Kienast, F. (1996). Model convergence and state variable update in forest gap models. *Ecological Modelling*, *89* (1), 197-208.

Bugmann, H. K. and A. M. Solomon (2000). Explaining Forest Composition and Biomass across Multiple Biogeographical Regions. *Ecological Applications*, *10* (1), 95-114.

Bugmann, H. K. (2001). A review of forest gap models. *Climatic Change*, *51*, 259-305.

Bulygina, O., Korshunova, N. N., Razuvaev, V. N., & Groisman, P. Y. (2014, December). Climate Extreme Events over Northern Eurasia in Changing Climate. In: AGU Fall Meeting Abstracts (Vol. 1, p. 0453).

Bunn, A. G., Goetz, S. J., Kimball, J. S., & Zhang, K. (2007). Northern High-Latitude Ecosystems Respond to Climate Change. *EOS Transactions*, *88*, 333-335.

Burton, P. J., Kneeshaw, D. D., & Coates, K. D. (1999). Managing forest harvesting to maintain old growth in boreal and sub-boreal forests. *The Forestry Chronicle*, *75* (4), 623-631.

Burton, P. J., Messier, C., and Smith, D. W., eds. *Towards Sustainable Management of the Boreal Forest*. Ottawa, ON, CAN: NRC Research Press, 2003.

Buryak, L. V., Kalenskaya, O. P., Tolmachev, A. V., & Yankovskii, R. V. (2009). Forest fires and their after-effects in the Sushensky Bor National Park. *Lesnoe Khozyaistvo*, *3*, 37-39.

Buryak, L. V., Sukhinin, A. I., Kalenskaya, O. P., & Ponomarev, E. I. (2011). Effects of fires in ribbon-like pine forests of southern Siberia. *Contemporary Problems of Ecology*, *4* (3), 248-253.

Busing, R. T. and A. M. Solomon (2004) A comparison of forest survey data with forest dynamics simulators FORCLIM and ZELIG along climatic gradients in the Pacific Northwest. U. S. Geological Survey Scientific Investigations Report 2004-5087.

Busing, R. T. and D. Mailly (2004) Advances in spatial, individual-based modeling of forest dynamics. *Journal of Vegetation Science*, *15*, 831-842.

Cale, W. G., O'Neill, R. V., & Shugart, H. H. (1983). Development and application of desirable ecological models. *Ecological Modelling*, *18* (3), 171-186.

Campbell, G. S. (1977). *An Introductions to Environmental Biophysics*. Springer-Verlag, New York, NY.

Campbell, G. S. and J. M. Norman (1998). *An Introduction to Environmental Biophysics*. Springer Science & Business Media, LLC, New York, New York.

Chapin III, F. S., Callaghan, T. V., Bergeron, Y., Fukuda, M., Johnstone, J. F., Juday, G., & Zimov, S. A. (2004). Global change and the boreal forest: thresholds, shifting states or gradual change? *AMBIO: A Journal of the Human Environment*, *33* (6), 361-365.

Chapin, F. S. III, Oswood, M. W., Van Cleve, K., Viereck, L. A., and D. L. Verbyla. (2006a). Alaska's Changing Boreal Forest. Oxford University Press, Oxford, UK.

Chapin III, F. S., Viereck, L. A., Adams, P., Van Cleve, K., Fastie, C. L., Ott, R. A., ... & Johnstone, J. F. (2006b). Successional processes in the Alaskan boreal forest. In: *Alaska's changing boreal forest*. Oxford University Press, Oxford, p100-120.

Chen, J.M., & Black, T.A. (1992). Defining leaf area index for non-flat leaves. Plant, *Cell & Environment*, *15* (4), 421-429.

Chen, J., Franklin, J. F., & Spies, T. A. (1992). Vegetation responses to edge environments in old-growth Douglas-fir forests. *Ecological Applications*, *2* (4), 387-396.

Chen, J. M. (1996). Optically-based methods for measuring seasonal variation of leaf area index in boreal conifer stands. *Agricultural and Forest Meteorology*, *80* (2), 135-163.

Chen, J. M., Rich, P. M., Gower, S. T., Norman, J. M., & Plummer, S. (1997). Leaf area index of boreal forests: theory, techniques, and measurements. *Journal of Geophysical Research: Atmospheres (1984-2012)*, *102* (D24), 29429-29443.

Chen, J. M., Pavlic, G., Brown, L., Cihlar, J., Leblanc, S. G., White, H. P., Hall, R. J., Peddle, D. R., King, D. J., Trofymow, J. A., Swift, E., Van der Sanden, J. & Pellikka, P. K. E. (2002). Derivation and validation of Canada-wide coarse-resolution leaf area index maps using high-resolution satellite imagery and ground measurements. *Remote Sensing of Environment*, *80* (1), 165-184.

Chen, X., Vierling, L., Deering, D., & Conley, A. (2005). Monitoring boreal forest leaf area index across a Siberian burn chronosequence: a MODIS validation study. *International Journal of Remote Sensing*, *26* (24), 5433-5451.

Chlachula, J., & Sukhova, M. G. (2011). Regional manifestations of present climate change in the Altai, Siberia. International Proceedings of Chemical, Biological and Environmental Engineering. Environmental Engineering and Applications, Edited by Li Xuan, *17*, 134-139.

Chytry, M., Danihelka, J., Kubesova, S., Lustyk, P., Ermakov, N., Hajek, M., ... & Pisut, I. (2008). Diversity of forest vegetation across a strong gradient of climatic continentality: Western Sayan Mountains, southern Siberia. *Plant Ecology*, *196* (1), 61-83.

Clark, W. C., Jones, D. D., & Holling, C. S. (1979). Lessons for ecological policy design: a case study of ecosystem management. *Ecological Modelling*, *7* (1), 1-53.

Clark, J. S. (1998). Why trees migrate so fast: confronting theory with dispersal biology and the paleorecord. *The American Naturalist*, *152* (2), 204-224.

Cochrane, M. A., Alencar, A., Schulze, M. D., Souza, C. M., Nepstad, D. C., Lefebvre, P., & Davidson, E. A. (1999). Positive feedbacks in the fire dynamic of closed canopy tropical forests. *Science*, *284* (5421), 1832-1835.

Coffin, D. P., & Urban, D. L. (1993). Implications of natural history traits to system-level dynamics: comparisons of a grassland and a forest. *Ecological Modelling*, *67* (2), 147-178.

Collinge, S. K. (1996). Ecological consequences of habitat fragmentation: implications for landscape architecture and planning. *Landscape and Urban Planning*, *36* (1), 59-77.

Conard, S. G., Sukhinin, A. I., Stocks, B. J., Cahoon, D. R., Davidenko, E. P. and G. A. Ivanova (2002) Determining effects of area burned and fire severity on carbon cycling and emissions in Siberia. *Climatic Change*, *55*, 197-211.

Conard, S. G., Sukhinin, A. I., Ivanova, G. A., Hao, W. M., & McRae, D. J. (2004). Modeling and monitoring effects of area burned and fire severity on carbon cycling, emissions, and forest health and sustainability in Central Siberia: February 2004 Progress Report, 36 p.

Cox, P. M., Betts, R. A., Jones, C. D., Spall, S. A., & Totterdell, I. J. (2000). Acceleration of global warming due to carbon-cycle feedbacks in a coupled climate model. *Nature*, *408* (6809), 184-187.

Crawford, R. M. M., Jeffree, C. E., & Rees, W. G. (2003). Paludification and forest retreat in northern oceanic environments. *Annals of Botany*, *91* (2), 213-226.

Cuevas-Gonzales, M. A. R. Í. A., Gerard, F., Balzter, H., & Riano, D. (2009). Analysing forest recovery after wildfire disturbance in boreal Siberia using remotely sensed vegetation indices. *Global Change Biology*, *15* (3), 561-577.

Curtis, P. S., Vogel, C. S., Wang, X., Pregitzer, K. S., Zak, D. R., Lussenhop, J., Kubiske, M., & Teeri, J. A. (2000). Gas exchange, leaf nitrogen, and growth efficiency of Populus tremuloides in a CO_2-enriched atmosphere. *Ecological Applications*, *10* (1), 3-17.

Cvetkov, P.A. (2002) Determination of fire danger in Siberian forests. *Lesnoe Khozaistvo*, 5, 43-45. (in Russian)

Dale, V. H., Joyce, L. A., McNulty, S., Neilson, R. P., Ayres, M. P., Flannigan, M. D., ... & Michael Wotton, B. (2001). Climate change and forest disturbances: climate change can affect forests by altering the frequency, intensity, duration, and timing of fire, drought, introduced species, insect and pathogen outbreaks, hurricanes, windstorms, ice storms, or landslides. *BioScience*, *51* (9), 723-734.

de Groot, W. J., Cantin, A. S., Flannigan, M. D., Soja, A. J., Gowman, L. M., & Newbery, A. (2013). A comparison of Canadian and Russian boreal forest fire regimes. *Forest Ecology and Management*, *294*, 23-34.

Denman, K.L. et al. (2007). In: *Climate Change 2007: The Physical Science Basis. Contribution of Working Group I to the Fourth Assessment Report of the Intergovernmental Panel on Climate Change*, S. Solomon et al., Eds. (Cambridge Univ. Press, Cambridge, 2007) pp. 499-587.

Devi, N., Hagedorn, F., Moiseev, P., Bugmann, H., Shiyatov, S., Mazepa, V., & Rigling, A. (2008). Expanding forests and changing growth forms of Siberian larch at the Polar Urals treeline during the 20th century. *Global Change Biology*, *14* (7), 1581-1591.

Deyeva N. M. (1985). Biomass amount in forest communities of the northern-western part of Plateau Putorana, *Botanicheskii Zhurnal* (Russian Botanical Journal), *70* (1), 54-58. (in Russian)

Deyeva N. M. (1987). Vegetative mass structure in forest phytocoenoses of the northern-western part of Plateau Putorana, *Botanicheskii Zhurnal* (Russian Botanical Journal), *72* (4), 505-511. (in Russian)

Dirnbock, T., Dullinger, S., & Grabherr, G. (2003). A regional impact assessment of climate and land-use change on alpine vegetation. *Journal of Biogeography*, *30* (3), 401-417.

Dislich, C. and A. Huth (2012). Modelling the impact of shallow landslides on forest structure in tropical montane forests. *Ecological Modelling*, *239*, 40-53, DOI: 10.1016/j.ecolmodel.2012.04.016

Dore, S., Kolb, T. E., Montes-Helu, M., Sullivan, B. W., Winslow, W. D., Hart, S. C., ... & Hungate, B. A. (2008). Long-term impact of a stand-replacing fire on ecosystem CO_2 exchange of a Ponderosa pine forest. *Global Change Biology*, *14* (8), 1801-1820.

Dulamsuren, C., Hauck, M., & Mühlenberg, M. (2005a) Vegetation at the taiga forest-steppe borderline in the western Khentey Mountains, northern Mongolia. In: *Annales Botanici Fennici* (pp. 411-426). Finnish Zoological and Botanical Publishing Board.

Dulamsuren, C., Hauck, M., & Mühlenberg, M. (2005b) Ground vegetation in the Mongolian taiga forest-steppe ecotone does not offer evidence for the human origin of grasslands. *Applied Vegetation Science*, *8* (2), 149-154.

Dulamsuren, C., Hauck, M., Bader, M., Osokhjargal, D., Oyungerel, S., Nyambayar, S., ... & Leuschner, C. (2009). Water relations and photosynthetic performance in Larix sibirica growing in the forest-steppe ecotone of northern Mongolia. *Tree Physiology*, *29* (1), 99-110.

Dulamsuren, C., Hauck, M., Leuschner, H. H., & Leuschner, C. (2011). Climate response of tree-ring width in Larix sibirica growing in the drought-stressed forest-steppe ecotone of northern Mongolia. *Annals of Forest Science*, *68* (2), 275-282.

Dymond, C. C., Neilson, E. T., Stinson, G., Porter, K., MacLean, D. A., Gray, D. R., ... & Kurz, W. A. (2010). Future spruce budworm outbreak may create a carbon source in eastern Canadian forests. *Ecosystems*, *13* (6), 917-931.

Easterling, D. R., Horton, B., Jones, P. D., Peterson, T. C., Karl, T. R., Parker, D. E. et al (1997). Maximum and minimum temperature trends for the globe. *Science*, *277*, 364-367.

Eguchi, N., Fukatsu, E., Funada, R., Tobita, H., Kitao, M., Maruyama, Y., & Koike, T. (2004). Changes in morphology, anatomy, and photosynthetic capacity of needles of Japanese larch (*Larix kaempferi*) seedlings grown in high CO_2 concentrations. *Photosynthetica*, *42* (2), 173-178.

Emanuel, W. R., Shugart, H. H. and M. P. Stevenson (1985). Climate change and the broad scale distribution of terrestrial ecosystem complexes. *Climatic Change*, *7*, 29-43.

Englhart, S., Keuck, V., & Siegert, F. (2011). Aboveground biomass retrieval in tropical forests - The potential of combined X-and L-band SAR data use. *Remote Sensing of Environment*, *115* (5), 1260-1271.

Erler, A. E. T., Shuman, J. K., Soukhavolosky, V., Kovalev, A., Stevens, T. and H. H. Shugart (2008). Modeling and assessing insect disturbance on boreal forests in the Krasnoyarsk region of Russia by employing the FAREAST gap model and local forest inventory and disturbance data. Poster at the American Geophysical Union conference, San Francisco, CA, USA.

Ermolova, L. S., & Utkin, A. I. (1998). Specific leaf area of dominant forest-forming species of Russia. *Russian Journal of Ecology*, *29* (3), 152-156.

Ershov, D.V. and Isaev, A.S., eds. (2006). GIS database of Siberian Silkworm forest damages in Usolsky forest enterprise of the Krasnoyarsk region. Russian Academy of Science Center for Froest Ecology and Productivity Forest Ecosystems Monitoring Laboratory, Moscow, Russia.

Esper, J., & Schweingruber, F. H. (2004). Large-scale treeline changes recorded in Siberia. *Geophysical Research Letters*, *31* (6). DOI: 10.1029/2003GL019178

ESRI 2012 ESRI ArcGIS version 10.1 [computer program] ESRI, Redlands, CA, USA .

Falster, D. S., Duursma, R. A., Ishihara, M. I., Barneche, D. R., FitzJohn, R. G., Varhammar, A., ... & McCulloh, K. (2015). BAAD: a Biomass And Allometry Database for woody plants. *Ecological Archives* E096-128.

Ferreira, L. V., & Laurance, W. F. (1997). Effects of forest fragmentation on mortality and damage of selected trees in central Amazonia. *Conservation Biology*, 797-801.

Fisher, J. B., Whittaker, R. J., & Malhi, Y. (2011). ET come home: potential evapotranspiration in geographical ecology. *Global Ecology and Biogeography*, *20* (1), 1-18.

Folland, C. K. and T. R. Karl. (2001) Observed climate variability and change. In: *Climate change 2001: the scientific basis. Contribution of WORKING Group 1 to the third IPCC scientific assessment*. Edited by Houghton, J. T., Ding, Y., Griggs, D. J., Noguer, M., Van der Linden, P. J., Xiaosu, D., Maskell, K., and C. A. Johnson. Campridge University Press, Cambridge, UK. pp. 99-182.

Fransson, J. E. S. (1999). Estimation of stem volume in boreal forests using ERS-1 C-and JERS-1 L-band SAR data. *International Journal of Remote Sensing*, *20* (1), 123-137.

Fu, P., & Rich, P. M. (2002). A geometric solar radiation model with applications in agriculture and forestry. *Computers and electronics in agriculture*, *37* (1), 25-35.

Furyaev, V.V., Pleshnikov, F.I., Zlobina, L.P, and E.A. Furyaev. (2004). Transformation of structure and ecological function of forests under the influence of fire in central Siberia. *Lesovedenie*, *6*, 50-57.

Gerard, F., Plummer, S., Wadsworth, R., Sanfeliu, A. F., Iliffe, L., Balzter, H., & Wyatt, B. (2003). Forest fire scar detection in the boreal forest with multitemporal SPOT-VEGETATION data. *IEEE Transactions on Geoscience and Remote Sensing*, *41* (11), 2575-2585.

Germania, I.G. (2003) Global and regional problems of forest fires. (in Russian)

Germino, M. J., Smith, W. K., & Resor, A. C. (2002). Conifer seedling distribution and survival in an alpine-treeline ecotone. *Plant Ecology*, *162* (2), 157-168.

Goetz, S. J., Mack, M. C., Gurney, K. R., Randerson, J. T., & Houghton, R. A. (2007). Ecosystem responses to recent climate change and fire disturbance at northern high latitudes: observations and model results contrasting northern Eurasia and North America. *Environmental Research Letters*, *2* (4), 045031.

Goodale, G. L., Apps, M. J., Birdsey, R. A., Field, C. B., Heath, L. S., Houghton, R. A., Jenkins, J. C., Kohlmaier, G. H., Kurz, W., Liu, S., Nabuurs, G. H., Nilsson, S. and A. Z. Shvidenko (2002) Forest carbon sinks in the Northern Hemisphere. *Ecological Applications*, *12*, 891-899.

Gorchakovsky, P. L., & Shiyatov, S. G. (1978). The upper forest limit in the mountains of the boreal zone of the USSR. *Arctic and Alpine Research*, *10* (2), 349-363.

Goulden, M. L., Munger, J. W., Fan, S. M., Daube, B. C., & Wofsy, S. C. (1996). Exchange of carbon dioxide by a deciduous forest: response to interannual climate variability. *Science*, *271* (5255), 1576-1578.

Gower, S. T., & Richards, J. H. (1990). Larches: deciduous conifers in an evergreen world. *BioScience*, *40* (11), 818-826.

Gower, S. T., Kucharik, C. J., & Norman, J. M. (1999). Direct and indirect estimation of leaf area index, f APAR, and net primary production of terrestrial ecosystems. *Remote Sensing of Environment*, *70* (1), 29-51.

Gower, S. T., Krankina, O., Olson, R. J., Apps, M., Linder, S., & Wang, C. (2001). Net primary production and carbon allocation patterns of boreal forest ecosystems. *Ecological Applications*, *11* (5), 1395-1411.

Grace, J., Lloyd, J., McIntyre, J., Miranda, A. C., Meir, P., Miranda, H. S., ... & Gash, J. (1995). Carbon dioxide uptake by an undisturbed tropical rain forest in southwest Amazonia, 1992 to 1993. SCIENCE-NEW YORK THEN WASHINGTON-, 778-778.

Grace, J., Berninger, F., & Nagy, L. (2002). Impacts of climate change on the tree line. *Annals of Botany*, *90* (4), 537-544.

Grimm, V., & Railsback, S. F. (2005). *Individual-based modeling and ecology*. Princeton University Press, Princeton, New Jersey, USA.

Grimm, V., Revilla, E., Berger, U., Jeltsch, F., Mooij, W. M., Railsback, S. F., et al. (2005). Pattern-oriented modeling of agent-based complex systems: lessons from ecology. *Science*, *310* (5750), 987-991.

Groisman, P. Y., Sherstyukov, B. G., Razuvaev, V. N., Knight, R. W., Enloe, J. G., Stroumentova, N. S., ... & Karl, T. R. (2007). Potential forest fire danger over Northern Eurasia: changes during the 20th century. *Global and Planetary Change*, *56* (3), 371-386.

Groisman, P., & Soja, A. J. (2009). Ongoing climatic change in Northern Eurasia: justification for expedient research. *Environmental Research Letters*, *4* (4), 045002.

Groisman, P. Y., Blyakharchuk, T. A., Chernokulsky, A. V., Arzhanov, M. M., Marchesini, L. B., Bogdanova, E. G., et al. (2013). Climate changes in Siberia. In *Regional Environmental Changes in Siberia and Their Global Consequences*. Springer Netherlands. p. 57-109.

Groisman, P. Y., & Gutman, G. (2013). *Environmental Changes in Siberia: Regional Changes and their Global Consequences*. Springer, Dordrecht. 357p.

Gruza, G. V., Ran'kova, E. Y., Razuvaev, V. N., and O. N. Bulygina. (1999). Indicators of climate change in the Russian Federation. In Weather and climate extremes. Edited by Karl, T., R., Nicholls, N., and A. Ghazi. Kluwer Academic Publishers, Dordrecht, Netherlands. p. 219-242.

Gruza, G.V., Bardin, M.Yu, Rankova, E.Ya., Rocheva, E.V, Platova, T.V, et al. (2015) A Report on Climate Features on the Territory of the Russian Federation in 2014. Obtained from http://www.meteorf.ru (in Russian)

Gustafson, E. J., Shvidenko, A. Z., Sturtevant, B. R., & Scheller, R. M. (2010). Predicting global change effects on forest biomass and composition in south-central Siberia. *Ecological Applications*, *20* (3), 700-715.

Hamilton, R. A. Woodland Owner Notes: Forest Soils and Site Index. North Carolina Cooperative Extension Service, USDA.

Hansen, J., Ruedy, R., Glascoe, J. and M. Sato. (1999). GISS analysis of surface temperature change. *Journal of Geophysical Research*, *104*, 30997-31022.

Hansen, M. C., Potapov, P. V., Moore, R., Hancher, M., Turubanova, S. A., Tyukavina, A., ... & Townshend, J. R. G. (2013). High-resolution global maps of 21st-century forest cover change. *Science*, *342* (6160), 850-853.

Hayden, B. P. (1998). Ecosystem feedbacks on climate at the landscape scale. *Philosophical Transactions of the Royal Society of London B: Biological Sciences*, *353* (1365), 5-18.

Hely, C., Flannigan, M., Bergeron, Y., & McRae, D. (2001). Role of vegetation and weather on fire behavior in the Canadian mixedwood boreal forest using two fire behavior prediction systems. *Canadian Journal of Forest Research*, *31* (3), 430-441.

Hoffmann, C. W., & Usoltsev, V. A. (2002). Tree-crown biomass estimation in forest species of the Ural and of Kazakhstan. *Forest Ecology and Management*, *158* (1), 59-69.

Hogg, E. H., Brandt, J. P., & Michaelian, M. (2008). Impacts of a regional drought on the productivity, dieback, and biomass of western Canadian aspen forests. *Canadian Journal of Forest Research*, *38* (6), 1373-1384.

Hogg, E. H., & Hurdle, P. A. (1995). The aspen parkland in western Canada: a dry-climate analogue for the future boreal forest? Springer Netherlands. pp. 391-400.

Holcomb, S. S. (2001). An examination of the riparian bottomland forest in North Central Texas through ecology, history, field study, and computer simulation (Doctoral dissertation, University of North Texas).

Hollinger, D. Y., Ollinger, S. V., Richardson, A. D., Meyers, T. P., Dail, D. B., Martin, M. E., Scott, N. A., Arkebauer, T. J., Baldocchi, D. D., and K. L. Clark. (2010). Albedo estimates for land surface models and support for a new paradigm based on foliage nitrogen concentrations. *Global Change Biology*, *16*, 696-710.

Holm, J. A., Shugart, H. H., Van Bloem, S. J. and G. Larocque. (2012) Gap model validation in a subtropical dry forest and predicting poor transition of abandoned fields into secondary forests in Puerto Rico. *Ecological Modelling*, *233*, 70-82.

Holm, J. A., Chambers, J. Q., Collins, W. D., & Higuchi, N. (2014). Forest response to increased disturbance in the central Amazon and comparison to western Amazonian forests. *Biogeosciences*, *11* (20), 5773-5794.

Holtmeier, F. K., & Broll, G. (2005). Sensitivity and response of northern hemisphere altitudinal and polar treelines to environmental change at landscape and local scales. *Global Ecology and Biogeography*, *14* (5), 395-410.

Houghton, R. A., Butman, D., Bunn, A. G., Krankina, O. N., Schlesinger, P., and T. A. Stone. (2007). Mapping Russian forest biomass with data from satellites and forest inventories. *Environmental Research Letters*, *2*, 045032, doi:10.1088/1748-9326/2/4/045032

Huth, A., Ditzer, T., & Bossel, H. (1998). *The rain forest growth model FORMIX3: model description and analysis of forest growth and logging scenarios for the Deramakot Forest Reserve (Malaysia).*

Hüttich, C., Korets, M., Bartalev, S., Zharko, V., Schepaschenko, D., Shvidenko, A., and Schmullius, C. (2014): Exploiting Growing Stock Volume Maps for Large Scale Forest Resource Assessment: Cross-Comparisons of ASAR- and PALSAR-Based GSV Estimates with Forest Inventory in Central Siberia. *Forests*, *5* (8), 1753-1776.

Hytteborn, H., Maslov, A.A., Nazimova, D.I. and L.P. Rysin (2005). Boreal Forests of Eurasia. In: F Andersson (editor) *Ecosystems of the World, 6: Coniferous Forests*. Elsevier B V, Amsterdam, Netherlands. p23-99.

IPCC, 2007: Climate Change 2007: The Physical Science Basis. Contribution of Working Group I to the Fourth Assessment Report of the Intergovernmental Panel on Climate Change [Solomon, S., D. Qin, M. Manning, Z. Chen, M. Marquis, K.B. Averyt, M.Tignor and H.L. Miller (eds.)]. Cambridge University Press, Cambridge, United Kingdom and New York, NY, USA.

IPCC, 2013: Climate Change 2013: The Physical Science Basis. Contribution of Working Group I to the Fifth Assessment Report of the Intergovernmental Panel on Climate Change [Stocker, T.G., Qin, D., Plattner, G.-K., Tignor,

M., Allen, S.K., Boschung, J., Nauels, A., Xia, Y., Bex, V. and P.M. Midgley (eds.)]. Cambridge University Press, Cambridge, UK and New York, NY, 1535 pp.

Isachenko, A. G. (1985). *Landscapes of the USSR* (map atlas). Leningrad University Press, USSR, 320pp.

Isaev A.S., Ovchinnikova T.M., Pal'nikova E.N., Sukhovolski V.G.and O. V. Tarasova (2000) The influence of insects on boreal ecosystems under global climate change. - In: *Disturbance of Boreal Forest Ecosystem: Human Impacts and Natural Processes* (International Boreal Forest Research Association 1997 Annual Meeting Proceedings). US Department of Agriculture Forest Service. North Central Research Station General Technical Report NC-209, pp.115-123.

Isaev, A. S., Khlebopros, R. G., Nedorezov, L. V., Kondakov, Yu. P., Kiselev, V. V., and V. G. Sukhovol'sky. (2001). *Population dynamic of forest insects*. Nauka (Science), Moscow, Russia. (In Russian)

Isachenko, A.G., Shlyapnikov, A.A., Robozertseva, O.D., and A. Z. Filipetskaya (1988) The landscape map of the USSR. General Ministry of Geodesy and Cartography of the USSR, Moscow, USSR. (in Russian).

Istomov, S. V. (2005). The current dynamics of the upper treeline in West Sayan mountains, actual questions of research and protection of the plant world. Transactions of the Reserve - Tigiretky, 211-214.

Ivanova, G. A., Ivanov, V. A., Kukavskaya, E. A., & Soja, A. J. (2010). The frequency of forest fires in Scots pine stands of Tuva, Russia. *Environmental Research Letters*, *5* (1), 015002.

Jackson, R. B., Randerson, J. T., Canadell, J. G., Anderson, R. G., Avissar, R., Baldocchi, D. D., ... & Pataki, D. E. (2008). Protecting climate with forests. *Environmental Research Letters*, *3* (4), 044006.

Jiang, H., Peng, C., Apps, M. J., Zhang, Y., Woodard, P. M. and Z. Wang (1999) Modelling the next primary productivity of temperate forest ecosystems in China with a GAP model. *Ecological Modelling*, *122*, 225-238.

Johnstone, J. F., Chapin III, F. S., Foote, J., Kemmett, S., Price, K., & Viereck, L. (2004). Decadal observations of tree regeneration following fire in boreal forests. *Canadian Journal of Forest Research*, *34* (2), 267-273.

Jupp, T. E., Taylor, C. M., Balzter, H., & George, C. T. (2006). A statistical model linking Siberian forest fire scars with early summer rainfall anomalies. *Geophysical Research Letters*, *33* (14).

Kajimoto, T., Matsuura, Y., Sofronov, M. A., Volokitina, A. V., Mori, S., Osawa, A., & Abaimov, A. P. (1999). Above- and belowground biomass and net primary productivity of a *Larix gmelinii* stand near Tura, central Siberia. *Tree Physiology*, *19* (12), 815-822.

Kammer, P. M., Schöb, C., & Choler, P. (2007). Increasing species richness on mountain summits: Upward migration due to anthropogenic climate change or re-colonisation? *Journal of Vegetation Science*, *18* (2), 301-306.

Kashian, D. M., Romme, W. H., Tinker, D. B., Turner, M. G., & Ryan, M. G. (2006). Carbon storage on landscapes with stand-replacing fires. *BioScience*, *56* (7), 598-606.

Kasischke, E. S., Christensen, N. L., Jr. and Stocks, B. J. (1994). Fire, global warming and the mass carbon balance in boreal forests. *Ecological Applications*, *5*, 437-451.

Kasischke, E. S. and N. H. F. French (1995) Locating and estimating the areal extent of wildfires in Alaskan boreal forests using multiple-season AVHRR NDVI composite data. *Remote Sensing of Environment*, *51*, 263-275.

Kasischke E.S., Hyer E.J., French N.H.F., Suchinin A.I., Hewson J.H., Stocks B.J. (2004). Carbon emissions from boreal forest fires: 1996 to 2002. *Global Biogeochemical Cycles*, *19*:GB1012, doi:10.1029/2004, GB002300

Keane, R. E., Austin, M., Field, C., Huth, A., Lexer, M. J., Peters, D., ... & Wyckoff, P. (2001). Tree mortality in gap models: application to climate change. *Climatic Change*, *51* (3-4), 509-540.

Kharuk, V. I., & Fedotova, E. V. (2003). Forest-tundra ecotone dynamics. Arctic environment variability in the context of global change, 281-299.

Kharuk, V. I., Ranson, K. J., Kuz'michev, V. V., & Im, S. T. (2003). Landsat-based analysis of insect outbreaks in southern Siberia. *Canadian Journal of Remote Sensing*, *29* (2), 286-297.

Kharuk, V. I., Dvinskaya, M. L., & Ranson, K. J. (2005). The spatiotemporal pattern of fires in northern Taiga larch forests of central Siberia. *Russian Journal of Ecology*, *36* (5), 302-311.

Kharuk, V. I., Ranson, K. J., Im, S. T., & Naurzbaev, M. M. (2006). Forest-tundra larch forests and climatic trends. *Russian Journal of Ecology*, *37* (5), 291-298.

Kharuk, V. I., Ranson, K. and M. Dvinskaya. (2007). Evidence of evergreen conifer invasion into Larch dominated forests during recent decades in central Siberia. *Eurasian Journal of Forest Research*, *10*, 163-171.

Kharuk, V. I., Ranson, K. J., Sergey, T. I. and M. L. Dvinskaya. (2009). Response of *Pinus sibirica* and *Larix sibirica* to climate change in southern Siberian alpine forest-tundra ecotone. *Scandinavian Journal of Forest Research*, *24*, 130-139.

Kharuk, V. I., Im, S. T., & Dvinskaya, M. L. (2010a). Forest-tundra ecotone response to climate change in the Western Sayan Mountains, Siberia. *Scandinavian Journal of Forest Research*, *25* (3), 224-233.

Kharuk, V. I., Ranson, K. J., Im, S. T., & Vdovin, A. S. (2010b). Spatial distribution and temporal dynamics of high-elevation forest stands in southern Siberia. *Global Ecology and Biogeography*, *19* (6), 822-830.

Kharuk, V. I., Im, S. T., Dvinskaya, M. L., & Ranson, K. J. (2010c). Climate-induced mountain tree-line evolution in southern Siberia. *Scandinavian Journal of Forest Research*, *25* (5), 446-454.

Kharuk V.I., Ranson K.J., and Dvinskaya M.L. (2010d) Wildfire dynamics in Mid-Siberian larch dominated forests. In: Balzter H (ed) *Environmental Change in Siberia*. Springer, London, pp 83-100.

Kharuk, V. I., Ranson, K. J., Dvinskaya, M. L., & Im, S. T. (2011). Wildfires in northern Siberian larch dominated communities. *Environmental Research Letters*, *6* (4), 045208.

Kharuk, V. I., Ranson, K. J., Oskorbin, P. A., Im, S. T., & Dvinskaya, M. L. (2013a). Climate induced birch mortality in Trans-Baikal lake region, Siberia. *Forest Ecology and Management*, *289*, 385-392.

Kharuk, V. I., Im, S. T., Oskorbin, P. A., Petrov, I. A., & Ranson, K. J. (2013b). Siberian pine decline and mortality in southern siberian mountains. *Forest Ecology and Management*, *310*, 312-320.

King, G. A., & Neilson, R. P. (1992). The transient response of vegetation to climate change: a potential source of CO2 to the atmosphere. *Water, Air, and Soil Pollution*, *64* (1-2), 365-383.

Kloeppel, B. D., Gower, S. T., Treichel, I. W., & Kharuk, S. (1998). Foliar carbon isotope discrimination in Larix species and sympatric evergreen conifers: a global comparison. *Oecologia*, *114* (2), 153-159.

Knorre, A. A., Kirdyanov, A. V., & Vaganov, E. A. (2006). Climatically induced interannual variability in aboveground production in forest-tundra and northern taiga of central Siberia. *Oecologia*, *147* (1), 86-95.

Kobak, K. I. (1988). Budyko, M. I. (ed). *Biotic components of the carbon cycle*. Gidrometeoizdat, Leningrad, USSR.

Kobayashi, H., Delbart, N., Suzuki, R., & Kushida, K. (2010). A satellite-based method for monitoring seasonality in the overstory leaf area index of Siberian larch forest. *Journal of Geophysical Research: Biogeosciences* (2005-2012), *115* (G1).

Kohler, P., Chave, J., Riera, B., Huth, A. (2003). Simulating long-term response of tropical wet forests to fragmentation. *Ecosystems*, *6* (2), 0114-0128.

Köhler, P., & Huth, A. (2007). Impacts of recruitment limitation and canopy disturbance on tropical tree species richness. *Ecological Modelling*, *203* (3), 511-517.

Kohyama, T. (2005). Scaling up from shifting-gap mosaic to geographic distribution in the modeling of forest dynamics. *Ecological Research*, *20*, 305-312.

Kolchugina, T. P., & Vinson, T. S. (1995). Role of Russian forests in the global carbon balance. *Ambio*, 258-264.

Kolosova, L.N., ed. (1982). Geographic Atlas for school teachers, 4th ed. General Ministry of Geodesy and Cartography of the USSR, Moscow, USSR. (in Russian)

Kondakov, Y. (1974). Regularities of the Siberian moth outbreaks. Ecology of forest animal populations. Nauka, Novosibirsk, Russia. pp.206-265. (in Russian)

Kondakov, Y.L. (2002). Massive outbreaks of Siberian silkmoth in forests of Krasnoyarsky Krai. *Entomological Investigations in Siberia*, *2*, 25-74. (in Russian)

Körner, C. (1998). A re-assessment of high elevation treeline positions and their explanation. *Oecologia*, *115* (4), 445-459.

Korovin, G. N. (1996). Analysis of the distribution of forest fires in Russia. In: *Fire in ecosystems of boreal Eurasia*. Springer Netherlands. pp. 112-128.

Korpachev, V.P., Perezhilin, A.I., Andriyas, A.A., and Y.I. Ryabakon. (2010). Pollution of reservoirs HES by woody debris, organic entities, and their effect on water quality. Yestestvoznanie Academy Press, Moscow, Russia. (in Russian)

Kotlyakov, V. and T. Khromova. (2002). Maps of permafrost and ground ice. In Stolbovoi V. and I. McCallum, eds. Land Resources of Russia. Laxenburg, Austria: International Institute for Applied Systems Analysis and the Russian Academy of Science. CD-ROM. Distributed by the National Snow and Ice Data Center, Boulder.

Krankina, O. N., & Dixon, R. K. (1992). Forest management in Russia: challenges and opportunities in the era of perestroika. *Journal of Forestry* (USA).

Krankina, O. N., & Dixon, R. K. (1994). Forest management options to conserve and sequester terrestrial carbon in the Russian Federation. *World Resources Review*, *6* (1), 88-101.

Krankina, O. N., Harmon, M. E., & Winjum, J. K. (1996). Carbon storage and sequestration in the Russian forest sector. *AMBIO*, *25*, 284-288.

Krankina, O. N., Houghton, R. A., Harmon, M. E., Hogg, E. H., Butman, D., Yatskov, M., Huso, M., Treyfeld, R. F., Razuvaev, V. N., and G. Spycher. (2005) Effects of climate, disturbance, and species on forest biomass across Russia. *Canadian Journal of Forest Research*, *35*, 2281-2293.

Kryuchkov, V.V. (1973). The effect of permafrost on the northern tree line. In Permafrost: Proceedings of the Second International Conference (USSR Contribution), pp.136-138. Washington, D.C.: National Academy of Science.

Kukavskaya, E. A., Buryak, L. V., Ivanova, G. A., Conard, S. G., Kalenskaya, O. P., Zhila, S. V., & McRae, D. J. (2013). Influence of logging on the effects of wildfire in Siberia. *Environmental Research Letters*, *8* (4), 045034.

Kukavskaya, E., Buryak, L. V., Conard, S. G., Petkov, A., Barrett, K., Kalenskaya, O. P., & Ivanova, G. (2014). Effects of Repeated Fires in the Forest Ecosystems of the Zabaikalye Region, Southern Siberia. In: AGU Fall Meeting Abstracts (Vol. 1, p. 0456).

Kulagin, A. Y., Davydychev, A. N., & Zaitsev, G. A. (2006). Specific features of the growth of Siberian spruce (Picea obovata Ledeb.) at early stages of ontogeny in broadleaf-conifer forests of the Ufa plateau. *Russian Journal of Ecology*, *37* (1), 66-69.

Kull, O., & Tulva, I. (2000). Modelling canopy growth and steady-state leaf area index in an aspen stand. Annals of forest science, 57(5), 611-621.

Kullman, L. (2000). Tree-limit rise and recent warming: a geoecological case study from the Swedish Scandes. *Norsk Geografisk Tidsskrift*, *54* (2), 49-59.

Kullman, L. (2001). 20th century climate warming and tree-limit rise in the southern Scandes of Sweden. *Ambio: A journal of the Human Environment*, *30* (2), 72-80.

Kullman, L. (2004). A face of global warming - "ice birches" and a changing alpine plant cover. *Geoöko*, *25*, 181-202.

Kullman, L., & Kjällgren, L. (2006). Holocene pine tree-line evolution in the Swedish Scandes: Recent tree-line rise and climate change in a long-term perspective. *Boreas*, *35* (1), 159-168.

Kulmala, M., Suni, T., Lehtinen, K. E. J., Maso, M. D., Boy, M., Reissell, A., ... & Hari, P. (2004). A new feedback mechanism linking forests, aerosols, and climate. *Atmospheric Chemistry and Physics*, *4* (2), 557-562.

Kurz, W. A., Apps, M. J., Stocks, B. J., & Volney, W. J. A. (1995a). *Global climate change: disturbance regimes and biospheric feedbacks of temperate and boreal forests*. Oxford University Press, New York. p199-133.

Kurz, W. A., Apps, M. J., Beukema, S. J., & Lekstrum, T. (1995b). 20th century carbon budget of Canadian forests. *Tellus B*, *47* (1-2), 170-177.

Kurz, W. A. and M. J. Apps (1999) A 70-year retrospective analysis of carbon fluxes in the Canadian forest sector. *Ecological Applications*, *9*, 526-547.

Kurz, W. A., Dymond, C. C., Stinson, G., Rampley, G. J., Neilson, E. T., Carroll, A. L., ... & Safranyik, L. (2008). Mountain pine beetle and forest carbon feedback to climate change. *Nature*, *452* (7190), 987-990.

Kuusinen, N., Tomppo, E., Shuai, Y., & Berninger, F. (2014). Effects of forest age on albedo in boreal forests estimated from MODIS and Landsat albedo retrievals. *Remote Sensing of Environment*, *145*, 145-153.

Landsberg, J. J., & Gower, S. T. (1997). *Applications of physiological ecology to forest management*. Academic Press.

Larcher, W. (1995). *Plant physiological ecology*. Springer, Berlin, Germany.

Larocque, G. R., Archambault, L. and C. Delisle. (2006) Modelling forest succession in two southeastern Canadian mixedwood ecosystem types using the ZELIG model. *Ecological Modelling*, *199*, 350-362.

Larocque, G. R., Archambault, L. and C. Delisle. (2011) Development of the gap model ZELIG-CFS to predict the dynamics of American mixed forest types with complex structures. *Ecological Modelling*, *222*, 2570-2583.

Larocque, G.R., H.H. Shugart, W. Xi and J.A. Holm. (2016). Forest succession models (in press). G.R. Larocque (ed.), *Ecological Forest Management Handbook*. CRC Press, Taylor and Frances Group, London.

Lauenroth, W. K., Urban, D. L., Coffin, D. P., Parton, W. J., Shugart, H. H., Kirchner, T. B., and T. M. Smith (1993) Modeling vegetation structure - ecosystem process interactions across sites and ecosystems. *Ecological Modelling*, *67*, 49-80.

Laurance, W. F., Delamônica, P., Laurance, S. G., Vasconcelos, H. L., & Lovejoy, T. E. (2000). Conservation: rainforest fragmentation kills big trees. *Nature*, *404* (6780), 836-836.

Laurance, W. F., Lovejoy, T. E., Vasconcelos, H. L., Bruna, E. M., Didham, R. K., Stouffer, P. C., ... & Sampaio, E. (2002). Ecosystem decay of Amazonian forest fragments: a 22-year investigation. *Conservation Biology*, *16* (3), 605-618.

Laurance, W. F. (2008). Theory meets reality: how habitat fragmentation research has transcended island biogeographic theory. *Biological Conservation*, *141* (7), 1731-1744.

Law, B. E. (2014). Regional analysis of drought and heat impacts on forests: current and future science directions. *Global Change Biology*, *20* (12), 3595-3599.

Lawrence, P. J., Feddema, J. J., Bonan, G. B., Meehl, G. A., O'Neill, B. C., Oleson, K. W., ... & Thornton, P. E. (2012). Simulating the biogeochemical and biogeophysical impacts of transient land cover change and wood harvest in the Community Climate System Model (CCSM4) from 1850 to 2100. *Journal of Climate*, *25* (9), 3071-3095.

Le Toan, T., Beaudoin, A., Riom, J., & Guyon, D. (1992). Relating forest biomass to SAR data. *Geoscience and Remote Sensing, IEEE Transactions on*, *30* (2), 403-411.

Leemans, R. and Prentice, I. C. (1989) *FORSKA, a General Forest Succession Model*. Institute of Ecological Botany, Uppsala, pp. 70.

Lenoir, J., Gégout, J. C., Marquet, P. A., De Ruffray, P., & Brisse, H. (2008). A significant upward shift in plant species optimum elevation during the 20th century. *Science*, *320* (5884), 1768-1771.

Lindroth, A., Grelle, A., & Morén, A. S. (1998). Long-term measurements of boreal forest carbon balance reveal large temperature sensitivity. *Global Change Biology*, *4* (4), 443-450.

Lindroth, A., Lagergren, F., Aurela, M., Bjarnadottir, B., Christensen, T., Dellwik, E., ... & Vesala, T. (2008). Leaf area index is the principal scaling parameter for both gross photosynthesis and ecosystem respiration of Northern deciduous and coniferous forests. *Tellus B*, *60* (2), 129-142.

Liu, J., & Ashton, P. S. (1998). FORMOSAIC: an individual-based spatially explicit model for simulating forest dynamics in landscape mosaics. *Ecological Modelling*, *106* (2), 177-200.

Liu, H., Randerson, J. T., Lindfors, J., & Chapin, F. S. (2005). Changes in the surface energy budget after fire in boreal ecosystems of interior Alaska: An annual perspective. *Journal of Geophysical Research: Atmospheres* (1984-2012), *110* (D13).

Loboda, T. V., & Csiszar, I. A. (2007). Reconstruction of fire spread within wildland fire events in Northern Eurasia from the MODIS active fire product. *Global and Planetary Change*, *56* (3), 258-273.

Logan, J. A., J. Régnière and J. A. Powell (2003) Assessing the impacts of global warming on forest pest dynamics. *Frontiers in Ecology and in the Environment*, *1*, 130-137.

Luyssaert, S., Schulze, E. D., Börner, A., Knohl, A., Hessenmöller, D., Law, B. E., ... & Grace, J. (2008). Old-growth forests as global carbon sinks. *Nature*, *455* (7210), 213-215.

Lyamzev, N. and A. Isaev (2002) in Stolbovoi and McCallum.

Lydolph, P. E. (1977). *Climates of the Soviet Union. World Survey of Climatology*, vol. 7. Elsevier Scientific Publishing Company, New York.

Ma, Z., Peng, C., Zhu, Q., Chen, H., Yu, G., Li, W., ... & Zhang, W. (2012). Regional drought-induced reduction in the biomass carbon sink of Canada's boreal forests. *Proceedings of the National Academy of Sciences*, *109* (7), 2423-2427.

MacDonald, G. M., Velichko, A. A., Kremenetski, C. V., Borisova, O. K., Goleva, A. A., Andreev, A. A., Cwynar, L.C., Riding, R.T., Forman, S.L., Edwards, T.W.D., Aravena, R., Hammarlund, D., Szeicz, J.M., and Gattaulin, V. N. (2000). Holocene treeline history and climate change across northern Eurasia. *Quaternary Research*, *53* (3), 302-311.

Malevsky-Malevich, S. P., Molkentin, E. K., Nadyozhina, E. D., & Shklyarevich, O. B. (2008). An assessment of potential change in wildfire activity in the Russian boreal forest zone induced by climate warming during the twenty-first century. *Climatic Change*, *86* (3-4), 463-474.

Malysheva, N.V. (1993). Forest density map. In: *Ecological Atlas of Russia* (2002). Kiselyova, N.M., ed. "Karta" Publishing House, St. Petersburg, Russia.

Manabe, S. and R. J. Stouffer (1980) Sensitivity of a global climate to an increase in CO_2 concentration in the atmosphere. *Journal of Geophysical Research*, *85*, 5529-5554.

Mankin, J B, R V O'Neil, H H Shugart and B W Rust (1977). The importance of validation in ecosystem analysis. In: G. S. Innis (editor) *New Directions in the Analysis of Ecological Systems, Part I: Simulation Councils*, La Jolla, CA. p63-71.

Matsumoto, K., Ohta, T., Nakai, T., Kuwada, T., Daikoku, K. I., Iida, S. I., ... & Hattori, S. (2008). Energy consumption and evapotranspiration at several boreal and temperate forests in the Far East. *Agricultural and Forest Meteorology*, *148* (12), 1978-1989.

Maximov, T., Ohta, T., & Dolman, A. J. (2008). Water and energy exchange in East Siberian forest: A synthesis. *Agricultural and Forest Meteorology*, *148* (12), 2013-2018.

McDowell, N. G., Beerling, D. J., Breshears, D. D., Fisher, R. A., Raffa, K. F., & Stitt, M. (2011). The interdependence of mechanisms underlying climate-driven vegetation mortality. *Trends in Ecology & Evolution*, *26* (10), 523-532.

Meleshko, V. P., Kattsov, V. M., Govorkova, V. A., Sporyshev, P. V., Shkol'nik, I. M., & Shneerov, B. E. (2008). Climate of Russia in the 21st century. Part 3. Future climate changes calculated with an ensemble of coupled atmosphere-ocean general circulation CMIP3 models. *Russian Meteorology and Hydrology*, *33* (9), 541-552. (in Russian)

Messier, C., Smith, D. W., & Adamowicz, W. L. (Eds.). (2003). *Towards sustainable management of the boreal forest* . Ottawa, Ont: NRC Research Press. pp. 1-40

METI and NASA Release Version 2 ASTER Global DEM (2011). U.S. Geological Survey / NASA LP DAAC. Retrieved 13 November 2013.

Miao, Z., & Li, C. (2007). *Biomass estimates for major boreal forest species in west-central Canada* (Vol. 2). Canadian Wood Fibre Centre.

Mielke, D.L., Shugart, H.H., and D.C. West. (1978) Stand model for upland forests of Southern Arkansas (No. ORNL/TM-6225). Oak Ridge National Lab, Tennessee, USA.

Milakovsky, B., Frey, B., & James, T. (2012). Carbon dynamics in the boreal forest. In: *Managing Forest Carbon in a Changing Climate*. Springer Netherlands. p 109-135.

Miller, C. and D. L. Urban (1999) A model of surface fire, climate and forest pattern in the Sierra Nevada, California. *Ecological Modelling*, *114*, 113-135.

Mitrofanov D. P. (1977) *Chemical composition of forest plants in Siberia*. Nauka, Novosibirsk, USSR. 120 pp. (in Russian)

Mladenoff, D. J., & He, H. S. (1999). Design, behavior and application of LANDIS, an object-oriented model of forest landscape disturbance and succession. Spatial modeling of forest landscape change: approaches and applications. Cambridge University Press, Cambridge, UK, 125-162.

Mladenoff, D. J. (2004). LANDIS and forest landscape models. *Ecological Modelling*, *180* (1), 7-19.

Moiseev, P. A. (2002). Effect of climatic changes on radial increment and age structure formation in high-mountain larch forests of the Kuznetsk Ala Tau. *Russian Journal of Ecology*, *33* (1), 7-13.

Mokhov, I. I., Chernokulsky, A. V., & Shkolnik, I. M. (2006, December). Regional model assessments of fire risks under global climate changes. In: *Doklady earth sciences* (Vol. 411, No. 2, pp. 1485-1488). MAIK Nauka/Interperiodica.

Mokhov, I. I., & Chernokulsky, A. V. (2010). Regional model assessments of forest fire risks in the Asian part of Russia under climate change. *Geography and Natural Resources*, *31* (2), 165-169.

Mollicone, D., Eva, H. D., & Achard, F. (2006). Ecology: human role in Russian wild fires. *Nature*, *440* (7083), 436-437.

Monserud, R. A., Tchebakova, N. M., & Leemans, R. (1993). Global vegetation change predicted by the modified Budyko model. *Climatic Change*, *25* (1), 59-83.

Monserud, R. A., & Tchebakova, N. M. (1996). A vegetation model for the Sayan Mountains, southern Siberia. *Canadian Journal of Forest Research*, *26* (6), 1055-1068.

Monsi, M., Uchijima, Z., & Oikawa, T. (1973). Structure of foliage canopies and photosynthesis. *Annual Review of Ecology and Systematics*, 301-327.

Morris, R. F. (1963). The dynamics of epidemic spruce budworm populations. *Memoirs of the Entomological Society of Canada*, *95* (31), 1-12.

Nakai, Y., Matsuura, Y., Kajimoto, T., Abaimov, A. P., Yamamoto, S., & Zyryanova, O. A. (2008). Eddy covariance CO_2 flux above a Gmelin larch forest on continuous permafrost in Central Siberia during a growing season. *Theoretical and Applied Climatology*, *93* (3-4), 133-147.

National Climate Data Center (NCDC). (1998). Technical Report 98-03. Available from NOAA National Climatic Data Center, Asheville, NC, USA.

National Climate Data Center (NCDC). (2005a). Global Synoptic Climatology Network C the former USSR Version 1.0. Available from NOAA National Climatic Data Center, Asheville, NC, USA.

National Climate Data Center (NCDC). (2005b). Daily and sub-daily precipitation for the former USSR Version 1.0. Available from NOAA National Climatic Data Center, Asheville, NC, USA.

Neigh, C. S., Nelson, R. F., Ranson, K. J., Margolis, H. A., Montesano, P. M., Sun, G., ... & Andersen, H. E. (2013). Taking stock of circumboreal forest carbon with ground measurements, airborne and spaceborne LiDAR. *Remote Sensing of Environment*, *137*, 274-287.

Niinemets, U., PORTSMUTH, A., & Truus, L. (2002). Leaf structural and photosynthetic characteristics, and biomass allocation to foliage in relation to foliar nitrogen content and tree size in three Betula species. *Annals of Botany*, *89* (2), 191-204.

Nikolov N. and H. Helmisaari. (1992). Silvics of the circumpolar boreal forest tree species, pp 9-84. In: Shugart H. H., R. Leemans and G.B. Bonan (eds). *A systems analysis of the global boreal forest*. Cambridge University Press, Cambridge, UK.

Noskova, N.E. and I.N. Tretyakova. (2006). The effects of stress on reproductive abilities of pine. *Conifers of the Boreal Zone*, *23* (3), 54-63.

Noskova, N.E., Tretyakova, I.N., and E.N. Muratova. (2009) Microsporogenesis and pollen formation in Scotch pine (*Pinus sylvestris* L.) under modern climatic conditions of Siberia. *Biology Bulletin*, *36* (3), 317-322.

Ogureeva, G.N. (1973). *Botanical geography of Altay*. Russian Academy of Sciences Press, Moscow, USSR. 188p.

Ohta, T., Maximov, T. C., Dolman, A. J., Nakai, T., van der Molen, M. K., Kononov, A. V., ... & Yabuki, H. (2008). Interannual variation of water balance and summer evapotranspiration in an eastern Siberian larch forest over a 7-year period (1998-2006). *Agricultural and Forest Meteorology*, *148* (12), 1941-1953.

Oker-Blom, P. (1986). Photosynthetic radiation regime and canopy structure in modeled forest stands. *Acta Forestalia Fennica*, *197*, 1-44.

Olchev, A., & Novenko, E. (2011). Estimation of potential and actual evapotranspiration of boreal forest ecosystems in the European part of Russia during the Holocene. *Environmental Research Letters*, *6* (4), 045213.

Oleson KW, Lawrence DM, Bonan GB et al. (2013) Technical Description of Version 4.5 of the Community Land Model (CLM), pp. 308-310. National Center for Atmospheric Research, Boulder, CO.

Ollinger, S. V., Richardson, A. D., Martin, M. E., Hollinger, D. Y., Frolking, S. E., Reich, P. B., ... & Schmid, H. P. (2008). Canopy nitrogen, carbon assimilation, and albedo in temperate and boreal forests: Functional relations and potential climate feedbacks. *Proceedings of the National Academy of Sciences*, *105* (49), 19336-19341.

Onuchin, V.S. (1962). Several morphological features of Siberian larch in Tuva. In: *Larch: compilation*. Krasnoyarsk: STI, 29(1), 22-35. (in Russian)

Onuchin A. A. (1986). Transformation of solid precipitation with forests of Khamar-Daban Mountans: Dissertation. Krasnoyarsk: V.N. Sukachev Forest Institute, 182 p. (in Russian).

Osawa, A., Zyryanova, O. A., Matsuura, Y., Kajimoto, T., and R. W. Wein (2010). *Permafrost Ecosystems: Siberian Larch Forests, Ecological Studies*. Springer, New York, NY.

Ovchinnikov, D.V. and E.A. Vaganov (1999). Dendrochronological characteristics of Larix sibirica L. at the upper treeline in Mountain Altai. *Nauka*, *6* (2), 145-152. (in Russian)

Pabst, R. J., Goslin, M. N., Spies, T. A., and S. L. Garman. (2006). Use of the ZELIG forest simulation model in the coastal landscape analysis and modeling study (CLAMS). Presentation to Spanish forestry researchers (Sept 22, 2006), Corvallis, OR.

Pabst, R. J., Goslin, M. N., Garman, S. L., & Spies, T. A. (2008). Calibrating and testing a gap model for simulating forest management in the Oregon Coast Range. *Forest Ecology and Management*, *256* (5), 958-972.

Pacala, S. W., Canham, C. D., & Silander Jr, J. A. (1993). Forest models defined by field measurements: I. The design of a northeastern forest simulator. *Canadian Journal of Forest Research*, *23* (10), 1980-1988.

Pastor, J. and W. M. Post. (1986). Influence of climate, soil moisture, and succession on forest carbon and nitrogetn cycles. *Biogeochemistry*, *2*, 3-27.

Pastor, J. and W. M. Post. (1988). Response of northern forests to CO_2-induced climate change. *Letters to Nature*, *334*, 55-58.

Patenaude, G., Hill, R. A., Milne, R., Gaveau, D. L., Briggs, B. B. J., & Dawson, T. P. (2004). Quantifying forest above ground carbon content using LiDAR remote sensing. *Remote Sensing of Environment*, *93* (3), 368-380.

Pautova V. N. (1976). Aboveground plant mass and transpiration of some communities in forest-tundra zone. *Transactions of Limnological Institute of SO AN USSR*, *22* (42), 92-128. (in Russian)

Petrov, V. V., & N. B. Ponomareva (1977). Initial States of Secondary Successional Growth Post Fire in Coniferous Forest. *Vestnik Moskovskogo Universiteta: Biologia*, Moscow State University Press, Moscow, USSR.

Pielke, R. A., & Vidale, P. L. (1995). The boreal forest and the polar front. *Journal of Geophysical Research: Atmospheres (1984-2012)*, *100* (D12), 25755-25758.

Polikarpov, N. P., Chebakova, N. M., & Nazimova, D. I. (1986). *Klimat i gornye lesa Sibiri* (Climate and mountain forests of Siberia). Nauka Publishing House, Novosibirsk, USSR.

Post, W. M. and J. Pastor (1996) Linkages - an individual-based forest ecosystem model. *Climatic Change*, *34*, 253-261.

Prentice, K. C. and I Y. Fung (1990). The sensitivity of terrestrial carbon storage to climate change. *Nature*, *346*, 48-51.

Prentice, I. C., Sykes, M. T., & Cramer, W. (1993). A simulation model for the transient effects of climate change on forest landscapes. *Ecological Modelling*, *65* (1), 51-70.

Purves, D. and S. Pacala (2008). Predictive Models of Forest Dynamics Science, *Science*, *320* (5882) 1452-1453.

Purves, D.W., Lichstein, J.W., Strigul, N, and S.W. Pacala. (2008). Predicting and understanding forest dynamics using a simple tractable model. *Proceedings of the National Academy of Sciences*, *105* (44), 17-18-17022.

Radkevich, V. A. (1997) *Ecology textbook*. 3rd ed. Ministry of Higher Education. 159pp.

Rakovskaya, E.M., and M.I. Davydova. (1990). *Physical Geography of USSR*, v2. "Akademiya" Publishing House, Moscow, USSR.

Randerson, J. T., Liu, H., Flanner, M. G., Chambers, S. D., Jin, Y., Hess, P. G., ... & Zender, C. S. (2006). The impact of boreal forest fire on climate warming. *Science*, *314* (5802), 1130-1132.

Reimers, N.F. (1990). *Nature utilization: dictionary-encyclopedia*. Thought Press, Moscow, USSR.

Reiners, W. A., & Driese, K. L. (2004). *Transport processes in nature: propagation of ecological influences through environmental space* (Vol. 1). Cambridge University Press.

Repola, J., Ojansuu, R., & Kukkola, M. (2007). Biomass functions for Scots pine, Norway spruce and birch in Finland. In: *Working Papers of the Finnish Forest Research Institute* 53. Finnish Forest Research Institute.

Resler, L. M., Butler, D. R., & Malanson, G. P. (2005). Topographic shelter and conifer establishment and mortality in an alpine environment, Glacier National Park, Montana. *Physical Geography*, *26* (2), 112-125.

Rogers, B. M., Soja, A. J., Goulden, M. L., & Randerson, J. T. (2015). Influence of tree species on continental differences in boreal fires and climate feedbacks. *Nature Geoscience*.

Röser, C., Montagnani, L., Schulze, E. D., Mollicone, D., Kolle, O., Meroni, M., et al. (2002). Net CO_2 exchange rates in three different successional stages of the Dark Taiga of central Siberia. *Tellus B*, *54* (5), 642-654.

Running, S. W., Nemani, R. R. and R. D. Hungerford (1987) Extrapolation of synoptic meteorological data in mountainous terrain and its use for simulating forest evapotranspiration and photosynthesis. *Canadian Journal of Forest Research*, *17*, 472-483.

Samoilova, G. S. (1973). *Types of landscapes in mountains of Southern Siberia*. Neklyudova, M.P., ed. Moscow State University Press, Moscow, USSR. (in Russian)

SAS v9.3 (2010) SAS Institute Inc., Cary, NC, USA.

Savva, Y. V., Schweingruber, F. H., Vaganov, E. A., & Milyutin, L. I. (2003). Influence of climate changes on treering characteristics of Scots pine provenances in southern Siberia (forest-steppe). *IAWA Journal*, *24* (4), 371-383.

Saxton, K.E., and W.J. Rawls. (2006). Soil Water Characteristic estimates by texture and organic matter for hydrologic solutions. *Soil Science Society of America Journal*, *70* (5), 1569-1578.

Scheller, R.M., and J.B. Domingo. (2012) LANDIS-II Base Fire v3.0 Extension User Guide. University of Wisconsin, Madison, Wisconsin, USA. (http://www.landis-ii.org/extensions/base-fire)

Scholze, M., Knorr, W., Arnell, N. W., & Prentice, I. C. (2006). A climate-change risk analysis for world ecosystems. *Proceedings of the National Academy of Sciences*, *103* (35), 13116-13120.

Schepashenko, D., Shvidenko, A., & Nilsson, S. (1998). Phytomass (live biomass) and carbon of Siberian forests. *Biomass and Bioenergy*, *14* (1), 21-31.

Schepaschenko D, McCallum I, Shvidenko A, Fritz S, Kraxner F, Obersteiner M (2010) A new hybrid land cover dataset for Russia: a methodology for integrating statistics, remote sensing and in-situ information. J Land Use Sci. doi: 10.1080/1747423X.2010.511681 (Published online 22 Dec 2010)

Schulze, E. D. (1982). Plant life forms and their carbon, water and nutrient relations. In: *Physiological Plant Ecology* II. Springer Berlin Heidelberg. pp. 615-676.

Schulze, E. D., Schulze, W., Koch, H., Arneth, A., Bauer, G., Kelliher, F. M., ... & Issajev, A. (1995). Aboveground biomass and nitrogen nutrition in a chronosequence of pristine Dahurian Larix stands in eastern Siberia. *Canadian Journal of Forest Research*, *25* (6), 943-960.

Schulze, E. D., Vygodskaya, N. N., Tchebakova, N. M., Czimczik, C. I., Kozlov, D. N., Lloyd, J., ... & Wirth, C. (2002). The Eurosiberian Transect: an introduction to the experimental region. *Tellus B*, *54* (5), 421-428.

Schulze ED, Wirth C, Mollicone D, Ziegler W. (2005). Succession after stand replacing disturbances by fire, wind throw, and insects in the dark taiga of Central Siberia. *Oecologia*, *146* (1),77-88.

Schuur, E. A. G., McGuire, A. D., Schädel, C., Grosse, G., Harden, J. W., Hayes, D. J., ... & Vonk, J. E. (2015). Climate change and the permafrost carbon feedback. *Nature*, *520* (7546), 171-179.

Scurlock, J. M. O., Asner, G. P., & Gower, S. T. (2001). Worldwide historical estimates of leaf area index, 1932-2000. ORNL Technical Memorandum ORNL/TM-2001/268. Oak Ridge National Laboratory, Oak Ridge, Tenn. http://www.osti.gov/bridge.

Sedel'nikov, V.P. (1979) *Flora and vegetation of high-mountain areas in the Kusnetsk Altay*. Nauka, Novosibirsk, USSR. (in Russian)

Seedre, M., Taylor, A. R., Chen, H. Y. H., and K. Jogiste. (2013). Deadwood density of five boreal tree species in relation to field-assignment decay class. *Forest Science*, *59* (3), 261-266.

Serreze, M. C., Walsh, J. E., Chapin, F. S., III, Osterkamp, T., Dyurgerov, M., Romanovsky, V., Oechel, W. C., Morison, J., Zhang, T., and R. G. Barry (2000) Observational evidence of recent change in the Northern high-latitude environment. *Climatic Change*, *46*, 159-207.

Shibistova, O., Lloyd, J. O. N., Evgrafova, S., Savushkina, N., Zrazhevskaya, G., Arneth, A., ... & SCHULZE, E. D. (2002a). Seasonal and spatial variability in soil CO_2 efflux rates for a central Siberian Pinus sylvestris forest. *Tellus B*, *54* (5), 552-567.

Shibistova, O., Lloyd, J., Zrazhevskaya, G., Arneth, A., Kolle, O., Knohl, A., ... & Schmerler, J. (2002b). Annual ecosystem respiration budget for a Pinus sylvestris stand in central Siberia. *Tellus B*, *54* (5), 568-589.

Shinozaki, K., Yoda, K., Hozumi, K., & Kira, T. (1964). A quantitative analysis of plant form-the pipe model theory: I. Basic analyses. *Japanese Journal of Ecology*, *14* (3), 97-105.

Shugart, H. H. and D. C. West (1977) Development of an Appalachian deciduous forest succession model and its application to assessment of the impact of the chestnut blight. *Journal of Environmental Management*, *5*, 161-179.

Shugart, H. H. and D. C. West (1979) Size and pattern of simulated forest stands. *Forest Science*, *25*, 120-122.

Shugart, H.H. and D.C. West (1980). Forest Succession models. *Biosciences*, *30*, 308-313.

Shugart, H. H. (1984). *A theory of forest dynamics*. Springer-Verlag, New York.

Shugart, H.H., Antonovsky, M.J., Jarvis P.G., and Sandford A.P. (1986). CO_2, climatic change and forest ecosystems: Assessing the response of global forests to the direct effects of increasing CO_2 and climatic change pp. 475-521.

In: *The Greenhouse Effect, Climatic Change and Ecosystems (SCOPE 29)* eds. Bolin, B., Döös, B.R., Jager J. and Warrick R.A. (eds). John Wiley & Sons, New York.

Shugart, H. H. (1987). Dynamic Ecosystem Consequences of Tree Birth and Death Patterns. *Biosciences*, *37* (8), 596-601.

Shugart, H.H., Bonan, G.B. & Rastetter, E.B. (1988a). Niche theory and community organization. *Canadian Journal of Botany*, *66*, 2634-2639.

Shugart, H.H., P.J. Michaels, T.M. Smith, D.A. Weinstein and E.B. Rastetter. (1988b). Simulation Models of Forest Succession. In: T. Rosswall, R.G. Woodmansee and P.G. Risser (eds.), *Scales and Global Changes: Spatial and Temporal Variability in Biospheric and Geospheric Processes*. John Wiley and Sons, Ltd., London. pp. 125-151.

Shugart, H. H., Leemans, R. and G. B. Bonan, eds. (1992a). *A Systems Analysis of the Global Boreal Forest*. Cambridge University Press, Cambridge.

Shugart, H. H., Smith, T. M. and W. M. Post. (1992b). The potential for application of individual-based simulation models for assessing the effects of global change. *Annual Reviews of Ecology and Systematics*, *23*, 15-38.

Shugart, H. H., Emanuel, W. R. and G. Shao. (1996). Models of forest structure for conditions of climatic change. *Commonwealth Forestry Review*, *75*, 51-64.

Shugart, H. H. (1998). *Terrestrial ecosystems in changing environments*. Cambridge University Press, Cambridge.

Shugart, H. H. (2000). The importance of structure in the longer-term dynamics of ecosystems. *Journal of Geophysical Research - Atmospheres*, *105*, 20065-20075.

Shugart, H. H. (2003). *A theory of forest dynamics: The ecological implications of forest succession models*. Blackburn Press, Caldwell, NJ.

Shugart, H. H., Shuman, J. K., Yan, X., and N. Zhang. (2006). Eurasian forest cover and climate feedbacks. *iLEAPS Newsletter*, *3*, 20-21.

Shugart, H. H. (2007). *How the earthquake bird got its name and other tales of an unbalanced nature*. Yale University Press, USA.

Shugart, H. H. and F. I. Woodward. (2011). *Global Change and the Terrestrial Biosphere: Achievements and Challenges*. Wiley-Blackwell, Oxford, UK.

Shkol'nik, I., V. Meleshko, S. Efimov, and E. Stafeeva, (2012). Changes in climate extremes on the territory of Siberia by the middle of the 21st century: An ensemble forecast based on the MGO regional climate model. *Russian Meteorology and Hydrology*, *37*, 71-84.

Shuman, J.K. and H. H. Shugart. (2009). Evaluating the sensitivity of Eurasian forest biomass to climate change using a dynamic vegetation model. *Environmental Research Letters*, *4*, 045024.

Shuman, J.K. (2010). Dissertation: Russian forest dynamics and response to changing climate: A simulation study. University of Virginia, Charlottesville, VA.

Shuman, J. K., H. H. Shugart and T. L. O'Halloran. (2011). Sensitivity of Siberian larch forest to climate change. *Global Change Biology*, *17*, 2370-2384.

Shumilova, L. V. (1962). *Botanical geography of Siberia*. Tomsk State University, Tomsk, USSR. 440p.

Shvidenko, A. Z., & Nilsson, S. (2000). Fire and the carbon budget of Russian forests. In: *Fire, climate change, and carbon cycling in the boreal forest*. Springer New York. pp. 289-311.

Shvidenko, A., & Nilsson, S. (2002). Dynamics of Russian forests and the carbon budget in 1961-1998: An assessment based on long-term forest inventory data. *Climatic change*, *55* (1-2), 5-37.

Shvidenko, A. and S. Nilsson. (2003). Dynamics of Russian forests and the carbon budget in 1961-1998: An assessment based on long-term forest inventory data. *Climatic change*, *55* (1-2), 5-37.

Shvidenko, A. and S. Nilsson. (2003b). A synthesis of the impact of Russian forests on the global carbon budget for 1961-1998. *Tellus*, *55B*, 391-415.

Shvidenko, A. Z., Schepaschenko, D. G., Nilsson, C., and Yu. I. Buluy. (2006). *Tables and models of growth and productivity of forests of major forest forming species of northern Eurasia* (standard and reference materials). Ministry of Natural Resources of the Russian Federation, Moscow, Russia.

Simard, M., Pinto, N., Fisher, J. B., & Baccini, A. (2011). Mapping forest canopy height globally with spaceborne lidar. *Journal of Geophysical Research: Biogeosciences* (2005-2012), *116* (G4).

Sitch, S., Huntingford, C., Gedney, N., Levy, P. E., Lomas, M., Piao, S. L., ... & Woodward, F. I. (2008). Evaluation of the terrestrial carbon cycle, future plant geography and climate-carbon cycle feedbacks using five Dynamic Global Vegetation Models (DGVMs). *Global Change Biology*, *14* (9), 2015-2039.

Smith, T. M. and D. L. Urban. (1988). Scale and the resolution of forest structural pattern. *Vegetatio*, *74*, 143-150.

Smith, T. M., Shugart, H. H., Bonan, G. B., and J. B. Smith. (1992). Modeling the potential response of vegetation to global climate change. *Advances in Ecological Research*, *22*, 93-116.

Smith, T. M. and H. H. Shugart. (1993). The transient response of terrestrial carbon storage to a perturbed climate. *Nature*, *361*, 523-526.

Smith, W. K., Hinckley, T. M., & Ewel, K. C. (1995). Ecophysiology of coniferous forests. *Trends in Ecology and Evolution*, *10* (8), 343.

Sofronov, M.A., Sofronova, T.M., and A.V. Volokitina. (2004). Evaluation of fire danger based on weather conditions using meteorological forecasts. *Lesnoe Khozaistvo*, *6*, 31-32. (in Russian)

Soja, A. J., Cofer, W. R., Shugart, H. H., Sukhinin, A. I., Stackhouse, P. W., McRae, D. J., and S. G. Conard. (2004). Estimating fire emissions and disparities in boreal Siberia (1998-2002). *Journal of Geophysical Research*, *109* (D14S06) doi:10.1029/2004JD004570.

Soja, A. J., Shugart, H. H., Sukhinin, A., Conard, S., & Stackhouse Jr, P. W. (2006). Satellite-derived mean fire return intervals as indicators of change in Siberia (1995-2002). *Mitigation and Adaptation Strategies for Global Change*, *11* (1), 75-96.

Soja, A. J., Tchebakova, N. M., French, N. H., Flannigan, M. D., Shugart, H. H., Stocks, B. J., Sukhinin, A. I., Parfenova, E. I., and F. S. Chapin III. (2007). Climate-induced boreal forest change: Predictions versus current observations. *Global and Planetary Change*, *56*, 274-296.

Solomon, A. M. (1986). Transient Response of Forests to CO_2 Induced Climate Change: Simulation Modeling Experiments in Eastern North America. *Oecologia*, *68*, 567-579.

Spracklen, D. V., Bonn, B., & Carslaw, K. S. (2008). Boreal forests, aerosols and the impacts on clouds and climate. *Philosophical Transactions of the Royal Society A: Mathematical, Physical and Engineering Sciences*, *366* (1885), 4613-4626.

Stepanovskikh, A. S. (2003) *Applied Ecology: preservation of environment*. Unity-Dana Press, Moscow, Russia.

Stevens, G. C., & Fox, J. F. (1991). The causes of treeline. *Annual Review of Ecology and Systematics*, 177-191.

Stocks, B. J., Fosberg, M. A., Lynham, T. J., Mearns, L., Wotton, B. M., Yang, Q., ... & McKenney, D. W. (1998). Climate change and forest fire potential in Russian and Canadian boreal forests. *Climatic Change*, *38* (1), 1-13.

Stolbovoi, V. and I. McCallum, eds. (2002). CD-ROM Land Resources of Russia. International Institute for Applied Systems Analysis and the Russian Academy of Science, Laxenburg, Austria.

Stolbovoi, V. and I. Savin. (2002). Maps of soil characteristics. In Stolbovoi, V. and I. McCallum, eds (2002) CD-ROM Land Resources of Russia. International Institute for Applied Systems Analysis and the Russian Academy of Science, Laxenburg, Austria.

Strauss, J., Schirrmeister, L., Grosse, G., Wetterich, S., Ulrich, M., Herzschuh, U., and H.-W. Hubberten. (2013). The deep permafrost carbon pool of the yedoma region in Siberia and Alaska. *Geophys Research Letters*, *40*, 6165-6170.

Sturtevant, B.R., Miranda, B.R., Scheller, R.M., and D. Shinneman. (2008). LANDIS-II dynamic fire system extension. Verion 1. User guide. Univeristy of Wisconsin, Madison, Wisconsin, USA.

Sturtevant, B.R., R.M. Scheller, B.R. Miranda, D. Shinneman, A.D. Syphard. (2009). Simulating dynamic and mixed-severity fire regimes: A process-based fire extension for LANDIS-II. *Ecological Modelling*, *220*, 3380-3393.

Sullivan, A. D., & Clutter, J. L. (1972). A simultaneous growth and yield model for loblolly pine. *Forest Science*, *18* (1), 76-86.

Sun, G., Ranson, K. J., Kharuk, V. I., Im, S. T., & Naurzbaev, M. M. (2011). Characterization and monitoring of tundra-taiga transition zone with multi-sensor satellite data. In: *Eurasian Arctic Land Cover and Land Use in a Changing Climate*, pp. 53-77. Springer Netherlands.

Suzuki, K. and T. Ohta. (2003). Effect of larch forest density on snow surface energy balance. *Journal of Hydrometeorology*, *4*, 1181-1193.

Sykes, M. T., & Prentice, I. C. (1995). Boreal forest futures: modelling the controls on tree species range limits and transient responses to climate change. In: *Boreal Forests and Global Change*, pp. 415-428. Springer Netherlands.

Tarnocai, C., Canadell, J. G., Schuur, E. A. G., Kuhry, P., Mazhitova, G., & Zimov, S. (2009). Soil organic carbon pools in the northern circumpolar permafrost region. *Global Biogeochemical Cycles*, *23* (2).

Tchebakova, N. M., Monserud, R. A., & Parfenova, E. I. (2001). *Phytomass change in the mountain forests of southern Siberia under climate warming*. US Department of Energy National Energy Technology Laboratory.

Tchebakova, N.M. (2006). Dissertation (doctorate): Possible transformation of vegetation cover in Siberia for different climate change scenarios. Krasnoyarsk, Russia. 60pp. (in Russian)

Tchebakova, N. M., & Parfenova, E. I. (2006). Prediction of forest shifts under climate change at the end of the 20th century in Central Siberia. *Computer Technology*, *11* (part 3), 77-86.

Tchebakova, N. M., Parfenova, E., & Soja, A. J. (2009a). The effects of climate, permafrost and fire on vegetation change in Siberia in a changing climate. *Environmental Research Letters*, *4* (4), 045013.

Tchebakova, N. M., Rehfeldt, G. E. and E. I. Parfenova. (2009b). From vegetation zones to climatypes: Effect of climate warming on Siberian exosystems, pp. 427-447. In: Osawa, A., Zyranova, O. A., Matsurura, Y., Kajimoto, T. and R. W. Wein (eds). *Permafrost Ecosystems of Siberian Larch Forests*. Springer-Verlag, New York.

Tchebakova, N. M., Parfenova, E. I., & Soja, A. J. (2011). Climate change and climate-induced hot spots in forest shifts in central Siberia from observed data. *Regional Environmental Change*, *11* (4), 817-827.

Thornthwaite, C. W. and J. R. Mather. (1957). Instructions and tables for computing potential evapotranspiration and the water balance. *Publications in Climatology*, *10*, 183-311.

Tietjen, B., & Huth, A. (2006). Modelling dynamics of managed tropical rainforests - aggregated approach. *Ecological Modelling*, *199* (4), 421-432.

Timoshok, E. E., Narozhnyi, Y. K., Dirks, M. N., & Berezov, A. A. (2003). Experience in combined glaciological and botanical studies on the primary plant successions on young moraines in the Central Altai. *Russian Journal of Ecology*, *34* (2), 91-97.

Timoshok, E. E., Timoshok, E. N., & Skorokhodov, S. N. (2014). Ecology of Siberian stone pine (Pinus sibirica Du Tour) and Siberian larch (Larix sibirica Ledeb.) in the Altai mountain glacial basins. *Russian Journal of Ecology*, *45* (3), 194-200.

Tinner, W., & Kaltenrieder, P. (2005). Rapid responses of high-mountain vegetation to early Holocene environmental changes in the Swiss Alps. *Journal of Ecology*, *93* (5), 936-947.

Tjoelker, M. G., Oleksyn, J., & Reich, P. B. (1998). Seedlings of five boreal tree species differ in acclimation of net photosynthesis to elevated CO_2 and temperature. *Tree Physiology*, *18* (11), 715-726.

Tretyakova, I.N. and N.E. Noskova. (2004). Scotch pine pollen under conditions of environmental stress. *Russian Journal of Ecology*, *35* (1), 20-26.

Tretyakova, I. N. (2006). Characteristics of organ formation and their morphogenetic potential in Siberian larch. *Achievements of Modern Biology*, *126* (5), 472-480. (in Russian)

Urban, D.L. (1990). A versatile model to simulate forest pattern: A user's guide to ZELIG version 1.0. Department of Environmental Sciences, University of Virginia, Charlottesville, VA, 108 pp.

Urban, D.L., G.B. Bonan, T.M. Smith, and H.H. Shugart. (1991). Spatial applications of gap models. *Forest Ecology and Management*, *42*, 95-110.

Urban, D. L., & Shugart, H. H. (1992). Individual-based models of forest succession. In: *Plant succession: theory and prediction*. Chapman and Hall, London. pp. 249-292.

Urban, D. L. Harmon, M. E. and C. B. Halpern. (1993). Potential response of Pacific Northwest forests to climatic change, effects of stand age and initial composition. *Climatic Change*, *23*, 247-266.

Urban, D. L. (2000). Using model analysis to design monitoring programs for landscape management and impact assessment. *Ecological Applications*, *10*, 1820-1832.

Valendik, E. N. (1996). Temporal and spatial distribution of forest fires in Siberia. In: *Fire in Ecosystems of Boreal Eurasia*. Springer Netherlands. pp. 129-138.

Valendik, E.N., Verkhovec, S.V., Kisilyakhov, E.K. and A.Yu. Lantukh. (2004a). The role of the silkworm in the fire potential of forests of the Lower Angara river basin. *Lesnoe Khozaistvo*, *6*, 27-29. (In Russian)

Valendik, E.N., Verkhovec, S.V., Kisilyakhov, E.K., Kosov, I.V. and N.A. Tyul'panov. (2004b). Preparation of silkworm-infested forest for regeneration through fire. *Lesnoe Khozaistvo*, *3*, 41-42. (In Russian)

Vaschuk, L. N. and A. Z. Shvidenko. (2006). *Dynamics of Forests of Irkutsk Region*. Irkutsk printing house N1, Irkutsk, Russia.

Vertessy, R. A., Benyon, R. G., O'sullivan, S. K., & Gribben, P. R. (1995). Relationships between stem diameter, sapwood area, leaf area and transpiration in a young mountain ash forest. *Tree Physiology*, *15* (9), 559-567.

Viereck, L. A., Van Cleve, K., & Dyrness, C. T. (1986). Forest ecosystem distribution in the taiga environment. In: *Forest ecosystems in the Alaskan taiga*. Springer New York. pp. 22-43.

Volney, W. J. A. and R. A. Fleming. (2000). Climate Change and impacts of boreal forest insects. *Agriculture, Ecosystems and Environment*, *82*, 283-294.

Vygodskaya, N. N., Groisman, P. Ya., Tchebakova, N. M., Kurbatova, J. A., Panfyorov, O., Parfenova, E. I., and A. F. Sogachev. (2007). Ecosystems and climate interactions in the boreal zone of northern Eurasia. *Environmental Research Letters*, *2*, 045033.

Wang, J., Zhang, C., Xia, F., Zhao, X., Wu, L., & Gadow, K. V. (2011). Biomass structure and allometry of Abies nephrolepis (Maxim) in Northeast China. *Silva Fennica*, *45* (2), 211-226.

Waring, R. H., Schroeder, P. E., & Oren, R. (1982). Application of the pipe model theory to predict canopy leaf area. *Canadian Journal of Forest Research*, *12* (3), 556-560.

Waring, R. H., & Schlesinger, W. H. (1985). *Forest ecosystems: concepts and management*. Academic Press, Inc. Harcourt Brace Jovanovich, Publishers.

Watt, A. S. (1947). Pattern and process in the plant community. *The Journal of Ecology*, *35*, 1-22.

Wegge, P., Rølstad, J., & Gjerde, I. (1992). Effects of boreal forest fragmentation on capercaillie grouse: empirical evidence and management implications. In: *Wildlife 2001: populations*. Springer Netherlands. pp. 738-749.

Weishampel, J.F., D.L. Urban, H.H. Shugart, and J.B. Smith. (1992). A comparison of semivariagrams from a forest transect gap model and remotely sensed data. *Journal of Vegetation Science*, *3*, 521-526.

Weishampel, J.F. (1994). Dissertation: Spatial dynamics of primary forest succession: Modeling the Glacier Bay 'chronosequence'. University of Virginia, Charlottesville, VA.

Weishampel, J. F., & Urban, D. L. (1996). Coupling a spatially-explicit forest gap model with a 3-D solar routine to simulate latitudinal effects. *Ecological Modelling*, *86* (1), 101-111.

Welp, L. R., Randerson, J. T., & Liu, H. P. (2007). The sensitivity of carbon fluxes to spring warming and summer drought depends on plant functional type in boreal forest ecosystems. *Agricultural and Forest Meteorology*, *147* (3), 172-185.

Wertin, T. M., McGuire, M. A., & Teskey, R. O. (2012). Effects of predicted future and current atmospheric temperature and [CO_2] and high and low soil moisture on gas exchange and growth of Pinus taeda seedlings at cool and warm sites in the species range. *Tree Physiology*, *32* (7), 847-858.

Westerling, A. L., Hidalgo, H. G., Cayan, D. R., and T. W. Swetnam. (2006). Warming and earlier spring increase western US forest wildfire activity. *Science*, *313*, 940-943.

Wilmking, M., Juday, G. P., Barber, V. A., & Zald, H. S. (2004). Recent climate warming forces contrasting growth responses of white spruce at treeline in Alaska through temperature thresholds. *Global Change Biology*, *10* (10), 1724-1736.

Winjum, J. K., Dixon, R. K., & Schroeder, P. E. (1992). Estimating the global potential of forest and agroforest management practices to sequester carbon. In: *Natural Sinks of :math:'CO_2'*. Springer Netherlands. pp. 213-227.

Wirth, C., Schulze, E. D., Lühker, B., Grigoriev, S., Siry, M., Hardes, G., ... & Vygodskaya, N. N. (2002). Fire and site type effects on the long-term carbon and nitrogen balance in pristine Siberian Scots pine forests. *Plant and Soil*, *242* (1), 41-63.

Wirth, C. (2005). Fire regime and tree diversity in boreal forests: implications for the carbon cycle. In: *Forest Diversity and Function*. Springer Berlin Heidelberg. pp. 309-344.

Woodward, F. I. (1987). *Climate and Plant Distribution*. Cambridge University Press, Cambridge.

Yamazaki, T., Yabuki, H., Ishii, Y., Ohta, T., & Ohata, T. (2004). Water and energy exchanges at forests and a grassland in eastern Siberia evaluated using a one-dimensional land surface model. *Journal of Hydrometeorology*, *5* (3), 504-515.

Yan X. and H. H. Shugart. (2005). A forest gap model to simulate dynamics and patterns of eastern Eurasian forests. *Journal of Biogeography*, *32*, 1641-1658.

Yan, M. J., Yamanaka, N., Yamamoto, F., & Du, S. (2010). Responses of leaf gas exchange, water relations, and water consumption in seedlings of four semiarid tree species to soil drying. *Acta Physiologiae Plantarum*, *32* (1), 183-189.

Yang, J., He, H. S., & Gustafson, E. J. (2004). A hierarchical fire frequency model to simulate temporal patterns of fire regimes in LANDIS. *Ecological Modelling*, *180* (1), 119-133.

Yatskov, M., Harmon, M. E., & Krankina, O. N. (2003). A chronosequence of wood decomposition in the boreal forests of Russia. *Canadian Journal of Forest Research*, *33* (7), 1211-1226.

Zhang, N., Shugart, H. H. and X. Yan. (2009). Simulating the effects of climate changes on eastern Eurasian forests. *Climatic Change*, *95*, 341-361.

Zhang, K., Kimball, J. S., Nemani, R. R., & Running, S. W. (2010). A continuous satellite-derived global record of land surface evapotranspiration from 1983 to 2006. *Water Resources Research*, *46* (9).

Zhang, N., Yasunari, T., & Ohta, T. (2011). Dynamics of the larch taiga-permafrost coupled system in Siberia under climate change. *Environmental Research Letters*, *6* (2), 024003.